

Evaluation of icing design criteria for lattice towers

By
Oleksiy Korotkov

A thesis submitted to
the Faculty of Graduate Studies
in partial fulfilment of
the requirements for the degree of
Master of Science

Department of Civil Engineering
Faculty of Engineering
University of Manitoba
Winnipeg, Manitoba

April 2010

Copyright © 2010 by Oleksiy Korotkov

ABSTRACT

Atmospheric icing is a major design factor for guyed lattice masts and transmission lines in Canada and many other countries with cold climate. Tall and slender guyed lattice towers are particularly sensitive to ice accretion, wind or combination of both, as they are often located in remote areas, where meteorological data are limited. The variation of local topography and seasonal climate affects icing conditions and complicates standardization of icing accretion design guidelines.

Icing design criteria was evaluated in this study through an extensive literature review of current design standards for latticed structures subjected to ice and wind load and/or a combination of both, field and laboratory work.

The experimental program was carried out for a prototype 7 m (21 ft) tall fibre reinforced polymer (FRP) guyed lattice tower to investigate its behavior under wind and/or ice loads. The accumulation of glaze, soft rime and hard rime icing was studied on the members of steel and FRP lattice tower sections oriented at 0, 30 and 90 degree angles to the icing wind at the University of Manitoba Icing and Wind Tunnel Facility. The effectiveness of using the low friction icephobic coating Wearlon Super F-1 Ice as a possible ice mitigation technique for lattice towers was also studied.

The tower was installed at the outdoor laboratory at the University of Manitoba and monitored from February 12 to March 1, 2009. The wind speed during the time of observation (February 12 to March 1, 2009) varied between 0 km/h and 37.8 km/h. The strain readings were collected by the strain gauges located along the tower span and accelerations were measured by two three axis accelerometers. The results from the field

study showed that maximum tensile and compressive stresses in the members of FRP tower section were well below the ultimate tensile and compressive strength of the material. The growth of strain can be attributed to extended period of relaxation of the material under fluctuating wind load. Since no natural icing was observed during the observation time the tower was artificially sprayed with chilled mist water. Moderate glaze icing of the tower did not contribute significantly to these stresses. The vibration amplitude decreased due to an increased weight of the structure and the low wind velocity. Currently natural frequencies are not used in design, with the possible exception of earthquake loading provisions. However, values obtained through testing can be used as a reference in a future dynamic analysis of similar guyed FRP lattice towers, since the lattice tower tested at the University of Manitoba is the first of its kind.

The study showed that there was no significant difference on ice accretion on steel and FRP tower sections with nearly identical cross sections. However, the angle of orientation of the segments to the icing wind affected ice accumulation. The lowest ice accretion was observed at 0 degree angle for the glaze ice. Based on the test results in this study the maximum ice thickness of glaze ice equal to 32 mm for both FRP and steel was observed. Thus, similar ice loads as those used in steel structures are recommended for the analysis of guyed FRP towers.

The FRP and steel tower surfaces were coated with low friction icephobic coating Wearlon Super F-1 Ice. The coating did not prevent ice accretion. However, a 14 % reduction in ice weight was observed on FRP section. Both steel and FRP segments showed reduction in adhesive strength of ice after the glaze icing test.

ACKNOWLEDGEMENTS

The author would like to express sincere gratitude and appreciation to the following individuals for ongoing support during the project:

- Dr. Dimos Polyzois, P.Eng., Advisor
- Dr. Eric Bibeau, P.Eng., Advisory committee member
- Prof. Fariborz Hashemian, P.Eng., Advisory committee member
- Greg Moneta, Lab and field support
- Chad Klowak, P.Eng., McQuade Structures Lab
- Grant Whiteside, Technician, McQuade Structures Lab
- Hugues Vogel, Civionics EIT, ISIS Canada
- Evangeline Rivera, Manager, ISIS Canada
- Sami Alshurafa, Phd student
- Bruce Ellis, Technician, UMITF Lab support
- John Kell, P.Eng., Manitoba Hydro
- Greg Friesen, P.Eng., Manitoba Hydro
- Dave Tataryn-tower installation
- Fellow graduate students

This project was funded by Manitoba Hydro and NSERC Wind Energy Strategic Network (WESNet).

TABLE OF CONTENTS

ABSTRACT	ii
ACKNOWLEDGEMENTS	iv
TABLE OF CONTENTS.....	v
LIST OF TABLES	ix
LIST OF FIGURES	xi
LIST OF COPYRIGHTED MATERIAL	xvii
1 INTRODUCTION	1
1.1 General	1
1.2 Objectives.....	5
1.3 Scope	5
2 LITERATURE REVIEW	6
2.1 Introduction	6
2.2 Design standards for ice loading	6
2.2.1 CAN/CSA S37 -01 Antennas, Towers, and Antenna-Supporting Structures	6
2.2.2 Structural Standard for Antenna Supporting Structures and Antennas. ANSI/TIA 222-G-2005.....	12
2.2.3 Manitoba Hydro Specifications	17
2.2.4 CAN/CSA-C22.3 NO. 1-06. Overhead Systems	18

2.2.4.1	Design loads for wire and cable attachments	19
2.2.4.2	Loads on supports.....	19
2.2.5	CAN/CSA-C22.3 NO. 60826-06. Design Criteria for Overhead Transmission Lines	21
2.2.6	ISO 12494: Atmospheric Icing of Structures.....	23
2.3	Icing failures of guyed lattice structures	26
2.4	Atmospheric ice on towers.....	29
2.5	Estimation of ice accretion on structures.	33
2.6	Variation of ice amounts with height.....	39
2.7	Prevention and shedding methods.....	41
2.8	Summary	44
3	FIELD AND LABORATORY WORK.....	47
3.1	Introduction	47
3.2	Field testing of FRP lattice tower under environmental loads.	50
3.2.1	Tower modifications	50
3.2.2	Tower erection	55
3.2.3	Site layout and sensors.....	58
3.2.4	Data acquisition system (DAQ).....	60
3.2.5	Test procedure.....	61
3.3	Icing tunnel tests.....	69

3.3.1	Design and manufacturing of steel tower section	70
3.3.2	Test procedure.....	71
3.3.3	Application of an icephobic coating.	73
4	RESULTS AND DISCUSSION.....	75
4.1	Strains.....	75
4.2	Vibrations.....	81
4.2.1	Theoretical background	81
4.2.2	Results.....	82
4.3	Icing tunnel test results.....	88
4.3.1	Test 1. Accumulation of glaze icing on the FRP section at 90 degree angle..	88
4.3.2	Test 2. Accumulation of soft rime icing on the FRP section at 90 degree angle.....	91
4.3.3	Test 3. Accumulation of hard rime icing on the FRP tower section at 90 degree angle.	94
4.3.4	Test 4. Accumulation of glaze icing on the steel section at 90 degree angle.	95
4.3.5	Test 5. Accumulation of soft rime icing on the steel tower section at 90 degree angle.	97
4.3.6	Test 6. Accumulation of hard rime icing on the steel section at 90 degree angle.....	98

4.3.7	Accumulation of icing at 0 and 30 degree angles to the face.	101
4.4	Evaluation of effectiveness of the icephobic coating Wearlon Super F-1 Ice.	106
5	SUMMARY AND CONCLUSIONS	115
	REFERENCES	122
	APPENDICES	127
	APPENDIX A: Design criteria maps.....	127
	APPENDIX B: Wind speed and wind directions from field experiment	131
	APPENDIX C: Strains from the FRP tower.	143
	APPENDIX D: Vibration frequency spectra of the FRP tower.....	159

LIST OF TABLES

Table 2.1: Minimum design ice thickness	7
Table 2.2: Examples of damaging ice storms in Manitoba.....	17
Table 2.3: Deterministic weather loads	18
Table 2.4: Damage and failure limits of structures.....	20
Table 2.5: Ratios of weight of ice to structure weight	23
Table 2.6: Failures of guyed masts by cause and height.....	26
Table 2.7: Physical properties of ice.....	30
Table 2.8: Meteorological parameters controlling ice accretion.....	32
Table 2.9: Underestimated radial ice accretion.....	34
Table 2.10: Summary of the icing design criteria from the Standards	46
Table 4.1: Accumulation of glaze ice on steel and FRP tower sections at 90 degree angle	96
Table 4.2: Accumulation of soft rime ice on steel and FRP tower sections at 90 degree angle	98
Table 4.3: Accumulation of hard rime ice on steel and FRP tower sections at 90 degree angle	100
Table 4.4: Accumulation of glaze ice on steel and FRP tower sections at 0 degree angle	102

Table 4.5: Accumulation of soft rime ice on steel and FRP tower sections at 0 degree angle	102
Table 4.6: Accumulation of hard rime ice on steel and FRP tower sections at 0 degree angle	102
Table 4.7: Accumulation of glaze ice on steel and FRP tower sections at 30 degree angle	103
Table 4.8: Accumulation of soft rime ice on steel and FRP tower sections at 30 degree angle	103
Table 4.9: Accumulation of hard rime ice on steel and FRP tower sections at 30 degree angle	103
Table 4.10: Total accreted masses of ice at 0, 30 and 90 degree angles, (grams)	104
Table 4.11: Maximum ice thicknesses of ice at 0, 30 and 90 degree angles, (mm)	104
Table 4.12: Masses of ice per unit length at 0, 30 and 90 degree angles, (kg/m)	105
Table 4.13: Accumulation of glaze ice on steel and FRP tower sections coated with Wearlon Super F-1 Ice at 90 degree angle	106
Table 4.14: Accumulation of soft rime ice on steel and FRP tower sections coated with Wearlon Super F-1 Ice at 90 degree angle	109
Table 4.15: Accumulation of hard rime ice on steel and FRP tower sections coated with Wearlon Super F-1 Ice at 90 degree angle	112
Table 4.16: Accretion of ice on uncoated segments and coated with Wearlon Super F-1 Ice at 90 degree angle	113

LIST OF FIGURES

Figure 1.1: Collapsed transmission towers in Quebec after 1998 ice storm.....	1
Figure 1.2: Severe icing on lattice tower in Sweden	2
Figure 1.3: Hydro-Quebec pylon collapsed under the weight of the ice, near Drummondville, Quebec, January 1998	2
Figure 1.4: Lattice guyed masts	3
Figure 1.5: Self-supporting communication tower (a) and transmission towers (b)	3
Figure 2.1: Face area of radial ice.....	7
Figure 2.2: Ice Map of Canada	8
Figure 2.3: Limits for wind shielding	10
Figure 2.4: Relation between radial ice thickness and member size	12
Figure 2.5: Projected area of ice	13
Figure 2.6: Outside dimensions for calculating ice weight	15
Figure 2.7: Reference icing amounts (mm)-50-year return period.....	22
Figure 2.8: Failures of guyed towers in Canada taller than 75m between 1955 and 1988 designed according to various standards.....	27
Figure 2.9: Failure factors leading to collapse	29
Figure 2.10: Glaze (a), soft rime (b) and hard rime(c) ice accretion on lattice tower	31
Figure 2.11: Type of accreted in-cloud icing as a function of wind speed and temperature	32

Figure 2.12: Ice map of Canada.....	34
Figure 2.13: Ice accretion amounts caused by freezing precipitation.....	36
Figure 2.14: Ice weight as a function of time	37
Figure 2.15: Variation of ice amount with height.....	40
Figure 2.16: Centrifuge ice adhesion reduction AMIL's results	44
Figure 3.1: FRP lattice tower segment.....	47
Figure 3.2: Fully raised FRP tower.....	49
Figure 3.3: PVC conduit inside the tower.....	51
Figure 3.4: Steel tower base.....	51
Figure 3.5: Pinned base of the tower	52
Figure 3.6: The voids filled with epoxy resin	53
Figure 3.7: Tower base foundation	53
Figure 3.8: Guy wire attachment bracket.....	54
Figure 3.9: Guy wire attachment bracket.....	54
Figure 3.10: Guy wire assembly sequence	56
Figure 3.11: Erection of the tower	56
Figure 3.12: Layout of the test site location	58
Figure 3.13: Layout of strain gauges and accelerometers.....	59
Figure 3.14: Installed meteorological instruments.....	60

Figure 3.15: DAQ system	60
Figure 3.16: Ice on the diagonal bracing of FRP tower	62
Figure 3.17: Iced chord of the FRP tower.....	62
Figure 3.18: Iced members of FRP tower	63
Figure 3.19: Temperature fluctuation during testing period	64
Figure 3.20: Wind direction at 3:02-3:32 PM on February 23, 2009	65
Figure 3.21: Wind speed at 3:02-3:32 PM on February 23, 2009	65
Figure 3.22: Wind direction at 10:47-11:01 AM on February 25, 2009.....	66
Figure 3.23: Wind speed at 10:47-11:01 on February 25, 2009	66
Figure 3.24: Wind direction at 11:54-12:12AM on February 26, 2009.....	67
Figure 3.25: Wind speed at 11:54-12:12AM on February 26, 2009.....	67
Figure 3.26: Wind direction at 1:56-2:12 PM on February 28, 2009	68
Figure 3.27: Wind speed at 1:56-2:12 PM on February 28, 2009	68
Figure 3.28: FRP section (left) and steel section (right).....	69
Figure 3.29: Wind direction is normal, parallel and 30 degrees angle to the face.....	70
Figure 3.30: FRP segment cross section.....	70
Figure 3.31: University of Manitoba Icing and Wind Tunnel	71
Figure 3.32: Tested segment placed in icing tunnel	72
Figure 3.33: Wearlon Super F1-Ice coating and hardener	73

Figure 3.34: Fiber glass tower section coated with Wearlon Super F1-Ice (light grey color)	74
Figure 4.1: Strains in chords at the top on February 23, 2009	76
Figure 4.2: Average wind direction (a) and location of strain gauges (b) on February 23, 2009.....	76
Figure 4.3: Strains in chords and diagonals at the top on February 26, 2009.....	78
Figure 4.4: Location of strain gauges and major wind direction at 11:54-12:12 on February 26, 2009	78
Figure 4.5: Strains in chords and diagonals at the top of the iced FRP tower on March 1, 2009.....	80
Figure 4.6: Directions of measured accelerations.....	82
Figure 4.7: Vibration frequency spectrum of FRP tower at 3.65 m on February 17, 2009	83
Figure 4.8: Vibration frequency spectrum of FRP tower at 7 m on February 17, 2009 ...	83
Figure 4.9: Vibration frequency spectrum of FRP tower at 3.65 m on February 23, 2009	84
Figure 4.10: Vibration frequency spectrum of FRP tower at 7 m on February 23, 2009 .	84
Figure 4.11: Vibration frequency spectrum of FRP tower on February 26, 2009	85
Figure 4.12: Test 1-glaze ice accumulation on the members of FRP tower section at 90 degree angle	88
Figure 4.13: Removed pieces of glaze ice	90

Figure 4.14: Test 2-soft rime ice accumulation on the members of FRP tower section at 90 degree angle	91
Figure 4.15: Appearance of rime ice on the members of FRP tower	93
Figure 4.16: Test 3-hard rime ice accumulation on the members of FRP tower section at 90 degree angle.	94
Figure 4.17: Soft rime ice accumulation at the wind speed of 5 m/s (a) and hard rime ice accumulation at the wind speed of 25m/s (b)	95
Figure 4.18: Test 4-glaze ice accumulation on the steel tower section at 90 degree angle.	96
Figure 4.19: Test 5-soft rime ice accumulation on the steel tower section at 90 degree angle.....	97
Figure 4.20: Hard rime ice accumulation on the members of the steel tower section at 90 degree angle	99
Figure 4.21: Glaze ice accumulation on the FRP tower section coated with Wearlon Super F-1 Ice at 90 degree angle.....	107
Figure 4.22: Glaze ice accumulation on the steel tower section coated with Wearlon Super F-1 Ice at 90 degree angle.....	108
Figure 4.23: Soft rime ice accumulation on the FRP tower section coated with Wearlon Super F-1 Ice at 90 degree angle.....	110
Figure 4.24: Soft rime ice accumulation on the steel tower section coated with Wearlon Super F-1 Ice at 90 degree angle.....	111

Figure 4.25: Hard rime ice accumulation on the steel tower section coated with Wearlon Super F-1 Ice at 90 degree angle..... 113

Figure 4.26: Hard rime ice accumulation on the FRP tower section coated with Wearlon Super F-1 Ice at 90 degree angle..... 114

Figure 5.1: Results from the icing tunnel testing of the FRP and steel lattice tower segments at 0, 30 and 90 degree angles 118

Figure 5.2: Results from the icing tunnel testing of the FRP and steel lattice tower segments coated with the icephobic coating Wearlon Super F-1 Ice at 90 degree angle 120

LIST OF COPYRIGHTED MATERIAL

Figure 2.1: Face area of radial ice (CSA, 2001), p. 7; Figure 2.3: Limits for wind shielding (CSA, 2001), p. 10 are reproduced with the permission of Canadian Standards Association from *S37-01 (R2006) - Antennas, Towers, and Antenna-Supporting Structures*, which is copyrighted by CSA, 5060 Spectrum Way, Mississauga ON, L4W 5N6 Canada. While use of this material has been authorized, CSA shall not be responsible for the manner in which the information is presented, nor for any interpretations thereof.

Figure 2.2: Ice Map of Canada (CSA, 2001) p. 8; Figure 2.12: Ice map of Canada (CSA, 2006c), p. 34 © Environment Canada

Figure 2.4: Relation between radial ice thickness and member size (Wahba et al., 1993), p. 12 © 2008 NRC Canada or its licensors. Reproduced with permission.

Figure 2.5: Projected area of ice (ANSI/TIA, 2005), p. 13; Figure 2.6: Outside dimensions for calculating ice weight (ANSI/TIA, 2005), p. 15 have been reproduced under written permission from Telecommunications Industry Association. Complete copies of all TIA standards can be purchased through IHS at 1-800-854-7179 or 303-397-7956 (www.ihs.com).

Table 2.3: Deterministic weather loads (CSA, 2006a), p. 18; Table 2.4: Damage and failure limits of structures (CSA, 2006a), p. 20; Figure A- 1: Loading map of Canada (CSA, 2006a), p. 127; Figure A- 2: Loading map of Manitoba (CSA, 2006a), p. 128 are reproduced with the permission of Canadian Standards Association from *CAN/CSA-C22.3 NO. 1-06 - Overhead Systems*, which is copyrighted by CSA, 5060 Spectrum Way, Mississauga ON, L4W 5N6 Canada. While use of this material has been authorized, CSA shall not be responsible for the manner in which the information is presented, nor for any interpretations thereof.

Figure 2.7: Reference icing amounts (mm)-50-year return period (CSA, 2006b), p. 22; Table 2.5: Ratios of weight of ice to structure weight (CSA, 2006b) p. 23; Table 2.7: Physical properties of ice (CSA, 2006b), p. 30; Table 2.8: Meteorological parameters controlling ice accretion (CSA, 2006b), p. 32; Figure 2.11: Type of accreted in-cloud icing as a function of wind speed and temperature (CSA, 2006b), p. 32 are reproduced with the permission of Canadian Standards Association from *CSA C22.3 No. 60826-06 - Design Criteria for Overhead Transmission Lines (Adopted CEI/IEC 60826:2003, third edition, 2003-10, with Canadian deviations)*, which is copyrighted by CSA, 5060 Spectrum Way, Mississauga ON, L4W 5N6 Canada. While use of this material has been authorized, CSA shall not be responsible for the manner in which the information is presented, nor for any interpretations thereof.

Table 2.6: Failures of guyed masts by cause and height (Smith, 2007), p. 26 © 2007 Brian W. Smith. Reproduced with permission.

Figure 2.8: Failures of guyed towers in Canada taller than 75m between 1955 and 1988 designed according to various standards (Magued et al., 1989), p. 27 © 2008 NRC Canada or its licensors. Reproduced with permission.

Figure 2.9: Failure factors leading to collapse (Mulherin, 1998), p. 29 © 1998 Elsevier. Reprinted with permission.

Table 2.9: Underestimated radial ice accretion (Wahba et al., 1993), p. 34 © 2008 NRC Canada or its licensors. Reproduced with permission.

Figure 2.13: Ice accretion amounts caused by freezing precipitation (Yip, 1995), p. 36; Figure 2.15: Variation of ice amount with height (Yip, 1995), p. 40 © 1995 Elsevier. Reprinted with permission.

Figure 2.14: Ice weight as a function of time (Makkonen & Oleskiw, 1997), p. 37 © 1995 Elsevier. Reprinted with permission.

Figure A- 3: 50-year mean recurrence interval uniform ice thicknesses due to freezing rain with concurrent 3-second gust speeds: contiguous 48 states (ASCE, 2005), p. 129; Figure A- 4 (continued): 50-year mean recurrence interval uniform ice thicknesses due to freezing rain with concurrent 3-second gust speeds: contiguous 48 states (ASCE, 2005), p. 130 © 2005 ASCE. Reproduced with permission.

1 INTRODUCTION

1.1 General

Atmospheric icing is known to occur in many northern countries, including Canada. Ice accretion on structures poses significant challenges for engineers, owners and the general population ranging from TV and radio signal disruption (Mulherin, 1986) to complete structure failures (Magued et al., 1989; Mulherin, 1998) to power outages and loss of human life (Phillips, 2002).

Goel (2008) reports that the ice storm in 1998 in eastern Ontario and southern Quebec brought down 1,300 transmission towers and 35,000 distribution structures, causing power outage for two million people. Restoration work cost nearly five billion dollars for the province of Quebec alone. An example of the icing effect on transmission structures is shown in Figures 1.1 to 1.3.^{1,2}

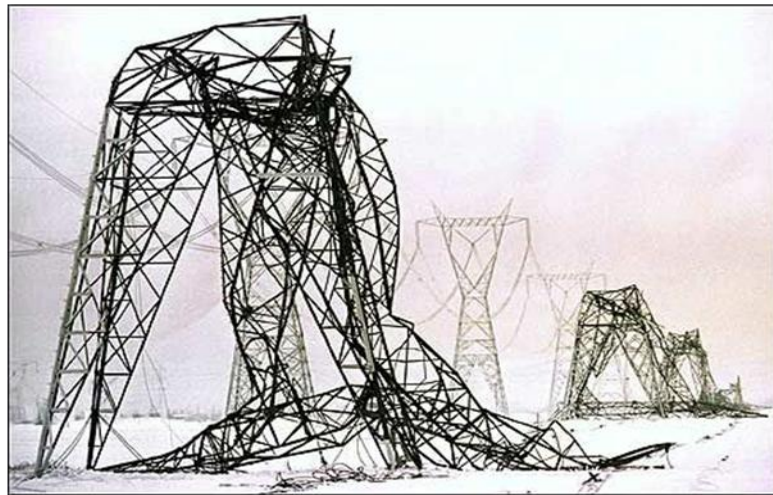


Figure 1.1: Collapsed transmission towers in Quebec after 1998 ice storm
(photo courtesy of http://www.galileo.org/tips/structures/collapsed_tower.jpg)

¹ Figure 1.2 © 1998 American Meteorological Society

² Figure 1.3 © 1998 Le Nouvelliste

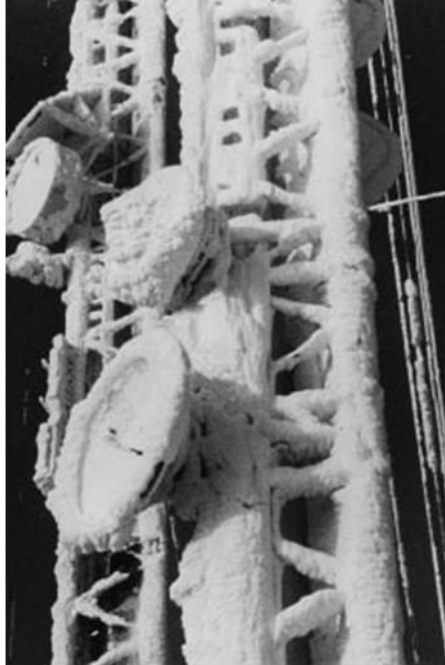


Figure 1.2: Severe icing on lattice tower in Sweden (Sundin & Makkonen, 1998)



Figure 1.3: Hydro-Quebec pylon collapsed under the weight of the ice, near Drummondville, Quebec, January 1998 (Abley, 1998)

Lattice structures are mainly used as a support for overhead power lines, wind turbines and communication towers and can be classified into two categories: lattice self-supporting towers, which can be classified into communication (Figure 1.5a) and transmission (Figure 1.5b) towers and lattice guyed masts (Figure 1.4). Lattice self-supporting communication towers are free standing towers square or triangular in cross section with a height up to 150m. Normally lattice tower vary in face width from bottom to the top and different bracing patterns are used depending on the type of load. Self-supporting towers possess good torsional rigidity and the elimination of stays saves area on the site. As a result they are more popular in populated areas, while communication towers are often guyed in rural areas (Smith, 2007). Lattice guyed masts are typically triangular or square in cross section, normally with constant face width from bottom to top. They are supported at various levels by guy wires anchored in the ground.



Figure 1.4: Lattice guyed masts

(Photo courtesy of Oleksiy Korotkov)



(a)



(b)

Figure 1.5: Self-supporting communication tower (a) and transmission towers (b)

(Photo courtesy of Oleksiy Korotkov)

Lattice guyed masts which can be as high as 600 m are lighter than similar height self-supporting towers, however they require larger site area. Guyed masts are more vulnerable to ice loading (Magued et al., 1989; Mulherin, 1998) due to uneven distribution and shedding of ice on guy wires and heavy icing on tower and guys (Smith, 2007).

The Structures Group of the Scientific Commission, appointed by the Government of Quebec created after 1998 ice storm in eastern Ontario and southern Quebec, recommended a review of the basic climatic loads and load combinations at high risk locations, in order to determine whether ice and wind on ice loads are currently adequate for design (Goel, 2008). The Commission also made a number of other observations and recommendations:

Observations:

- a) It was found that in some cases conductors and ground wires triggered collapse and overhead ground wires accumulated more ice than conductors.
- b) Several anchored angle towers did not have extra longitudinal or transverse strength required to stop the cascade failure.
- c) Collapse in some cases occurred under vertical load which was close to maximum design loads.

Recommendations:

- a) Carry out the review of basic climatic loads and load combinations at high risk locations. Effect of wind during and after ice build-up on conductors has to be included into modified maximum ice loading case.

- b) Conductor's tensile strength should be incorporated into the design of the anchored angled towers so they should be able to withstand cascading.
- c) Mechanical sturdiness of the lines can be improved by adding metal anti-cascading towers to all important wood portal lines.

1.2 Objectives

The objectives of this research investigation were to:

- a) Review the current design standards and specifications for ice and wind on ice load for lattice structures;
- b) Evaluate results from field testing of the FRP tower under wind and ice loads;
- c) Study ice buildup and effect of the FRP and steel lattice tower sections orientation to the icing wind direction in a wind tunnel;
- d) Evaluate the effectiveness of using icephobic coating as a possible mitigation technique for FRP and steel latticed towers.

1.3 Scope

The thesis consists of five chapters. In **Chapter 1**, a general introduction to the project is given, followed by project objectives and scope. Review of current design standards and specifications of icing on structures and related literature on atmospheric icing and estimation of ice accretion is presented in **Chapter 2**. Field testing of a composite lattice tower subjected to wind and ice loads and an examination of the ice buildup on a tower section in the icing tunnel is covered in **Chapter 3**. The assessment and discussion of the results are presented in **Chapter 4**. The summary of the work carried out and conclusions are presented in **Chapter 5**.

2 LITERATURE REVIEW

2.1 Introduction

In this chapter, current design standards for latticed structures subjected to ice and wind load and/or combination of both are reviewed and discussed. These include the CAN/CSA S37-01 Standard (CSA, 2001); the EIA/TIA-222-G (ANSI/TIA, 2005); the Manitoba Hydro Specifications (Friesen & Kell, 2009); the CAN/CSA-C22.3 NO. 1-06 (CSA, 2006a); the CAN/CSA-C22.3 NO. 60826-06 (CSA, 2006b) and ISO 12494: Atmospheric Icing of Structures (ISO, 2001). In addition, related literature dealing with atmospheric icing, icing failures of guyed lattice structures, and estimation of ice accretion and mitigation techniques is also reviewed.

2.2 Design standards for ice loading

2.2.1 CAN/CSA S37 -01 Antennas, Towers, and Antenna-Supporting Structures

The Canadian Standard CSA-S37-01 (CSA, 2001) is applicable to structural design, fabrication, erection of new structural antennas, towers, antenna-supporting structures and their components, as well as modification of existing ones.

Ice load, as a design load, is defined in this Standard as the weight of glaze ice (with a density of 900 kg/m^3) on all exposed surfaces of structure, including guy wires and attachments (Figure 2.1). If the gap between adjacent surfaces is less or equal to double the radial ice thickness, the whole surface is considered uniform and covered with ice. The minimum design ice thicknesses are listed in Table 2.1 and shown for different

regions in Canada in Figure 2.2. However local topography and site specific meteorological data should be considered in determining the class of icing.

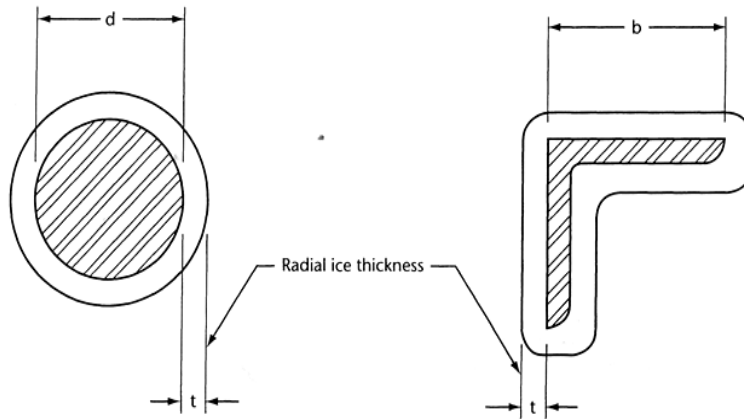


Figure 2.1: Face area of radial ice (CSA, 2001)

Table 2.1: Minimum design ice thickness (CSA, 2001)

Class*	Minimum design ice thickness, mm
I	10
II	25
III	40
IV	50

*Refer to Figure 2.2

The numbers shown in Figure 2.2 are based on ice accretion occurring from freezing rain falling through a layer of freezing air. Rime ice is not considered, as there are no instruments and methods to evaluate appropriate values. Ice thickness increases with height due to in-cloud icing or exposure of the site location to large bodies of water. However there is currently not sufficient data to evaluate this increase (Marshall et al., 2005).

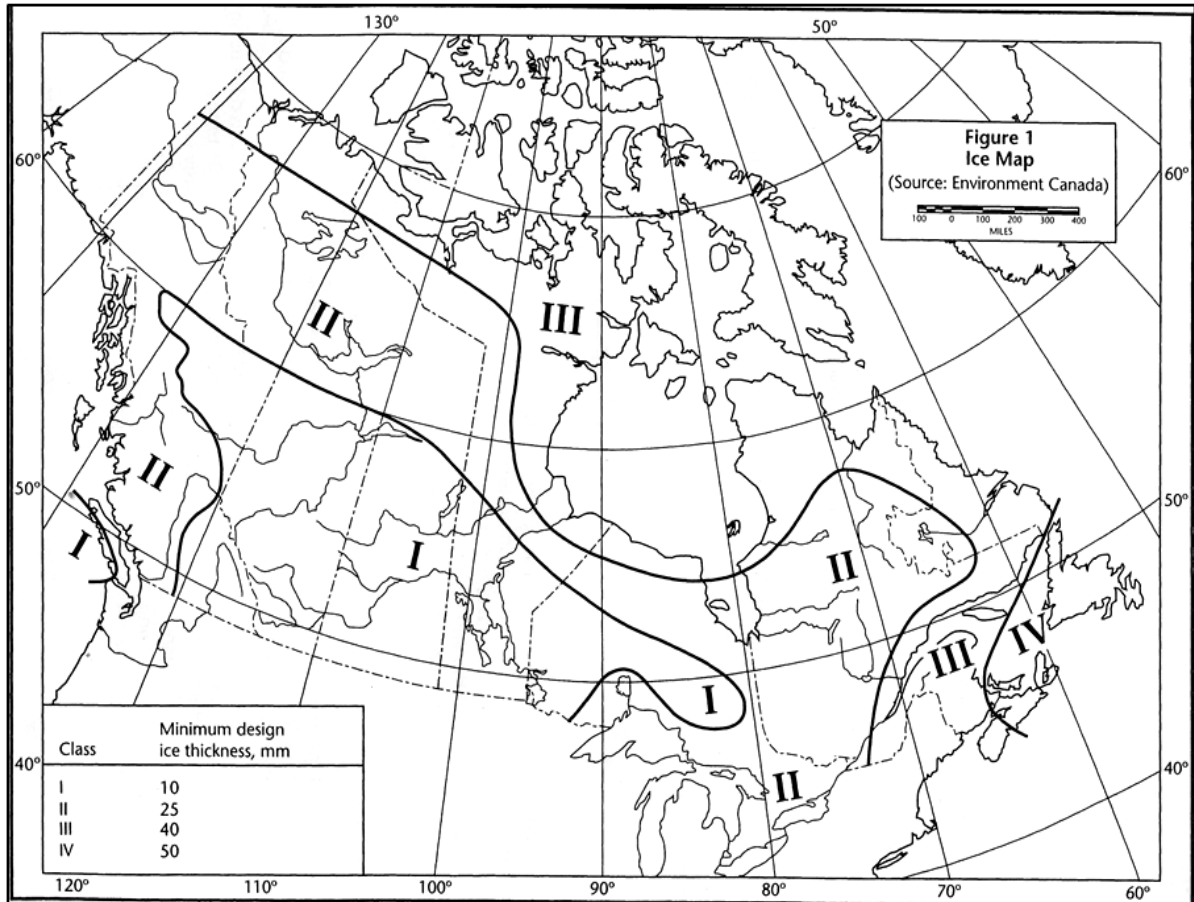


Figure 2.2: Ice Map of Canada (CSA, 2001)

The ice map shown in Figure 2.2 has been criticized by Wahba et al. (1993) for providing insufficient ice thicknesses in some parts of the country and excessive thicknesses in others, as compared to meteorological data which is based on 40-year return period (Wahba et al., 1993).

According to CSA-S37-01 (CSA, 2001) the wind load, W , for iced structures is given as the wind pressure, P , multiplied by the sum of the partial face areas times their appropriate drag factors $C_{d,i}$, as follows:

$$W = P (C_{df} \times A_f + C_{dr} \times A_r + C_{di} \times A_i) \quad (2.1)$$

where

W = wind load (N)

P = wind pressure (Pa)

C_{df} = drag factor for flat members

A_f = area for the bare flat members (m^2)

C_{dr} = drag factor for round members

A_r = face area of bare round members (m^2)

A_i = face area of radial ice (m^2)

Face areas are defined as the net areas of the members on one face of the structure, projected normal to that face. It can be calculated as follows,

$$A_f = b \times L \quad (2.2)$$

$$A_r = d \times L \quad (2.3)$$

$$A_i = 2t \times L \quad (2.4)$$

where

L = length of member

t = ice thickness (refer to Figure 2.1)

d = diameter of the round member (refer to Figure 2.1)

b = width of the flat member (refer to Figure 2.1)

The drag factor C_d for lattice towers is dependent on the solidity ratio, R_s , which is defined as

$$R_s = A_s/A_g \quad (2.5)$$

where

A_s = net area of one face of the structure, including ice thickness where appropriate (m^2)

A_g = gross area of one face of the structure, including ice thickness where appropriate (m^2)

Shielding of one member by another should be considered when the distance between two members is less than twice the projected width of the upwind member for bare case or twice the projected width plus radial thickness of the upwind member for iced member case. Limits for the wind shielding are shown in Figure 2.3.

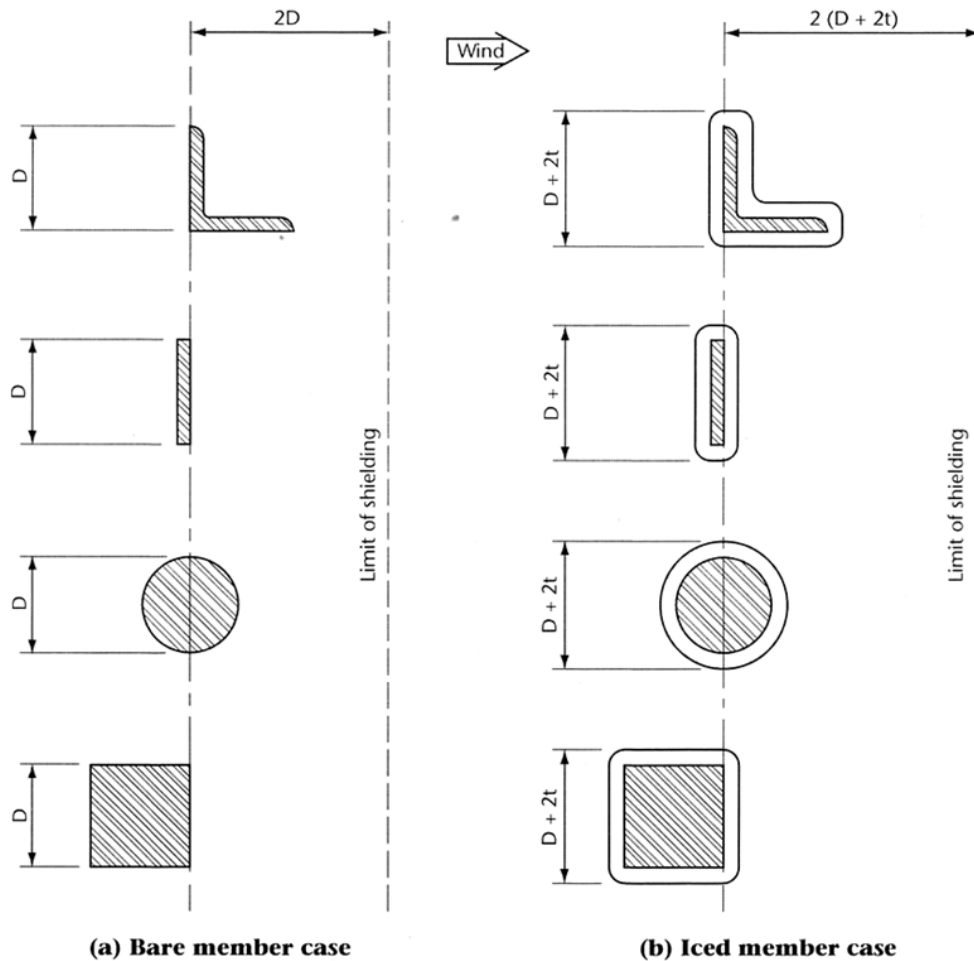


Figure 2.3: Limits for wind shielding (CSA, 2001)

When linear attachments shield, or is shielded by, the members forming face of the structure, they should be considered part of the net projected area A_s .

According to CSA-S37-01 (CSA, 2001) the load combination involving ice and wind load acting together should be less or equal resistance of the member and

can be considered as

$$R \geq D + W + I + T \quad (2.6)$$

where

D = dead load

W = wind load

I = ice load

T = temperature effects

Forces in members are computed using appropriate load factors α , load combination factor ψ and the importance factor γ and they should be less or equal to the factored resistance of the members, as follows:

$$\phi R \geq \alpha_D D + \gamma(\psi \alpha_W W + \alpha_I I + \alpha_T T) \quad (2.7)$$

Load combination factor ψ is specified as 0.5. It reflects low probability of extreme ice and wind load acting together. However in locations where extreme ice and wind can occur at the same time, an increased value of ψ equal up to 1 can be considered.

The ice load factor, α_I in Eq. 2.7 equal to 1.5 and is applicable to the weight of the ice only.

According to Wahba et al. (1993) contrary to wind loads, there is no return period for the ice load specified in CSA-S37-01. Currently, the radial ice thickness is the same for all members irrespective of member size. However, taking into consideration member size, as shown in Figure 2.4, the ice thickness can be reduced, especially for self supporting lattice towers, where large member sizes are common.

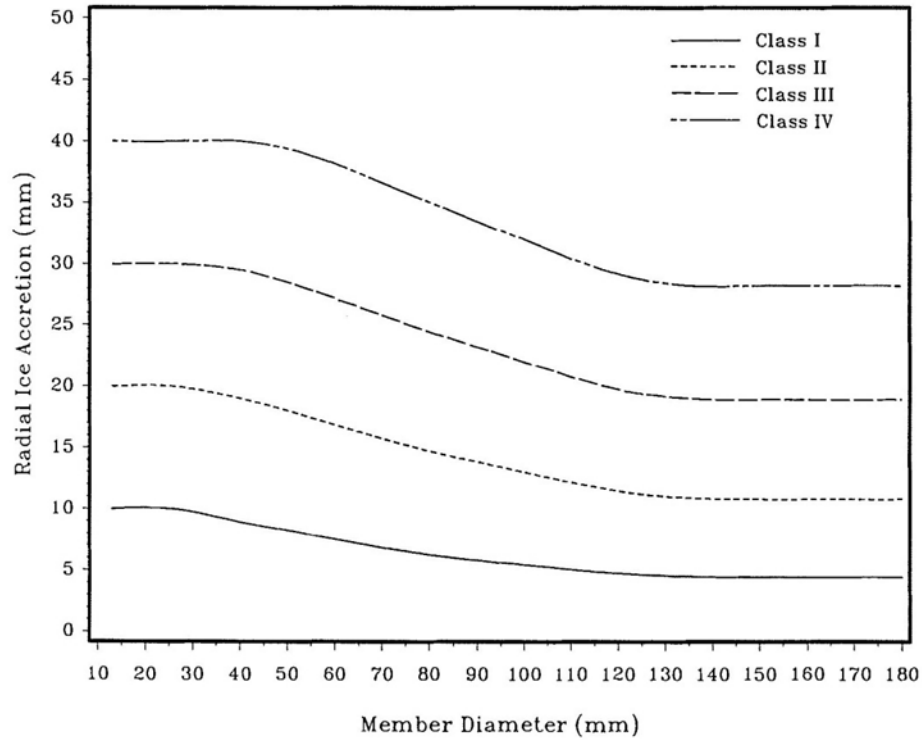


Figure 2.4: Relation between radial ice thickness and member size (Wahba et al., 1993)

Recommendations for the dynamic analysis due to wind loads included in CSA-S37-01, however, do not include the dynamic effect of wind on iced tower (Wahba et al., 1998).

The CSA-S37-01 Standard does not provide ice thickness increase with height. However, for taller towers and towers at higher elevation ice thickness should be increased (Marshall et al., 2005).

2.2.2 Structural Standard for Antenna Supporting Structures and Antennas.

ANSI/TIA 222-G-2005.

The Structural Standard for Antenna Supporting Structures and Antennas ANSI/TIA 222-G-2005 (ANSI/TIA, 2005) is a limit states design Standard, which

provides design and fabrication requirements for new and existing antennas and supporting structures.

One of the load combinations involving ice and wind load that should be considered for structure and foundation design to ensure design strength equals or exceeds factored loads is:

$$\phi R_n \geq 1.2D + 1.0D_g + 1.0D_i + 1.0W_i + 1.0T_i \quad (2.8)$$

where:

D = dead load of structure, excluding guy assemblies

D_g = dead load of guy assemblies

D_i = weight of ice with factored ice thickness

W_i = wind load with ice

T_i = temperature load effects

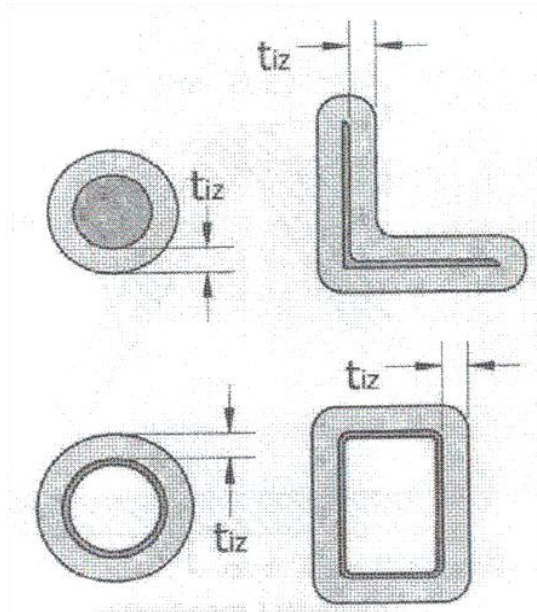


Figure 2.5: Projected area of ice (ANSI/TIA, 2005)

The design ice thickness, t_i , defined as radial thickness of glaze ice at 10m above terrain for a 50-year return period. It is evenly distributed around exposed structural member's surfaces, as shown in Figure 2.5.

The basic wind speeds with ice and design ice thickness are shown in Appendix A. The design ice thickness increases with height and can be calculated from the following equation:

$$t_{iz} = 2.0 t_i I K_{iz} (K_{zt})^{0.35} \quad (2.9)$$

where

$$K_{iz} = \left[\frac{z}{10}\right]^{0.10} \leq 1.4 z \quad (2.10)$$

t_{iz} = the factored thickness of radial ice

t_i = design thickness of ice (mm)

I = importance factor for the structure from the ANSI/TIA Standard (ANSI/TIA, 2005)

K_{iz} = ice escalation factor

K_{zt} = topographic factor from the ANSI/TIA Standard (ANSI/TIA, 2005)

z = height above the ground (m)

2.0 = limit state conversion factor

The weight of ice is calculated by multiplying the cross-sectional area of accreted ice by the density of the ice. The weight of ice should be based on a density of glaze ice of 8.8 kN/m^3 . The cross-sectional area of the ice at height z can be calculated from the following:

$$A_{iz} = \pi t_{iz} (D_c + t_{iz}) \quad (2.11)$$

where

D_c = largest out-to-out dimension of a member, as shown in Figure 2.6.

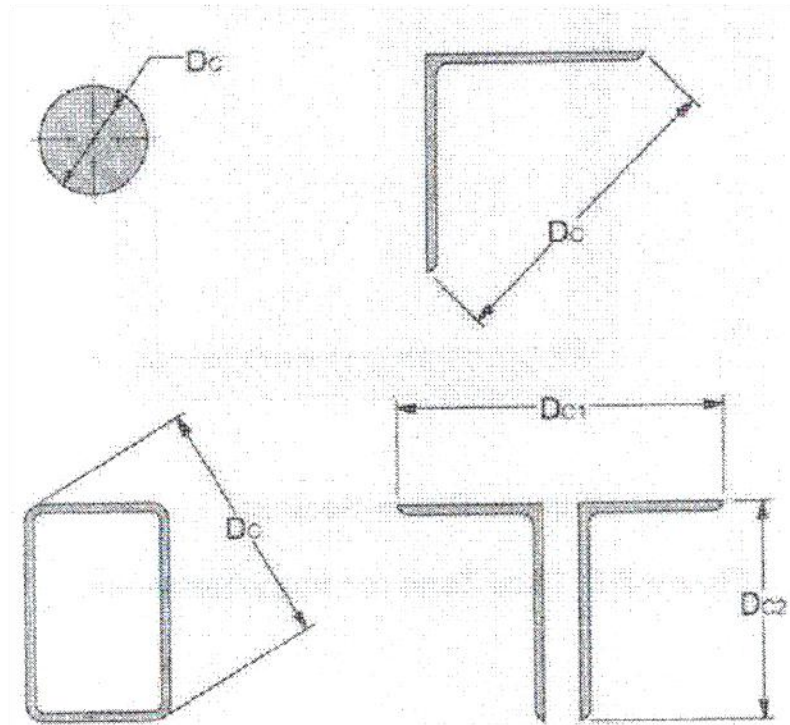


Figure 2.6: Outside dimensions for calculating ice weight (ANSI/TIA, 2005)

The wind load on ice covered lattice structures is dependent on the increased projected area due to ice accretion. The projected area should be increased by adding t_{iz} to all exposed edges of the projected area. Wind load should be calculated without ice, but should be modified based on effective projected area which includes ice. The solidity ratio, ε , should be based on the projected area including ice and can be calculated as:

$$\varepsilon = (A_f + A_r) / A_g \quad (2.12)$$

where

A_f = projected area of flat structural members of one face of the section

A_r = projected area of round structural members including the projected area of ice on flat and round members in one face of the section

A_g = gross area of one face of the structure

The design wind load and ice thickness applied to a section of the latticed structure can be based on the wind load and ice thickness values at mid-span of the section. The loads can be considered uniform if the section length does not exceed 18 m.

Shielding of elements should be considered when the distance between elements in the direction under examination is less than or equal two times smallest dimension of the element in the considered direction. Shielding is not considered when the distance between elements in the direction under examination is more than four times smallest dimension of the element in the considered direction.

2.2.3 Manitoba Hydro Specifications

Manitoba Hydro follows the CAN/CSA S37 -01 (CSA, 2001) and CAN/CSA-C22.3 NO. 1-06 Standard (CSA, 2006a). Typically, in design of lattice structures the following icing conditions are considered: 1 in (25 mm) ice accretion without wind and ½ in (13 mm) ice accretion with 56 mph (90 km/h) wind (Friesen & Kell, 2009). Design loads with 1 in (25 mm) ice thickness are based on criteria outlined in the CSA-C22.3 and were modified based on previous experiences, where large ice loads have been reported, as shown in the Table 2.2.

Table 2.2: Examples of damaging ice storms in Manitoba (CEATI, 2006)

#	Start date	End date	Location	Description
1	10/7/1959	10/15/1959	North-west North Dakota into south-east Manitoba	Ice more than 2 in (50 mm) thick and 30 mph wind brought down wires and caused extensive damage to rural system
2	4/2/1963	4/4/1963	southern Manitoba	Freezing rain followed by high winds caused accretion up to 2 in (50 mm) of ice
3	2/26/1983	3/12/1983	South-east Saskatchewan, southern Manitoba, most of North Dakota	Reported as one of the worst storms in Manitoba history. Freezing rain and wind caused collapse a number of communication towers. Accretion of 2 to 3 in (50-75 mm) of ice in Somerset was reported and utilities were rolling the ice off wires.
4	4/27/1984	4/29/1984	North Dakota into south Manitoba	This storm is worse than the one in 1983. Manitoba Hydro's 3500 poles were down and 12 steel towers were crumpled.

2.2.4 CAN/CSA-C22.3 NO. 1-06. Overhead Systems

The Canadian Standard CAN/CSA-C22.3 NO. 1-06 (CSA, 2006a) provides requirements for the construction of overhead systems. It is applicable to electric supply and communication lines and equipment located entirely outside of buildings and fenced supply stations. This Standard does not provide complete design or construction specifications of the components (such as supports, foundations, etc.); however, it provides minimum design requirements. It gives a choice between deterministic, i.e., design in which strength, load and load factors are specified and might not be related to the statistical data, or reliability-based design methods. The reliability-based design method is covered in CAN/CSA-C22.3 NO. 60826-06 (CSA, 2006b). Non-linear analysis, including stability (buckling) check, is the recommended method of analysis of the structures.

This Standard specifies weather loads to be applied in the design of supports (towers) and wire and cable attachments. Four deterministic load conditions are included: severe, heavy, medium loading A, medium loading B.

The radial ice thicknesses, the horizontal wind loading and temperature for each of the load conditions are listed in Table 2.3.

Table 2.3: Deterministic weather loads (CSA, 2006a)

Loading conditions	Severe	Heavy	Medium A	Medium B
Radial thickness of ice, mm	19	12.5	6.5	12.5
Horizontal wind loading, N/m ²	400	400	400	300
Temperature	-20°C	-20°C	-20°C	-20°C

Loading maps for Canada and Manitoba are given in Appendix A. Depicted loads in those maps are considered minimum and local areas can have higher icing and/or wind load. These maps are based on the Environment Canada data and information provided by the utilities across Canada (CSA, 2006a).

2.2.4.1 Design loads for wire and cable attachments

- a) The design vertical load, in N/m, of ice-covered wire and cable attachments are based on the radial ice thickness from Table 2.3 and ice density of 900 kg/m^3 ;
- b) The design transverse load, in N/m, is based on the wind loading (in N/m^2) as listed in Table 2.3, acting horizontally on ice-covered wire and cable attachments.

It is noted that maximum wind speeds are not generally associated with maximum icing.

2.2.4.2 Loads on supports

According to the CSA Standard C22.3 the following loads should be used in design of supports, including towers. Loads have to be combined vectorially. The service loads are multiplied by appropriate load factors in accordance with the Limit States Design approach.

- a) The vertical load on the structure consists of the vertical force created by its own mass plus the weight of all attachments. The radial thickness of ice is applied only to wire and cable attachments; i.e. the weight of ice on the lattice structure is not considered.
- b) The transverse load on the structure is created by the wire load plus the load from wind pressure (as specified in Table 2.3) on the surfaces of the structure without

an ice covering. For flat surfaced lattice structures, the exposed area of the lateral face should be increased by 50 % first to allow pressure on the leeward side and 100 % increase of the wind pressure from Table 2.3 should be applied after.

- c) Load on supports at various angles should be considered when change in direction of wire or cable attachment occurs. The wind pressure in this case should be taken in such a direction as to produce a maximum stress on the structure.

The CSA Standard C22.3 requires that support structures, such as transmission towers, should be able to withstand the design loads as well as any unbalanced loads due to uneven spans or uplift under wire load. Only negligible deformation of component parts is permitted in the design of metal towers and metal supports subjected to assumed loads. The damage and failure limits of support structures are listed in Table 2.4.

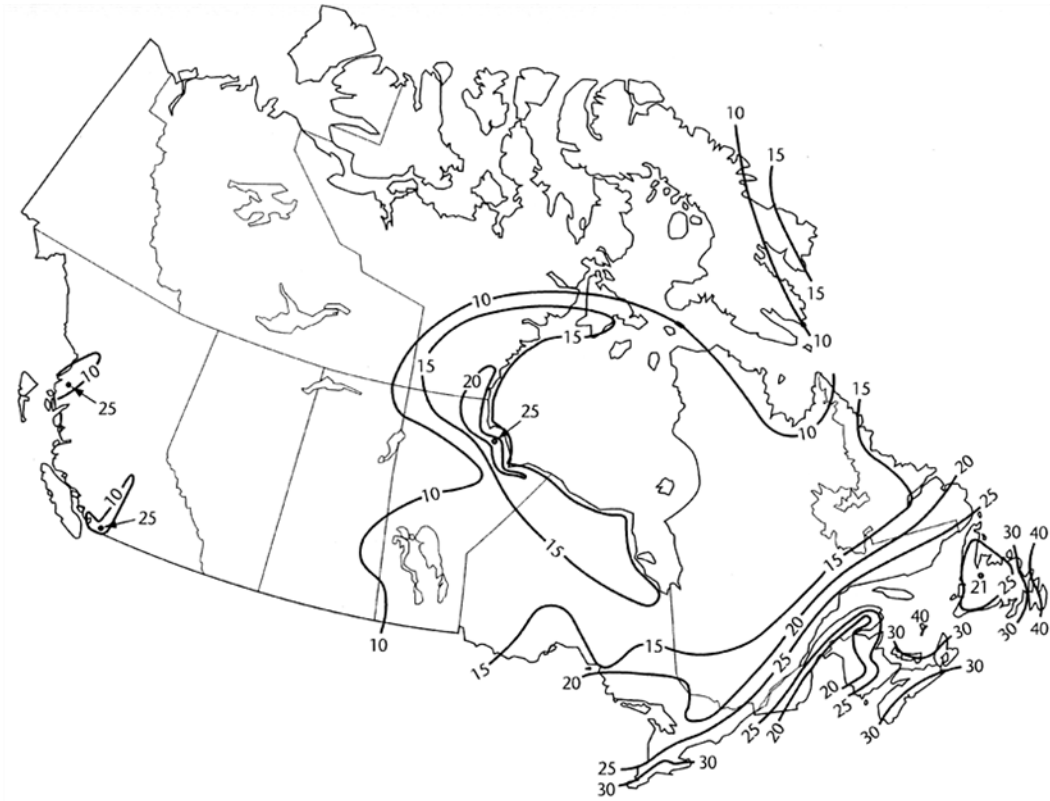
Table 2.4: Damage and failure limits of structures (CSA, 2006a)

Supports				
Support type	Material or elements	Loading-mode	Damage limit	Failure limit
Lattice tower (including guyed towers)	All elements except guys	Tension	Yield (elastic) stress	Ultimate tensile (breaking) stress
		Shear	90% (elastic) shear stress	Shear (breaking) stress
		Compression (buckling)	Non-elastic deformation* from L/500 to L/100	Collapse by instability
Steel guys		Tension	Lowest value of – yield stress (70% to 75% UTS) – deformation corresponding to a 5% reduction in the tower strength	Ultimate tensile stress

2.2.5 CAN/CSA-C22.3 NO. 60826-06. Design Criteria for Overhead Transmission Lines

CAN/CSA-C22.3 NO. 60826-06 (CSA, 2006b) is the Canadian adoption of the International Electrotechnical Commission Standard 60826. It specifies the loading and strength requirements of overhead transmission lines based on the reliability design method. This method particularly useful in areas where significant amounts of meteorological and strength data are available. Reliability requirements ensure that the lines can withstand defined climatic limit loads (wind, ice and wind with ice with a return period T) and the loads derived from these actions. Transmission lines can be designed for different reliability levels. For the purposes of this standard, reference reliability level is defined as the reliability of the line designed for a 50-year return period climatic event. Lines can be designed for a higher level of reference reliability by increasing the return period T for climatic events.

As there is no national ice accretion surveillance network, values of ice accretion were obtained by Environment Canada using the Chaîné model (Chaine & Skeates, 1974), which provides estimates of ice accumulation due to freezing rain at locations where standard hourly meteorological data is available. Values for a 50-year return period radial ice thickness of glaze ice due to freezing precipitation are shown in Figure 2.7. These values represent point loads; i.e., ice thickness measured at reference stations during specified ice storms, and there might be another point where more significant icing could occur.



Note: Values are point values of radial ice thickness resulting from precipitation icing. For more northern areas, contact Environment Canada.

Figure 2.7: Reference icing amounts (mm)-50-year return period (CSA, 2006b)

In the absence of local data, it is recommended to increase the values shown in Figure 2.7 by 50 % (spatial factor $S_a = 1.5$). Spatial factor also takes into consideration a height of up to 30 m, while the values in Figure 2.7 were modeled at height of 10 m above ground. It is noted that the weight of ice on lattice structures can be significant and can reach or exceed the weight of the structure itself.

The weight of the ice can be calculated using the geometry of the support members and the relevant thickness of ice accumulation. Alternatively, it can be estimated from Table 2.5.

Table 2.5: Ratios of weight of ice to structure weight (CSA, 2006b)

Ice thickness (mm)	15	25	30	35	40	45	50
Ratio of weight of ice to structure weight	0.57	1.00	1.23	1.48	1.73	2.00	2.28

2.2.6 ISO 12494: Atmospheric Icing of Structures.

ISO 12494: Atmospheric Icing of Structures (ISO, 2001) is international standard by the International Organization for Standardization. It provides general guidelines in determining ice and wind load on the iced structure. It is applicable to masts, towers, guy wires and other structures subjected to icing. The main purposes of the Standard are to specify dimensions, weight, shapes and drag coefficients of accreted ice.

These can be achieved by:

- a) collection of existing experience on icing;
- b) icing modeling based on meteorological data;
- c) direct extensive icing measurements.

The Standard introduces the “Ice Class”, which is defined as an expected amount of accreted ice at certain site. Ice Class is characterized by the 50-year return period of ice accretion on reference 30 mm diameter cylinder 0.5 m long placed at the height of 10 m above ground and slowly rotating about its axis.

Ice class for glaze (ICG) is defined as ice thickness on the reference ice collector. Ice thicknesses and corresponding masses are given in Table 3 of the ISO Standard (ISO, 2001).

Accretion models for glaze icing are shown in Figure 3 of the Standard (ISO, 2001). For sloping elements ice thickness is measured perpendicular to the axis of element and is uniform in all directions around the object.

Ice class for rime (ICR) is the ice mass on a reference ice collector. The interdependence between ice masses and ice dimensions, which are based on ice density, object shapes and dimensions are shown in Table 4 of the Standard (ISO, 2001). Rime ice is assumed to be vane shaped with length pointing windward. An example of ice vane dimensions for flat surfaces is shown in Figure 4 of the ISO Standard, where W is the width of the object (mm), t is ice thickness (mm), D is the total width of the object including ice (mm) and L is the length of the ice vane measured in the wind direction (mm).

The standard uses different icing models for the rime ice vane accretion for slender structural members with object width (W) less than 300 mm and single members with widths exceeding 300 mm.

Rime ice accretion on a lattice structures can either be estimated as the summation of ice amount on single members per meter unit length or as a “complete iced structure”, as icing can cover the whole width and become a solid structure. Icing on single members can be reduced due to overlapped structural members at intersection points (i.e. length of iced member is shorter than structural length of the member).

For the iced members inclined to the wind direction all dimensions are measured in horizontal plane, as shown in Figure 6 of the ISO Standard (ISO, 2001) therefore the ice mass along the axis of the member is $m \sin\alpha$, where m can be found from the Standard.

Wind action on the iced lattice structure should be calculated without considering ice. However the structural dimensions should be increased with the ice thickness and drag coefficients should be adjusted to accommodate these changes. Wind loading on lattice structures is dependent on the solidity ratio, τ . The modified solidity ratio, τ' , should be used to calculate the wind action on iced sections.

Rules for ice-free lattice structures should be applied in situations where low ice classes (both glaze and rime) exist, using just the drag coefficients and ice dimensions for iced members from this Standard. However for higher Ice Classes (especially rime) ice accretion could fuse into a solid structure resulting in an increased exposed wind area. The leeward part of lattice structure may have one lower Ice Class than the one specified for the windward side.

Combination of two ice and wind load cases should be considered. In combination one low probability of wind load combined with high probability of ice load and for second case high occurrence of wind action and low ice load, as shown in Table 26 of the Standard (ISO, 2001).

Factors φ_{ice} and φ_w are used to change loads from 50- to 3-years probability. Factor φ_{ice} reduces 50-year return period to 3-year and a value close to 0.3 is recommended. Factor φ_w should be taken from national standards for the possible decrease of wind load. Factor k depends on icing class and reduces wind pressure because of reduced probability of simultaneous occurrence of high wind and heavy snow.

Guyed masts need additional investigation on asymmetric ice accumulation on guys and tower itself.

2.3 Icing failures of guyed lattice structures

Latticed structures, particularly guyed lattice towers, are especially sensitive to environmental loads, such as ice and wind. Additional dead load due to ice accumulation can be significant. It can lead to higher wind load as well as uneven distribution of ice on guys when the ice sheds that can lead to bending effect on the structure. Ice accretion can cause complete tower failure (Magued et al., 1989; Mulherin, 1998). A number of failures of guyed masts during the last 40 years are listed in Table 2.6. Although a specific cause could not always be identified clearly, the trend is obvious: the majority of failures of masts comes from ice load or combination of ice and wind (Smith, 2007).

Table 2.6: Failures of guyed masts by cause and height (Smith, 2007)

Cause	Height, m											Total
	0-50	51-100	101-150	151-200	201-250	251-300	301-400	401-500	501-600	601+	Unknown	
Ice	14	34	19	21	6	8	11	7	1	1	19	141
Ice and wind	7	7		2	1	1	2	1		2	5	28
Wind	3	3	1	2	1			2	3		1	16
Oscillations	1	5	1	3	1	4	6				1	22
Guy failure		3	1	1		5		1				22
Outside damage		1										1
Lightning/insulators		2	2		1	4	1	1				11
Erection/maintenance	6	6	2	3	3	4	4	3	2	6		39
Design/materials	1	5	2	4	5	4	1				1	23
Plane impact		1			2	1	1	1				6
Vandals	1	1										2
Subsidence		1										1
Unknown		3	8	1	4			1			1	18
Total	33	72	36	37	24	31	26	17	6	9	28	319

Mulherin (1986) reported icing failure of three TV towers in Maine and one on Mt. Greylock, Massachusetts since 1983.

An early study by Magued et al. (1989) showed that the failure rate of guyed towers in Canada prior to the introduction of the CSA-S37-M86 Standard (CSA, 1986) was unacceptably high. Figure 2.8 shows reported failures of guyed towers due to wind load, ice load or combination of both, which exceeded values believed to be maximum during the design process. According to Magued et al. (1989) the approximate rate of failure of broadcasting guyed towers was 0.055% /year. Major factors leading to such high percentage included uncertainty in prediction of ice accumulation and the exclusion of ice accumulation on guy wires in earlier editions of S37 Standard. Magued et al. suggest that there is a need of creation of Canadian registry of tower performance in order to keep up to date information concerning tower failures and estimation of ice accumulation still carries large degree of uncertainty (Magued et al., 1989).

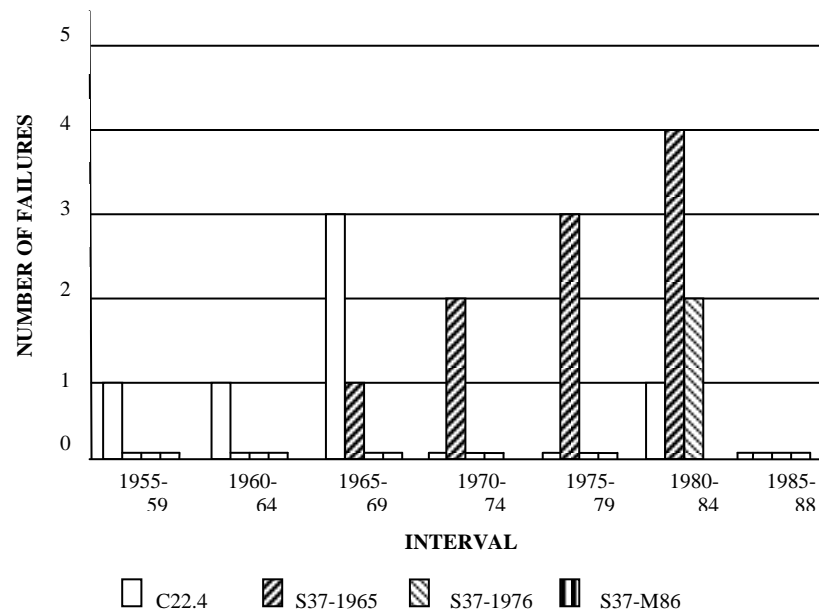


Figure 2.8: Failures of guyed towers in Canada taller than 75m between 1955 and 1988 designed according to various standards (Magued et al., 1989)

Sundin and Mulherin (1993) investigated icing related failures of 13 towers over 305m (1000 ft.) in the US and three towers in Finland and Sweden between 1973 and

1991. Both precipitation icing and in-cloud icing were identified as causes of collapse. However, precipitation icing in the form of freezing rain dominated the failures in flat terrain with high winds in the mid-west of the US. Frequent temperature fluctuations are common in those regions. The events that contributed to tower collapse were preceded by warm frontal-type weather conditions which led to collapse by loading the tower with large amount of ice. Nine of the 16 events induced moderate to heavy precipitation icing and eleven of the 16 were accompanied by moderate to heavy in-cloud icing. These conditions led to eleven of 16 cases where resulting tower accumulation were heavy to severe. Ice load alone may or may not be the cause of failure in all of these towers. Incomplete poor construction, loose bolts, brittle or fatigue failure steel, cable oscillations, ice shedding, increase/changing wind could also been contributing factors. High wind was a less predictor of failures. Only five of the 16 cases experienced high and severe winds and four out of these five cases were accompanied by heavy and severe ice loading (Sundin & Mulherin, 1993).

In the US, failures of 140 towers, ranging from 12 to 610 m in height, due to ice accretion were compiled into a database according to structural characteristics, geographic location, description of collapse, concurrent weather, and resulting damage. Mulherin (1998) showed that the largest number of failures involved guyed towers and only one tower was a free standing structure. The majority of failures occurred between December 1 and March 3 and two thirds of these occurred north of the N 37° latitude.

As shown in Figure 2.9, 56 % of the failures are related to combined wind and ice while 37 % were due to ice alone. Only 7 % of failures were attributed to wind (no ice). Mulherin (1998) reported that more extensive meteorological data is required to obtain a

better understanding of the failure rates and recommended to check the adequacy of ice and wind on ice design load at locations that pose a high risk to towers (Mulherin, 1998).

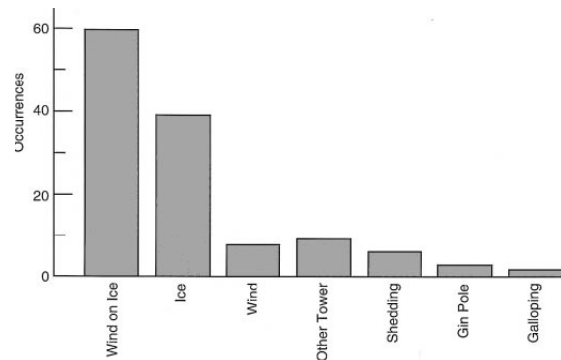


Figure 2.9: Failure factors leading to collapse (Mulherin, 1998)

El-Fashny et al. (1999) investigated the probability of structural failure for a self-supported telecommunication tower in Quebec. Uncertainty on the reliability of the structure was dominated by the uncertainty on the environmental load model, especially the type of distribution of wind and ice. The authors emphasized the need for more precise models for the distribution of extreme wind in the occurrence with ice accretion. They concluded that estimation of reliability of existing and future communication towers can be improved with better understanding of icing phenomena. There is a need for analysis of the frequency of icing events as a mean of location and a classification of their spatial area and severity (El-Fashny et al., 1999).

2.4 Atmospheric ice on towers

Ice accretion is the general definition for the process where the water freezes in the atmosphere and adheres to exposed objects. There are three major forms of icing leading to significant accretion on structures: glaze icing, rime icing and freezing wet snow (Smith, 2007). Characteristics of different types of ice are shown in Table 2.7.

Table 2.7: Physical properties of ice (CSA, 2006b)

Type of ice	Density kg/m ³	Adhesion	Appearance		Cohesion
			Color	Shape	
Glaze	700-900	Strong	Transparent	Cylindrical icicles	Strong
Hard rime	700-900	Strong	Opaque to transparent	Eccentric pennants into wind	Very strong
Soft rime	200-600	Medium	White	Eccentric pennants into wind	Low to medium
Wet snow	400-700	Medium	White	Cylindrical	Medium to strong

Glaze ice occurs when rain or drizzle fall through a layer of cold air. The precipitation freezes on contact with the ground or any object on their path. The resulting accumulation is normally clear, solid ice, often with icicles (see Figure 2.10a). This accretion is hard, strong and difficult to remove. The density is 800-900 kg/m³ and the thickness can be expected to be more than 50 mm on exposed structures located on the windward side of coastal slopes.

Rime icing occurs when supercooled water droplets in a cloud or fog freeze upon contact with objects. It is normally observed on structures located on mountain tops exceeding 1000 m in elevation and close to large sources of open water. Soft rime is usually opaque white in appearance (Figure 2.10b) with a density below 600 kg/m³. Hard rime ice is normally milky and opaque in appearance (Figure 2.10c), with a density in the range of 700-900 kg/m³.

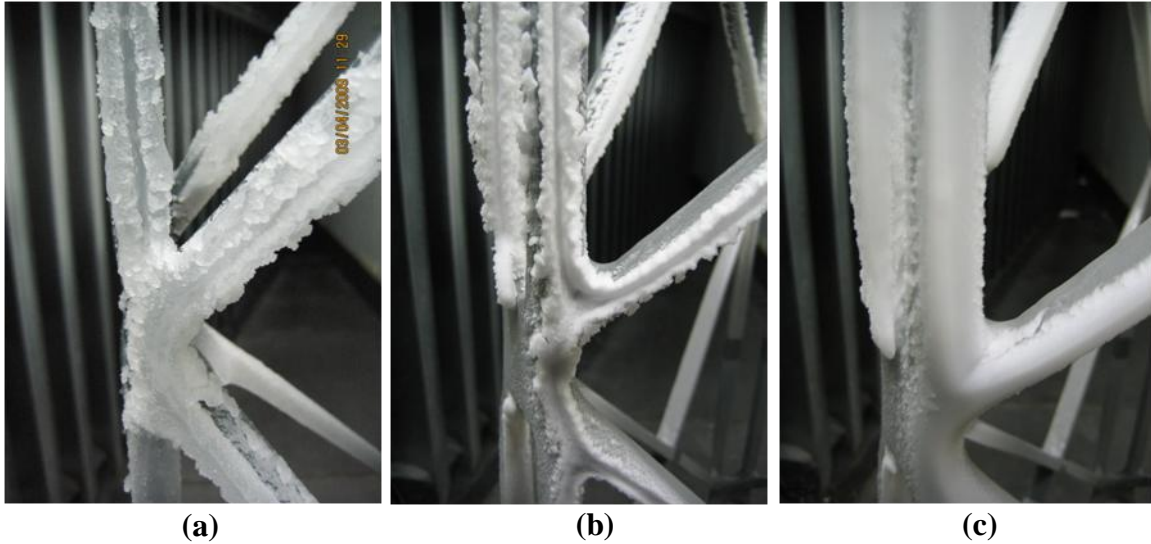


Figure 2.10: Glaze (a), soft rime (b) and hard rime(c) ice accretion on lattice tower

Freezing snow occurs when snow passes through a layer of air having temperature above 0°C and adheres to surface of the structure. When the air temperature drops below 0°C snow adhered to an object freezes. The thickness can be significant (up to few centimetres) and can occur anywhere across Canada. The density ranges from 400 to 700 kg/m³.

The type of ice is a function of a number of factors, such as,:

- Liquid water content of the air
- Droplet size
- Wind speed
- Temperature
- Dimensions of iced object

For the same conditions the ice accretion will be higher for smaller objects than for larger ones (CSA, 2006b). Typical parameters that control ice accretion are shown in Table 2.8.

Table 2.8: Meteorological parameters controlling ice accretion (CSA, 2006b)

Type of ice	Air temperature °C	Mean wind speed V m/s	Droplet size	Liquid water content	Typical storm duration
Glaze ice	$-10 < T < 0$	Any	Large	Medium	Hours
Wet snow	$0 < T < 3$	Any	Flakes	Very high	Hours
Hard rime	$-10 < T < 1$	$V > 10$	Medium	Medium to high	Days
Soft rime	$-20 < T < 1$	$V < 10$	Small	Low	Days

The transition between glaze, hard rime and soft rime icing is mainly a function of wind speed and air temperature, as shown in Figure 2.11. However curves shift to the right with increasing water content and decreasing object size.

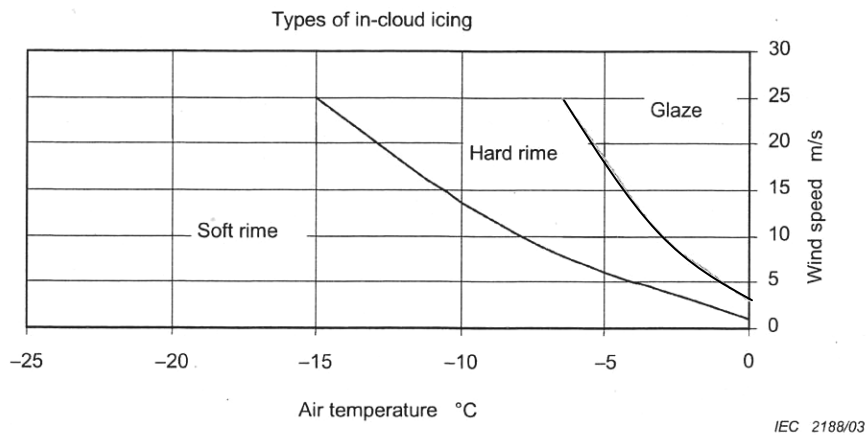


Figure 2.11: Type of accreted in-cloud icing as a function of wind speed and temperature (CSA, 2006b)

2.5 Estimation of ice accretion on structures.

Ice accretion on structures is a significant problem for engineers and utilities across Canada. Transmission lines and communication towers often are built through large and sparsely populated areas where meteorological data are limited.

In contrast to meteorological parameters such as temperature, precipitation, wind speed and snow depth there are limited data available on ice accretion. The variety of local topography, climate and icing conditions complicate standardization of actions by ice accretion (ISO, 2001).

There have been number of studies undertaken in Canada to collect ice accretion data. However, consistent and long term statistics are difficult and expensive to obtain and are not usually obtained through a meteorological observation network (Wahba et al.,1993;Yip, 1995)

Wahba et al. (1993) compared values of the maximum radial ice accretion (1 in 40 years probability) based on climatic data gathered from weather stations across Canada with data specified in the ice map provided in the CSA S37-M86 Standard (CSA, 1986).³ It should be noted that there are some differences between the two data sets. That radial ice accretion is overestimated in some parts of Canada while it is underestimated in others compared to those in the current standard, as shown in Table 2.9.

³ The ice map in the current CAN/CSA S37-01 Standard (CSA, 2001) is identical to that in CSA S37-M86 (CSA, 1986) shown in **Figure 2.2**.

Table 2.9: Underestimated radial ice accretion (Wahba et al., 1993)

Site	Radial ice accretion, mm			
	CSA S37-M86 (CSA, 1986)	1/40 years return (Chaine & Skeates, 1974)	CHBDC (CSA, 2006c)	Proposed map (Wahba et al., 1993)
Dauphin, MB	10	33	31	30
Gimli, MB	10	18	31	20
Winnipeg, MB	10	15	31	20
Kenora, ON	10	15	31	20
Thunder Bay, ON	10	26	31	30

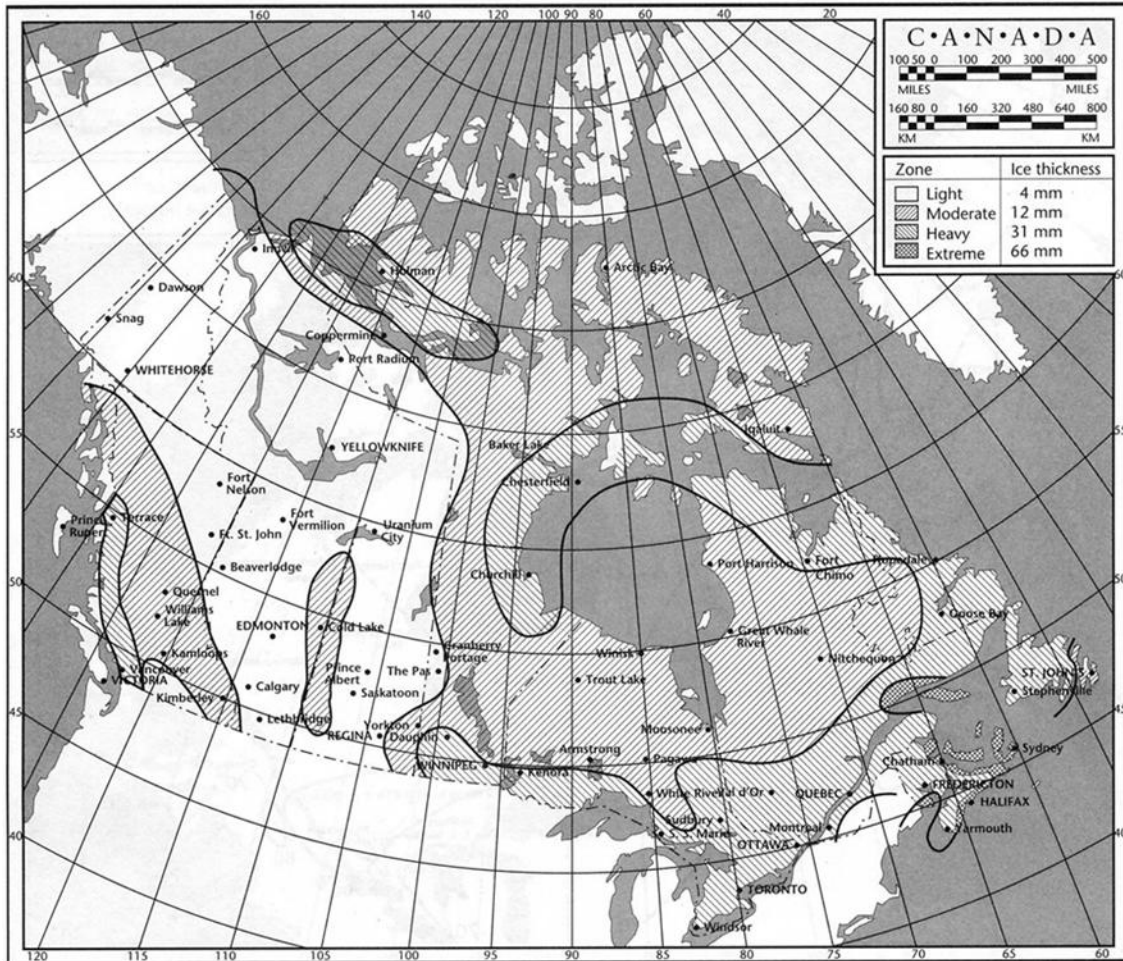


Figure 2.12: Ice map of Canada (CSA, 2006c)

Wahba et al. (1993) proposed a new map which is based on a uniform return period of 40 years. The proposed map is in agreement with the one provided by the Canadian Highway Bridge Design Code (CHBDC) (CSA, 2006c), which is also based on a model developed by Chaine and Skeates (Chaine & Skeates, 1974). The CHBDC ice accretion map is shown in Figure 2.12. The proposed map does not include in-cloud icing or wet snow and considers freezing precipitation only. Wahba et al. (1993) also suggest considering the diameter of the members when calculating ice thickness as the accumulated amount depends on size of the member. The change in ice thickness versus member diameter is plotted in Figure 2.4.

Yip (1995) used Chaine and Skeates's ice model (Chaine & Skeates, 1974) to simulate equivalent radial ice thickness on cylindrical rods. The Chaine and Skeates model tends to overestimate low icing episodes and underestimate high icing episodes. It is very sensitive to wind speed and precipitation rates. However, it is simple to use and economical to run. Results show that the simulated 30-year return period equivalent radial ice amounts based on data from 20 Quebec stations are compared reasonably well with corresponding Passive Ice Meter (PIM) observations from Quebec Hydro. Data from 303 stations across Canada were used to plot an ice map shown in Figure 2.13 which shows the equivalent radial ice thickness for freezing precipitation at the height of 10 m. using a 30-year return period. Yip (1995) points out that map needs to be validated by field ice observations and more work has to be done to include wet snow and in-cloud rime ice.

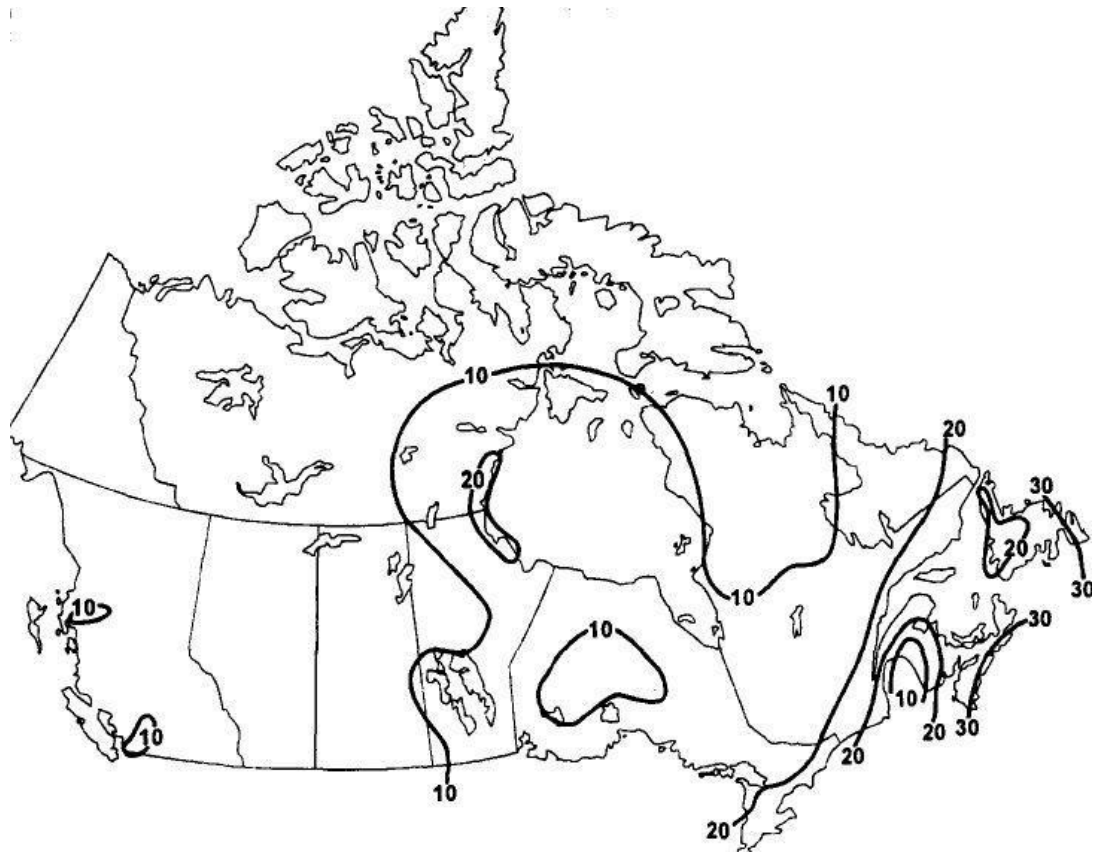


Figure 2.13: Ice accretion amounts caused by freezing precipitation (Yip, 1995)

A small scale experiment on rime icing modelling by Makkonen and Oleskiw (1997) showed that correct simulation is possible in theory, however difficult to attain in practice. The in service tower that was the basis of their simulation was located in Yllas, Finland, for which field ice data is available. For their experiment a 1:15.3 scaled replica of the tower's vertical lattice mast section was produced and tested in an icing wind tunnel. The general appearance and density of the simulated ice accretion was very similar to the ice characteristics observed in the field. The initial ice accretion was observed on the windward side with minimum thickness at stagnation line. Ice accumulated on leeward side and eventually filled the space within the lattice tower. The ice mass on the model at the end of the test was between 1 and 2 kg, which corresponds

to an ice load of 500 to 1000 kg per meter for the full scale tower. A special test was set to study time-dependent icing effects. The increase rate of ice mass as a function of time is shown Figure 2.14.

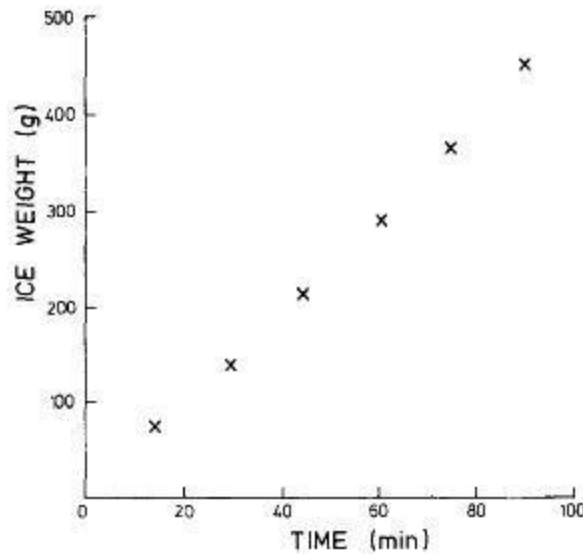


Figure 2.14: Ice weight as a function of time (Makkonen & Oleskiw, 1997)

The linear growth of ice mass observed in the experiment, together with a good agreement between the initial icing rate and theoretical estimates, suggests that the theoretical icing rate calculated for the non-iced mast may be assumed to be valid throughout the icing process. Small scale modelling of large and complex structures can be useful in studying the effects of structural design changes on relative ice loads.

A report published by the Canadian Electricity Association (CEA, 1998) validates three ice accretion models for freezing precipitation by analyzing data obtained from three full scale test sites during 1994-1997 in Eastern Canada. The models are based on work carried out by Chaine and Skeates (1974), Makkonen (1984) and MRI (1977). Based on data obtained during 20 storms, all three models show considerable scatter in their prediction. Contrary to report by Yip (1995), Chaine's model significantly

overestimated moderate to large loads (up to 70 %). The A-model developed by Makkonen (1984) overestimated ice loads by more than 10 N/m while the MRI model consistently underestimated ice loads. Thus these models need to be further improved and more data are required to verify these models.

Sundin and Makkonen (1998) carried out direct ice load measurements on a 323 m high lattice tower located at Arvidsjaur, Sweden, and compared those values with ice loads derived from a weather station data which is located 3 km from the tower. The data were collected at three hour intervals over seven winter periods. The loads in the legs of the tower were obtained from strain gauge readings. The estimation of ice loads due to in-cloud icing and freezing precipitation from meteorological data are based on procedures developed by Makkonen and Ahti (1995). The results show that most of the measured and predicted ice loads agree reasonably well. Only loads larger than 500 kN were considered significant enough for this tower, as the design allowed additional load in the legs of up to 9300 kN. Below 500 kN the loads were hardly observable. The Sundin and Makkonen (1998) study showed that in-cloud icing is the dominant icing load in this location. Unexpected icing events, such as melting and shedding, result in discrepancies between measured and predicted values. Sundin and Makkonen (1998) point out the importance of on-site temperature observations in order for cumulative loads to be modelled correctly.

A report published by the Canadian Electricity Association Technologies Inc. (CEATI, 2002) investigated differences in discontinuity of 50-year return period ice loads between the CSA Standard (CSA, 2006a) and the ASCE 7 Standard (ASCE, 2005). The examined area extends from eastern Michigan to Western New York and includes

northwest Ohio and Ontario. There are not many significant differences between Cold Regions Research and Engineering Laboratory (CRREL) and Environment Canada (EC) approaches in estimating extreme ice thickness and concurrent wind speed. The best approach to determine icing design conditions remains analysis of past record. The Chaine model (Chaine & Skeates, 1974) used in the EC method predicts thicker ice accretion on a 25.4 mm. diameter rod than the Simple model used in the CRREL method. However, the difference in the results between the two models is within 5 mm. for a 50-year return period for most of individual weather stations. However for a 200-year return period ice thicknesses exceed 5 mm. in over half of the stations. Based on this report (CEATI, 2002) the authors recommended using weather data from both the US and Canada for future ice accretion analyses and the development of related standards. A new method for determining extremes, called the Regional Frequency Analysis, should be investigated. To evaluate and improve the performance of ice accretion modeling used by CRREL and EC, concurrent ice load measurements should be obtained from weather stations where standard weather data are taken.

2.6 Variation of ice amounts with height

Mulherin (1986) surveyed data from 118 stations regarding icing and associated problems in the north eastern United States. Results showed that high towers on top of mountains were more likely to experience atmospheric icing and related problems. Fifteen of the 16 stations having top elevations of over 760 m, or mast heights higher than 275 m reported moderate or more severe icing. The findings were strengthened by a high percentage of users of the Icing Protection Devices (IPD), either active, such as electric antenna deicers or passive, such as radomes, polymer coatings, shields or wide

band antennas, in northern states with higher latitude such as Maine, Vermont and New Hampshire.

According to Yip (1995), simulated equivalent radial thickness estimated by the Chaîne model (Chaîne & Skeates, 1974) is more dependent on wind velocity and precipitation rate rather than temperature and conductor size. With an increase in structure height, wind speed will increase exponentially. Horizontal ice accretion, as it is dependent on the precipitation rate, will not be affected by increased wind speed. However, vertical accretion will increase. Yip (1995) used data from 15 locations across Canada to predict the 30-year return period for equivalent radial ice amounts at 10, 30, 50, 70, 100 and 150 m above ground for a 30-year return period. Ice thickness at 150 m is about 129 % of the ice at 10 m., except at three British Columbia locations, where the ice thickness was 119 % of the ice thickness at 10 m. This is partially attributed to surface roughness. The ratios of ice amounts at any height to ice amount at 10 m. as a function of height above ground for all stations, except three British Columbia locations are shown in Figure 2.15.

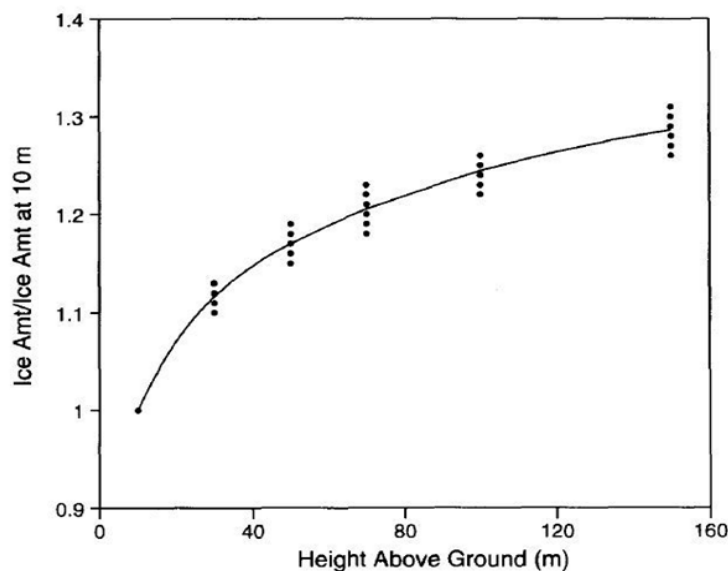


Figure 2.15: Variation of ice amount with height (Yip, 1995)

Ice amounts based on 30-year return period at different height levels can be calculated using the following relationship:

$$A_z = A_{10} \times [0.106 \times \ln Z + 0.755] \quad (2.13)$$

where A_z is the ice thickness at height z ; z is the height in meters; and A_{10} is the ice thickness at 10 m.

According to ISO 12494 (ISO, 2001) the ice amount can vary with the height above ground but there is no model to estimate this variation. Ice can be observed at higher levels and might not be observed at the ground and vice versa. A multiplying factor for ice masses for higher levels above ground is shown in Figure 2 of ISO Standard (ISO, 2001). It can be applied either for glaze or rime ice. The other way to consider height factor is to express different Ice Classes for different heights of the structure.

The current ASCE Standard 7 Sect. 10 (ASCE, 2005) and TIA-222-G (ANSI/TIA, 2005) provide a formula to increase radial ice thickness with height above the ground, however it should be used carefully, since icing approach is different from Canadian method (Marshall et al. 2005).

2.7 Prevention and shedding methods

A number of different approaches are available to mitigate ice accretion, to minimize its severity or assist in its removal. These can be grouped as anti-icing or deicing methods. Anti-icing methods are used to prevent or minimize ice accretion, while deicing methods help removal of already accreted ice. Due to the large size of the towers many of these methods have limited application due to high cost.

Mulherin (1986) reported that the most effective anti-icing method is electric heating, which is primarily utilized in transmitting elements of TV and FM antennas. Considering the size of the towers and the significant power demand, heating the entire tower may be too costly.

It has been noted by Wahba et al. (1993) that larger diameter of superstructure elements accretes less ice thickness, as shown in Figure 2.4.

Another anti-icing approach involves the use of icephobic or low adhesion coatings. The suitability of these coatings for lattice structures is debatable because of the high cost and the size of towers. Mulherin (1986) reported that up to that date no experimental work had been done to satisfy requirements of durability, low cost and ease of application of icephobic coatings on towers. However, he suggested that it could be feasible to coat critical sections of the tower for easier ice removal by natural or artificial means (i.e. wind, natural or artificial vibrations, heat etc.). Constant vibratory frequencies used to remove ice from stiff members may be too extreme and could compromise the whole tower integrity, according to Mulherin (1986). However this technique could be further explored, especially for de-icing of guy wires and flexible towers. Mulherin (1986) also suggested considering painting the towers with darker colors which absorb more solar energy and therefore can aid in melt off. Although there is a requirement to paint towers with a standard red/white pattern for better air traffic visibility, certain tower attachments or antenna parts could be darker to gain solar advantage.

Laforte et al. (2002) researched the adhesion reduction efficiency of seven icephobic coatings and five common protective coatings. The authors indicated that icephobic coating did not reduce ice accumulation on the surface. However, results

showed a wide variation in ice adhesion ranging from a 37 % decrease occurring in some samples and a 50 % increase in others compared to bare aluminum. The surface roughness is considered the most influential factor on ice adhesion, according to Laforte et al. (2002). The authors concluded that the adhesion reduction of icephobic coatings is comparable with commonly used protective coatings. None of the tested icephobic materials showed any significant reduction of ice adhesion or sufficient durability.

Mulherin and Haehnel (2003) investigated the effectiveness of commercially available, low friction surface coatings to determine whether icing control on hydropower and navigation projects could be more economical. Numerous construction materials and low friction coatings were examined to determine if they reduce adhesive shear strength of ice after laboratory and field testing. The durability after six months of field exposure was investigated as well. The study showed that icephobic materials do not prevent ice accretion on surfaces but can decrease the adhesion strength facilitating easier ice removal. Some of the icephobic coatings tested had one half to one third the adhesive strength of bare steel.

Adhesion reduction factors of several icephobic coatings were evaluated by Anti-Icing Materials International Laboratory (AMIL) as shown in Figure 2.16.

Industrial lubricants and greases were excluded from this experiment as their application is impractical on lattice towers. Wearlon had the highest ice reduction factor, as shown in Figure 2.16.

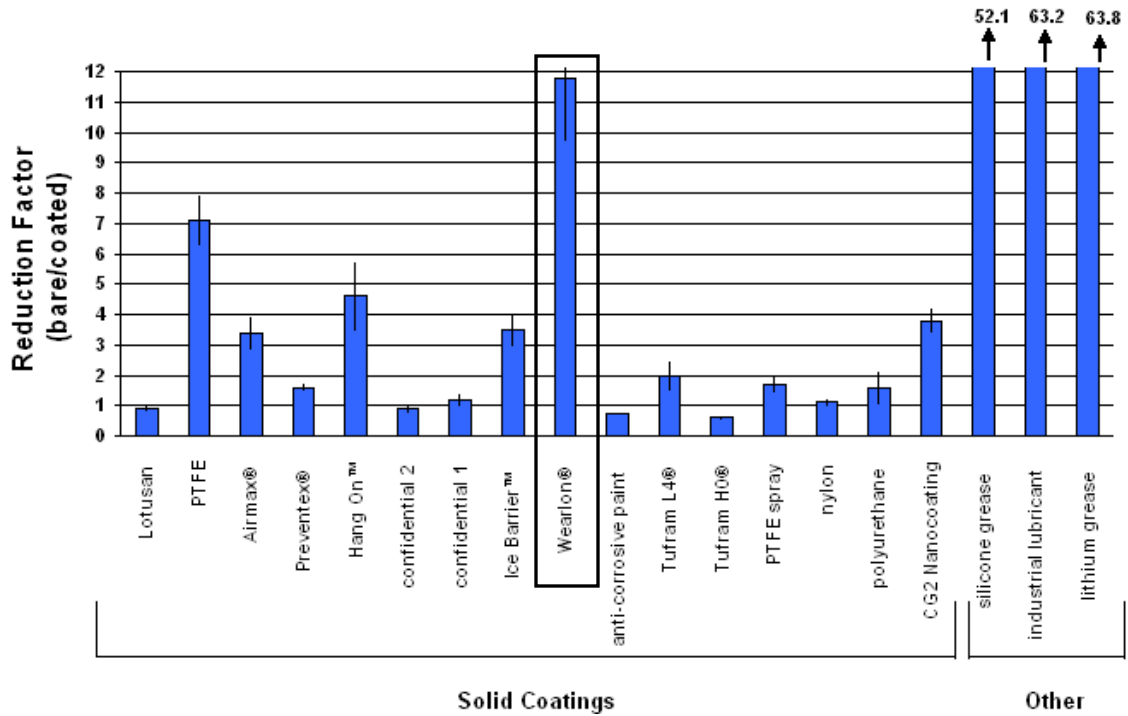


Figure 2.16: Centrifuge ice adhesion reduction AMIL's results (AMIL, 2009)

Ice adhesion to cold rolled steel was in the range of 1.38 MPa, while ice adhesion to Wearlon Super F-1 varied from 0.104 to 0.138 MPa (Mulherin & Haehnel, 2003; Ecological Coatings, 2009). Kraj (2007) reported that Wearlon icephobic surface coating in combination with another mitigation method reduced the ice adhesion force and the accumulated amount of ice on wind turbine blades. Wearlon Super F-1 Ice was selected as a deicing coating in this study. The physical properties of Wearlon Super F-1 and the results are discussed in the next chapter.

2.8 Summary

Atmospheric icing causes significant problems for engineers and utilities across Canada and other cold climate regions of the world. Tall and slender lattice structures and transmission lines are particularly affected by ice accretion, wind or combination of both, as they are often located in remote areas, where meteorological data are limited. The

variation of local topography and seasonal climate affect icing conditions and complicate standardization of icing accretion design guidelines.

The design criteria for ice loads can be obtained either through direct extensive ice load measurements at a specific site or through icing modeling using existing meteorological data. The correlation between field measurements and modeling can be low (CEA, 1998). Therefore models have to be further improved and verified by icing observations.

The summary of icing design criteria from the Standards is shown in Table 2.10. Ice accretion design thicknesses maps are provided in CAN/CSA S37-01 Standard (CSA, 2001); the EIA/TIA-222-G (ANSI/TIA, 2005); the CAN/CSA-C22.3 NO. 1-06 (CSA, 2006a); and, the CAN/CSA-C22.3 NO. 60826-06 (CSA, 2006b). However if local data and factors are available, they should be considered in determining design icing criteria. For example Manitoba Hydro Specifications (Friesen & Kell, 2009) are based partially on previous experience and observations. Measurements or modelling are required to obtain ice class (IC) for the specific site as specified in ISO 12494: Atmospheric Icing of Structures (ISO, 2001). Only EIA/TIA-222-G and ISO Standards provide ice thickness increase with height. None of the Standards provide information on type of the ice as a function of height.

Icephobic coatings do not prevent ice formation. However they lower the adhesive shear strength of ice, which can be subsequently removed. Application of icephobic materials may reduce energy and man-hours required to deice structures.

Wearlon Super F-1 icephobic has showed acceptable performance in reduction of ice adhesion. Lower adhesive strength and mass of accreted ice after application of Wearlon coating in conjunction with other deicing methods have also been reported.

Table 2.10: Summary of the icing design criteria from the Standards

	Type of ice	Ice thicknesses (mm)	Load factors for ice	Variation of icing amount with height
Antennas, Towers, and Antenna-Supporting Structures CAN/CSA S37-01	Glaze	min 10-50	1.2-1.5	-
Overhead Systems CAN/CSA-C22.3 NO. 1-06	Glaze	min 6.5-19	-	-
Design Criteria for Overhead Transmission Lines CAN/CSA-C22.3 NO. 60826-06	Glaze	min 10-40	Spatial factor $S_a=1.5$	Spatial factor accounts height up to 30 m above ground
Structural Standard for Antenna Supporting Structures and Antennas EIA/TIA-222-G	Glaze	Provided for each county	0-1.2	✓
Manitoba Hydro Specifications	Glaze	12.5 with 90 km/h wind; 25.4 without wind	-	-
ISO 12494: Atmospheric Icing of Structures	Glaze Rime	10-50+ Depends on icing class and density	-	✓

3 FIELD AND LABORATORY WORK

3.1 Introduction

Conventional steel lattice structures are subjected to corrosion, deterioration and therefore in need of expensive maintenance. The search for alternative corrosion and maintenance-free material for lattice structures led to a research program at the University of Manitoba to develop lattice tower using fiber reinforced polymers (FRP) (Ochonski, 2009). Some of the benefits using fiber reinforced polymers (FRP) are

- High strength to weight ratio
- Lightweight
- Low electrical conductivity
- Corrosion resistant
- Low maintenance requirements

Four 2143 mm (7 ft) fiber reinforced polymer (FRP) lattice tower segments have been manufactured through a continuous filament winding process at the University of Manitoba as shown in Figure 3.1. All sections were fabricated using E-Glass fibers with epoxy resin.



Figure 3.1: FRP lattice tower segment (Ochonski, 2009)

The process of design and manufacturing of this tower was discussed by Ochonski (2009) who also conducted static and dynamic laboratory tests. The tower was designed according to CSA S37-01 Standard (CSA, 2001).

The analysis was conducted using the finite element program ANSYS. Ochonski used 25 mm radial ice thickness in the analysis of the tower. The maximum chord force was equal to -34.73 kN due to factored wind and ice load and -18.43 kN for factored wind load only. The maximum combined compressive stress was equal to -78.63 MPa from dynamic analysis, which is higher than maximum compressive buckling strength of tower chords of 71 MPa. Ochonski recommends increasing the cross-section area of the chord.

While the design was based on current practice involving steel lattice towers, there were questions regarding ice loads used in the analysis. There is no information regarding ice accumulation on FRP tower, since the lattice tower tested at the University of Manitoba is the first of its kind.

The objective of this study was to examine ice load accumulation on FRP tower both in an ice tunnel and in the field.

The purpose of the field testing of the tower was to evaluate the performance of a fiber reinforced polymer (FRP) lattice tower under environmental loads (wind and/or ice). A segment consisting of three sections 2134 mm (7 ft) were installed in the Smartpark Area at the University of Manitoba as shown in Figure 3.2.

A fourth section 2134 mm (7 ft) tall was used for icing studies at the Icing and Wind tunnel facility of the University of Manitoba.

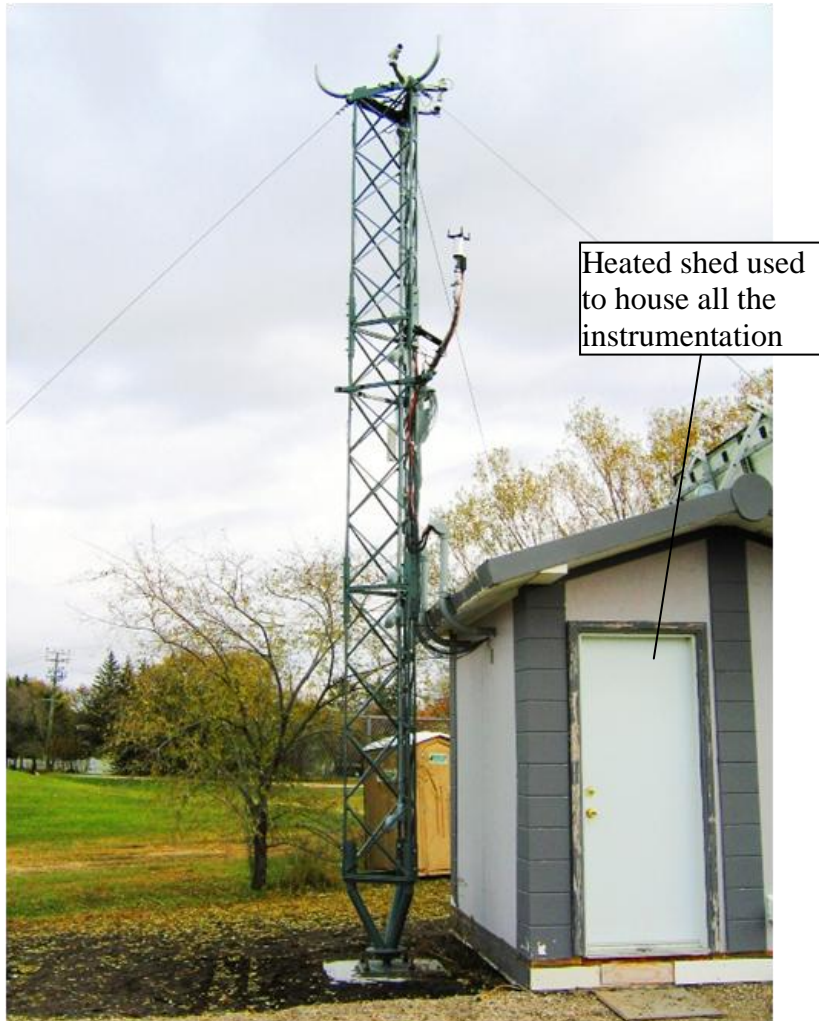


Figure 3.2: Fully raised FRP tower

3.2 Field testing of FRP lattice tower under environmental loads.

3.2.1 Tower modifications

Prior to field installation, the instrumentation used in the previous experimental program by Ochonski (2009) was checked to ensure compliance with outdoor testing. Preparation work included verification of the resistance of the strain gauges already installed and replacement of any damaged ones. The gauges used were FLA-6-11-5L with 120 Ohm resistance manufactured by Tokyo Sokki Kenkyujo Co. Verification of the 120 Ohm resistance was performed with a handheld ohmmeter. All signal wires were extended from their initial length to accommodate the longer distance to the Data Acquisition System housed in the heated shed shown in Figure 3.2. The wires were attached to the tower members and were coated with auto body filler for protection.

Two high sensitive three axis accelerometers CXL02LF3-R-AL manufactured by Crossbow Technologies were also attached to the tower. One was affixed in the middle of the second section at 3.65 m above the ground and one close to the guy wire attachment at 7 m above the ground.

A conduit designed and built using PVC pipes and PVC service heads were used to accommodate long sensor wires and shield them from the environment. The conduit was extended from the top and bottom of the tower to the junction box located 4 m above ground. It was attached to the cords of the tower with metal brackets and clamps, as shown in Figure 3.3.

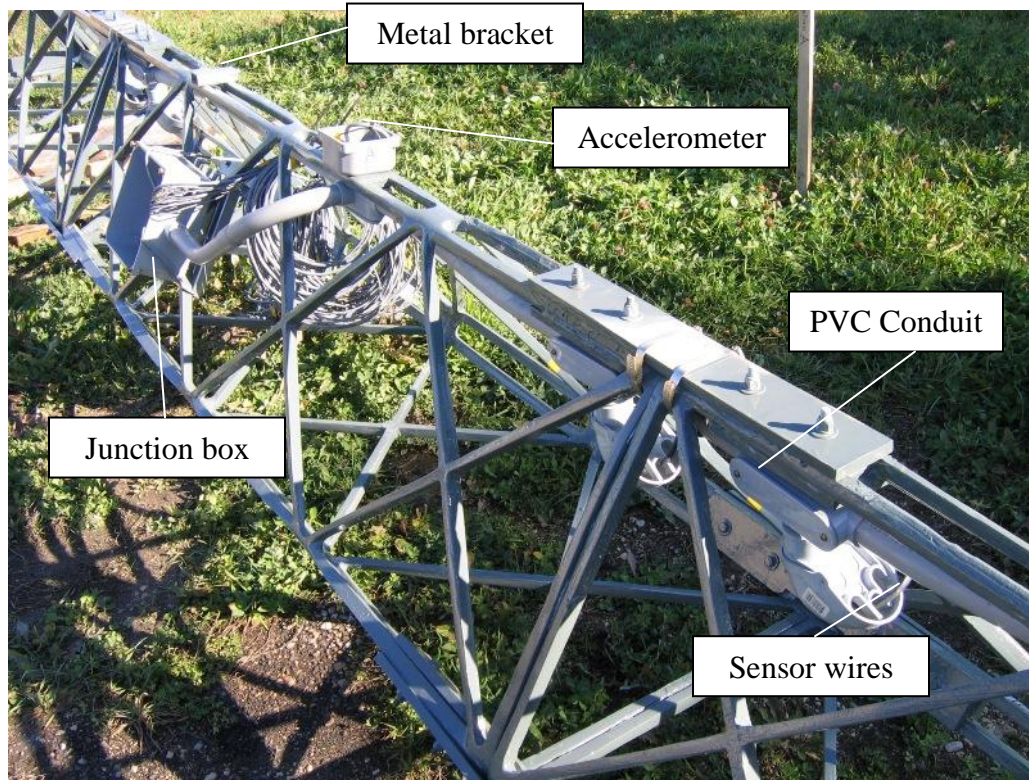


Figure 3.3: PVC conduit inside the tower

The tower was simply supported at the base and cable supported at the top. A pinned base reduces any bending effects on the tower and provides better stress distribution in lower section of the lattice tower (Smith, 2007). The tower base used by Ochonski (2009) was manufactured using 76.2 mm (3 in) steel pipes, L38.1x38.1x6.3 (1 ½ x 1 ½ x ¼) steel angles and round 12.7 mm (1/2 in) base plate, as shown in Figure 3.4.

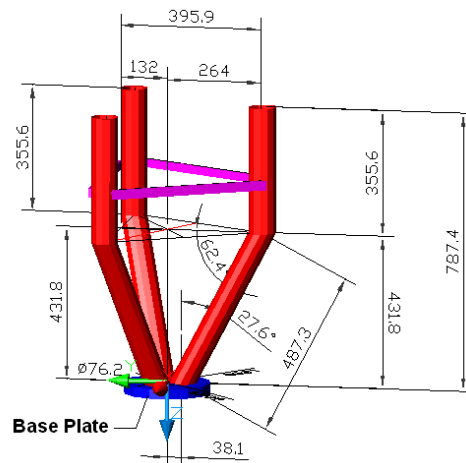


Figure 3.4: Steel tower base (Ochonski, 2009)

The legs of the base were connected to the bottom section of the tower by 12.7 mm (1/2 in) steel bolts.

A number of modifications were made to the base of the tower to facilitate the erection process. A 177.8x177.8x25.4 mm (7x7x1 in) steel plate was welded to the bottom of the base, as shown in Figure 3.5a, and a spherical bearing was welded to the foundation base plate as shown in Figure 3.5b. In addition, short pieces of steel angles were welded to the pipe legs of the base to provide better force transfer between the FRP tower and the base plate as shown in Figure 3.5a.

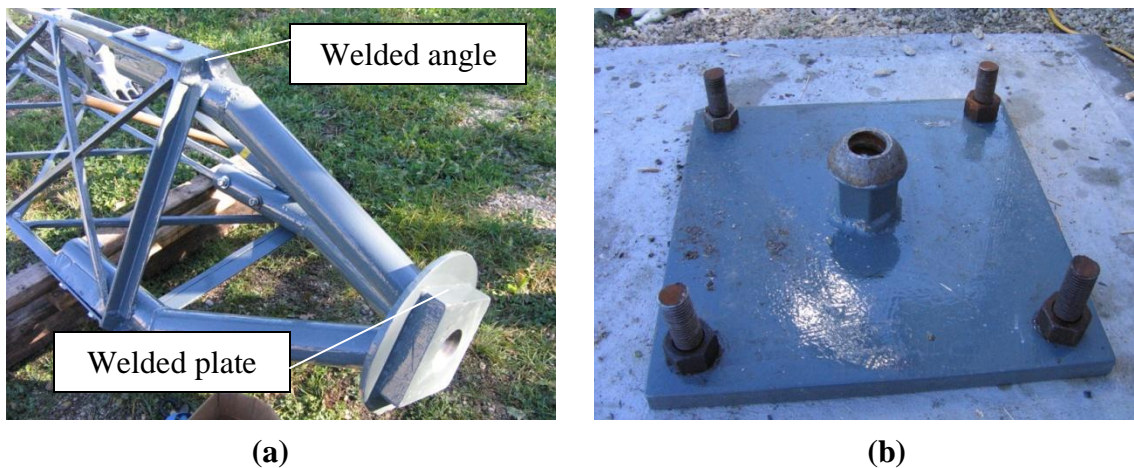


Figure 3.5: Pinned base of the tower

The voids between the bottom FRP tower segment and steel tubular legs of the base were filled with resin to provide a secure connection and more efficient force distribution between the tower and the base. The 105 Epoxy Resin with 205 Resin Fast Hardener manufactured by West Systems Inc. were mixed with the ratio of five parts of resin to one part of hardener to fill in the gaps. Epoxy was poured in small batches as it generates heat and large mass can be inflammable. Plywood, wrapped in a wax paper, and non-drying clay were used to contain and shape resin. The voids filled with resin are shown in Figure 3.6.

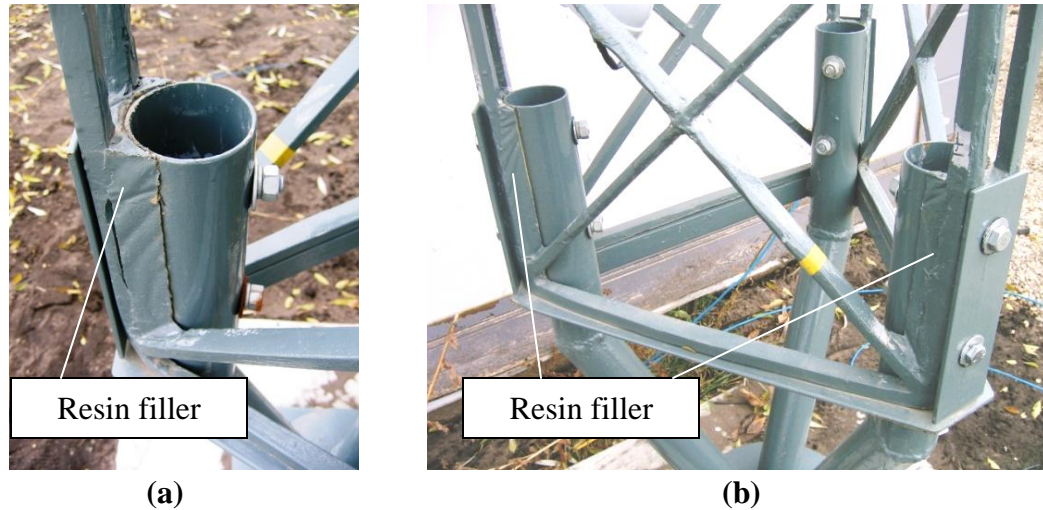


Figure 3.6: The voids filled with epoxy resin

The tower was placed on 800 x 800 x 300 mm concrete slab. The designated area was excavated approximately 500 mm. and four L 44 x 44 x 6.35 (L 1 ¾ x 1 ¾ x ¼) piles were driven into soil approximately 1 m deep. Compacted crushed stone 75 mm thick was used as a sub grade on undisturbed soil. Wooden formwork was set up and reinforcement consisting of eight M15 rebars, tied together, was laid down. Commercial concrete was mixed on site and used to cast the foundation. Four 25.4 mm (1 in) threaded rods were anchored in the concrete. The 406.4 x 406.4 x 25.4 mm (16x16x1 in) steel base plate was bolted to the foundation as shown in Figure 3.5b. The tower’s foundation details are shown in Figure 3.7.

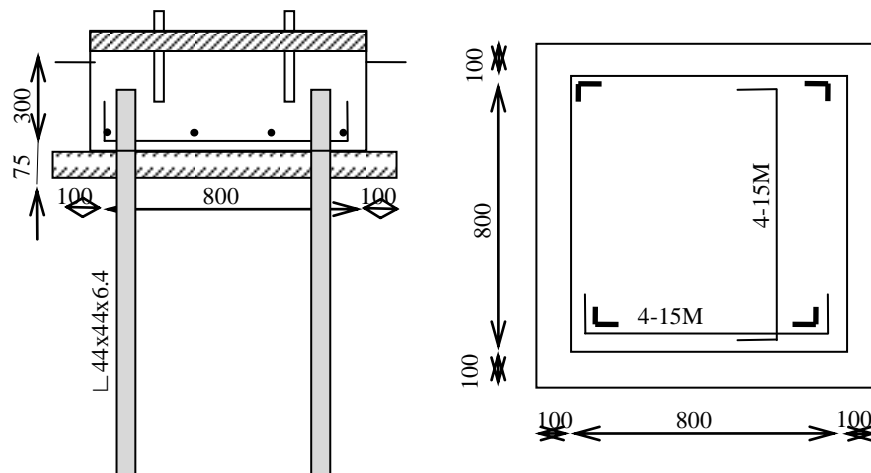


Figure 3.7: Tower base foundation

Steel bracing for the guy wire attachments was manufactured using L 63.5 x 63.5 x 6.35 (L 2 ½ x 2 ½ x ¼) angle and 63.5 x 63.5 x 6.35 (2 ½ x2 ½ x ¼) HSS sections, as shown in Figure 3.8. These were cut into 530 mm in length and welded together to fully cover the three sides of FRP tower. Holes were drilled in the steel hollow square sections to hold the 12.7 mm (½ in) bolts which were used to hold the guy wires as shown in Figure 3.9.

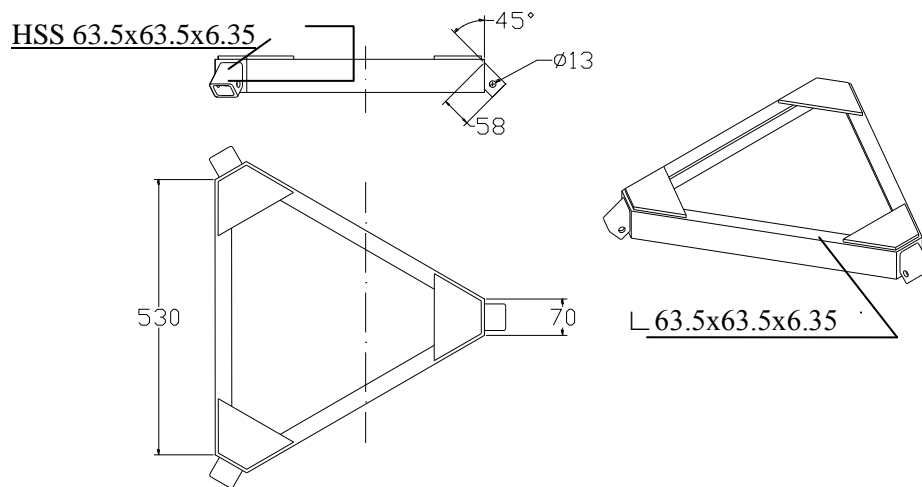


Figure 3.8: Guy wire attachment bracket



Figure 3.9: Guy wire attachment bracket

The tower was painted to protect it against environmental conditions and exposure to UV light. The tower sections were sanded and cleaned prior to applying the spray paint primer. The sections were coated with one layer of Tremclad® primer. The Tremclad® oil-based finish paint was rolled and hand brushed after primer dried up.

3.2.2 Tower erection

The tower erection process consisted of the following steps:

- a) Transportation;
- b) Assembly;
- c) Erection;
- d) Alignment;
- e) Cable tensioning.

The tower sections, base, guy wires, and hardware were transported from the University of Manitoba Structures Lab to the site on a flat bed truck. Due to the light weight of the assembled tower sections (approximately 50 kg) assistance of only three persons was required.

The assembly consisted of attaching the bottom tower section to the steel base using 12.7 mm (½ in) bolts, as shown in Figure 3.5a. The cable attachment bracket was inserted to the top of the tower and secured to the tower with three 6 mm (¼ in) bolts. The guy wires were looped through the anchor eyes and secured with three U-bolts at the dead end of each cable. Similarly, guy wires were looped through the bolts in the top cable attachment bracket shown in Figure 3.9. The guy wire assembly sequence is shown in Figure 3.10.

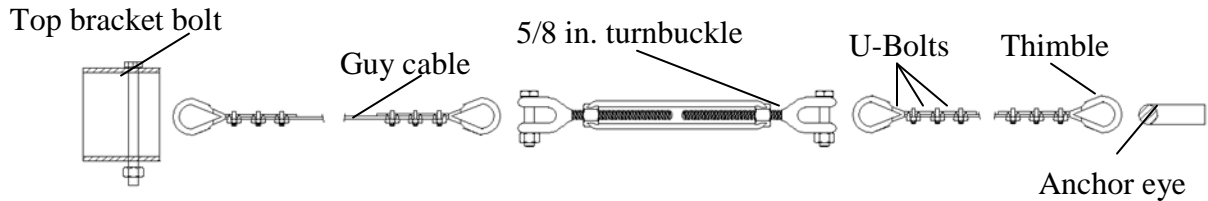


Figure 3.10: Guy wire assembly sequence

The tower was lifted about one meter from the ground and rested on temporary scaffolding. The lifting was done by one cable attached to a winch located on roof of the shed. The tower was stabilized by two guy wires, as shown in Figure 3.11.



Figure 3.11: Erection of the tower

The tower was lifted in stages at approximately 20 degrees at a time and the side guy wire tension was adjusted periodically. At approximately 45 degree angle, the cable opposite to the winch was fastened through its anchor and the tension was applied to this

cable during the final phase of the lift. The lifting was stopped when the top of the tower was just above the base. The tension was applied to all three cables. A carpenter's level was used to check the vertical alignment of the tower and proper adjustment of the tension force was given to the guy cables to ensure a perfect vertical position of the tower.

The tension in the guy wires was adjusted using the pulse technique described in the CSA-S37-01 (CSA, 2001) and was taken as 10 % of the breaking strength of the guys, which is 3.1 kN. The governing equation from CSA-S37-01 (CSA, 2001) is

$$T = \frac{4ML_c^2 n^2}{P^2} \quad (3.1)$$

where

T = average guy tension, N

M = mass of guy cable, kg/m

L_C = guy chord length, m

N = number of complete vibrations

P = time, measured while counting n vibrations, seconds

The time P = 1.3 sec. was measured for n = 9 vibrations to reach the required average tension of 3 kN in the guy wires.

The tension force in the guy cables was adjusted by rotating the turnbuckle.

The total height of the tower from the concrete foundation to the top was 7.08 m. (23 ft.-3 in.). The fully raised tower, along with several instruments, is shown in Figure 3.2.

3.2.3 Site layout and sensors.

The test site is located at the Alternative Village outdoor laboratory on the University of Manitoba campus, as shown in Figure 3.12.

The tower is supported by three sets of guy cables. The cables were PVC coated, 6.35 mm (1/4 in) in diameter, six strands, with a total breaking strength of 31 kN (7000 lb).

In the original testing by Ochonski (2009) a total of 24 strain gauges were affixed to one side of the tower to measure strains in the members of the tower during testing. These were still in working order for the present study. Additionally, two accelerometers were mounted to monitor vibrations of the tower, as shown in Figure 3.13. Accelerometer A was attached at the height of 3.65 m (12 ft) and accelerometer B at the height of 7 m (23 ft) above ground.



Figure 3.12: Layout of the test site location (Google Maps)

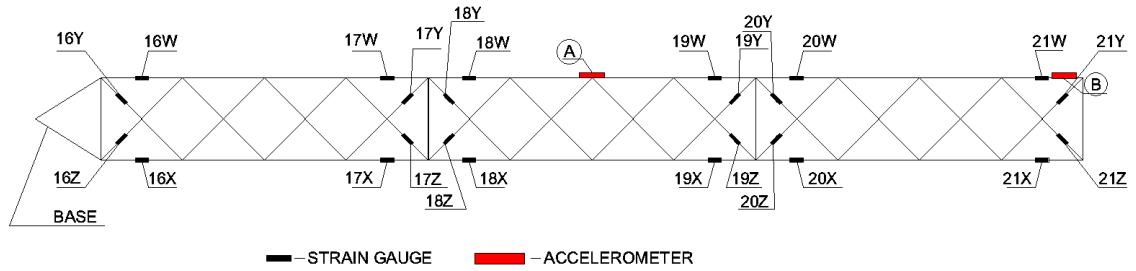


Figure 3.13: Layout of strain gauges and accelerometers

All sensors were connected to a data acquisition system housed at the shelter through the junction box located in the middle of the tower. All the sensor wires run through the PVC conduit and were protected from weather and UV light.

A number of meteorological instruments were also installed for another research project. They included a heated anemometer (measuring direction and wind speed) and icing sensors mounted on a 30 mm. diameter boom arm which was attached horizontally to the tower shaft approximately five meters above ground.

The YOUNG 85004 Ultrasonic Anemometer is a two-axis heated ultrasonic wind sensor with no moving parts manufactured by R.M. Young Company. Voltage outputs are provided for wind speed and direction measurements.

The Goodrich 0871LH1 freezing rain sensor detects presence of icing conditions. It is manufactured by Goodrich and distributed by Campbell Scientific (Canada). The presence of icing conditions is detected by ultrasonically vibrating probe.

The Ice Detection Controller LID-3210C is manufactured by Labkotec primarily used in wind energy industry. The detection of ice accumulated on sensor is based on measuring the strength of ultrasonic signal. The installed meteorological instrumentation is shown in Figure 3.14.

Freezing rain sensor and ice detection controller were not functional at the time of the testing

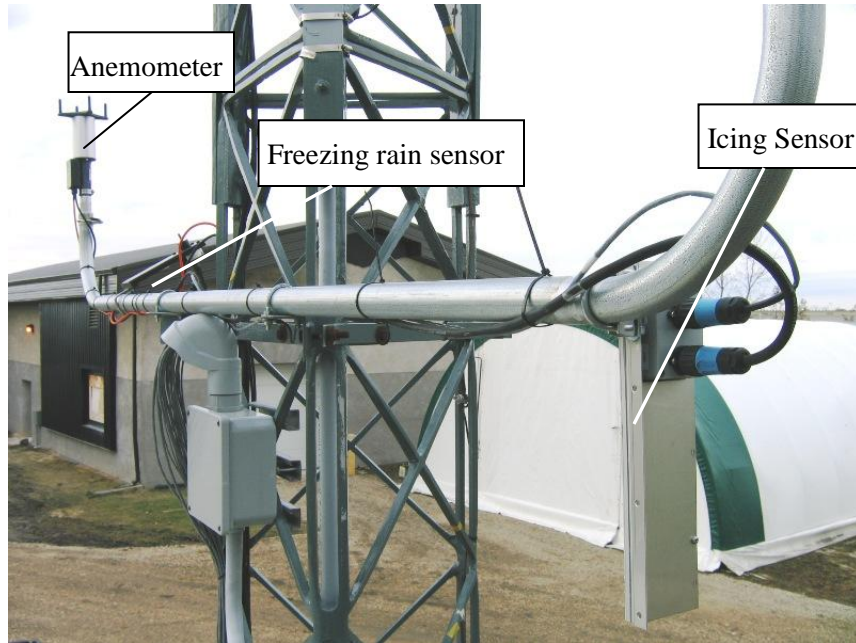


Figure 3.14: Installed meteorological instruments

3.2.4 Data acquisition system (DAQ)

The Data Acquisition System (DAQ) consisted of two data loggers and portable PC to display and store information, as shown in Figure 3.15.

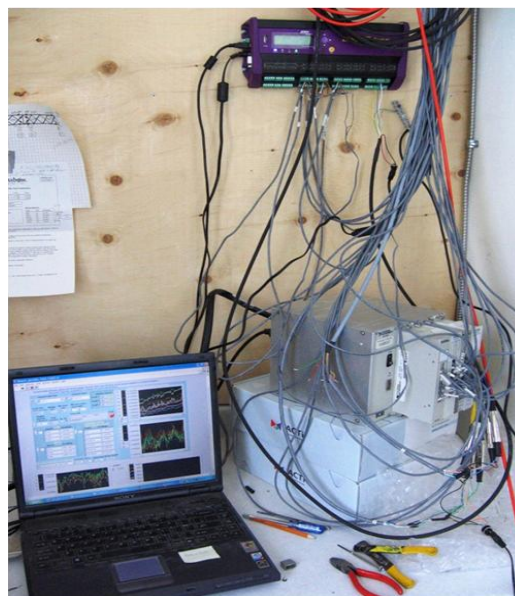


Figure 3.15: DAQ system

The DT-85 Data Logger was recording the output from eight strain gauges and the anemometer with 1 Hz sample frequency.

The NI SCXI-1000 Data Logger with four extension modules was recording values from the remaining strain gauges and two accelerometers. Two NI SCXI-1314 modules were used to record strains from 14 strain gauges. The readings from the two accelerometers were recorded by two NI SCXI-1320 modules. The data were sampled at the rate of 32Hz.

The DAQ system was manually operated everytime data were gathered.

The LabVIEW programming software was used to display and record the data obtained by the NI SCXI-1000 data logger and the DeLogger 5 program was used to display and record the data from the data logger DT-85.

3.2.5 Test procedure

Readings from the strain gauges, the accelerometers and the anemometer were recorded for the two week period in February of 2009. The initial readings were zeroed by the LabVIEW program. Each day the test lasted for approximately 15 min on average, except for days of calm weather. The duration of the test was limited due to the significant amount of data recorded. All gathered data were stored on a portable PC.

Since no icing events were noticed during that time period, the FRP tower was sprayed with chilled mist water on February 27, 2009. The accreted ice thickness was measured approximately 3 to 5 mm. Iced members of the tower are shown in Figures 3.16, 3.17 and 3.18. The strain gauge readings from the iced tower were measured on February 27, 28 and March 1, 2009.



Figure 3.16: Iced chord of the FRP tower



Figure 3.17: Ice on the diagonal bracing of FRP tower



Figure 3.18: Iced members of FRP tower

The highest wind was recorded on February 23, February 25, February 26 and February 28, 2009. The wind direction and wind speed are shown in Figures 3.20 to 3.27 for those dates. The averaged trend lines are shown for easier result interpretation. The south wind is dominant for February 23rd, north-west wind is dominant for February 25th, north-east wind is dominant for February 26th and north-west wind is dominant for February 28th. The highest wind gust was recorded on February 26th at 10.5 meters per second. The highest strains were recorded on February 23rd and February 26th. The wind direction and wind speed readings from the period of February 14, 2009 to March 1, 2009 are shown in Appendix B. The strain measurements between February 12, 2009 and March 1, 2009 are shown in Appendix C.

The ambient temperatures during the period of testing are shown in Figure 3.19.

The results are discussed in Chapter 4.

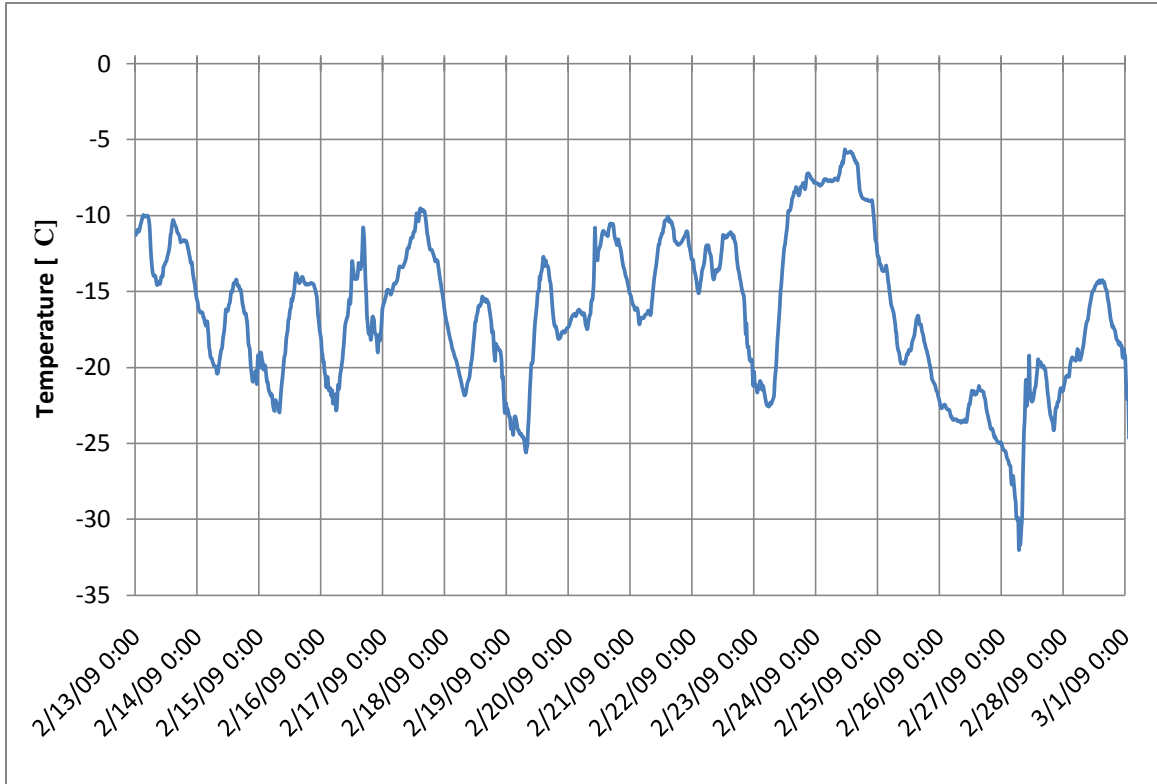


Figure 3.19: Temperature fluctuation during testing period (Department of Plant Science, 2009)

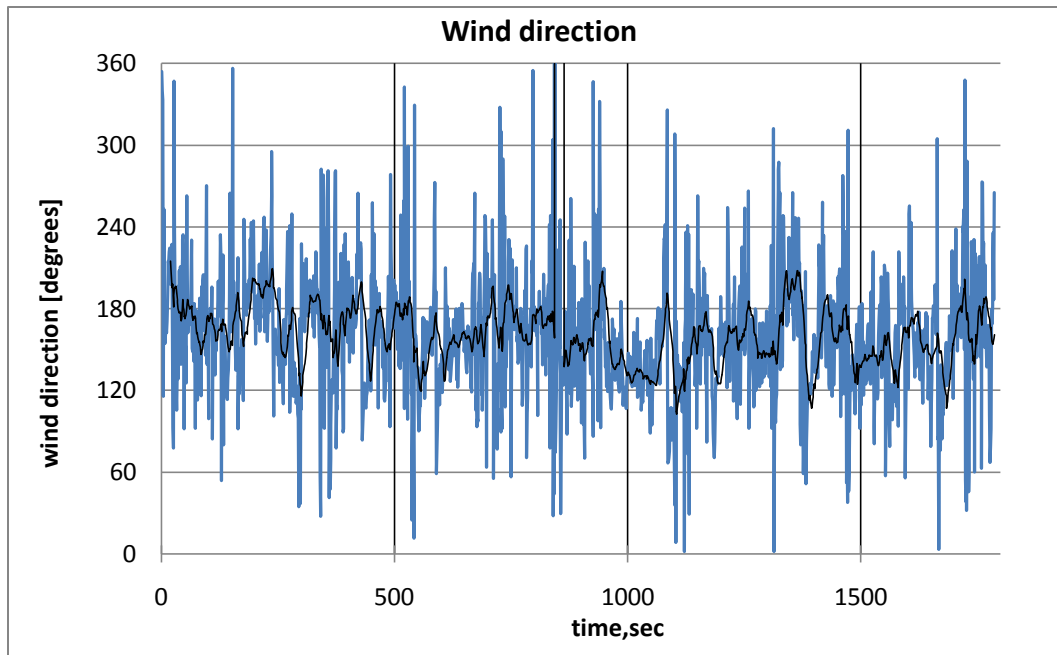


Figure 3.20: Wind direction at 3:02-3:32 PM on February 23, 2009

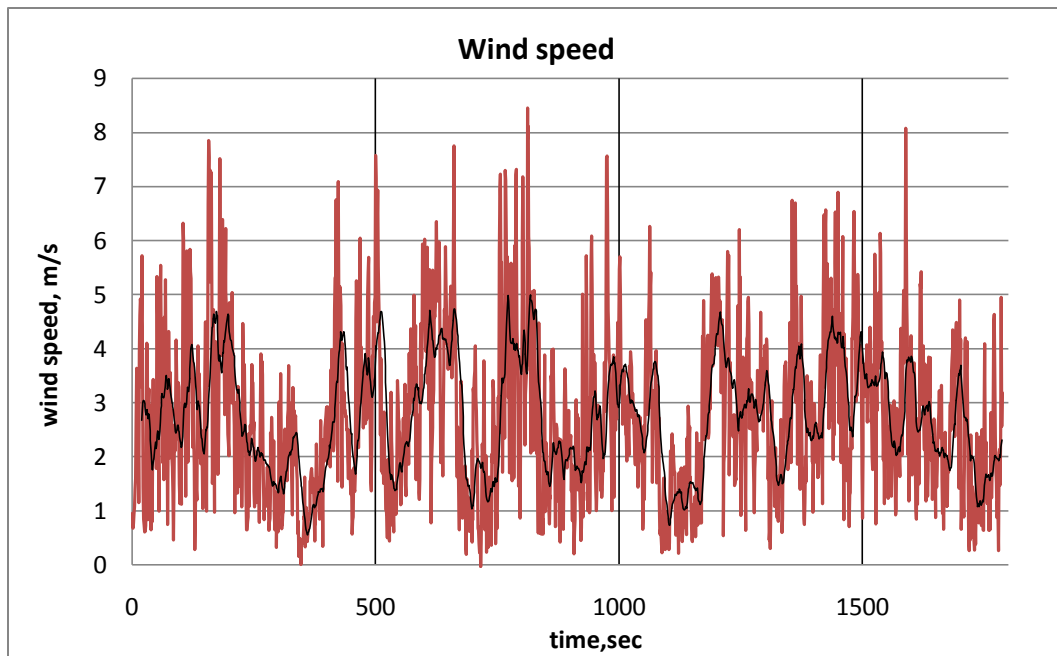


Figure 3.21: Wind speed at 3:02-3:32 PM on February 23, 2009

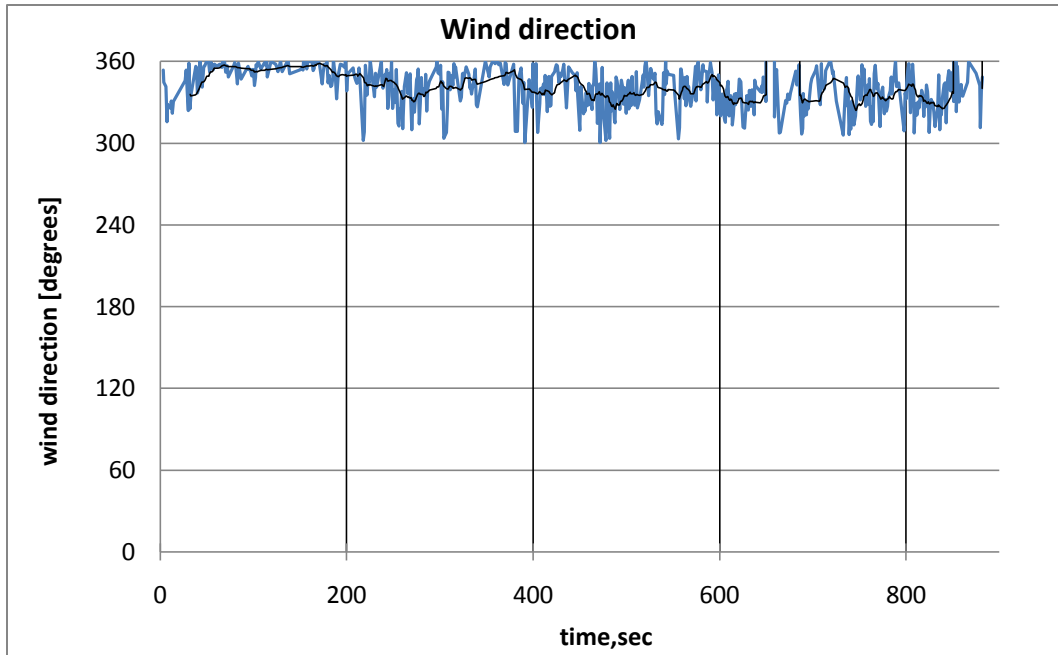


Figure 3.22: Wind direction at 10:47-11:01 AM on February 25, 2009

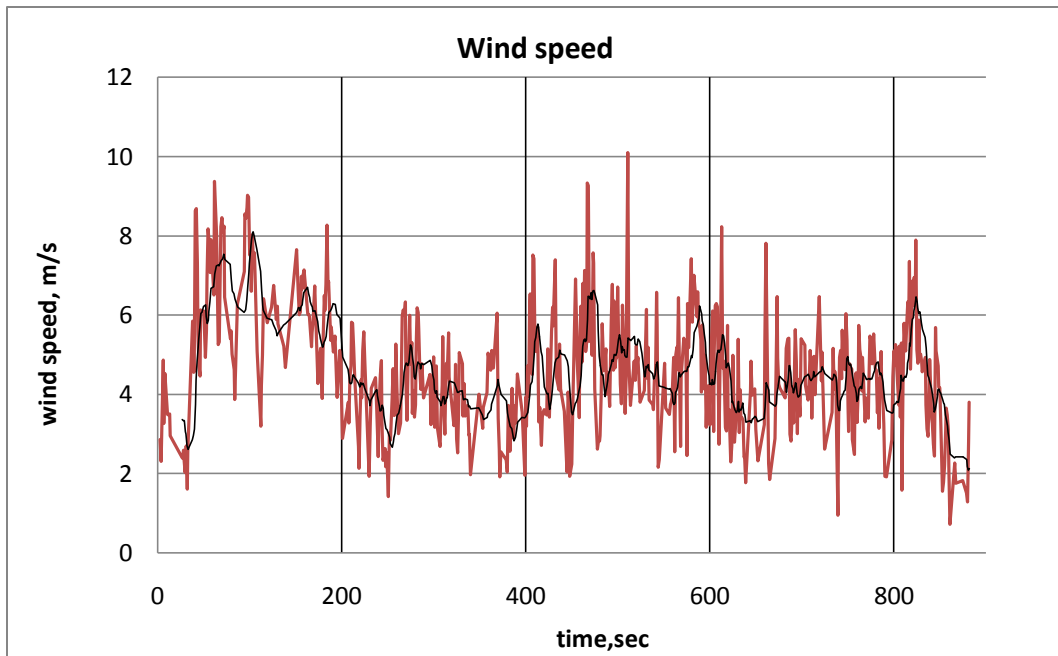


Figure 3.23: Wind speed at 10:47-11:01 on February 25, 2009

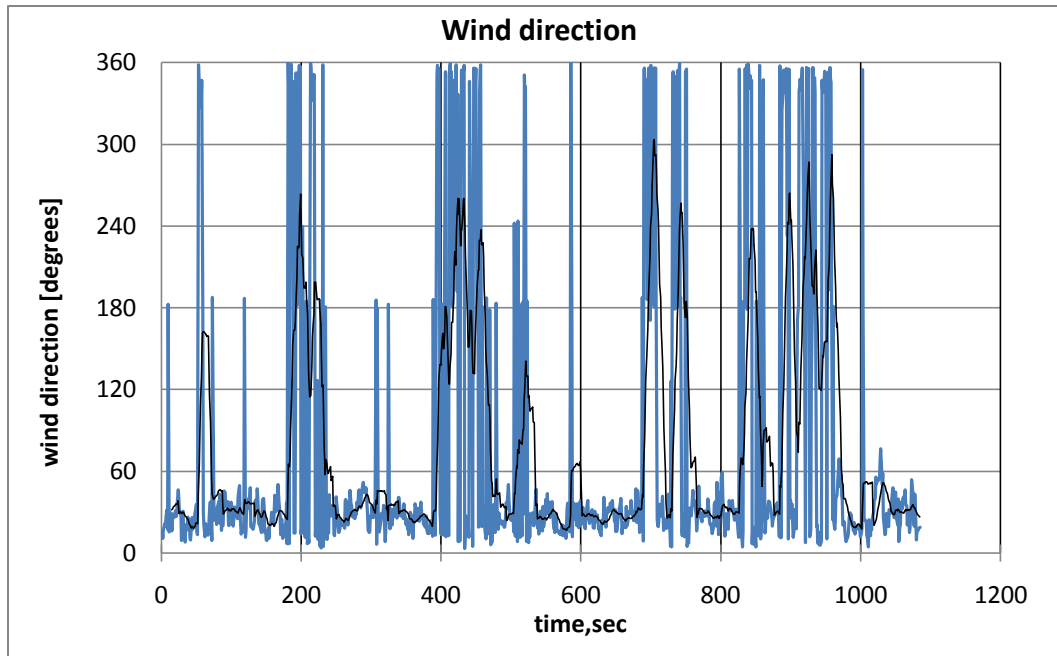


Figure 3.24: Wind direction at 11:54-12:12AM on February 26, 2009

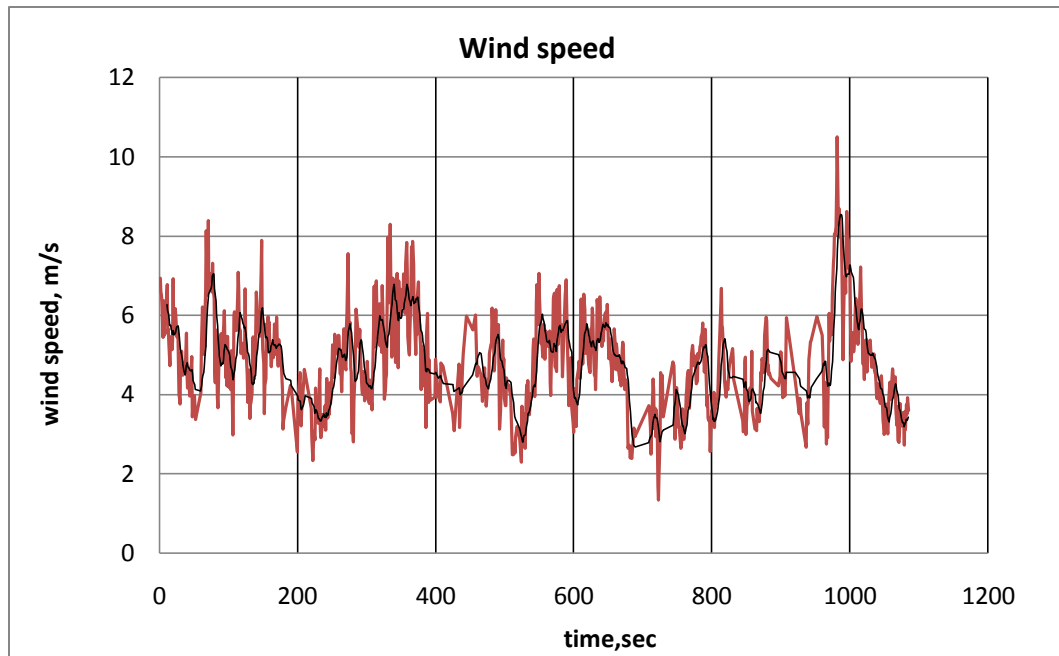


Figure 3.25: Wind speed at 11:54-12:12AM on February 26, 2009

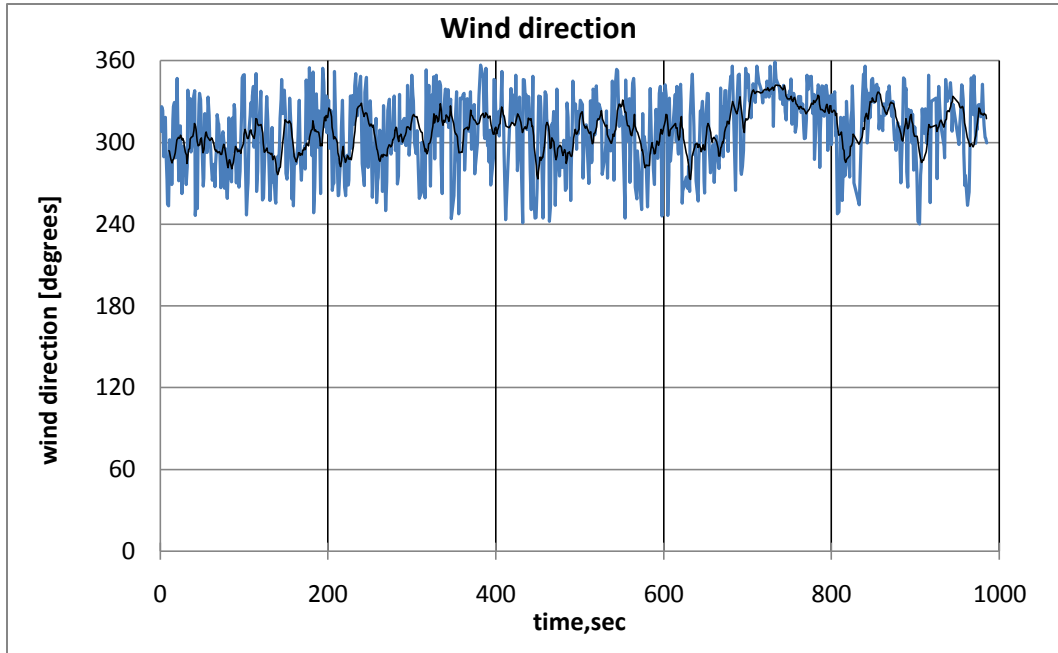


Figure 3.26: Wind direction at 1:56-2:12 PM on February 28, 2009

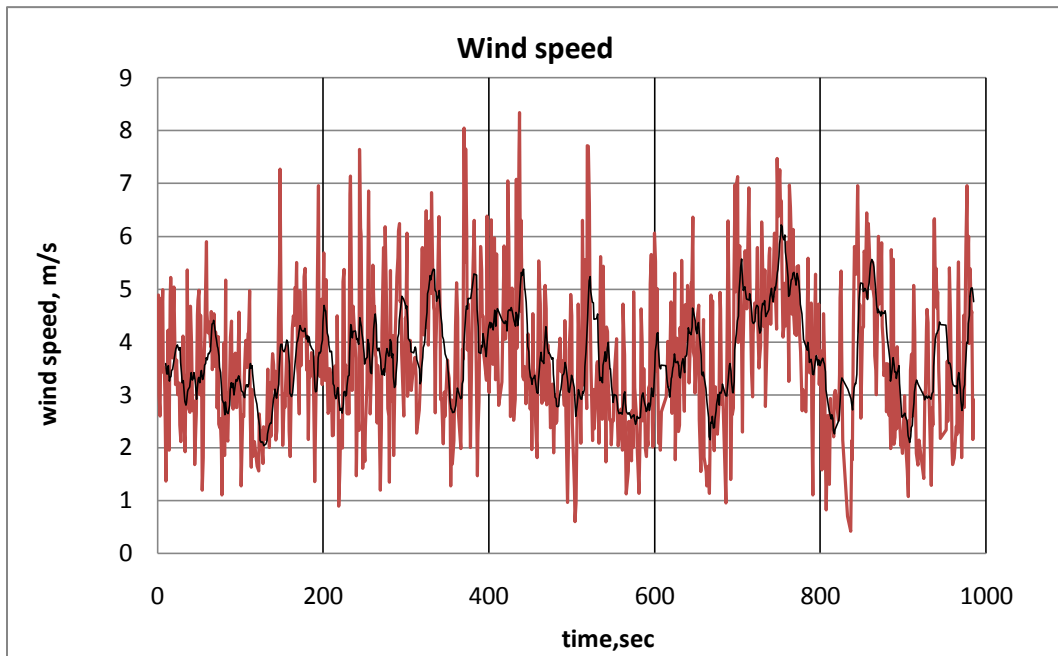


Figure 3.27: Wind speed at 1:56-2:12 PM on February 28, 2009

3.3 Icing tunnel tests

A 2134 mm (7 ft) segment of the FRP tower was used to examine ice build up on FRP towers. Testing took place at the Icing Wind Tunnel Facility of the University of Manitoba. A steel tower section with nearly identical geometrical properties to the FRP tower segment was also designed and manufactured for comparison purposes. The two tower segments are shown in Figure 3.28. Testing included examination of glaze and rime ice on tower segments under normal wind conditions (5 m/s wind speed) and high speed wind (25 m/s). The tower segments were oriented at different angles to the wind direction (0 degree, 30 degree and 90 degree angles) as shown in Figure 3.29. The effectiveness of an icephobic coating on the ice buildup in the tower segments was also examined.



Figure 3.28: FRP section (left) and steel section (right)

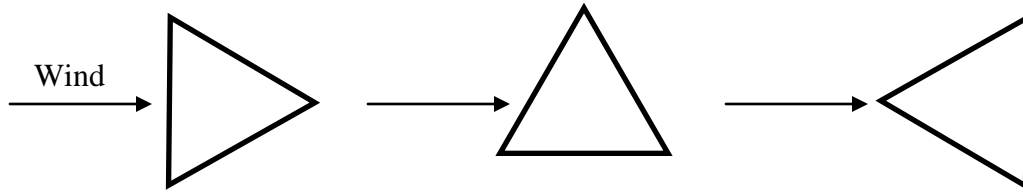


Figure 3.29: Wind direction is normal, parallel and 30 degree angle to the face

3.3.1 Design and manufacturing of steel tower section

The steel tower section was prefabricated using 12.5 mm x 19 mm ($\frac{1}{2}$ in x $\frac{3}{4}$ in) steel solid bar to replicate the FRP tower section shown in Figure 3.30. The solid bars were cut, bent and welded together. The voids in between steel chords at the joints were filled with auto body filler. The steel section was first coated with Tremclad oil based anticorrosion paint. The steel tower segment had a mass of 63.4 kg. (140 lb) compared to 14.8 kg. (32.5 lb) of the FRP section.

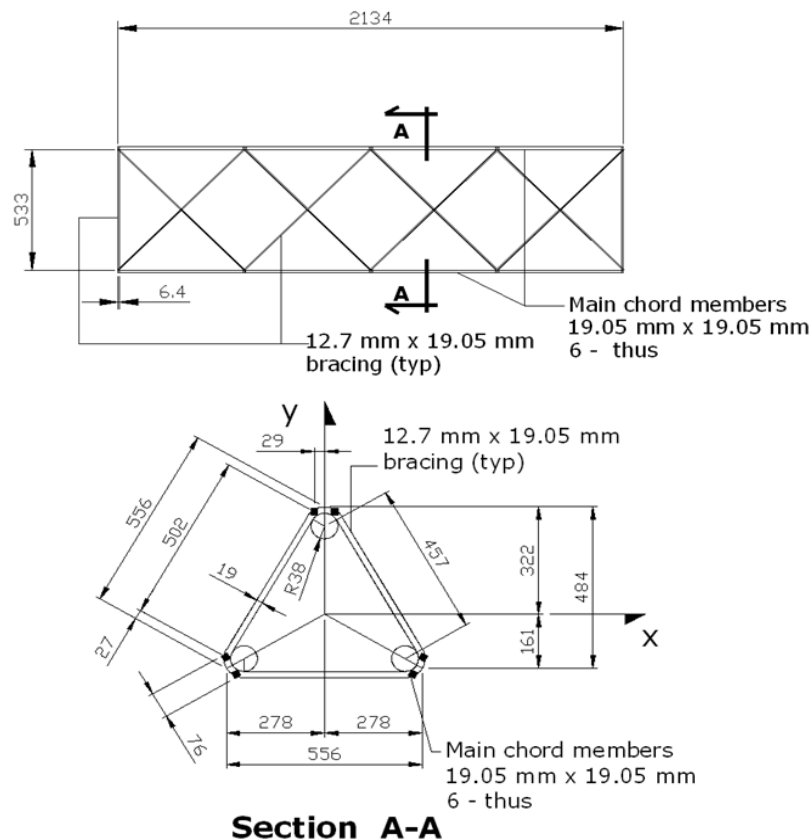


Figure 3.30: FRP segment cross section (Ochonski, 2009)

3.3.2 Test procedure

The University of Manitoba Icing Wind Tunnel Facility is capable of simulating the following environment conditions:

- Wind speed up: to 32 m/s (115 km/h)
- Temperature: -40 °C to +40 °C
- Ice: through a chilled water system installed to spray water to form ice on test specimen.

A layout of the Icing Facility is shown in Figure 3.31. It consists of a refrigeration system, a spray water system, a fan cabinet and the testing chamber.

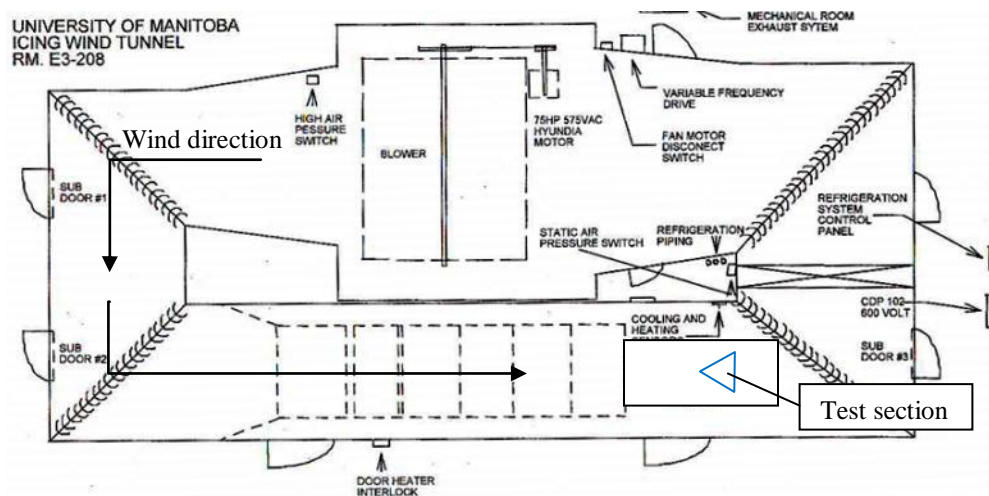


Figure 3.31: University of Manitoba Icing and Wind Tunnel

Both, the FRP and the steel sections were tested at 0 degree, 30 degree and 90 degree angles to the wind direction as shown in Figure 3.29.

Glaze, soft rime, and hard rime ice at high wind velocity were set as the icing conditions for the tower segments. For the glaze icing condition, the temperature was set at -5 °C and the wind speed was set at 5 m/s. The water content in the system affects both dry and wet condition of the ice. For glaze icing the water content was set at 5.5 gal/hr

with a water temperature of 1.5 °C (34.7 F). The soft rime ice environment was achieved by setting the temperature at -10 °C and the wind speed remained unchanged at 5 m/s. The water content was reduced to 2 gal/hr. Hard rime ice at high speed velocity was obtained by increasing the wind speed to 25 m/s without changing the other parameters.

The tower section was placed inside the test chamber and secured to the floor with weights as shown in Figure 3.32. One hour prior to testing the water system was cooled down gradually. During the rime ice tests a heater was used to prevent freezing of the spraying nozzle. After the system was cooled down to the required level spraying through the nozzles was initiated. The area affected by ice, shown in Figure 3.32, measured approximately 450 mm (1.5 ft). The spraying lasted 45 min. for each test.



Figure 3.32: Tested segment placed in icing tunnel

Glaze, soft rime and hard rime ice accretion on lattice tower sections are shown in Figure 2.10.

After 45 min the spraying was halted, ice accumulated on members was photographed and the thickness was measured. The accumulated ice was carefully detached from the section members and placed in a measuring pan and melted at room temperature to obtain the liquid water equivalent.

The amount of liquid water equivalent was compared to amounts obtained from other tests. The results are discussed in Chapter 4.

3.3.3 Application of an icephobic coating.

After both the steel and the FRP tower segments were tested for icing accumulation, they were both coated with the icephobic coating Wearlon Super F1-Ice shown in Figure 3.33. This coating is manufactured by Ecological Coatings, NY, USA.



Figure 3.33: Wearlon Super F1-Ice coating and hardener

It is a two component water based, room temperature cure, graphite silicone epoxy with increased silicone that improves the non-stick icephobic properties. It is commonly

used on roof edges, bridges, communication towers, wind turbines and other structures where ice buildup is of concern (Ecological Coatings, 2009).

The coated tower sections shown in Figure 3.34 were tested at 90 degree angle to the wind direction in the glaze ice environment. The tunnel setup conditions and the duration time of the test remained the same as the previous test.

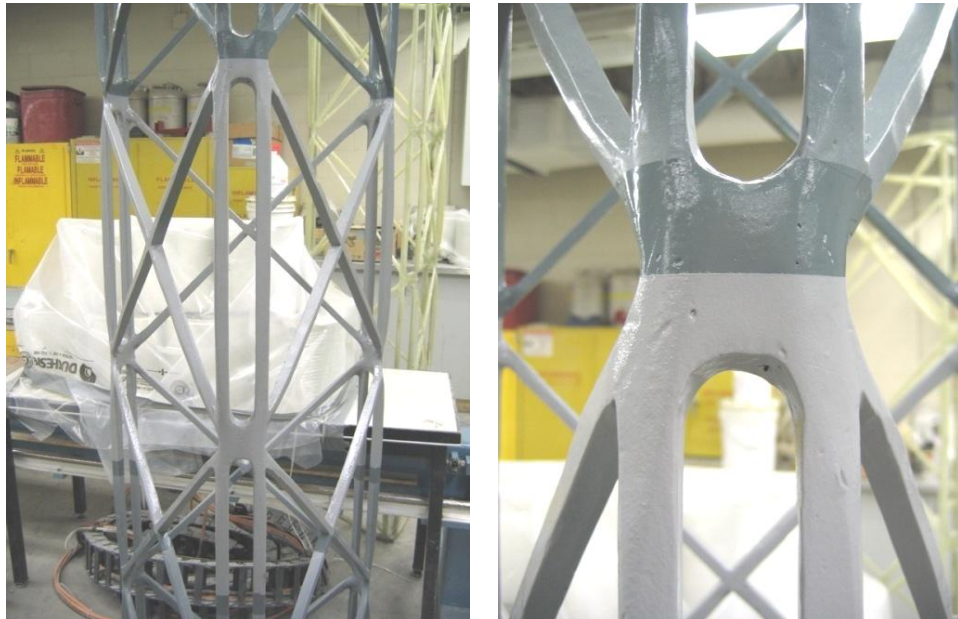


Figure 3.34: Fiber glass tower section coated with Wearlon Super F1-Ice (light grey color)

4 RESULTS AND DISCUSSION

The experimental test results for a 7 m (21 ft) FRP tower section under environmental loads and its measured vibrations are discussed in this chapter. Ice buildup results and the effects of varied orientations of tower sections to the icing direction, as shown in Figure 3.29, are presented and evaluated as well. Assessment of the efficiency of using the icephobic coating Wearlon Super F-1 Ice as a possible mitigation technique for FRP and steel latticed tower sections is also discussed.

4.1 Strains

The data obtained from the strain gauges located on the FRP tower, as shown in Figure 3.13, are presented in the plotted form of strain versus time. The measurements were obtained during the period of February 12 to March 1, 2009. All the strains presented and discussed in this section were recorded by NI SCXI-1000 data logger. The measurements from the DT-85 data logger were not taken into consideration since they were not consistent throughout the tests, thus their accuracy is questioned. The highest strains were recorded on February 23 and February 26, 2009. The corresponding wind direction and speed are shown in Figure 3.20 to 3.25. The strains were measured from 15:02 to 15:32 on February 23 and from 11:54 to 12:12 on February 26, 2009.

A typical strain diagram is shown in Figure 4.1. It indicates the presence of higher strain in member 21W. Chords and diagonals were placed in tension due to the eccentricity of the wind load, causing tower to twist, as shown in Figure 4.2 .

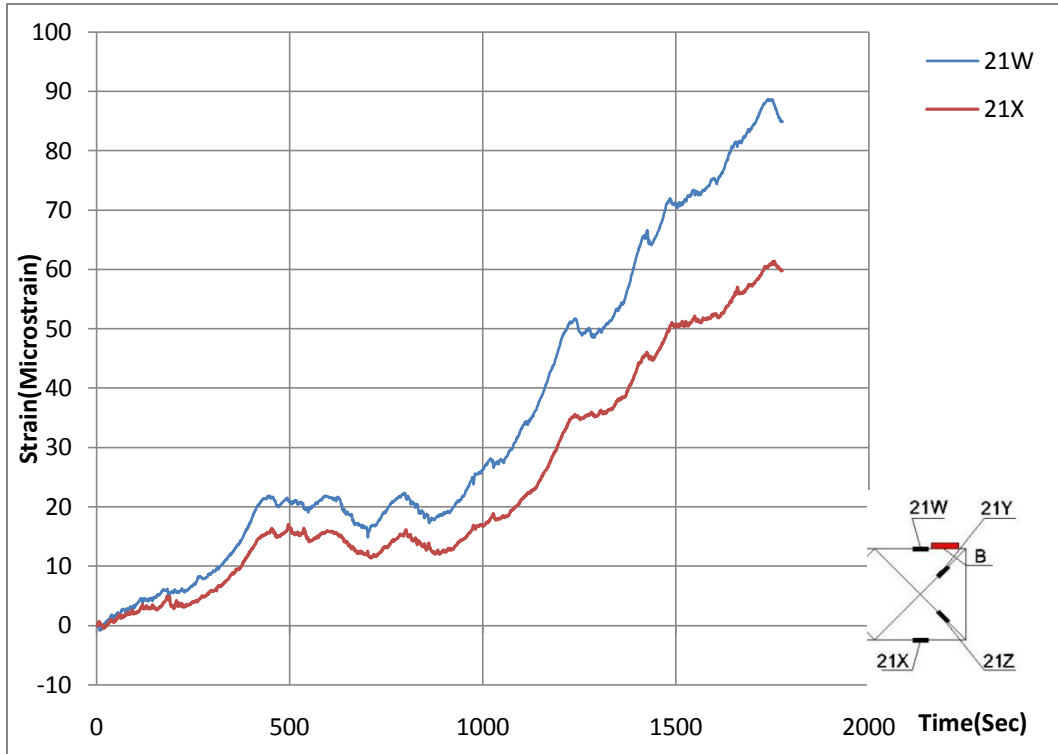


Figure 4.1: Strains in chords at the top on February 23, 2009

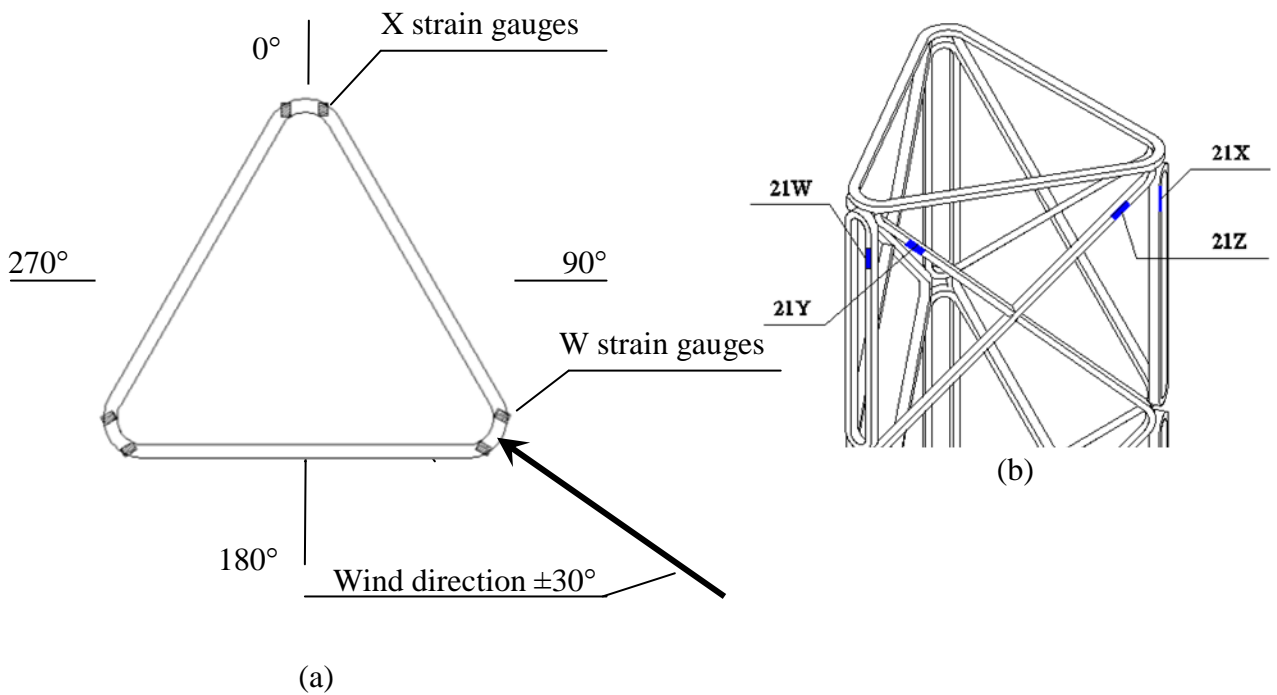


Figure 4.2: Average wind direction (a) and location of strain gauges (b) on February 23, 2009

The test results indicate that the strains continuously increase in tension from 0 seconds to 500 seconds and from 1000 seconds to 1800 seconds while wind load fluctuates with time. The strains are stabilized between 500 seconds and 1000 seconds. This non-linear behavior demonstrated by the strain diagram might be attributed to fluctuation of the wind load. However strain values remain low for the duration of the test period.

The maximum tensile strain in the chord was recorded by the strain gauge 21W and was equal to 86 micro strain. The corresponding stress equals to 2.19 MPa using a modulus of elasticity in the longitudinal direction equal to $E_1 = 25.44$ GPa. This stress is approximately 0.36 % of the ultimate tensile strength in the longitudinal direction which is equal to $F_1^u = 610.2$ MPa (Burachinsky, 2006).

The strains in the chords and the diagonal members between 11:54 and 12:12 on February 26, 2009, are shown in Figure 4.3. The dominating wind direction is shown in Figure 4.4. It should be pointed out that strain values were higher on February 26 than those on February 23, 2009, within the same time period. This can be attributed to the higher wind speed on February 26 and the fact that part of the tower was shielded from the southern wind by the instrumentation shelter and trees on February 23.

The maximum strain in the diagonal was recorded by strain gauge 21Z and was equal to 60 micro strain, as shown in Figure 4.3 . The corresponding stress equals to 1.52 MPa using a modulus of elasticity in the longitudinal direction equal to $E_1 = 25.44$ GPa. This stress accounts 0.25 % of the ultimate tensile strength in the longitudinal direction which is equal to $F_1^u = 610.2$ MPa (Burachinsky, 2006).

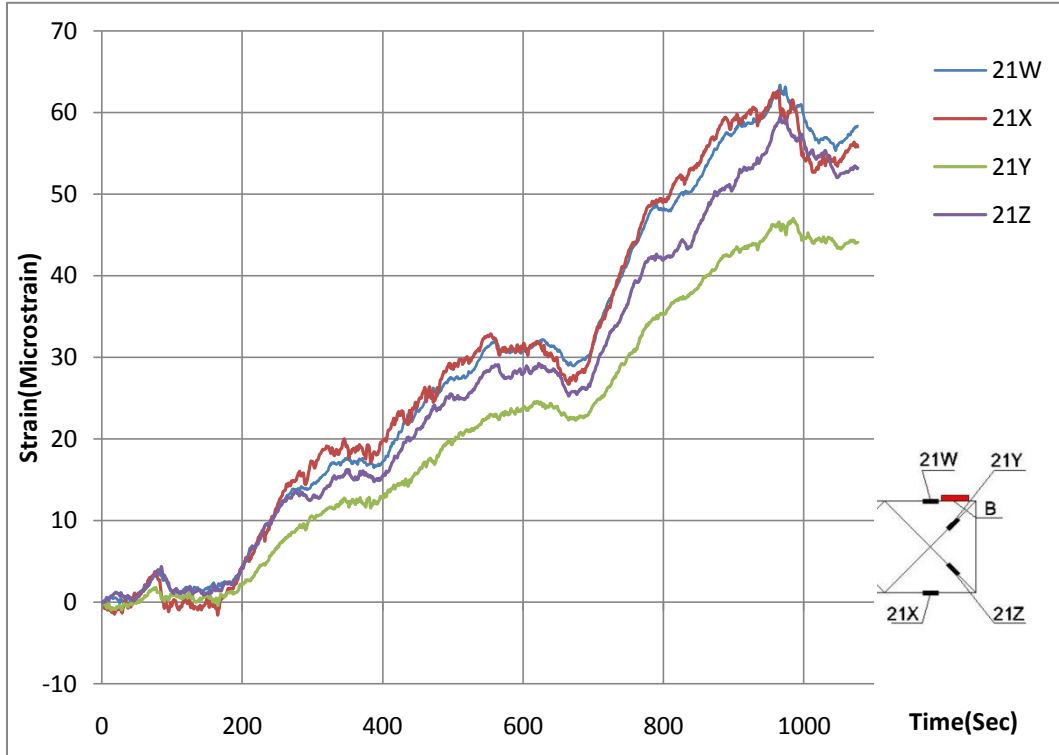


Figure 4.3: Strains in chords and diagonals at the top on February 26, 2009

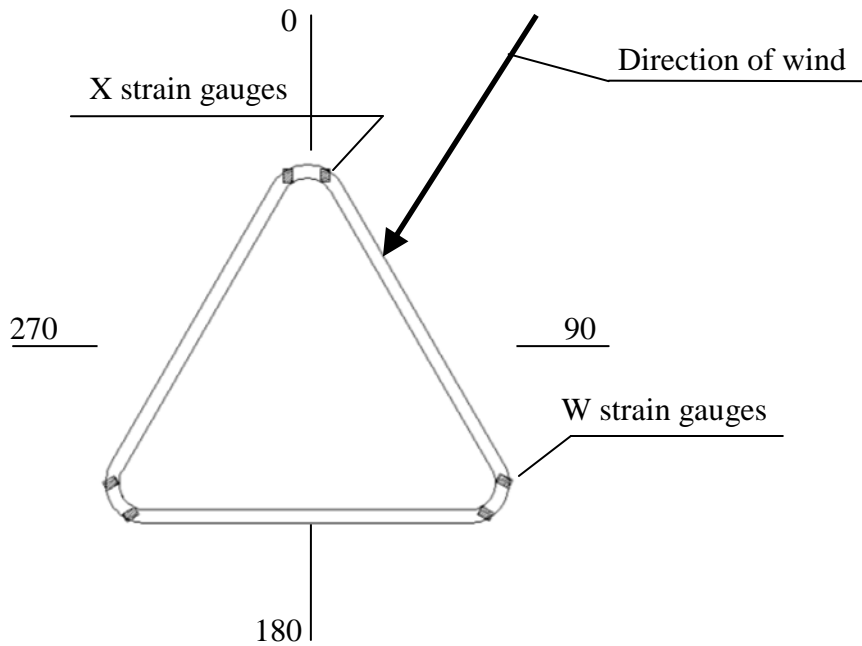


Figure 4.4: Location of strain gauges and major wind direction at 11:54-12:12 on February 26, 2009

The strain diagram shown in Figure 4.3 indicates that strain continuously increase in tension as well.

The strains recorded from February 12 to March 1, 2009 exhibit similar behaviors. The data recorded on February 13 and February 15 showed that the strains were relatively stable. The strains increased in compression on February 12(4:16-4:46pm), February 14, February 15(at 5:46-5:52pm), February 18, February 21, February 27, and March 1. The strains increased in tension on February 12 (11:36-11:52am), February 17, February 23, February 24, February 25, February 26 and February 28. The supplemental strain diagrams are shown in Appendix C. The strains recorded (compression or tension) were a function of the duration of the wind.

The strain values of the iced FRP lattice tower on February 27, 28 and March 1 were low. The strain values recorded for the top section on March 1, 2009 are shown in Figure 4.5.

The icing on the tower did not contribute significantly to the strain values. The results were varied from the 14 microstrain in tension to -10 microstrain in compression, as shown in Figure 4.5.

The low strain values can be attributed to relatively low wind velocity on March 1. The wind direction and wind speed are shown in Figure B- 23 and Figure B- 24 of Appendix B.

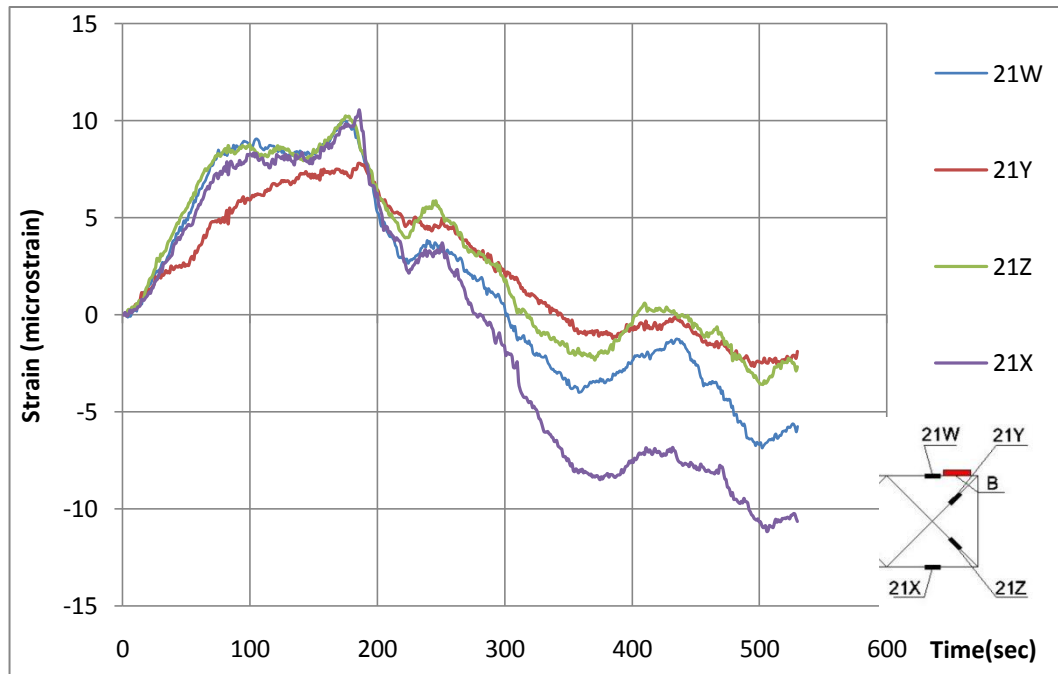


Figure 4.5: Strains in chords and diagonals at the top of the iced FRP tower on March 1, 2009

As was mentioned earlier the maximum tensile strain recorded by the strain gauge 21W was equal to 86 microstrain, which corresponds to a stress equal to 2.19 MPa. The maximum compressive strain was recorded by strain gauge 21W on February 12, 2009. It was equal to -36.8 microstrain. This strain corresponds to 0.936 MPa compressive stress using the value of the modulus of elasticity in the longitudinal direction equal to $E_1 = 25.44$ GPa. This stress accounts 0.27 % of the ultimate compressive strength in longitudinal direction equal to $F_1^{cu} = 342.7$ MPa (Burachinsky, 2006).

The results indicate that maximum strain values were low because of the low loads and the corresponding maximum stresses were well below maximum compressive and tensile strength limits.

4.2 Vibrations

4.2.1 Theoretical background

Natural frequencies and their mode shapes are important to assess if the structure is subject to large dynamic amplifications. The guyed towers can be excited in many modes due to their non-linear behavior and up to 15 vibration modes can contribute significantly to the response of the structure (Sparling & Wegner, 2006; Smith, 2007). Non-linear behavior is attributed to the change in cable stiffness with the change of guy wire tension (Wahba et al., 1998). Madugula et al. (1998) reported that increase in initial guy wire tension results in significant natural frequency increase. The height of the guyed mast has the greatest influence on the lowest natural frequencies as well.

According to Madugula et al. (1998) and Wahba et al. (1998) icing of the guyed towers results in significant reduction of natural frequencies, due to increased mass, making them more vulnerable to dynamic wind effects even at low wind speed. These authors also reported considerable increase in coupling action between the motion of the mast and guy wires and magnifying effect of guy motion on the tower were as well.

Galloping of the guy cables frequently observed when the guy cables are iced and usually in steady and low wind speeds. The motion of the heavily iced guys can generate negative aerodynamic damping that feeds additional energy into the system, therefore introducing source of potential instability (Madugula, 2002). Novak et al. (1978) reported that accretion of ice on the guy cables lead to galloping of the guys, resulting in high stress levels throughout a structure. Saxena et al. (1989) described several cases

when icing combined with moderate wind resulted in misalignment and failures of the towers. Fahleson (1995) reported strong dynamic effects observed on the guy cables.

4.2.2 Results

The FRP lattice tower was instrumented with two three-axis accelerometers located at 3.65 m and 7 m above the ground. The accelerations of the tower were recorded simultaneously with the strains and wind load. A measured acceleration response was recorded in three orthogonal local directions XYZ by the data acquisition system, as shown in Figure 4.6.

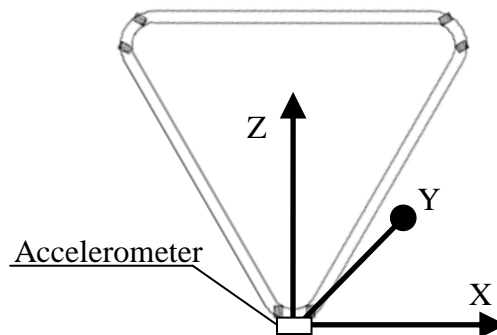


Figure 4.6: Directions of measured accelerations

The Data Processing Program developed by National Instruments was used to apply Fast Fourier Transform (FFT) to the acceleration signal to evaluate the power density distribution against the frequency domain.

Power spectra of the measured acceleration responses of the guyed FRP tower for February 17, 23 and 26 are shown in Figure 4.7 to 4.11.

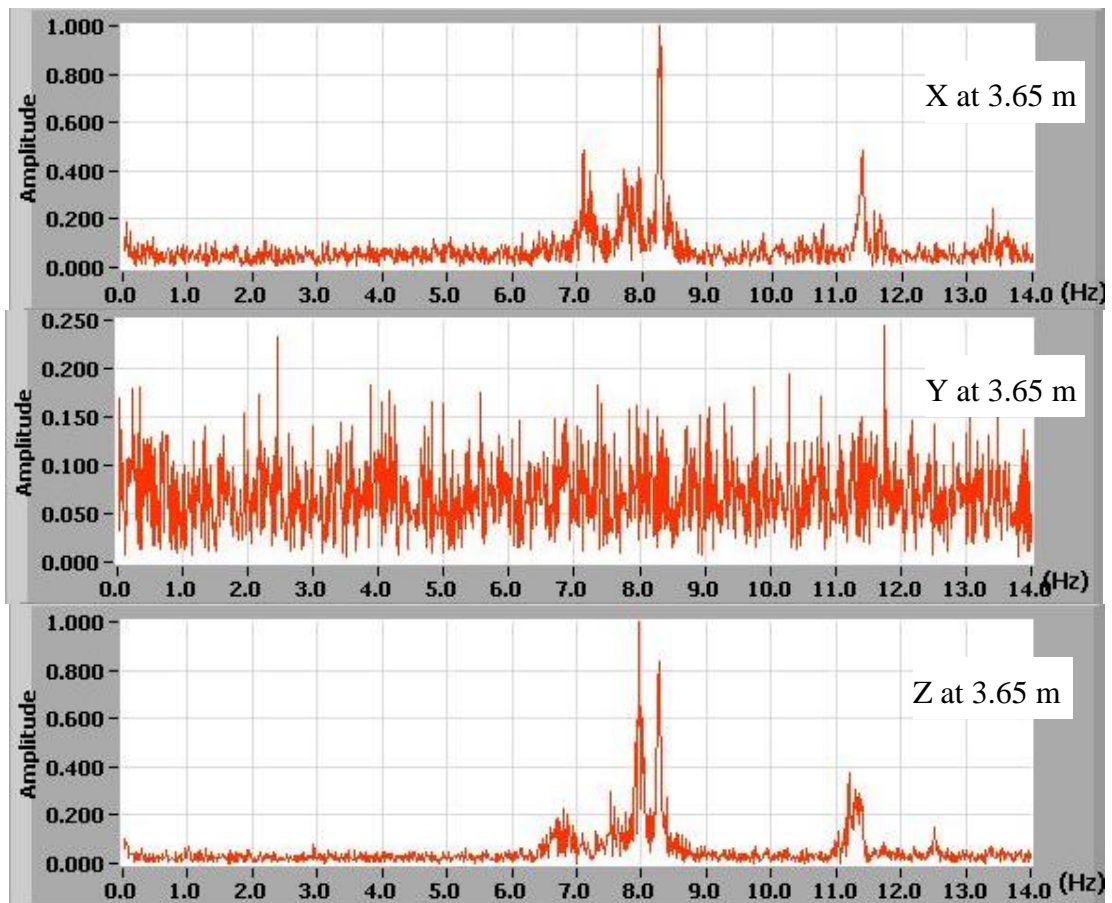


Figure 4.7: Vibration frequency spectrum of FRP tower at 3.65 m on February 17, 2009

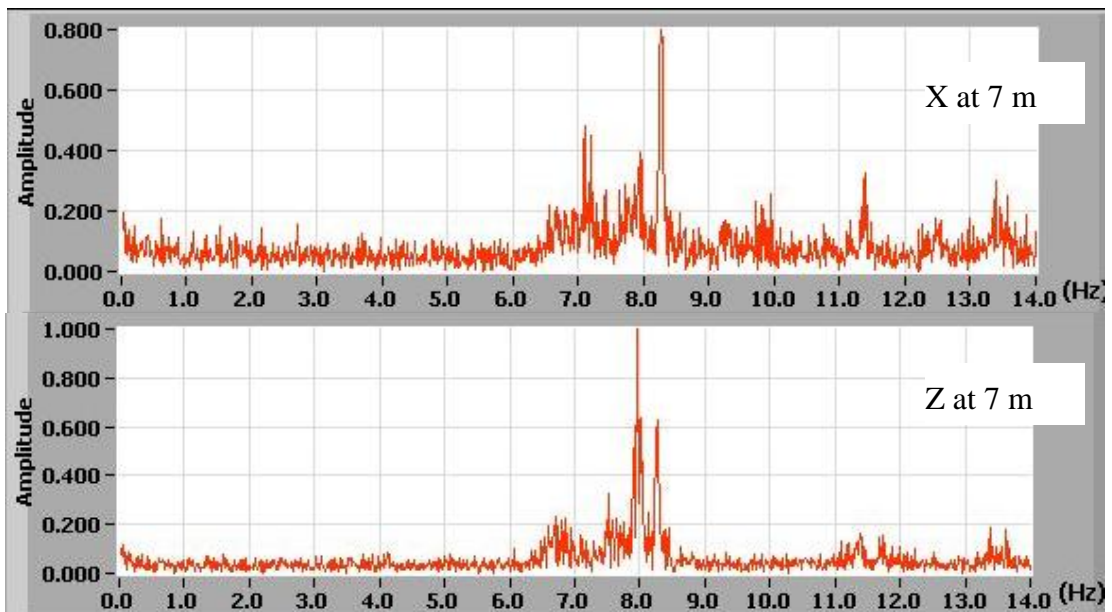


Figure 4.8: Vibration frequency spectrum of FRP tower at 7 m on February 17, 2009

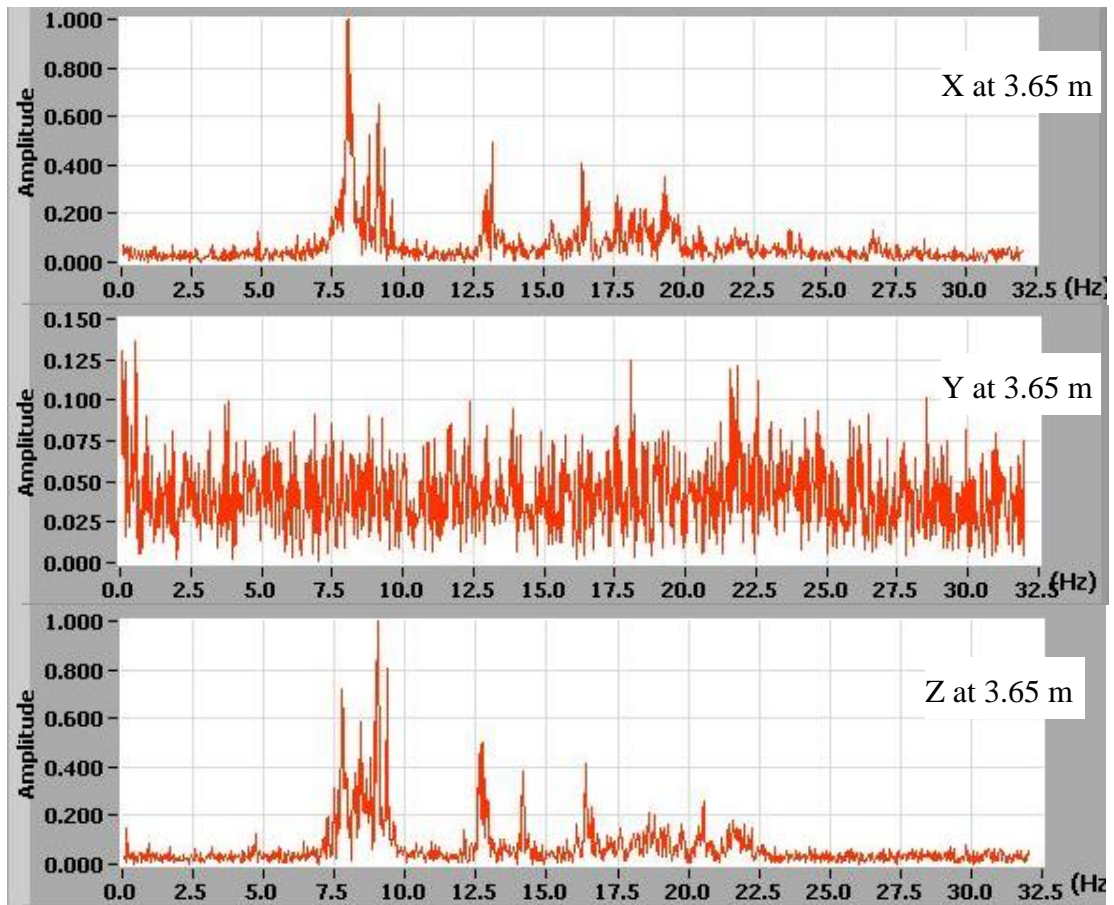


Figure 4.9: Vibration frequency spectrum of FRP tower at 3.65 m on February 23, 2009

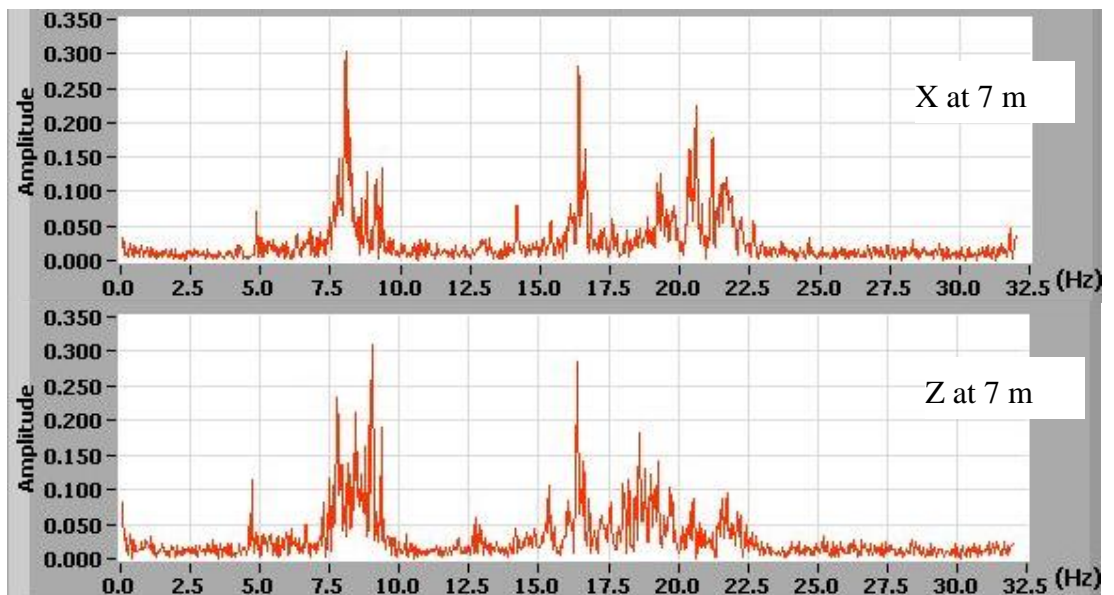


Figure 4.10: Vibration frequency spectrum of FRP tower at 7 m on February 23, 2009

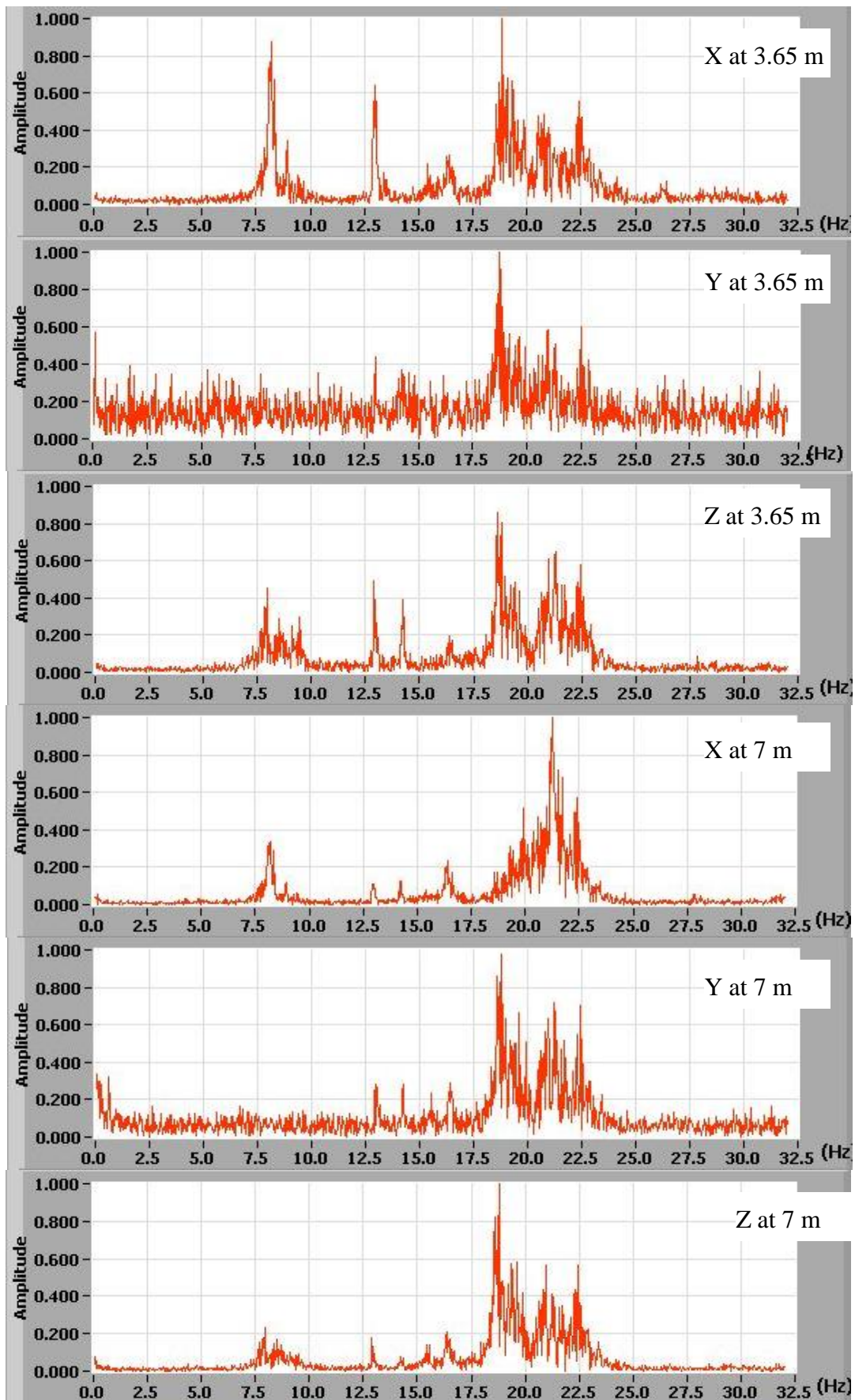


Figure 4.11: Vibration frequency spectrum of FRP tower on February 26, 2009

The spectra of measured acceleration responses to detect vibration modes of the guyed FRP tower indicate various peak responses in the X direction at both 3.65 m and 7 m at 7.08, 8.27 and 11.38 Hz on February 17. It should be pointed out that the vibrations in Y direction were minimal, as shown in Figure 4.7. The spectra of acceleration in Z direction at 3.65 m and 7 m show excitation peaks at 7.95, 8.25 and 11.21 Hz.

Vibration frequency spectra of the guyed FRP tower on February 23 are shown in Figure 4.9 and 4.10. The spectra of acceleration in the X direction at 3.65 m and 7 m peaked at 8.06, 9.12 and 13.15 Hz; however, the predominant peaks were observed at 8.06 Hz at 3.65 m and 7 m above the ground. Spectral peaks in Y direction were not significant. The excitation modes in Z direction were observed at 7.78, 8.4, 9.03, 16.37 Hz for both 3.65 and 7 m levels; however, the dominant peaks were observed to be at 9.03 Hz at 3.65 and 7 m. It should be pointed out that amplitude range was lower at 7 m height compared to 3.65 m level, as shown in Figure 4.10.

The significant excitation mode in the Y direction was observed on February 26, as shown in Figure 4.11. Spectral peak was recorded at 18.7 Hz at 3.65 and 7 m height.

Vibration frequency spectra of the iced FRP tower on February 27, 28 and March 1, 2009 are shown in Figure D- 12 to D-14. The results indicate that the amplitude of the vibration peaks at 3.65 m level was lower. It can be attributed to increased tower weight and lower wind speed; however, the dominant excitation mode was observed around 8 Hz.

The vibration frequency spectra indicate the closely spaced excitation modes of the guyed FRP tower and multimodal number of excitations. The fundamental mode of

vibration alone does not govern the design, as the modes are not well separated and many modes may contribute to the response of the structure to turbulent wind.

The modal and harmonic analysis was carried out by Ochonski (2009) for 8.53 m (28 ft) guyed FRP lattice tower to obtain natural frequencies and associated mode shapes. The first eight modes of modal analysis have associated natural frequency at 0.17 Hz, 4.292 Hz, 4.308 Hz, 11.351 Hz, 12.177 Hz, 12.219 Hz, 23.446 Hz, 23.595 Hz, respectively. The results from the harmonic analysis showed natural frequencies 4.292 Hz, 11.351 Hz, 12.177 Hz 23.466 Hz for mode 2, mode 4, mode 5, and mode 7, respectively. The first natural frequency obtained from laboratory tests was equal to 4.31 Hz. The first natural frequency of the analyzed 45 m FRP tower was 0.219 Hz, which is lower by a factor of 20.

The natural frequencies obtained from the field testing of the FRP tower are within the range of those reported by Ochonski (2009), the difference can be attributed to smaller tower section and higher pretension of guy cables. It should be also pointed out that it is difficult to differentiate between the movement simply caused by gust pressure fluctuations and resonant vibrations, meaning that not all of the peaks are necessarily natural frequencies of the system. Some are merely due to the fact that the wind gusts are changing with time.

At present, dynamic response is not considered in any way in design, according to CSA S37-01 (CSA, 2001). Therefore, natural frequencies are not used in design, with the possible exception of earthquake loading provisions (which are only referred to in an Appendix to the standard) (Sparling,2010). However obtained values can be used as a

reference in a future dynamic analysis of similar guyed FRP lattice towers, since the lattice tower tested at the University of Manitoba is the first of its kind.

The supplemental vibration frequency spectra are provided in Appendix D.

4.3 Icing tunnel test results

4.3.1 Test 1. Accumulation of glaze icing on the FRP section at 90 degree angle.

The FRP tower section was placed in the icing tunnel at 90 degree angle to the icing wind, as shown in Figure 3.29.

The ice accumulation on the members of the FRP tower segment is shown in Figure 4.12.



(a) Thickness of the glaze ice



(b) Measured thickness of the glaze ice

Figure 4.12: Test 1-glaze ice accumulation on the members of FRP tower section at 90 degree angle



(c) Front view of the iced section



(d) Side view of the iced section

Figure 4.12 (continued): Test 1-glaze ice accumulation on the members of FRP tower section at 90 degree angle

After 45 min in the icing tunnel, ice thickness varied from 6.35 mm ($\frac{1}{4}$ in) to 31.75 mm ($1 \frac{1}{4}$ in). The ice accreted on the windward side and no ice accumulation was observed on the leeward side. The heaviest accumulation was observed in the middle of the tower surface and the ice thickness gradually decreased towards the end of area affected by wind flow, as shown in Figure 3.32. The overall appearance of the glaze ice found to be similar to the one observed in nature. The accreted glaze ice found to be transparent, with cylindrical icicles growing into the wind, strong adhesion to the surface and strong cohesion. The ice often was removed from the tower section in a single piece which measured more than 300 mm in length, as shown in Figure 4.13.



Figure 4.13: Removed pieces of glaze ice

The total ice accumulation in water equivalent was measured 840 ml or 840 grams. It corresponds to an ice mass of approximately 1.87 kg per meter of tower length. The glaze ice built up was the heaviest among other types of ice because of the high water content.

4.3.2 Test 2. Accumulation of soft rime icing on the FRP section at 90 degree angle.

In the test the section remained at 90 degree angle, however air water content and temperature were modified, as described in Section 3.3.2. Figure 4.14 shows soft rime ice accumulation on the members of FRP tower section.



(a) Measured thickness
of the soft rime ice

Figure 4.14: Test 2-soft rime ice accumulation on the members of FRP tower section at 90 degree angle



(b) Front view of the iced section



(c) Side view of the iced section

Figure 4.14(continued): Test 2-soft rime ice accumulation on the members of FRP tower section at 90 degree angle

Due to the lower water content and lower temperature the rime ice buildup was not as intensive as the glaze ice buildup in Test 1. The ice thickness varied from 12.7 mm ($\frac{1}{2}$ in) to 19.05 mm ($\frac{3}{4}$ in). The accreted rime ice appeared white in color, flaky, with low cohesion and medium adhesion to the tower surface. Ice pennants accreted on windward side only. The ice accretion had a minimum ice thickness at the stagnation line and ‘horns’ were grown on both sides of this line on the surfaces perpendicular to the wind direction, as shown in Figure 4.15. However on the inclined diagonal members this phenomenon was not observed. A similar observation was made by Makkonen & Oleskiw (1997) on small scale experiments on rime icing.

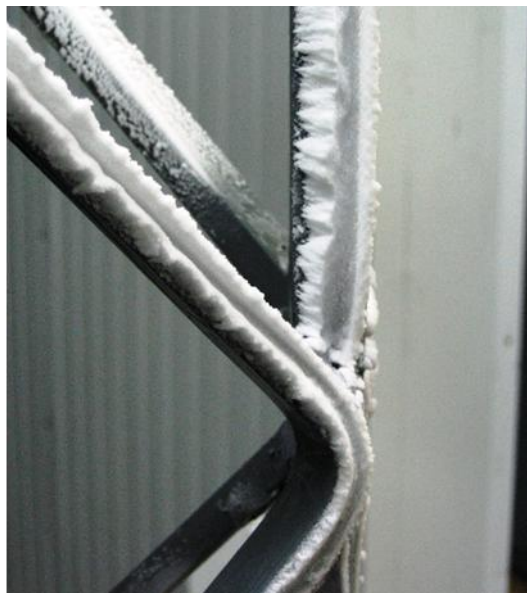


Figure 4.15: Appearance of rime ice on the members of FRP tower

The total ice accumulation in water equivalent was measured to be 100 ml or 100 grams. It corresponds to an ice mass of approximately 0.22 kg per meter of tower length. The estimation was based on 100 grams per 450 mm length of tower tested. The rime ice buildup was the lightest among other types of ice because of the low water content and low temperature.

4.3.3 Test 3. Accumulation of hard rime icing on the FRP tower section at 90 degree angle.

The conditions for this test were similar to those in Test 2, but the wind speed was increased to 25 m/s the reference velocity wind speed used by Manitoba Hydro in their specifications. It corresponds to a reference velocity pressure of 403 Pa. The rime ice thickness varied from 6.35 mm ($\frac{1}{4}$ in) to 12.7 mm ($\frac{1}{2}$ in). Figure 4.16 shows accumulation of the hard rime ice on the members of the FRP tower.



(a) Hard rime ice accretion on chords and diagonals

(b) Front view of the iced section

Figure 4.16: Test 3-hard rime ice accumulation on the members of FRP tower section at 90 degree angle.

Hard rime ice is solid, opaque, with the sharp edges and extremely difficult to remove. A stronger ice adhesion force was observed due to the higher wind speed when compared to results from Tests 1 and 2.

Figure 4.17 shows accumulation of soft rime ice at 5 m/s and hard rime ice at 25 m/s wind speed. The ‘knife’ edge shape of hard rime ice can be attributed to the rime surface erosion, which becomes significant at wind speeds near 20 meters per second (Makkonen & Oleskiw, 1997).

Ice accumulation in liquid water equivalent was measured 220 ml or 220 grams. It corresponds to an ice load of approximately 0.49 kg per meter of tower length. The hard rime ice built up was the second after glaze ice because of the higher wind speed.

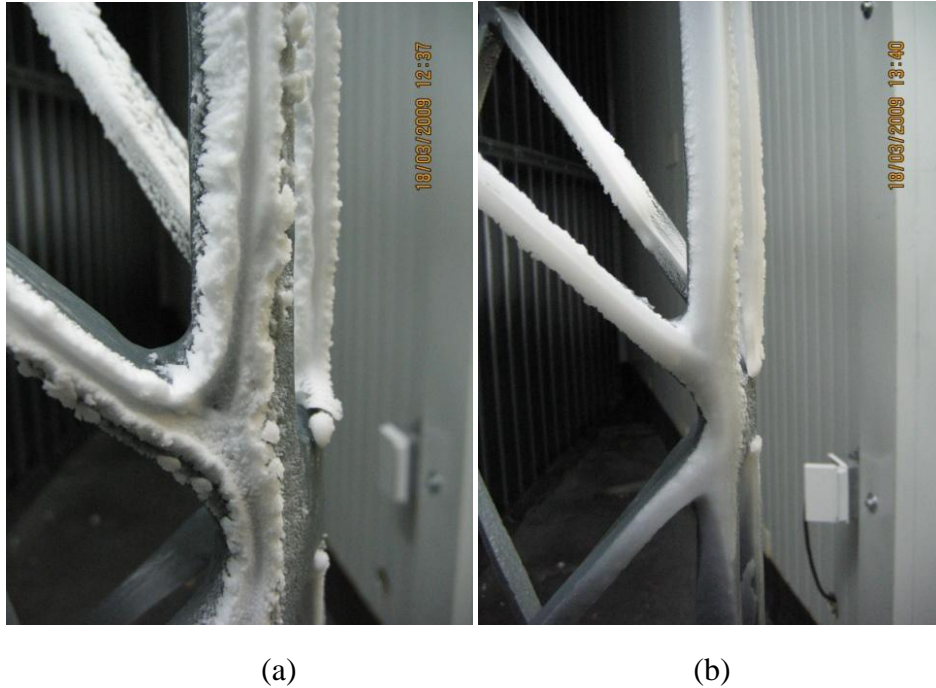


Figure 4.17: Soft rime ice accumulation at the wind speed of 5 m/s (a) and hard rime ice accumulation at the wind speed of 25 m/s (b)

4.3.4 Test 4. Accumulation of glaze icing on the steel section at 90 degree angle.

Test 4 is a repeat of test 1 with the exception that the steel section was tested instead of FRP section. The process of design and manufacturing of the steel tower section, which is nearly identical to FRP segment, is described in Section 3.3.1. The ice built up thickness varied from 6.35 mm ($\frac{1}{4}$ in) to 31.75 mm (1 $\frac{1}{4}$ in). The ice accumulation in water equivalent was measured 730 ml or 730 grams, which corresponds to an ice mass of approximately 1.62 kg per meter of tower length.

The measured liquid mass is slightly higher in the FRP tower section than the steel section, as shown in Table 4.1. This could be due to the larger sectional properties of

chord members in the FRP tower (19.05 mm x 19.05 mm) than the steel chord member (13 mm x 19.05 mm). The appearance of the glaze ice on the steel tower section is similar to that in FRP section. The glaze ice accumulation on the members of the steel tower at 90 degree angle is shown in Figure 4.18.

Table 4.1: Accumulation of glaze ice on steel and FRP tower sections at 90 degree angle

Tower section	Total accreted mass of glaze ice, (g)	Max. ice thickness, mm	Mass of glaze ice per unit length, (kg/m)
Steel	730	31.75	1.62
FRP	840	31.75	1.87



Figure 4.18: Test 4-glaze ice accumulation on the steel tower section at 90 degree angle.

4.3.5 Test 5. Accumulation of soft rime icing on the steel tower section at 90 degree angle.

Test 5 is a repeat of test 2 with exception of that the steel tower segments was tested. The shape and appearance of soft rime ice were similar to those observed in test 2 and are shown in Figure 4.19.



(a) Measured thickness of the soft rime ice

(b) Appearance of the soft rime ice

Figure 4.19: Test 5-soft rime ice accumulation on the steel tower section at 90 degree angle.

The thickness of the soft rime ice varied from 12.7 mm ($\frac{1}{2}$ in) to 15.9 mm ($\frac{5}{8}$ in). The ice accumulation in liquid equivalent form was measured to be 82 ml or 82 grams. It corresponds to an ice mass of approximately 0.18 kg per meter of the tower length.

The comparison of accreted ice values on steel and FRP tower sections is shown in Table 4.2.

Table 4.2: Accumulation of soft rime ice on steel and FRP tower sections at 90 degree angle

Tower section	Total accreted mass of soft rime ice, (g)	Max. ice thickness, mm	Mass of soft rime ice per unit length, (kg/m)
Steel	82	15.9	0.18
FRP	100	19.05	0.22

The results indicate that the weight of soft rime accreted on FRP tower is 18 % higher than the one accreted on the steel tower. As it was mentioned before chord members of FRP segment are slightly wider than the corresponding members of steel segment. Accretion of the soft rime ice was the lightest accumulation among other types of ice on the members of both steel and FRP segments. It can be explained by low water content and low temperature. However rime ice has a tendency to fill the empty space within the lattice tower and grow into solid structure, increasing wind drag coefficient (ISO, 2001; Smith, 2007).

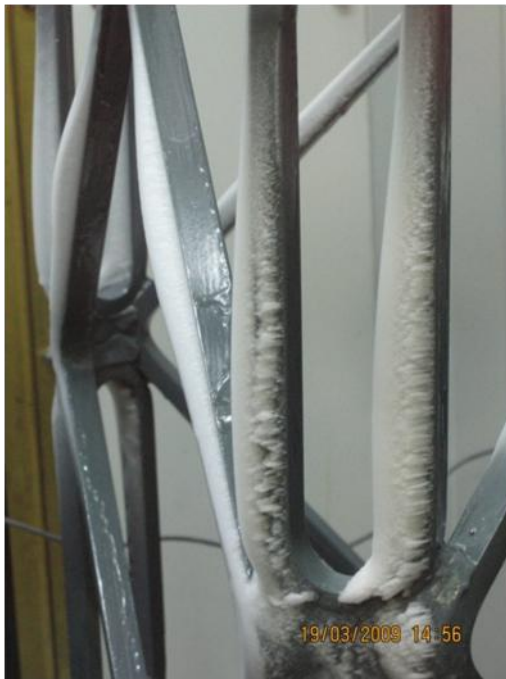
4.3.6 Test 6. Accumulation of hard rime icing on the steel section at 90 degree angle.

The experimental set-up was similar to Test 3 with exception of steel segment being tested. The spraying of the steel section lasted 45 min. The shape and appearance of hard rime ice were found similar to those observed in Test 3.

The accumulation of the hard rime ice on the members of the steel tower is shown in Figure 4.20.



(a) Measured thickness of the hard rime ice



(b) Side view of the iced section



(c) Appearance of the hard rime ice

Figure 4.20: Hard rime ice accumulation on the members of the steel tower section at 90 degree angle

The ice thickness varied from 6.35 mm ($\frac{1}{4}$ in) to 12.7 mm ($\frac{1}{2}$ in). Similar to Test 3, the ice adhesion force was higher than the one in Tests 4 and 5. Ice accumulation in water equivalent was measured to be 212 ml or 212 grams. It corresponds to an ice mass of approximately 0.47 kg per meter of the tower length.

The results from Test 3 and 6 are summarized in Table 4.3.

Table 4.3: Accumulation of hard rime ice on steel and FRP tower sections at 90 degree angle

Tower section	Total accreted mass of hard rime ice, (g)	Max. ice thickness, mm	Mass of hard rime ice per unit length, (kg/m)
Steel	212	12.7	0.47
FRP	220	12.7	0.49

The FRP tower section accreted more ice than the steel section, as shown in Table 4.3. It can be attributed to a higher solidity ratio of the FRP segment, which is defined as ratio of net area of the face of the structure to the gross area of the face of the structure, than the corresponding solidity ratio of the steel section, as discussed previously. The weight of hard rime ice was the second largest after the weight of glaze ice, shown in Table 4.1. The measured ice thickness in Tests 3 and 6 was lower than the one measured in Tests 2 and 5, but the weight per meter of length was higher because of higher density.

4.3.7 Accumulation of icing at 0 and 30 degree angles to the face.

The test setup for tests at 0 and 30 degree angles to the face was similar to those in Tests 1 to 6, but the orientation of the tower segments was changed to 0 and 30 degrees, as shown in Figure 3.29.

The appearance and shape of the accreted ice was found to be identical to those in Tests 1 to 6. The experimental results are summarized in Table 4.4 to 4.9.

The accumulated amounts of glaze, soft rime and hard rime ice at 0 degree angle on the members of steel and FRP tower sections are shown in Table 4.4 to 4.6. Ice accretion at 0 degree angle was almost 50 % lower than the accretion on the members at 30 and 90 degree angles, respectively. The lower rates may be due to shielding of the tower face parallel to the wind direction, as shown in Figure 3.29. Glaze ice accretion was slightly higher on the steel tower section, as shown in Table 4.4. It can be attributed to fabrication differences between the two types of tower, leading to a higher accretion at 0 degree angle.

Results for glaze, soft rime and hard rime icing accreted at 30 degree angle on the members of steel and FRP tower sections are shown in Table 4.7 to 4.9. As expected the highest ice accretion was observed for the glaze ice on the FRP tower section. The glaze ice accumulation in water equivalent was measured to be 850 ml or 850 grams. It corresponds to an ice mass of, approximately, 1.89 kg per meter of the tower length, which was the highest value observed in all tests.

The estimated mass of ice per unit length does not imply a uniform distribution around the section, as the ice formed only on the windward side of the members, but they can be used as reference accretion amounts for this type of lattice structure.

Table 4.4: Accumulation of glaze ice on steel and FRP tower sections at 0 degree angle

Tower section	Total accreted mass of glaze ice, (g)	Max. ice thickness, mm	Mass of glaze ice per unit length, (kg/m)
Steel	543	31.75	1.21
FRP	446	31.75	0.99

Table 4.5: Accumulation of soft rime ice on steel and FRP tower sections at 0 degree angle

Tower section	Total accreted mass of soft rime ice, (g)	Max. ice thickness, mm	Mass of soft rime ice per unit length, (kg/m)
Steel	50	12.7	0.11
FRP	52	12.7	0.115

Table 4.6: Accumulation of hard rime ice on steel and FRP tower sections at 0 degree angle

Tower section	Total accreted mass of hard rime ice, (g)	Max. ice thickness, mm	Mass of hard rime ice per unit length, (kg/m)
Steel	128	12.7	0.284
FRP	146	12.7	0.324

Table 4.7: Accumulation of glaze ice on steel and FRP tower sections at 30 degree angle

Tower section	Total accreted mass of glaze ice, (g)	Max. ice thickness, mm	Mass of glaze ice per unit length, (kg/m)
Steel	802	31.75	1.78
FRP	850	31.75	1.89

Table 4.8: Accumulation of soft rime ice on steel and FRP tower sections at 30 degree angle

Tower section	Total accreted mass of soft rime ice, (g)	Max. ice thickness, mm	Mass of soft rime ice per unit length, (kg/m)
Steel	116	12.7	0.26
FRP	100	12.7	0.22

Table 4.9: Accumulation of hard rime ice on steel and FRP tower sections at 30 degree angle

Tower section	Total accreted mass of hard rime ice, (g)	Max. ice thickness, (mm)	Mass of hard rime ice per unit length, (kg/m)
Steel	248	12.7	0.55
FRP	270	12.7	0.6

The results from the icing tunnel testing of FRP and steel tower segments at 0, 30 and 90 degree angles are summarized in Table 4.10-4.12.

Table 4.10: Total accreted masses of ice at 0, 30 and 90 degree angles, (grams)

Icing type	Material type	0 degrees	30 degrees	90 degrees
Glaze	Steel	543	802	730
	FRP	446	850	840
Soft Rime	Steel	50	116	82
	FRP	52	100	100
Hard Rime	Steel	128	248	212
	FRP	146	270	220

Table 4.11: Maximum ice thicknesses of ice at 0, 30 and 90 degree angles, (mm)

Icing type	Material type	0 degrees	30 degrees	90 degrees
Glaze	Steel	31.75	31.75	31.75
	FRP	31.75	31.75	31.75
Soft Rime	Steel	12.7	12.7	15.9
	FRP	12.7	12.7	19.05
Hard Rime	Steel	12.7	12.7	12.7
	FRP	12.7	12.7	12.7

Table 4.12: Masses of ice per unit length at 0, 30 and 90 degree angles, (kg/m)

Icing type	Material type	0 degrees	30 degrees	90 degrees
Glaze	Steel	1.21	1.78	1.62
	FRP	0.99	1.89	1.87
Soft Rime	Steel	0.11	0.26	0.18
	FRP	0.115	0.22	0.22
Hard Rime	Steel	0.284	0.55	0.47
	FRP	0.324	0.6	0.49

4.4 Evaluation of effectiveness of the icephobic coating Wearlon Super F-1 Ice.

Both the steel and the FRP tower segments were coated with one layer of icephobic coating Wearlon Super F-1 Ice as shown in Figure 3.34. The description of this low friction coating is provided in Section 3.3.3. The segments were tested at 90 degree angle to the wind direction in the Icing and Wind Tunnel Facility. Experiments included accumulation of the glaze ice, soft rime, and hard rime ice. The test setup was similar to that used in Tests 1 to 6.

The results from the glaze ice test are summarized in Table 4.13.

Table 4.13: Accumulation of glaze ice on steel and FRP tower sections coated with Wearlon Super F-1 Ice at 90 degree angle

Tower section	Total accreted mass of glaze ice, (g)	Max. ice thickness, mm	Mass of glaze ice per unit length, (kg/m)
Steel	734	38.1	1.63
FRP	724	31.75	1.61

The thickness of the glaze ice on steel tower section varied from 31.75 mm (1 ¼ in) to 38.1 mm (1 ½ in). The ice accumulation in liquid equivalent form was measured to be 734 ml or 734 grams. It corresponds to an ice mass of, approximately, 1.63 kg per meter of the tower length. No reduction of ice accretion on the steel section was observed and recorded values are nearly identical to those obtained in Test 4. Accreted glaze ice on the steel tower section is shown in Figure 4.22.

Formation of icicles was observed during the accretion of glaze ice on the FRP tower section. The ice thickness varied from 25.4 mm (1 in) to 31.75 mm (1 ¼ in), as shown in Figure 4.21.



(a) Appearance of the glaze ice on FRP section



(b) Measured thickness of the glaze ice on the FRP section

Figure 4.21: Glaze ice accumulation on the FRP tower section coated with Wearlon Super F-1 Ice at 90 degree angle.



(a) Accretion of glaze ice



(b) Measured thickness of the glaze ice

Figure 4.22: Glaze ice accumulation on the steel tower section coated with Wearlon Super F-1 Ice at 90 degree angle.

It should be pointed out that there was a 14 % reduction in ice accretion compared to values obtained in Test 1. Easier ice removal was also facilitated due to lower surface adhesion strength, which was empirically observed, but not quantified.

The accumulated amounts of soft rime ice on the members of steel and FRP tower segments are shown in Table 4.14.

Table 4.14: Accumulation of soft rime ice on steel and FRP tower sections coated with Wearlon Super F-1 Ice at 90 degree angle

Tower section	Total accreted mass of soft rime ice, (g)	Max. ice thickness, mm	Mass of soft rime ice per unit length, (kg/m)
Steel	126	15.8	0.28
FRP	117	15.8	0.26

Rime ice thickness varied from 12.7 mm (½ in) to 15.8 mm (5/8 in) for both steel and FRP segments, as shown in Figure 4.24 and 4.24. The accreted mass of soft rime ice on the steel segment was measured to be 126 ml or 126 grams in liquid equivalent form. This corresponds to an ice mass of approximately 0.28 kg per meter of tower length. The ice accumulation in liquid equivalent form for FRP section was 117 ml or 117 grams. It corresponds to an ice mass of approximately 0.26 kg per meter of tower length. Results indicate that there was no reduction in ice accumulation; moreover, the accreted masses are higher than those observed in Tests 2 and 5. Change in adhesive strength was not observed.

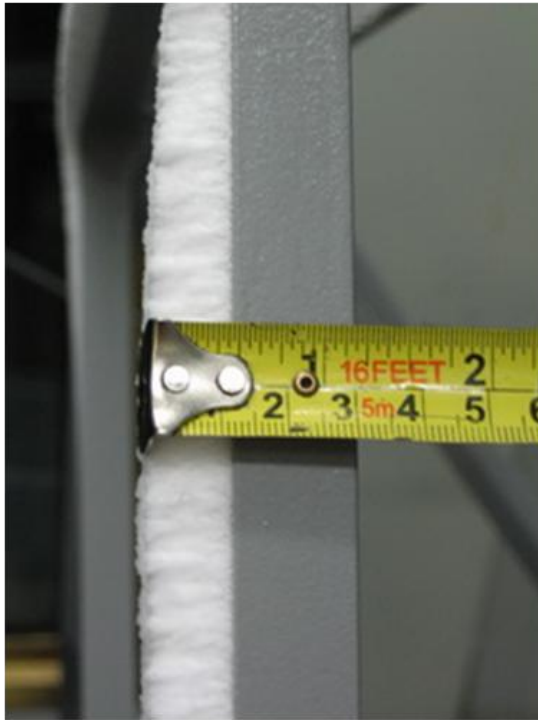


(a) Accretion of the soft rime ice on the diagonal



(b) Measured thickness of the soft rime ice on the FRP section

Figure 4.23: Soft rime ice accumulation on the FRP tower section coated with Wearlon Super F-1 Ice at 90 degree angle



(a) Accretion of the soft rime ice on the diagonal



(b) Measured thickness of the soft rime ice on the steel section

Figure 4.24: Soft rime ice accumulation on the steel tower section coated with Wearlon Super F-1 Ice at 90 degree angle

The measured values of accumulated hard rime ice on the members of steel and FRP tower sections coated with icephobic coating are shown in Table 4.15 .

Table 4.15: Accumulation of hard rime ice on steel and FRP tower sections coated with Wearlon Super F-1 Ice at 90 degree angle

Tower section	Total accreted mass of hard rime ice, (g)	Max. ice thickness, mm	Mass of hard rime ice per unit length, (kg/m)
Steel	283	15.8	0.63
FRP	220	15.8	0.49

Accumulated hard rime ice thickness varied from 12.7 mm ($\frac{1}{2}$ in) to 15.8 mm ($\frac{3}{4}$ in) for both steel and FRP segments, as shown in Figure 4.25 and 4.26. The accreted mass of hard rime ice on the steel segment was 283 ml or 283 grams in liquid equivalent form. This corresponds to an ice load of approximately 0.63 kg per meter of the tower length. The ice accumulation in liquid equivalent form for the FRP section was 220 ml or 220 grams, which corresponds to an ice load of approximately 0.49 kg per meter of the tower length. Reduction of ice accretion was not observed, as obtained values are nearly identical to those obtained in Tests 3 and 6. Results indicate that no reduction in ice accumulation for the FRP segment and an increase of accreted mass was observed for the steel section. Since the wind velocity was 25 m/s, ice adhesion was extremely strong and could not be differentiated from that observed in Tests 3 and 6.

The summary of results comparing ice accretion on uncoated segments and coated with Wearlon Super F-1 Ice is presented in Table 4.16.

Table 4.16: Accretion of ice on uncoated segments and coated with Wearlon Super F-1 Ice at 90 degree angle

Icing type	Material type	Total accreted mass of ice, (g)		Max. ice thicknesses, mm		Mass of ice per unit length, (kg/m)	
		uncoated	Wearlon Super F-1 Ice	uncoated	Wearlon Super F-1 Ice	uncoated	Wearlon Super F-1 Ice
glaze	Steel	730	734	31.75	38.1	1.62	1.63
	FRP	840	724	31.75	31.75	1.87	1.61
soft rime	Steel	82	126	15.9	15.8	0.18	0.28
	FRP	100	117	19.05	15.8	0.22	0.26
hard rime	Steel	212	283	12.7	15.8	0.47	0.63
	FRP	220	220	12.7	15.8	0.49	0.49



Figure 4.25: Hard rime ice accumulation on the steel tower section coated with Wearlon Super F-1 Ice at 90 degree angle



Figure 4.26: Hard rime ice accumulation on the FRP tower section coated with Wearlon Super F-1 Ice at 90 degree angle

5 SUMMARY AND CONCLUSIONS

Atmospheric icing is a major design criterion for guyed lattice masts and transmission lines in cold regions.

The evaluation of icing design criteria for lattice towers was carried out through an extensive literature, including current design standards for latticed structures subjected to ice and wind load and/or a combination of both, field and laboratory work. None of the Standards in Table 2.10 evaluate dynamic effect of wind on the iced tower and variation of icing type with height above ground. Variation of icing amount with height is provided only in ISO 12494 (ISO, 2001) and ANSI/TIA-222-G (ANSI/TIA, 2005) Standards. The icing map in CSA S37-01 (CSA, 2001) has not been updated since 1986 (CSA, 1986).

The response of 7 m guyed FRP lattice tower and its sections subjected to this type of environmental load was investigated in this study.

Conclusions from the field testing of the FRP lattice tower:

The experimental program was conducted for prototype FRP guyed lattice tower 7 m tall to investigate its behavior under wind and/or ice loads. The tower was installed at the outdoor laboratory at the University of Manitoba and monitored from February 14 to March 1, 2009. The strain readings were collected by the strain gauges located along the tower span and accelerations were measured by two three axis accelerometers. Wind speed and direction were measured by an ultrasonic anemometer. Since no icing was observed, the tower was sprayed with water mist to obtain artificial glaze ice varied from 3 to 5 mm thick. The readings from the iced tower were recorded on February 27, 28 and March 1. All data were recorded by a portable DAQ and stored on a PC. The results were

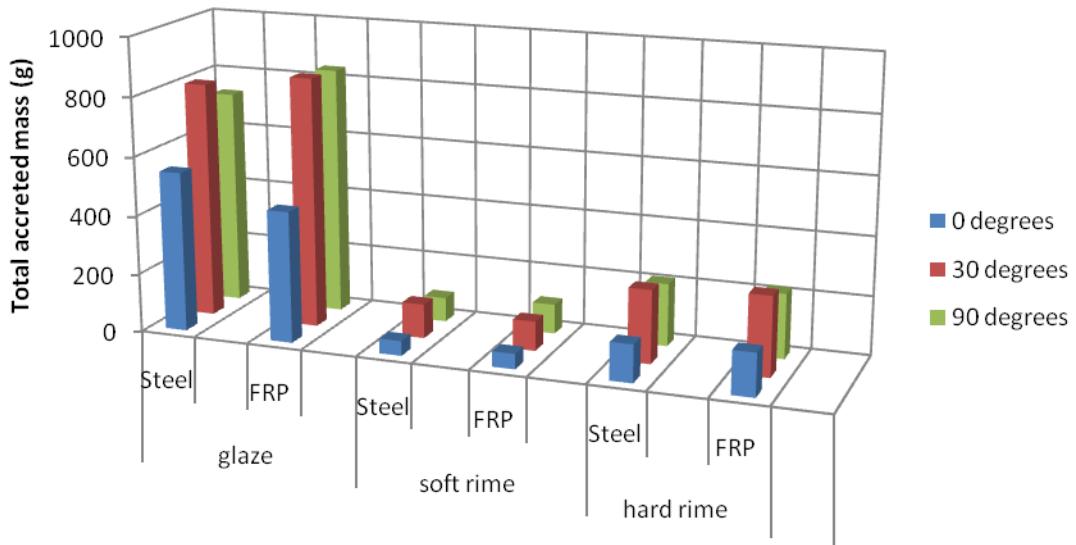
presented in the form of strain versus time diagrams and vibration frequency spectra for the FRP tower. The results showed that:

- The maximum tensile and compressive stresses recorded at the top of the FRP tower were 2.19 MPa and 0.936 MPa, respectively. These are quite small corresponding to 0.36 % and 0.27 % of the ultimate tensile and compressive strength of the material.
- The maximum tensile stress in diagonal was recorded at the top of the FRP tower and was equal 1.52 MPa. This stress accounts 0.25 % of the ultimate tensile strength in the longitudinal direction which is equal to $F_1^u = 610.2$ MPa.
- The constantly increasing strain, in either tension or compression, can be attributed to the extended period of relaxation of the material under fluctuating wind load.
- The iced FRP tower did not provide high strain values because of the low wind velocity.
- The vibration amplitude of the iced FRP tower was lower due to increased weight of the structure and lower wind velocity.
- At present, dynamic response is not considered in design, according to CSA S37-01 (CSA, 2001). Therefore, natural frequencies are not used in design, with the possible exception of earthquake loading provisions. However, values obtained through testing can be used as a reference to analyze of similar guyed FRP lattice towers, since the lattice tower tested at the University of Manitoba is the first of its kind.

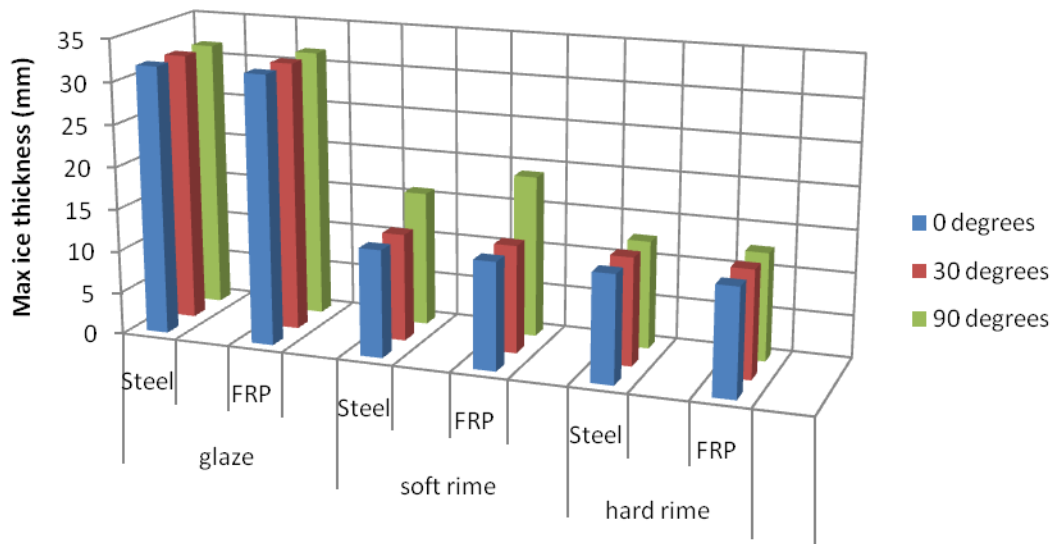
Conclusions from the icing tunnel testing of the FRP and steel lattice tower segments:

The accumulation of glaze, soft rime and hard rime icing was investigated for members of steel and FRP lattice tower sections at the University of Manitoba Icing and Wind Tunnel. The segments were tested at 0, 30 and 90 degree angles to the wind. Accreted ice was measured, photographed and melted to obtain the liquid water equivalent. Measured values were converted into relative ice loads per meter length of the tower. The results are summarized below.

- The heaviest accretion was observed for the glaze ice as shown in Figure 5.1a. The results confirm that the glaze ice is the dominant type of ice load as shown in the Standards summarized in Table 2.10.
- Based on the test results in this study the maximum ice thickness of glaze ice equal to 32 mm for both FRP and steel was observed. Thus, similar ice loads as those used in steel structures are recommended for the analysis of guyed FRP towers.
- The lowest ice accretion was observed at 0 degrees because of the shielded face parallel to the wind. The prevailing wind direction at the site is known normally, so it is desirable to position the communication towers and cables so that the wind load and ice accretion are minimized.
- The overall shape and appearance of glaze, soft rime and hard rime icing types were simulated well.

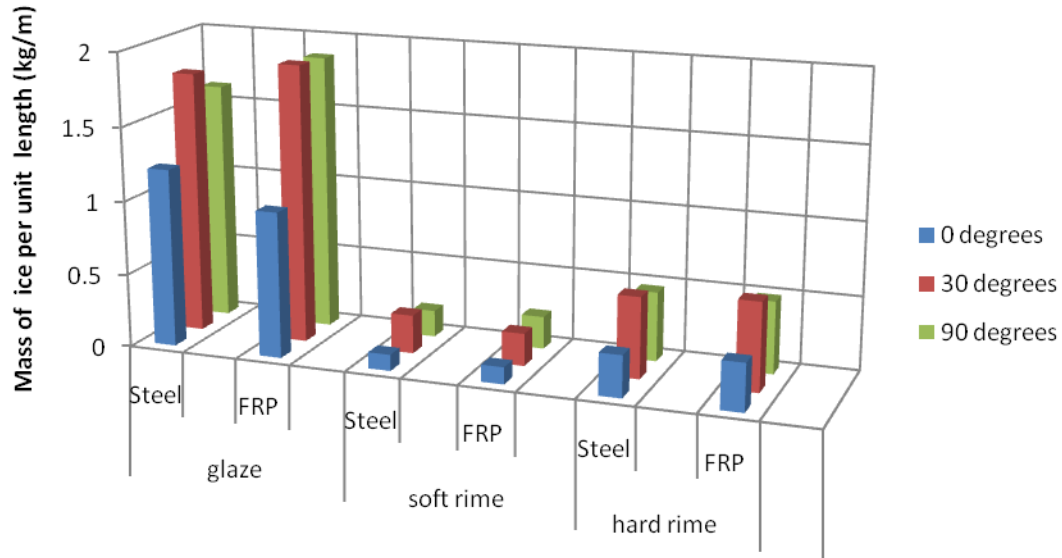


(a) Total accreted mass



(b) Maximum ice thickness

Figure 5.1: Results from the icing tunnel testing of the FRP and steel lattice tower segments at 0, 30 and 90 degree angles



(c) Mass of ice per unit length

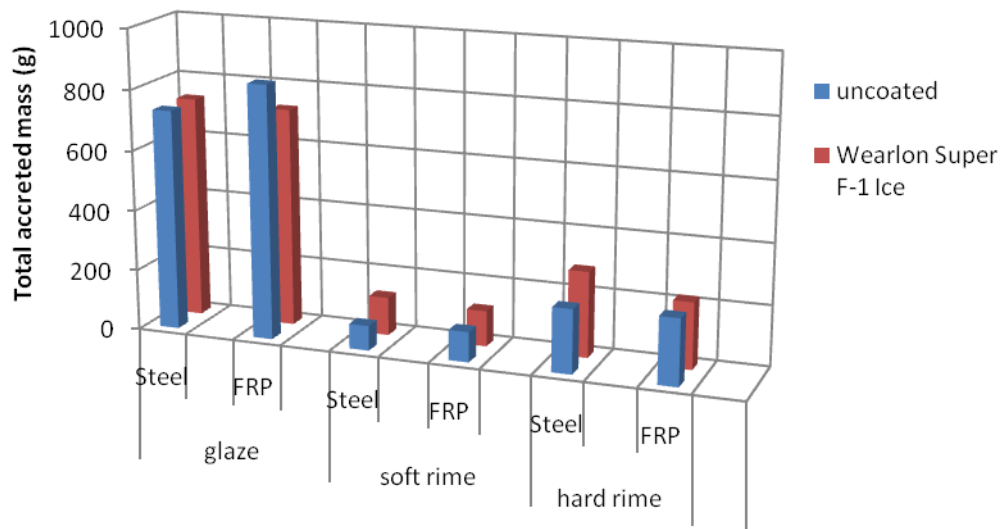
Figure 5.1 (continued): Results from the icing tunnel testing of the FRP and steel lattice tower segments at 0, 30 and 90 degree angles

Conclusions from the icing tunnel testing of the FRP and steel lattice tower segments coated with the icephobic coating Wearlon Super F-1 Ice:

The effectiveness of using the low friction icephobic coating Wearlon Super F-1 Ice was studied as a possible ice mitigation technique for lattice towers. The surfaces of steel and FRP tower sections were coated with Wearlon Super F-1 Ice and tested in glaze, soft rime and hard rime icing environments at 90 degree angle. The results showed that:

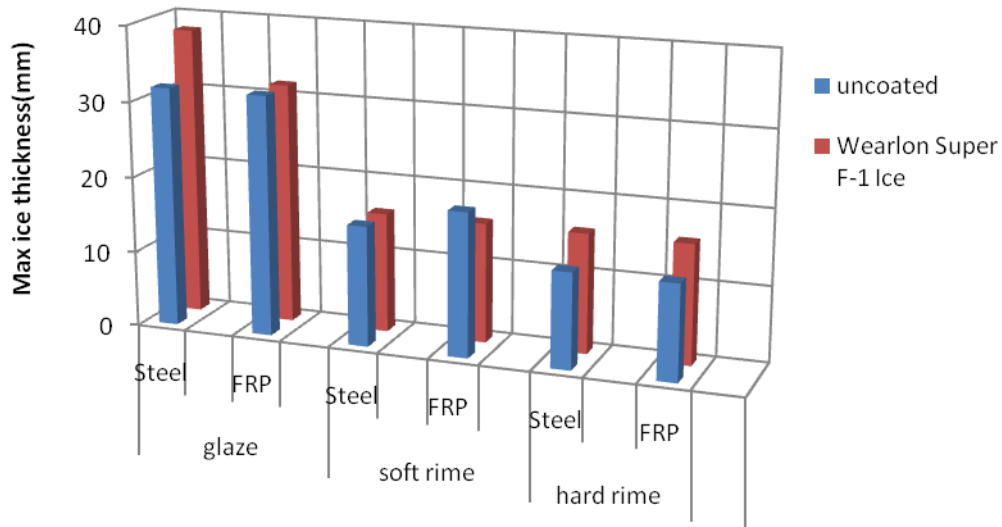
- FRP tower section showed 14 % reduction in accumulated ice mass compared to the uncoated one, as shown in Figure 5.2.
- Both steel and FRP sections showed reduction in adhesive strength of glaze ice after the test; however, it is recommended to verify these results in the field testing.

- The decrease of mass of soft and hard rime icing on the members of steel and FRP tower sections was not observed.
- No difference was noticed for soft and hard rime ice adhesive strength, when compared to uncoated sections.
- Considering the high cost of the coating and dimensions of full scale towers it might be feasible to coat critical sections of the tower for easier ice removal by natural or artificial means (i.e. wind, natural or artificial vibrations, sun light, heat etc.).

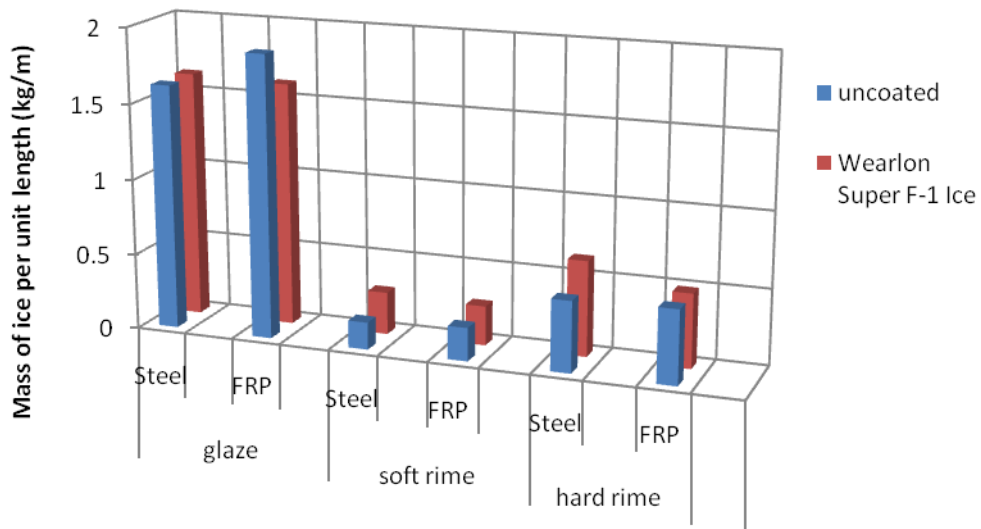


(a) Total accreted mass

Figure 5.2: Results from the icing tunnel testing of the FRP and steel lattice tower segments coated with the icephobic coating Wearlon Super F-1 Ice at 90 degree angle



(b) Maximum ice thickness



(c) Mass of ice per unit length

Figure 5.2 (continued): Results from the icing tunnel testing of the FRP and steel lattice tower segments coated with the icephobic coating Wearlon Super F-1 Ice at 90 degree angle

REFERENCES

- Abley, M. (1998). *The ice storm : an historic record in photographs of January 1998*. Toronto: Le Nouvelliste. Retrieved November 1, 2009, from Library and Archives Canada: <http://www.collectionscanada.gc.ca/obj/002028/f1/nlc010687-v6.jpg?PHPSESSID=cmmvold25ka5b323b0carl74n1>
- AMIL. (2009, November 1). *Centrifuge Ice Adhesion Reduction AMIL's Results*. Retrieved November 1, 2009, from ICEPHOBIC COATINGS EVALUATION: <http://www.uqac.ca/amil/en/icephobiccoatings/index.htm>
- ANSI/TIA. (2005). *Structural Standards for Steel Antenna Towers and Antenna Supporting Structures (ANSI/TIA 222-G-2005)*. TELECOMMUNICATIONS INDUSTRY ASSOCIATION.
- ASCE. (2005). *Minimum Design Loads for Buildings and Other Structures, ASCE Standard 7-05*. Reston, VA: American Society of Civil Engineers .
- Burachinsky, V. I. (2006). *Filament Winding of Long Tapered Tubes*. Winnipeg: University of Manitoba.
- CEA. (1998). *Validation of Ice Accretion Models For Freezing Precipitation Using Field Data. CEA 331 T992 (A–D)*. Montreal, QC: Canadian Electricity Association.
- CEATI. (2006). *Extreme Ice Thicknesses and Concurrent Wind Speeds in Canada Along the U.S. Border. T053700 3325 B*. Montreal, QC: CEA Technologies Inc.
- CEATI. (2002). *Investigation of the Differences in the Application of the Canadian and U.S. Methodology for Estimates of Ice Loads for a 50-yr Return Period. T003700 3306*. Montreal, QC: CEA Technologies Inc.

- Chaine, P. M., & Skeates, P. (1974). *Wind and Ice Loading Criteria Selection. Canadian Climate Centre Internal Report, Industrial Meteorology-Study III*. Downsview, ON: Atmospheric Environment Service.
- CSA. (2006a). *CAN/CSA-C22.3 NO. 1-06, Overhead Systems*. Mississauga, Ont.: Canadian Standards Association.
- CSA. (2006b). *CAN/CSA-C22.3 NO. 60826-06, Design Criteria for Overhead Transmission Lines*. Mississauga, Ont.: Canadian Standards Association.
- CSA. (2006c). *Canadian Highway Bridge Design Code*. Mississauga, Ont.: Canadian Standards Association.
- CSA. (2001). *CSA S37-01, Antennas, Towers and Antenna-Supporting Structures*. Mississauga, Ont.: Canadian Standards Association.
- CSA. (1986). *CSA S37-M86, Antennas, Towers and Antenna-Supporting Structures*. Mississauga: Canadian Standards Association.
- Department of Plant Science. (2009, 12 14). *Meteorological Report from "Point" Weather Station U of M for year 2009*. Retrieved 12 15, 2009, from The Point weather station: <http://home.cc.umanitoba.ca/~adam/weather.html>
- Ecological Coatings. (2009, 12 17). *ICEPHOBIC COATINGS*. Retrieved 12 17, 2009, from Wearlon® Industrial Coating Systems: <http://www.wearlon.com/Eice.htm>
- El-Fashny, K., Chouinard, L., & McClure, G. (1999). Reliability analysis of telecommunication tower. *Canadian Journal of Civil Engineering* , 26 (1), 1-12.
- Fahleson, C. (1995). *Ice and wind loads on guyed masts*. Doctoral thesis at Lulea University of Technology, Sweden.

- Friesen, G., & Kell, J. (2009). *Personal communication*. Winnipeg: MB Hydro.
- Goel, A. (2008). Design of Transmission Lines for Atmospheric Icing. In M. Farzaneh, *Atmospheric Icing of Power Networks* (pp. 328-371). Springer Science.
- ISO. (2001). *ISO 12494:Atmospheric icing of structures*. ISO/TC 98/SC 3.
- Kraj, G. A. (2007). *ICING CHARACTERISTICS AND MITIGATION STRATEGIES FOR WIND TURBINES IN COLD CLIMATES*. Winnipeg: University of Manitoba. Dept. of Mechanical Engineering Dissertations.
- Laforte, C., Carriere, J.-C., & Laforte, J.-L. (2002). How a Solid Coating Can Reduce Ice Adhesion on Structure. *Proceedings of the 10th International Workshop of Atmospheric Icing of Structures*. Brno, Czech Republic.
- Madugula, M. K. (2002). *Dynamic response of lattice towers and guyed masts*. Reston,VA: ASCE.
- Madugula, M. K., Wahba, Y. M., & Monforton, G. R. (1998). Dynamic response of guyed masts. *Engineering Structures* , 20 (12), 1097-1101.
- Magued, M. H., Bruneau, M., & Dryburgh, R. B. (1989). Evolution of design standards and recorded failures of guyed towers in Canada. *Canadian Journal of Civil Engineering* , 16, 725-732.
- Makkonen, L. (1984). Modelling of Ice Accretion on Wires. *Journal of Climate and Applied Meteorology* , 23 (6), 929-939.
- Makkonen, L., & Ahti, K. (1995). Climatic mapping of ice loads based on airport weather observations. *Atmospheric Research* , 36, 185-193.

- Makkonen, L., & Oleskiw, M. M. (1997). Small-scale experiments on rime icing. *Cold Regions Science and Technology* , 25 (3), 173-182.
- Marshall, D. G., Nightingale, A. J., & Dryburgh, R. B. (2005, May). *Comentary on CSA Standard S37-01 Antennas, Towers and Antenna Supporting Structures. Issue A*. Retrieved July 16, 2009, from http://www.noeticholdings.com/commentary_on_csa_s37/commentary_on_csa_standard_s37-01_antennas_towers_and_antenna-supporting_structures.pdf
- MRI. (1977). *Ontario Hydro Wind and Ice Loading Model. MRI 77 FR-1496*. Meteorological Research Incorporated.
- Mulherin, N. D. (1998). Atmospheric icing and communication tower failure in the United States. *Cold Regions Science and Technology* , 91-104.
- Mulherin, N. D. (1986). *Atmospheric icing on communication masts in New England*. Hanover, NH: US Army Corps of Engineers, Cold Regions Research & Engineering Laboratory .
- Mulherin, N. D., & Haehnel, R. B. (2003). *Ice Engineering: Progress in Evaluating Surface Coatings for Icing Control at Corps Hydraulic Structures*. HANOVER NH: ENGINEER RESEARCH AND DEVELOPMENT CENTER/COLD REGIONS RESEARCH AND ENGINEERING LAB.
- Novak, M., Davenport, A., & Tanaka, H. (1978). Vibration of towers due to galloping of iced cables. *Journal of Engineering Mechanics Division* (104), 457-473.
- Ochonski, A. (2009). *Development of latticed towers using advanced composite materials*. Winnipeg: University of Manitoba. Dept. of Civil Engineering Dissertations.

- Phillips, D. (2002, 08 26). *The worst ice storm in Canadian history?* Retrieved 07 27, 2009, from Ice storm 1998: http://www.msc-smc.ec.gc.ca/media/icestorm98/icestorm98_the_worst_e.cfm
- Saxena, R., Popplewell, N., Trainor, P., & Shah, A. (1989). Vibrations of complex guyed towers. *Proceedings of the 12th Biennial Conference on Mechanical Vibration and Noise Control*, (pp. 1-7). Montreal, Quebec, Canada.
- Smith, B. W. (2007). *Communication structures*. London: Thomas Telford.
- Sparling, B. F., & Wegner, L. D. (2006). Comparison of frequency- and time domain analyses for guyed masts in turbulent winds. *Canadian Journal of Civil Engineering* (33), 169-182.
- Sparling, B. (2010). *Personal communication*. Saskatoon: University of Saskatchewan.
- Sundin, E., & Makkonen, L. (1998). Ice loads on a lattice tower estimated by weather station data. *Journal of Applied Meteorology* , 523-529.
- Sundin, E., & Mulherin, N. (1993). Icing-related tower failures in the USA and Fenno-Scandinavia. *Proceeding Sixth International Workshop on Atmospheric Icing of Structures* (pp. 273-278). Budapest: Hungarian Electrotechnical Association.
- Wahba, Y. M., Madugula, M. K., & Monforton, G. R. (1993). Combined wind and ice loading on antenna towers. *Canadian Journal of Civil Engineering* , 1047-1056.
- Wahba, Y. M., Madugula, M. K., & Monforton, G. R. (1998). Effect of icing on the free vibration of guyed antenna towers. *Atmospheric Research* , 46 (1-2), 27-35.
- Yip, T.-C. (1995). Estimating icing amounts caused by freezing precipitation in Canada. *Atmospheric Research* , 36, 221-232.

APPENDICES

APPENDIX A: Design criteria maps.

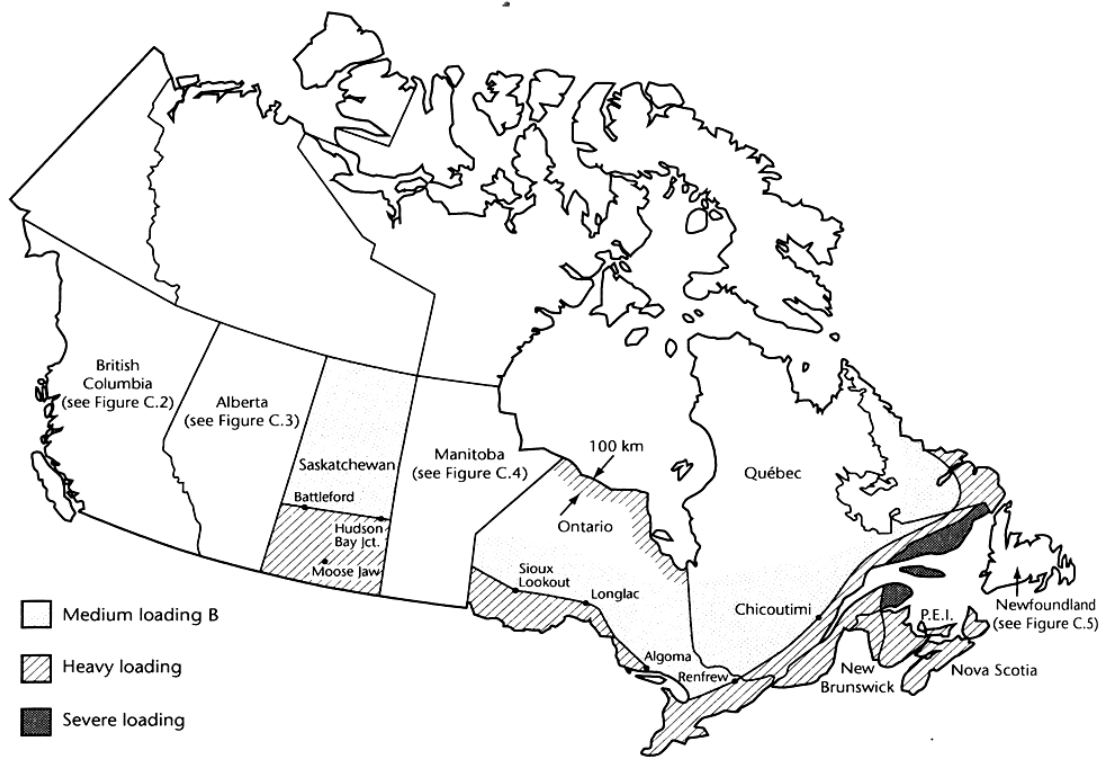


Figure A- 1: Loading map of Canada (CSA, 2006a)

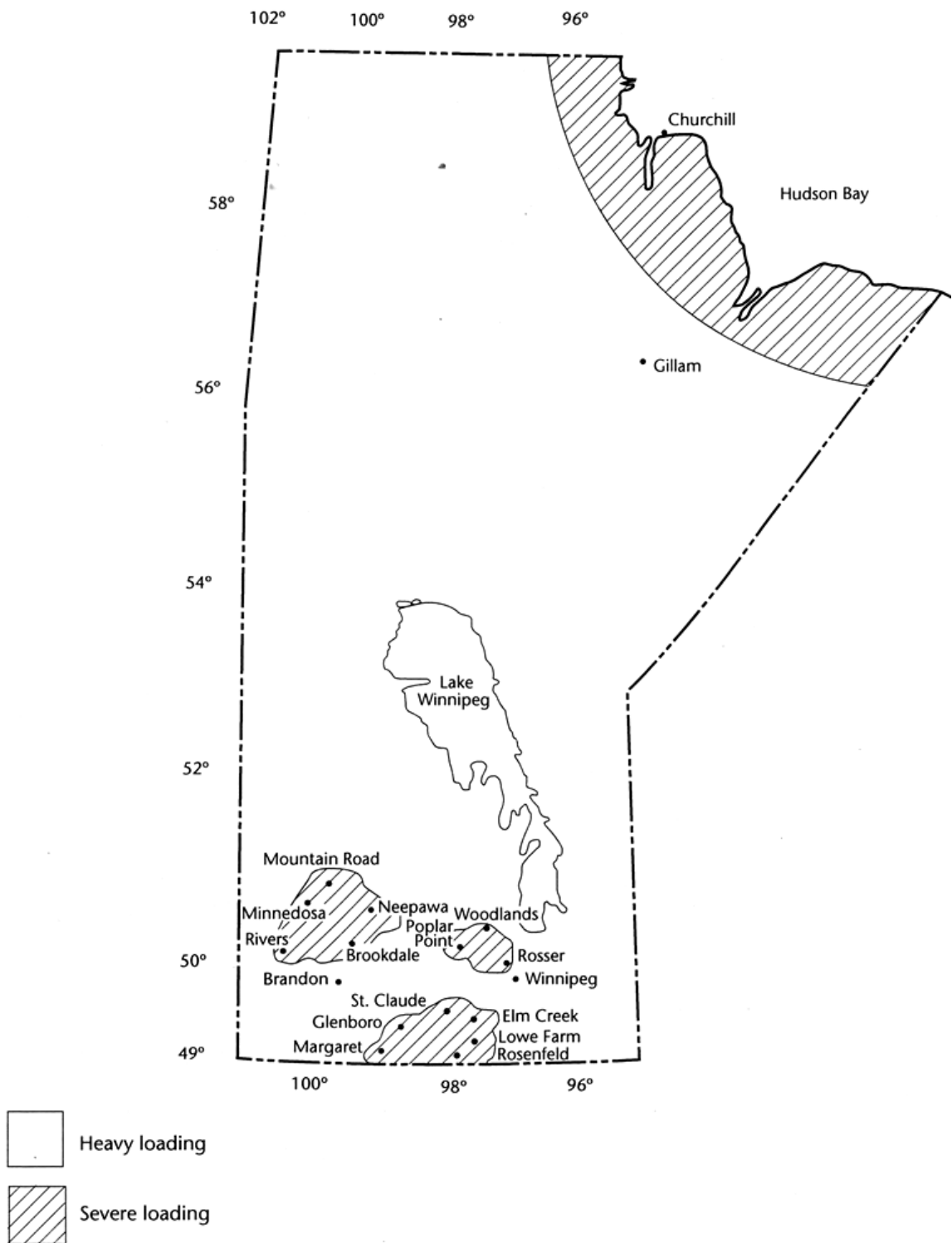


Figure A- 2: Loading map of Manitoba (CSA, 2006a)

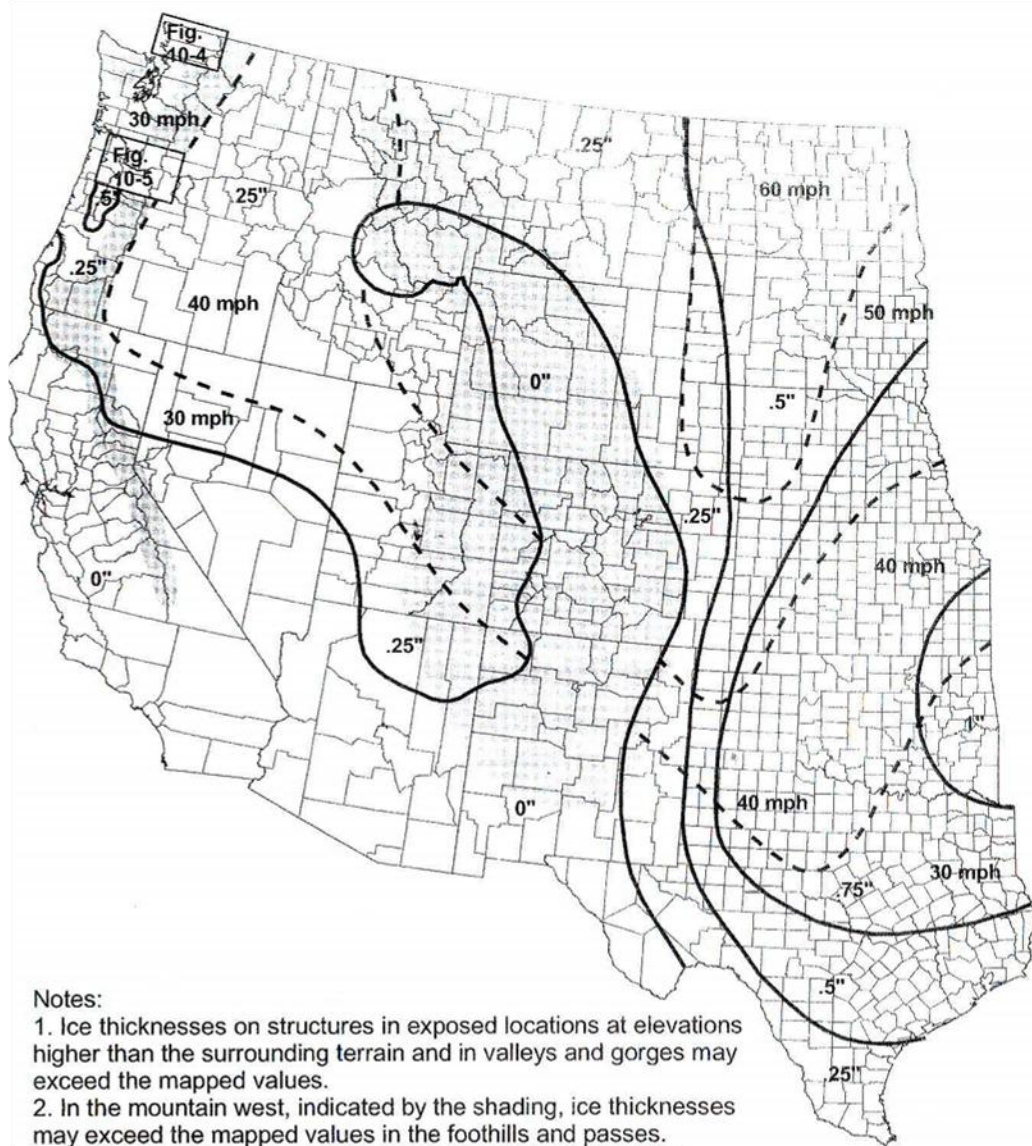


Figure A- 3: 50-year mean recurrence interval uniform ice thicknesses due to freezing rain with concurrent 3-second gust speeds: contiguous 48 states (ASCE, 2005)

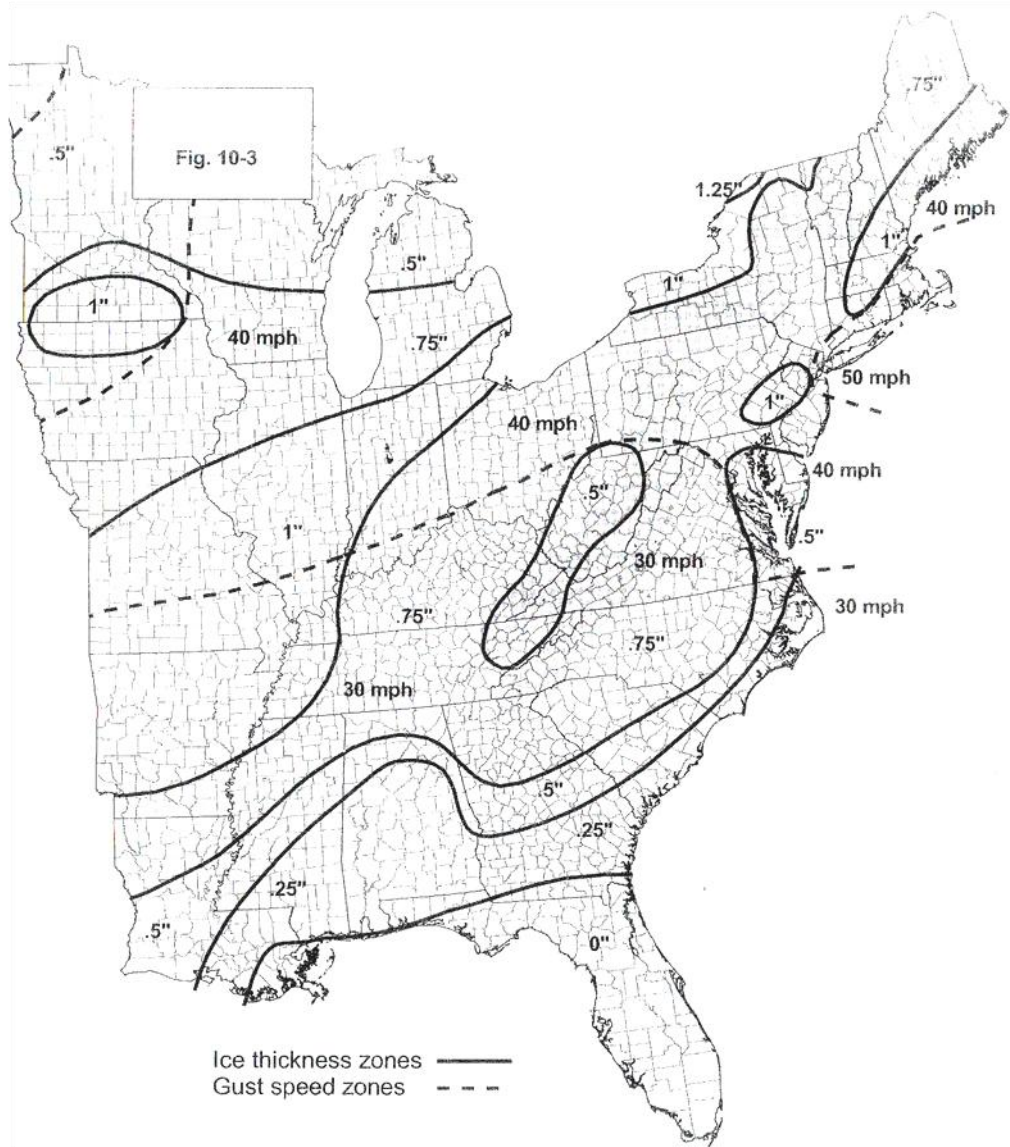


Figure A- 4 (continued): 50-year mean recurrence interval uniform ice thicknesses due to freezing rain with concurrent 3-second gust speeds: contiguous 48 states (ASCE, 2005)

APPENDIX B: Wind speed and wind directions from field experiment

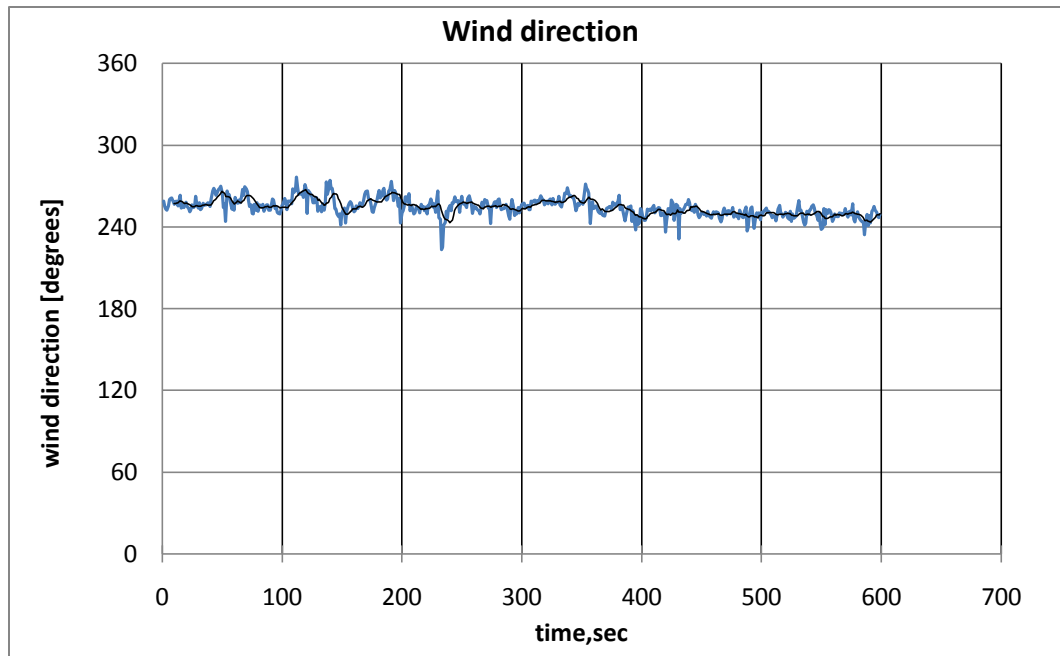


Figure B- 1: Wind direction on February 14, 2009 at 6:15-6:26PM

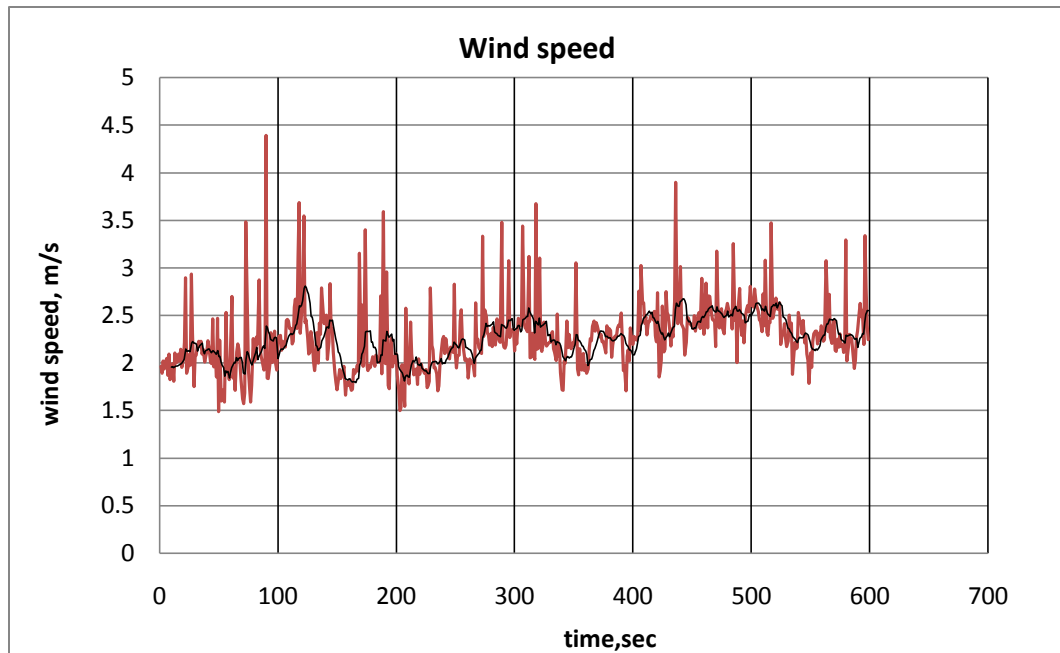


Figure B- 2: Wind speed on February 14, 2009 at 6:15-6:26PM

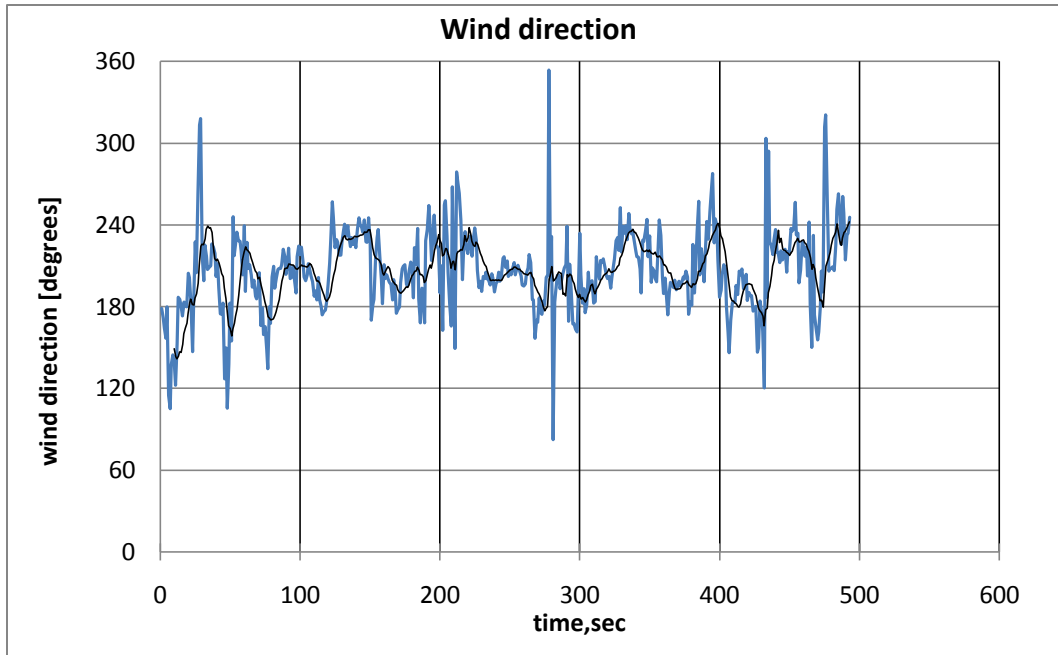


Figure B- 3: Wind direction on February 15, 2009 at 5:45-5:53 PM

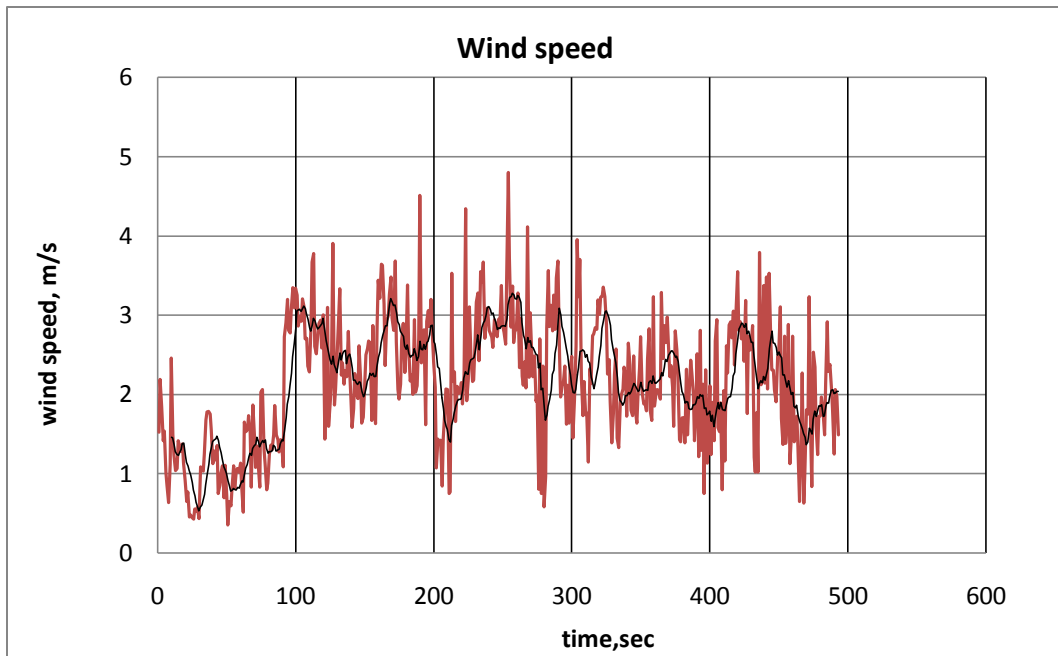


Figure B- 4: Wind speed on February 15, 2009 at 5:45-5:53 PM

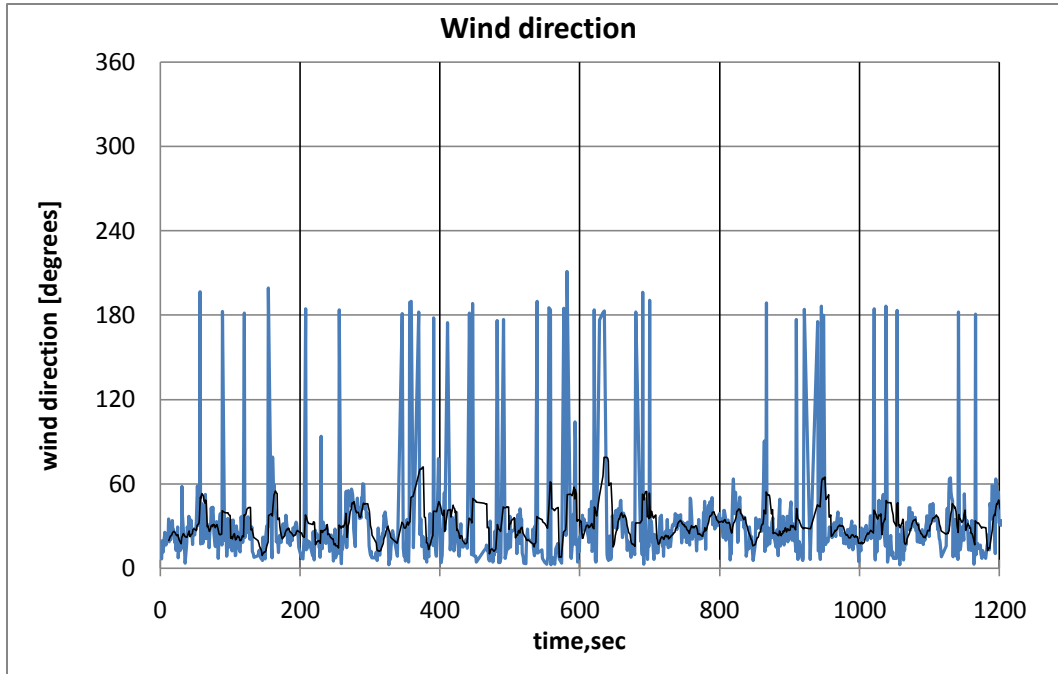


Figure B- 5: Wind direction on February 17, 2009 at 6:46-7:06 PM

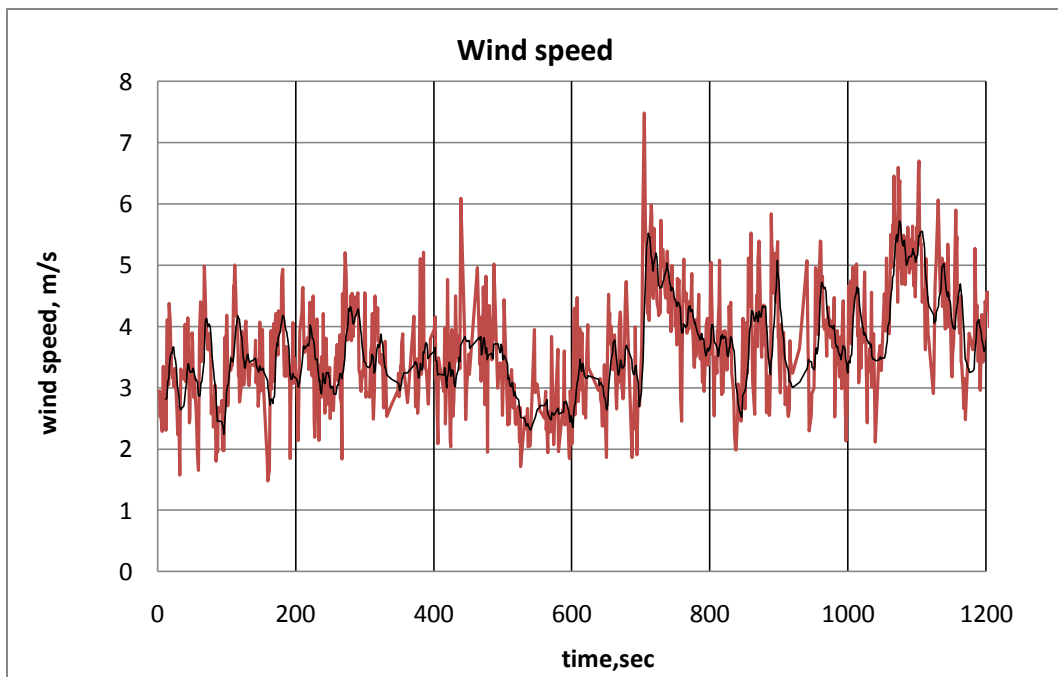


Figure B- 6: Wind speed on February 17, 2009 at 6:46-7:06 PM

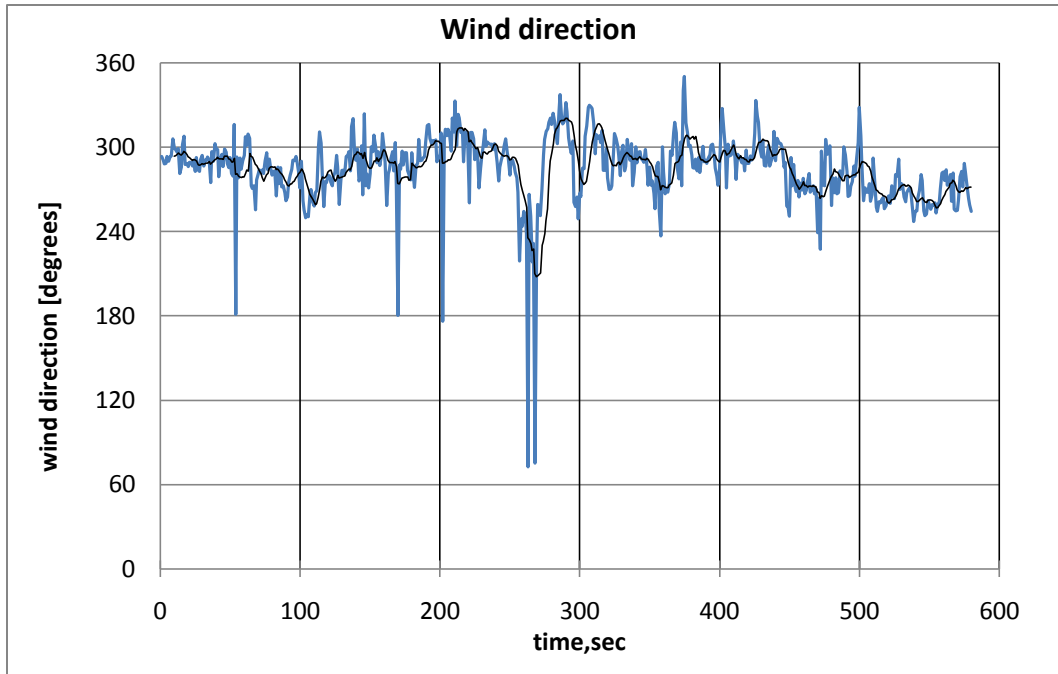


Figure B- 7: Wind direction on February 18, 2009 at 6:15-6:24 PM

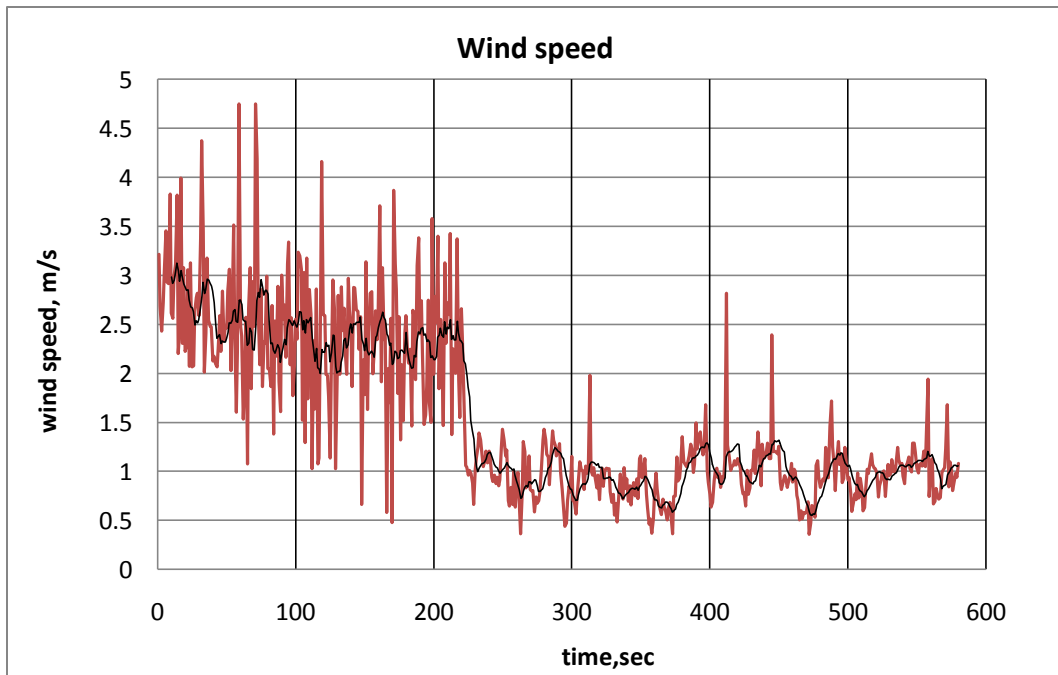


Figure B- 8: Wind speed on February 18, 2009 at 6:15-6:24 PM

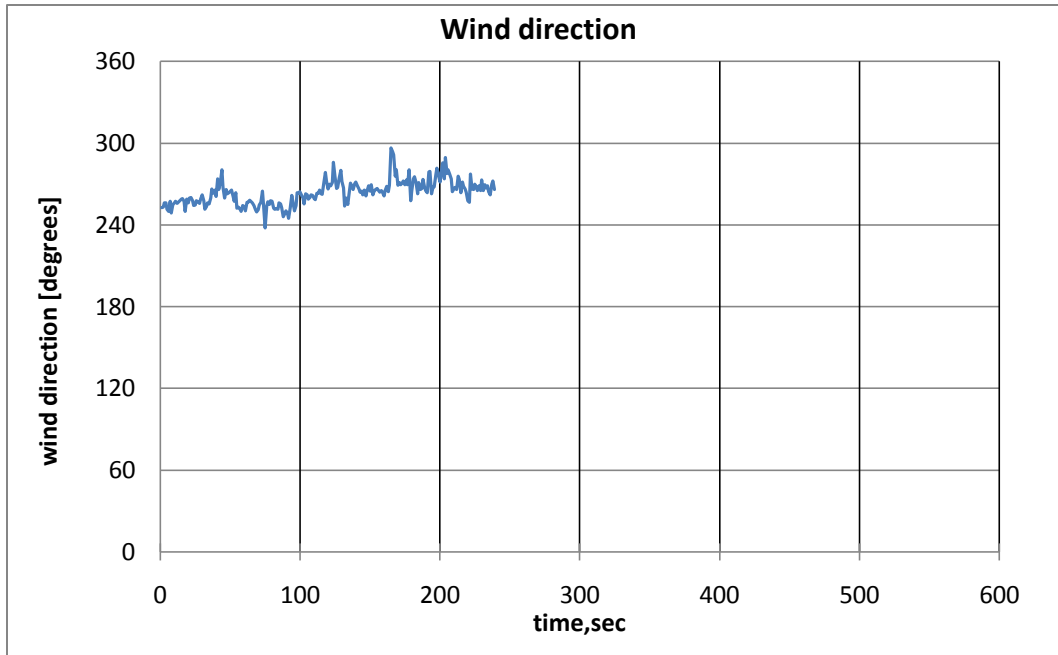


Figure B- 9: Wind direction on February 21, 2009 at 6:33-6:37 PM

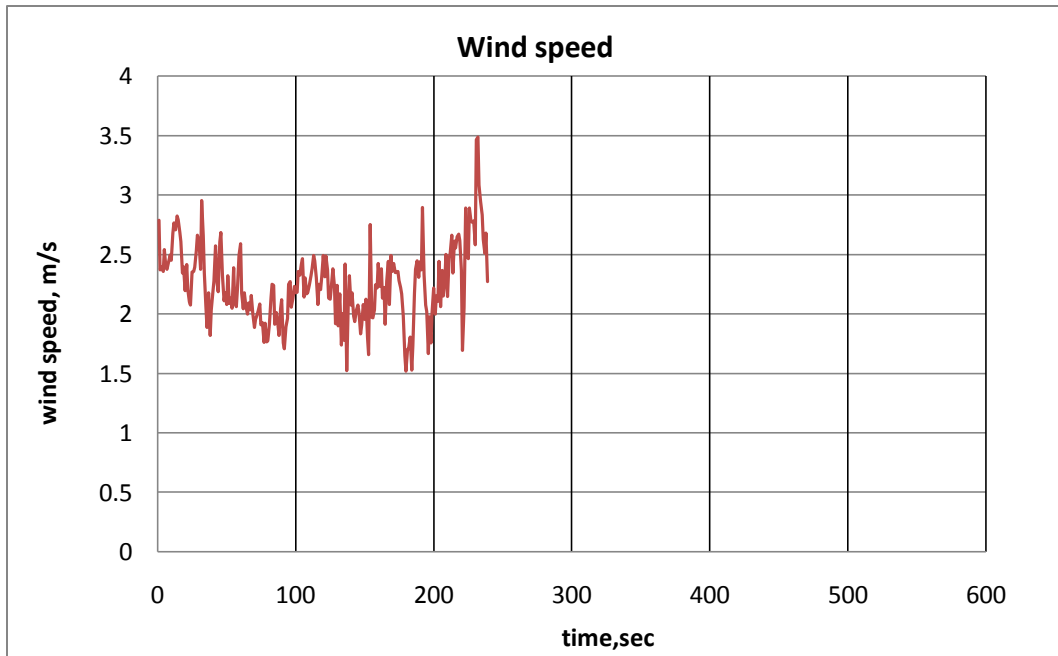


Figure B- 10: Wind speed on February 21, 2009 at 6:33-6:37 PM

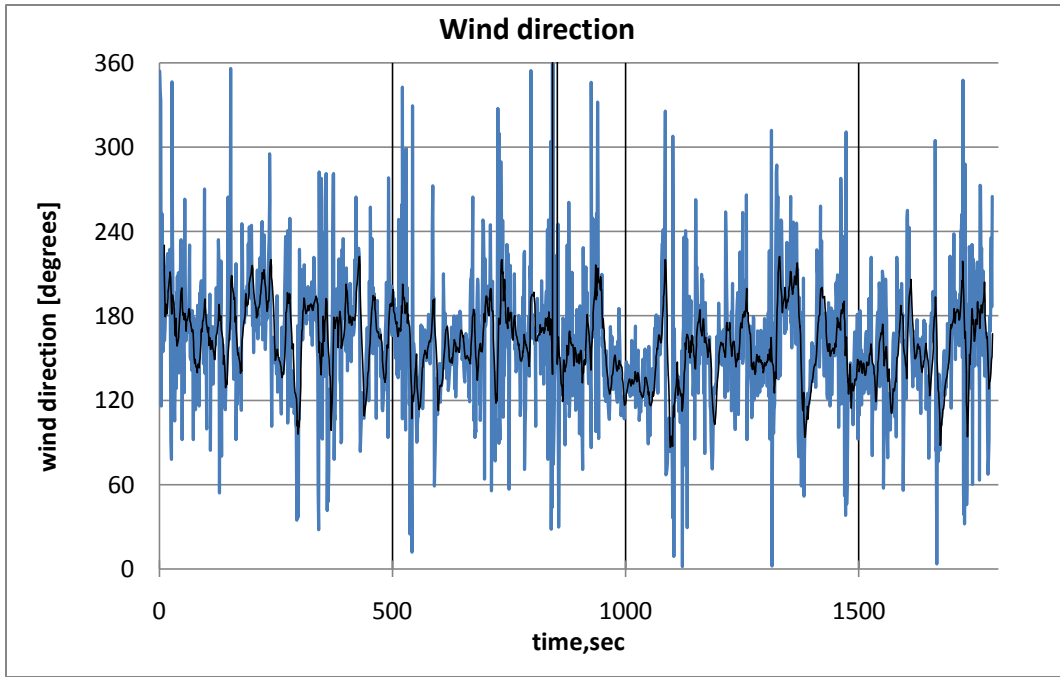


Figure B- 12: Wind direction on February 23, 2009 at 3:02-3:32 PM

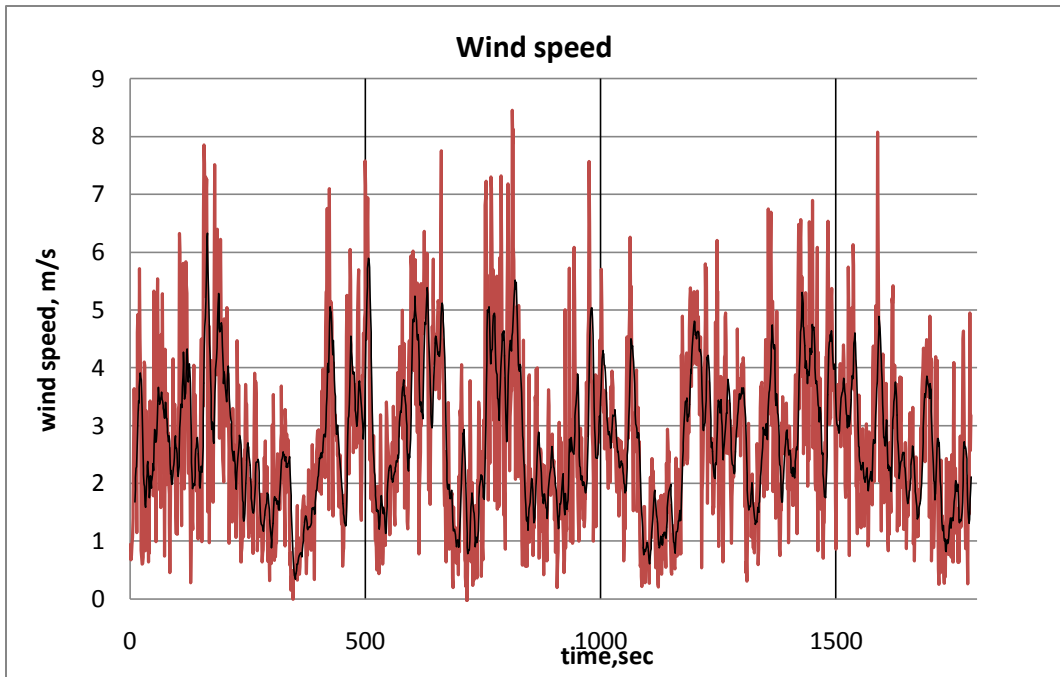


Figure B- 11: Wind speed on February 23, 2009 at 3:02-3:32 PM

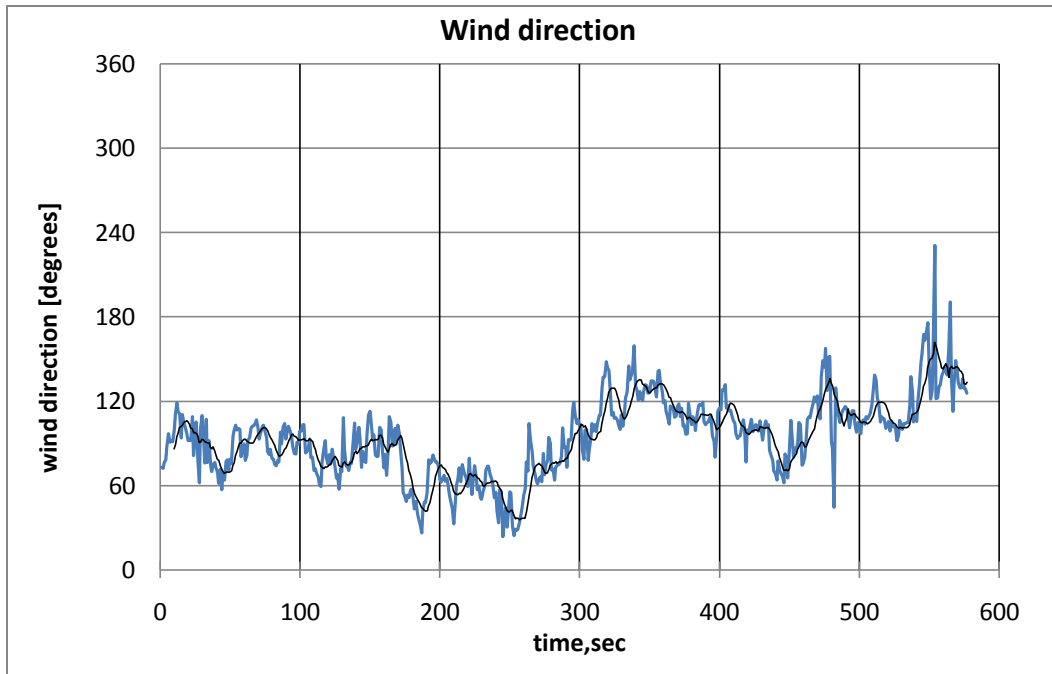


Figure B- 13: Wind direction on February 24, 2009 at 2:20-2:29 PM

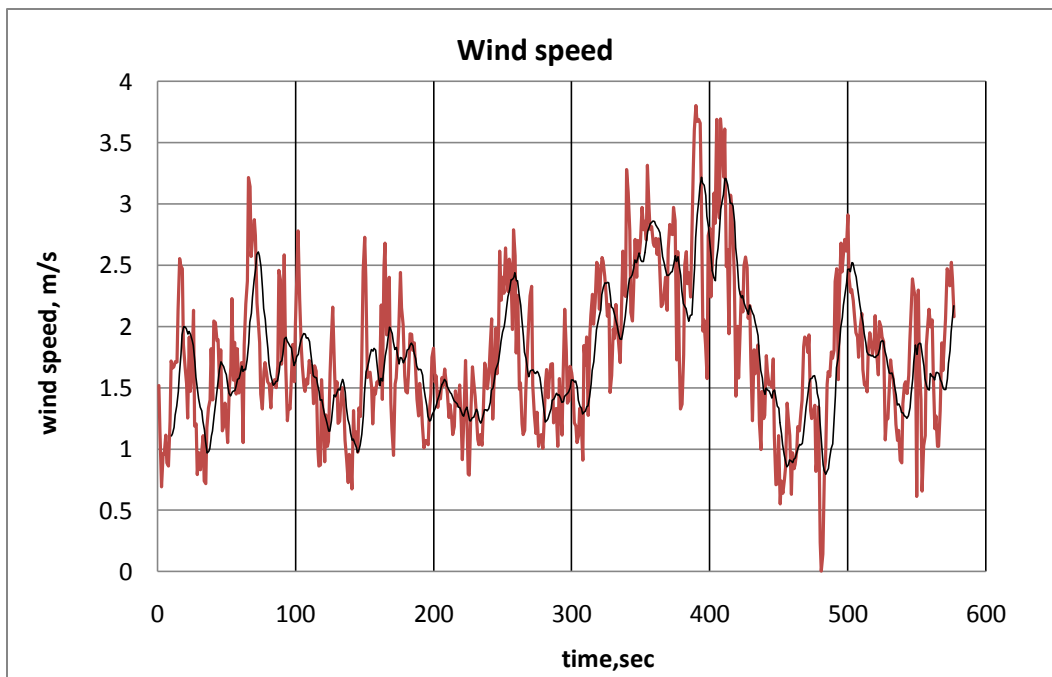


Figure B- 14: Wind speed on February 24, 2009 at 2:20-2:29 PM

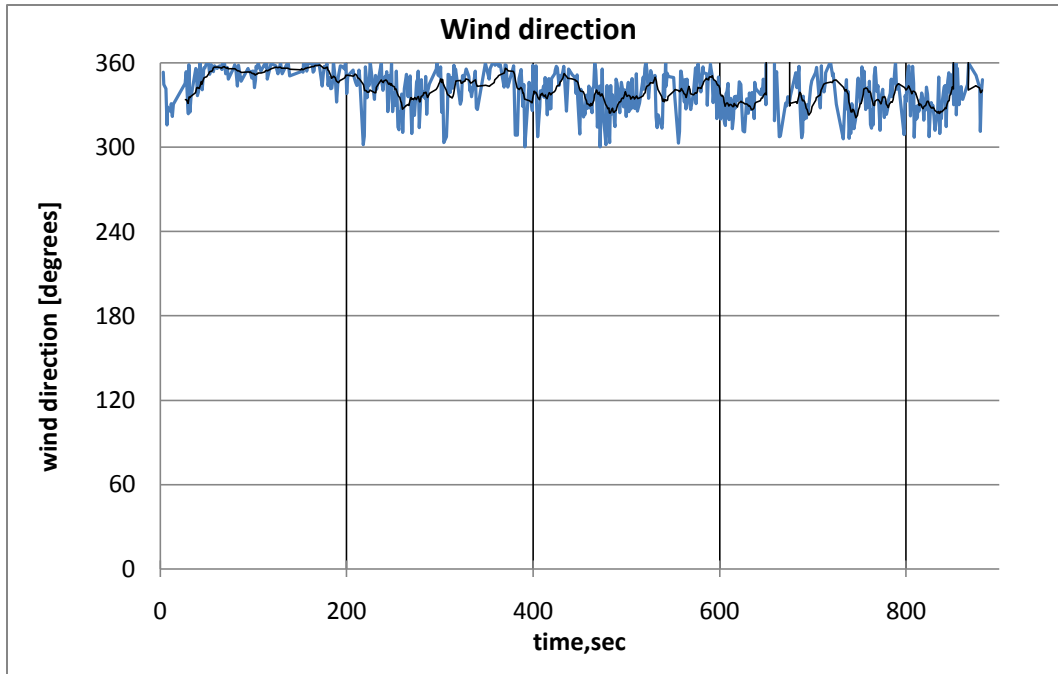


Figure B- 15: Wind direction on February 25, 2009 at 10:47-11:01 AM

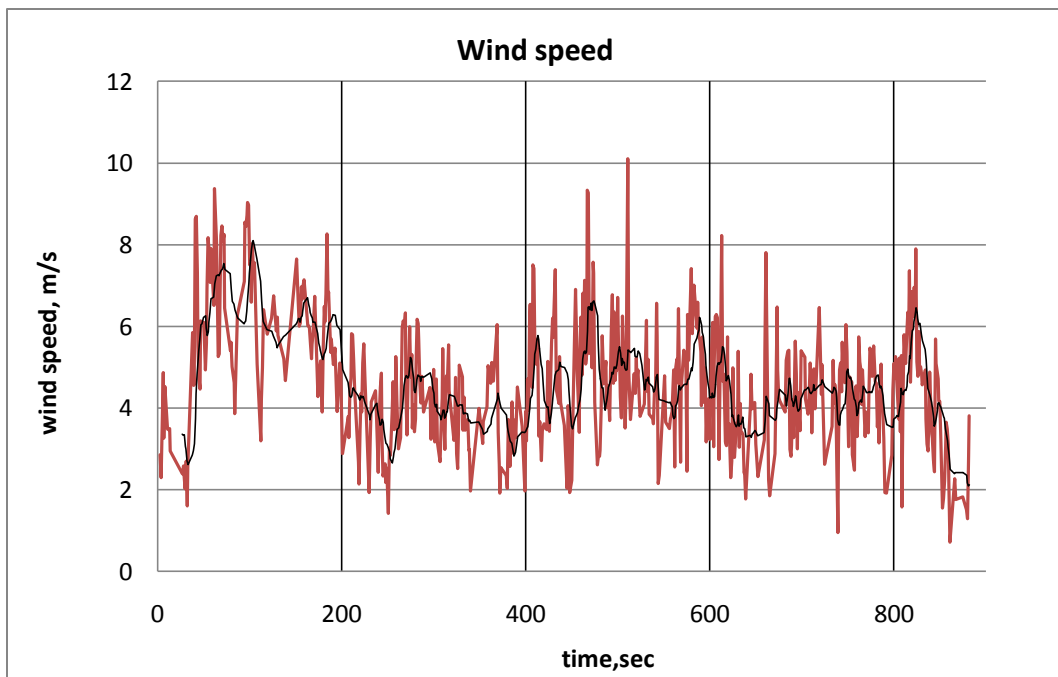


Figure B- 16: Wind speed on February 25, 2009 at 10:47-11:01 AM

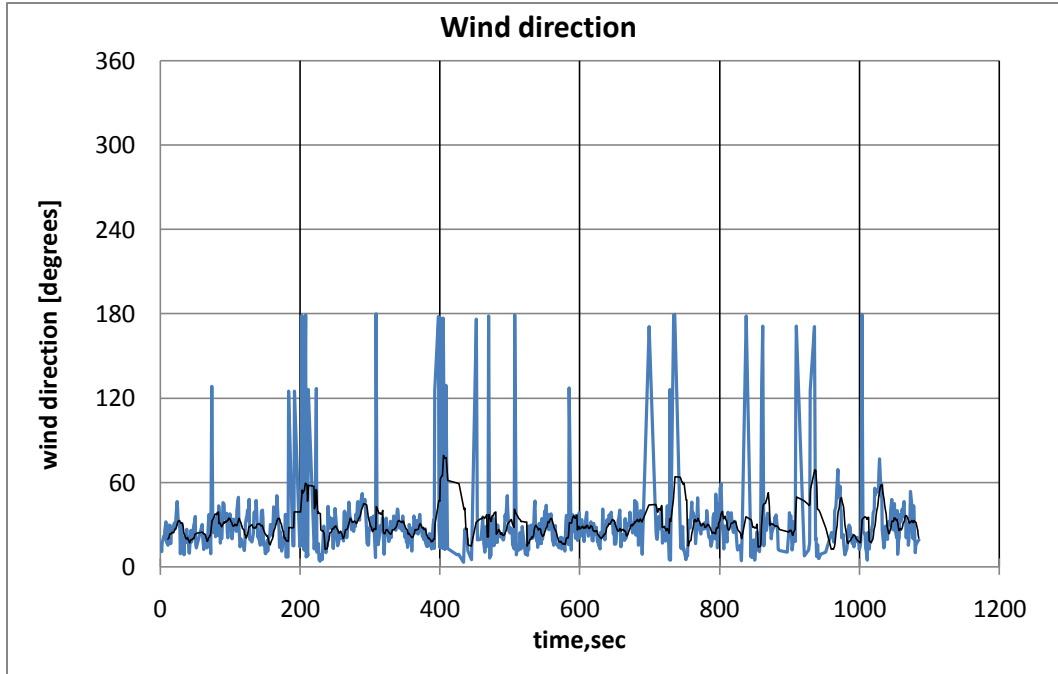


Figure B- 18: Wind direction on February 26, 2009 at 11:54-12:12 AM

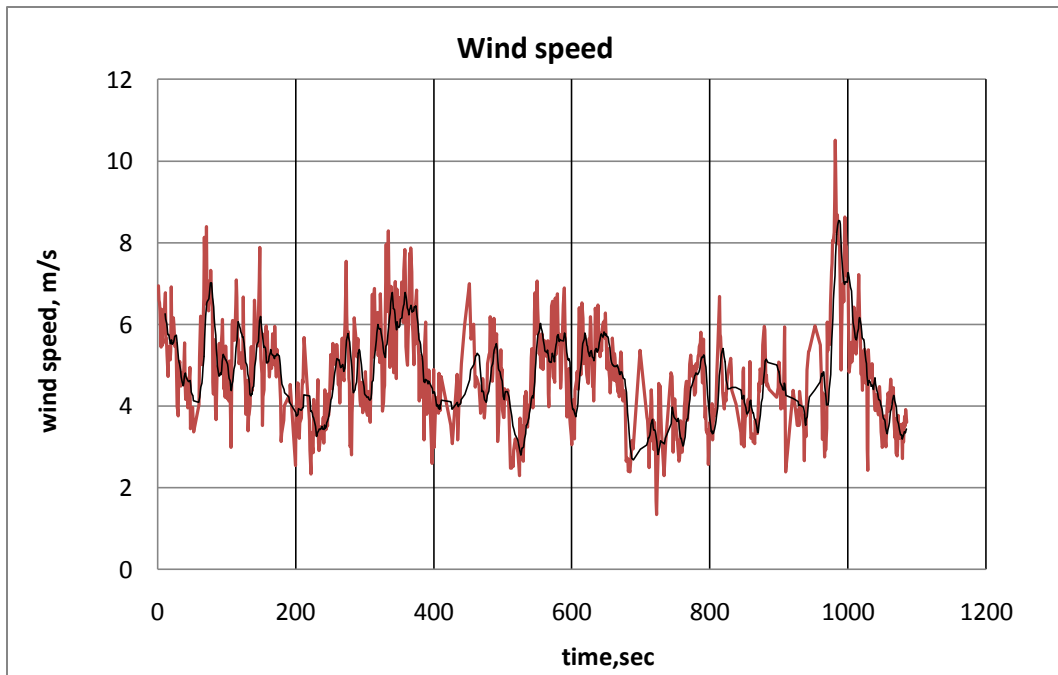


Figure B- 17: Wind speed on February 26, 2009 at 11:54-12:12 AM

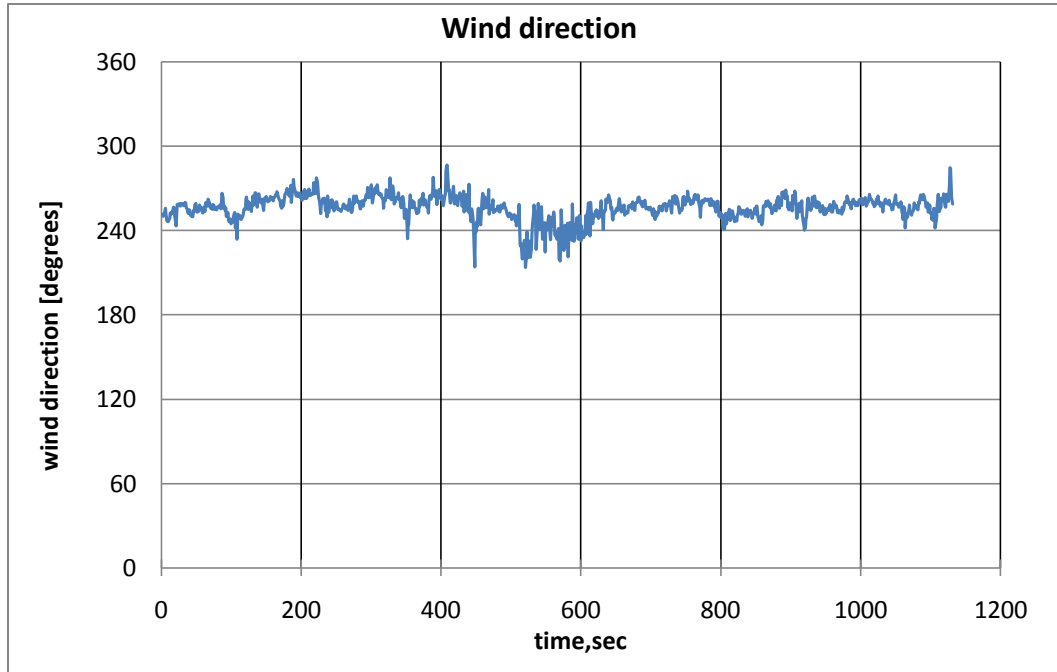


Figure B- 20: Wind direction on the iced tower on February 27, 2009 at 2:54-3:13 PM

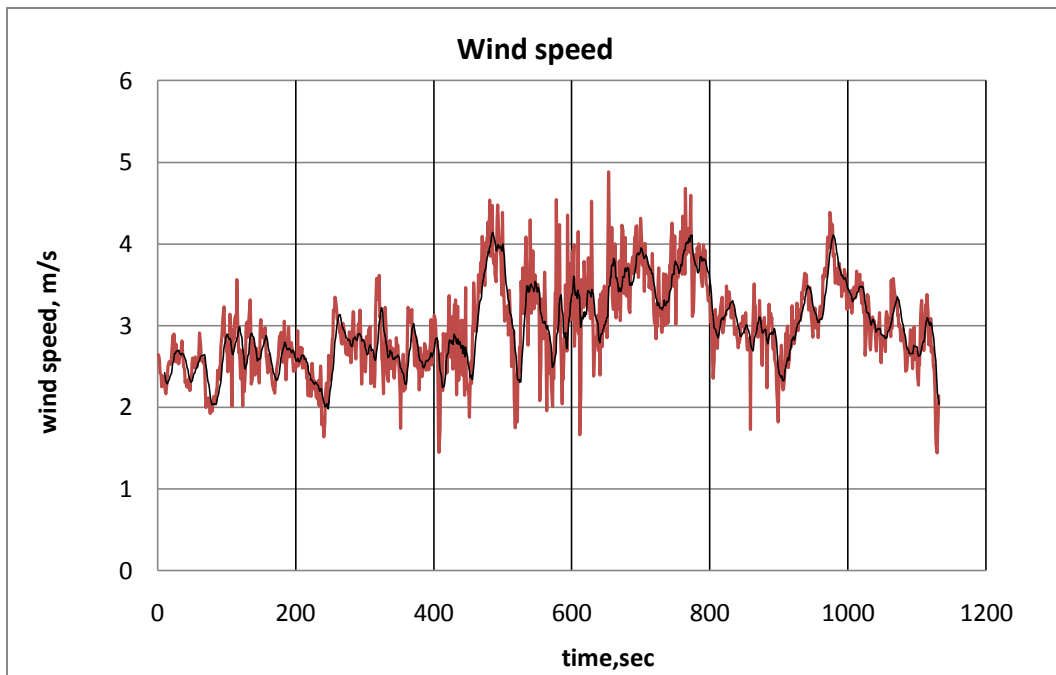


Figure B- 19: Wind speed on the iced tower on February 27, 2009 at 2:54-3:13 PM

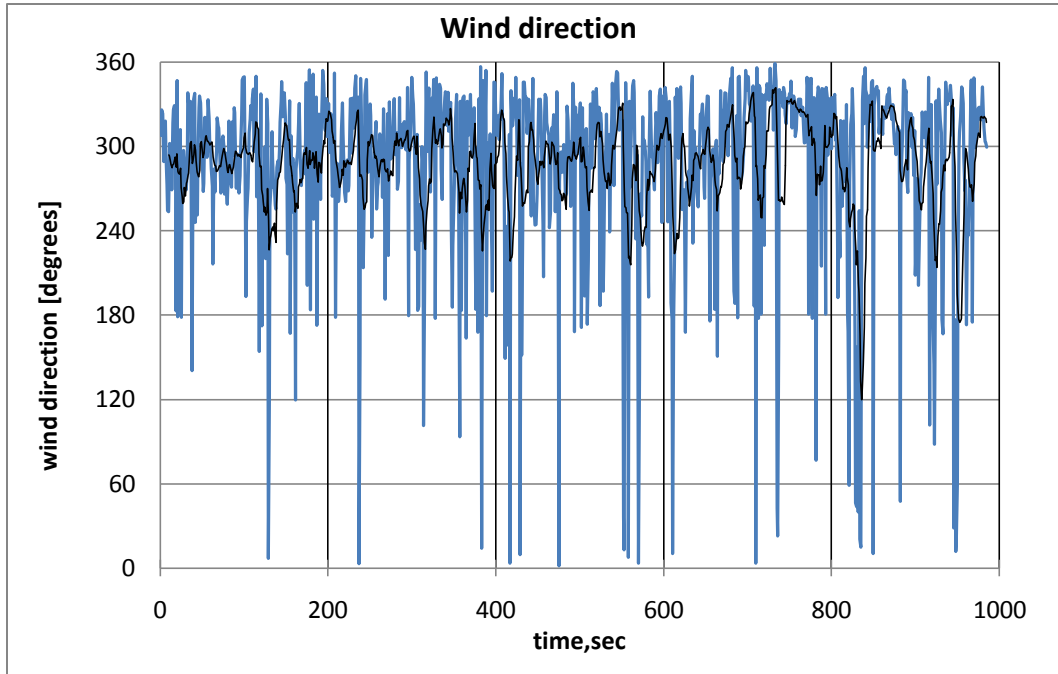


Figure B- 21: Wind direction on the iced tower on February 28, 2009 at 1:56-2:12 PM

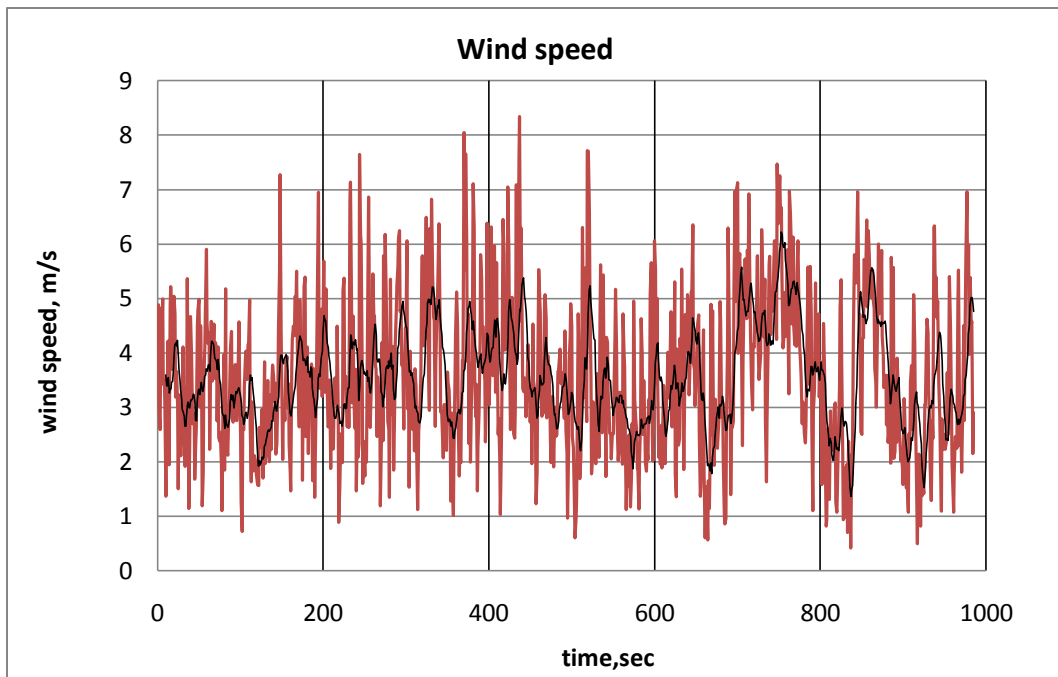


Figure B- 22: Wind speed on the iced tower on February 28, 2009 at 1:56-2:12 PM

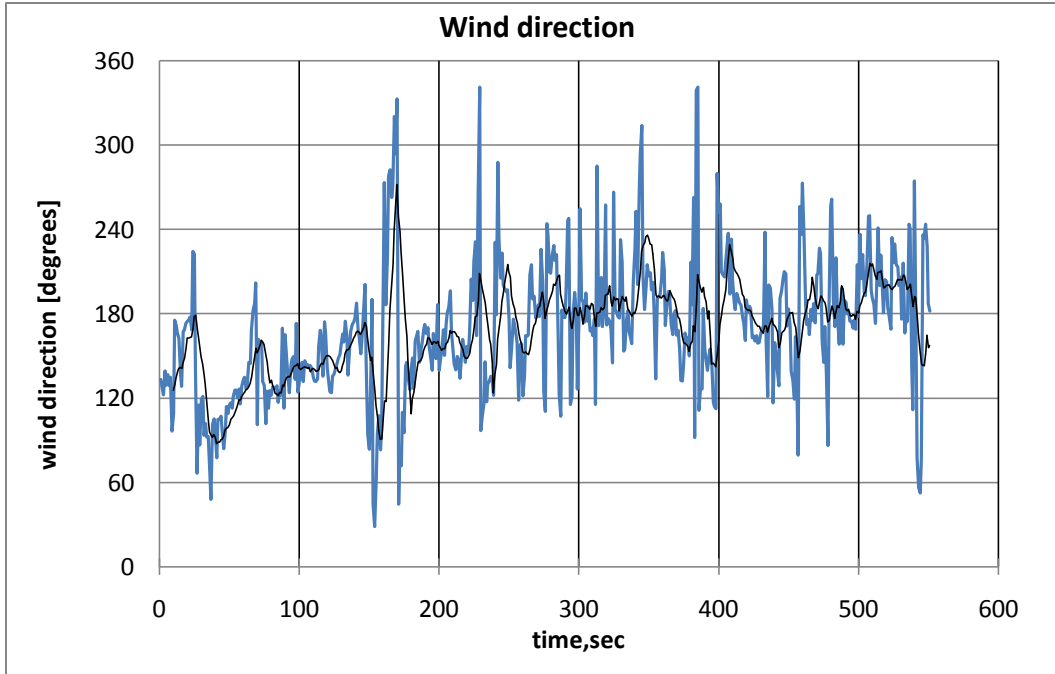


Figure B- 23: Wind direction on the iced tower on March 1, 2009 at 1:34-1:43 PM

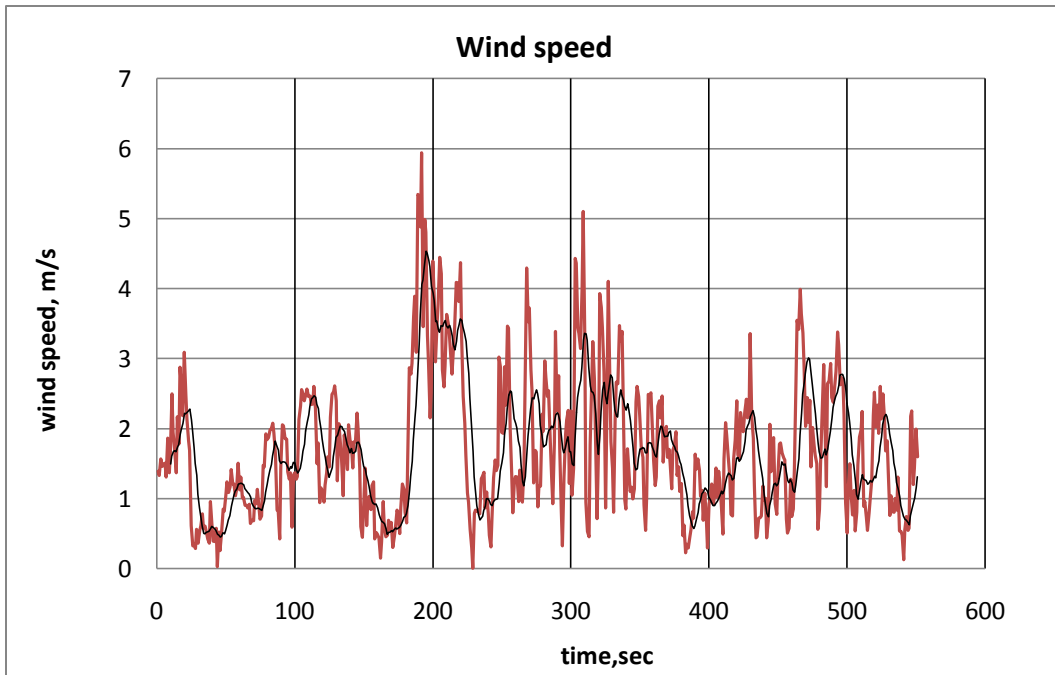


Figure B- 24: Wind speed on the iced tower on March 1, 2009 at 1:34-1:43 PM

APPENDIX C: Strains from the FRP tower.

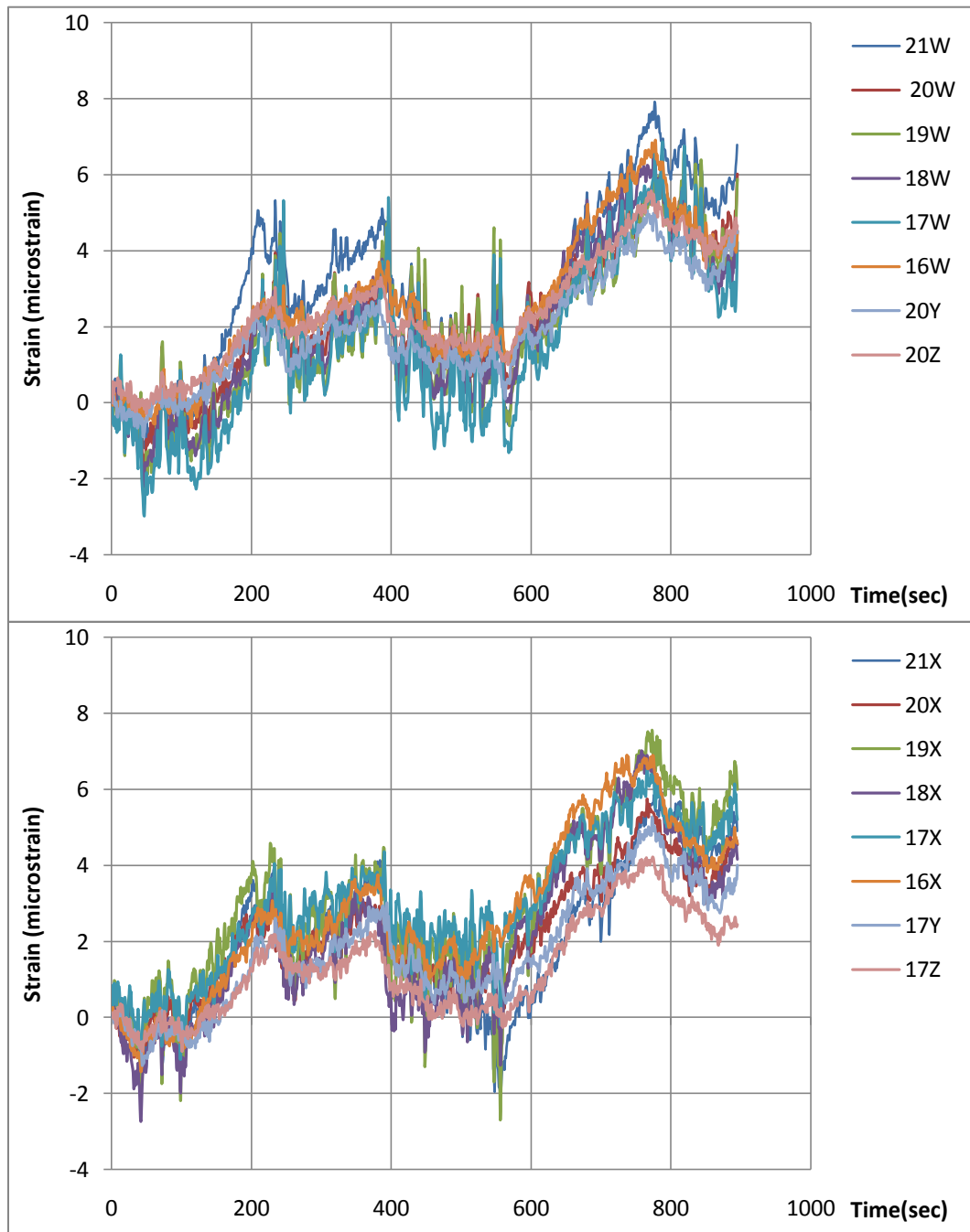


Figure C- 1: Strains in members of the FRP tower at 11:36-11:52AM on February 12,2009

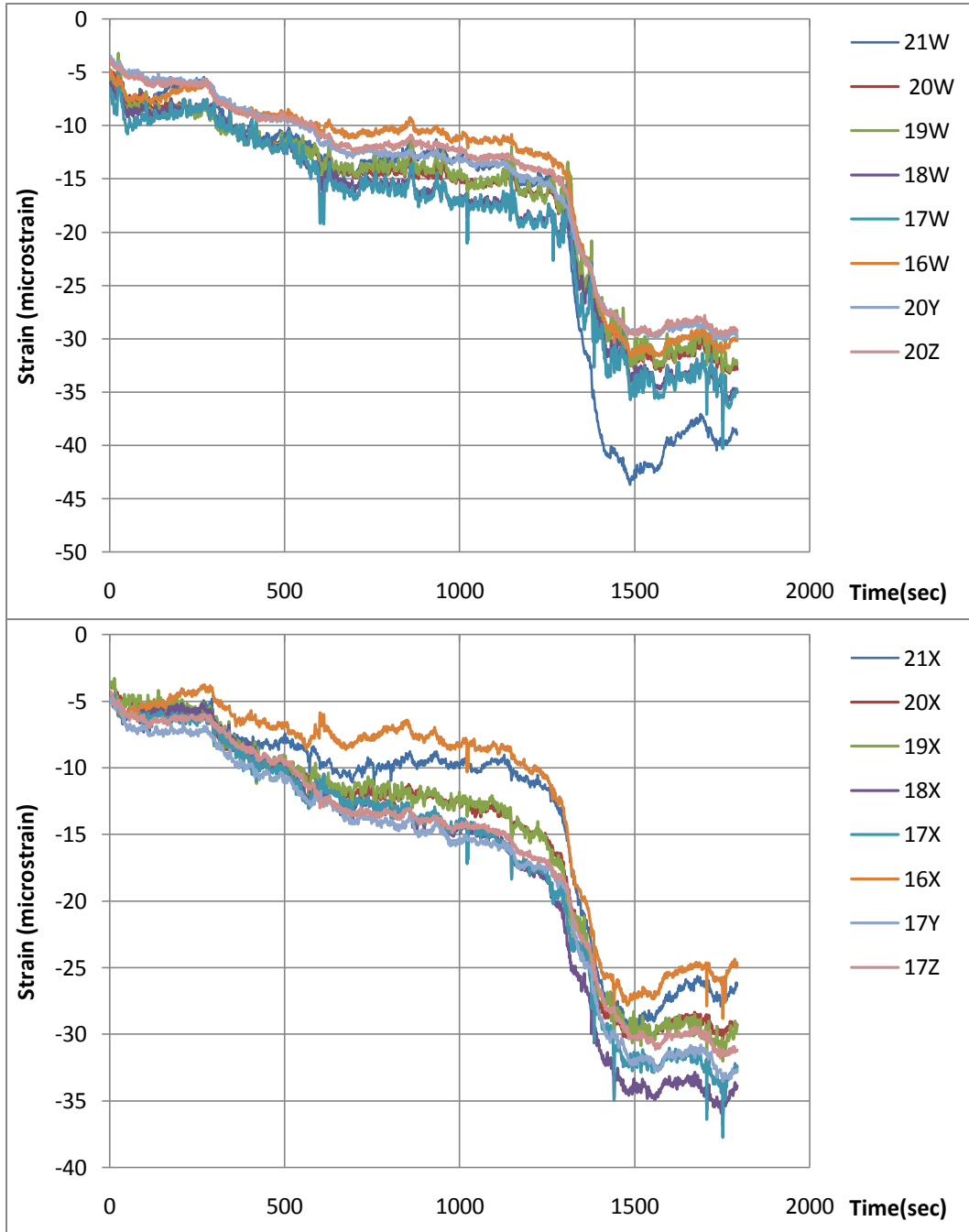


Figure C- 2: Strains in members of the FRP tower at 4:16-4:46PM on February 12, 2009

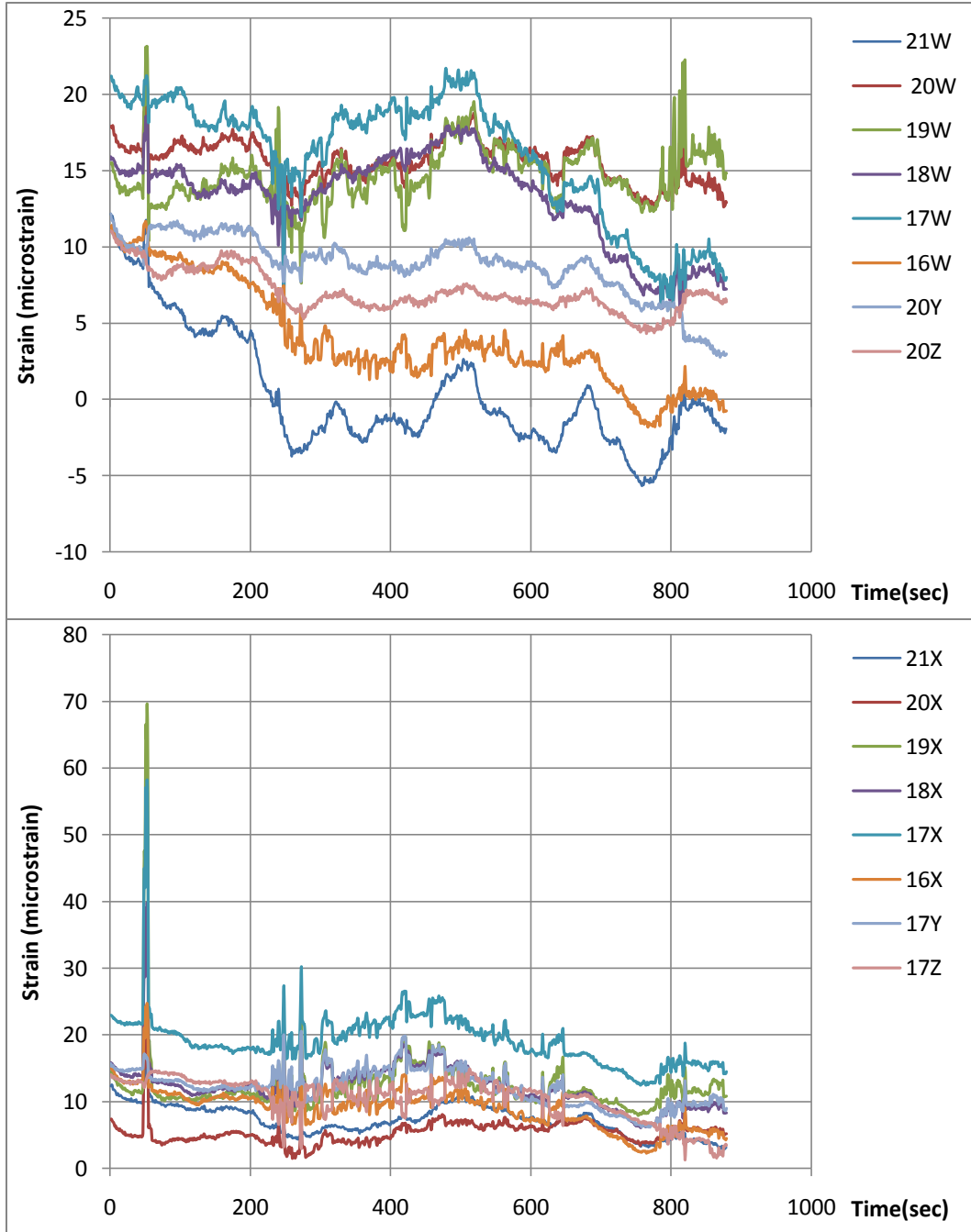


Figure C- 3: Strains in members of the FRP tower at 3:11-3:26PM on February 13, 2009

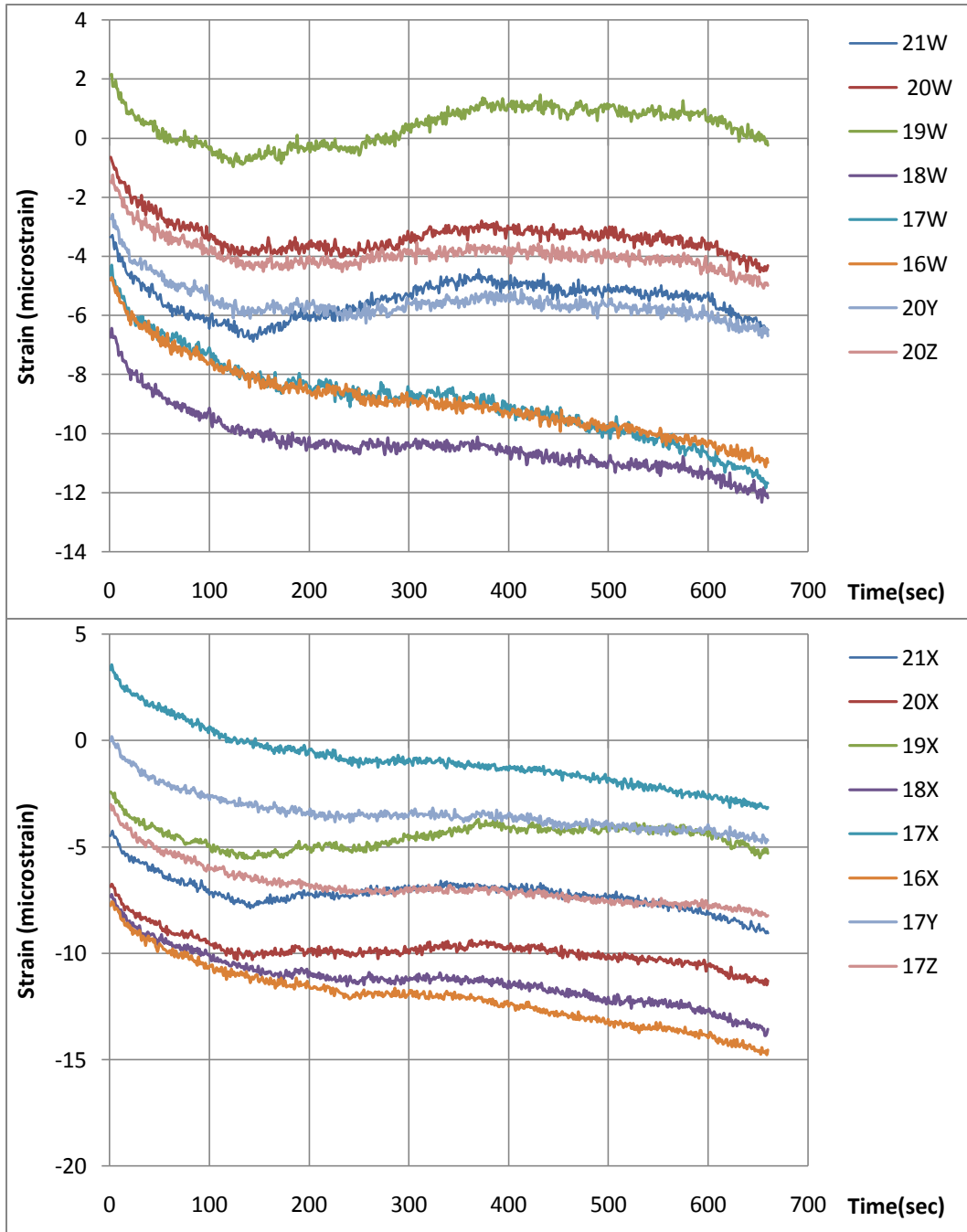


Figure C- 4: Strains in members of the FRP tower at 6:15-6:26PM on February 14, 2009

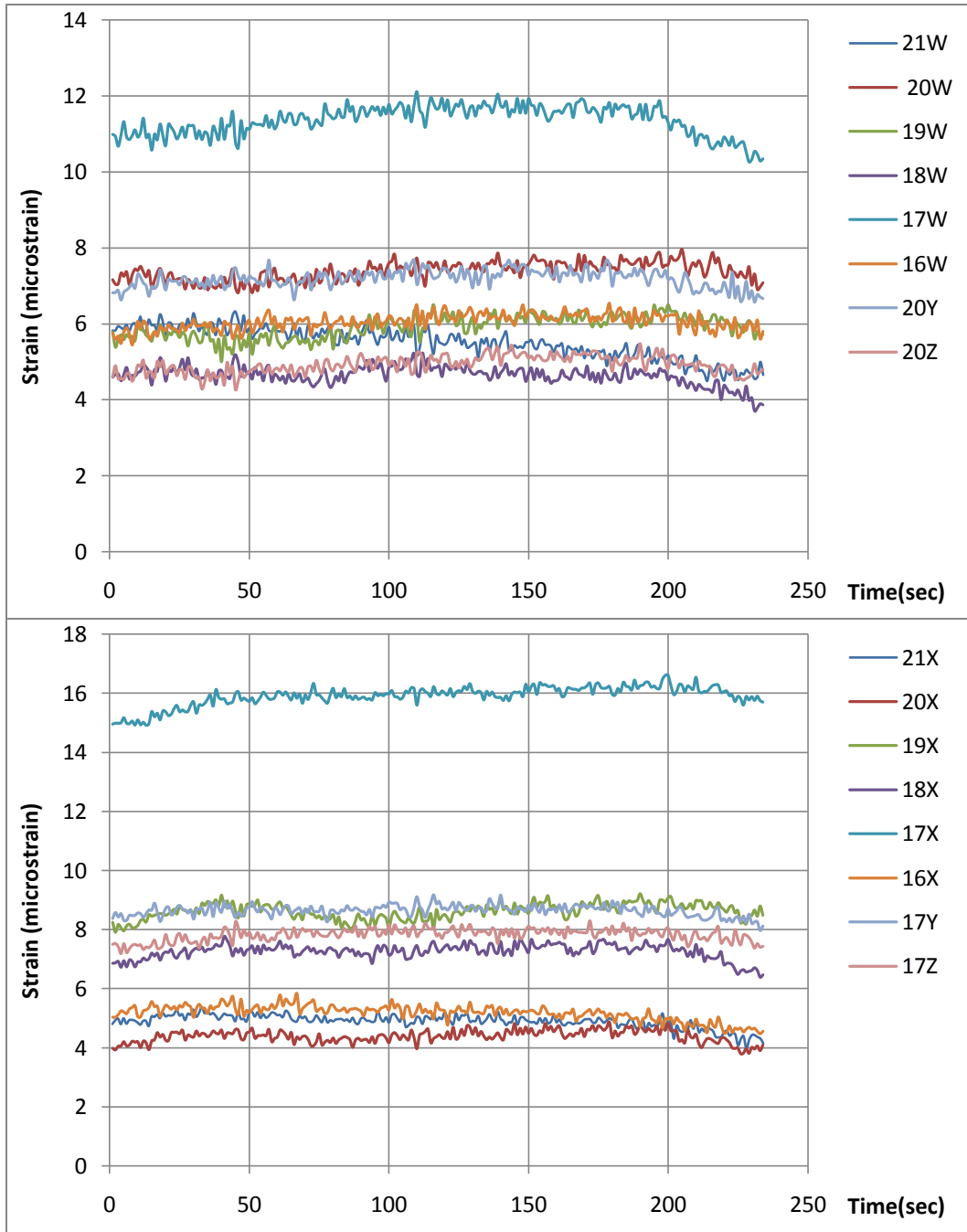


Figure C- 5: Strains in members of the FRP tower at 5:32-5:36PM on February 15, 2009

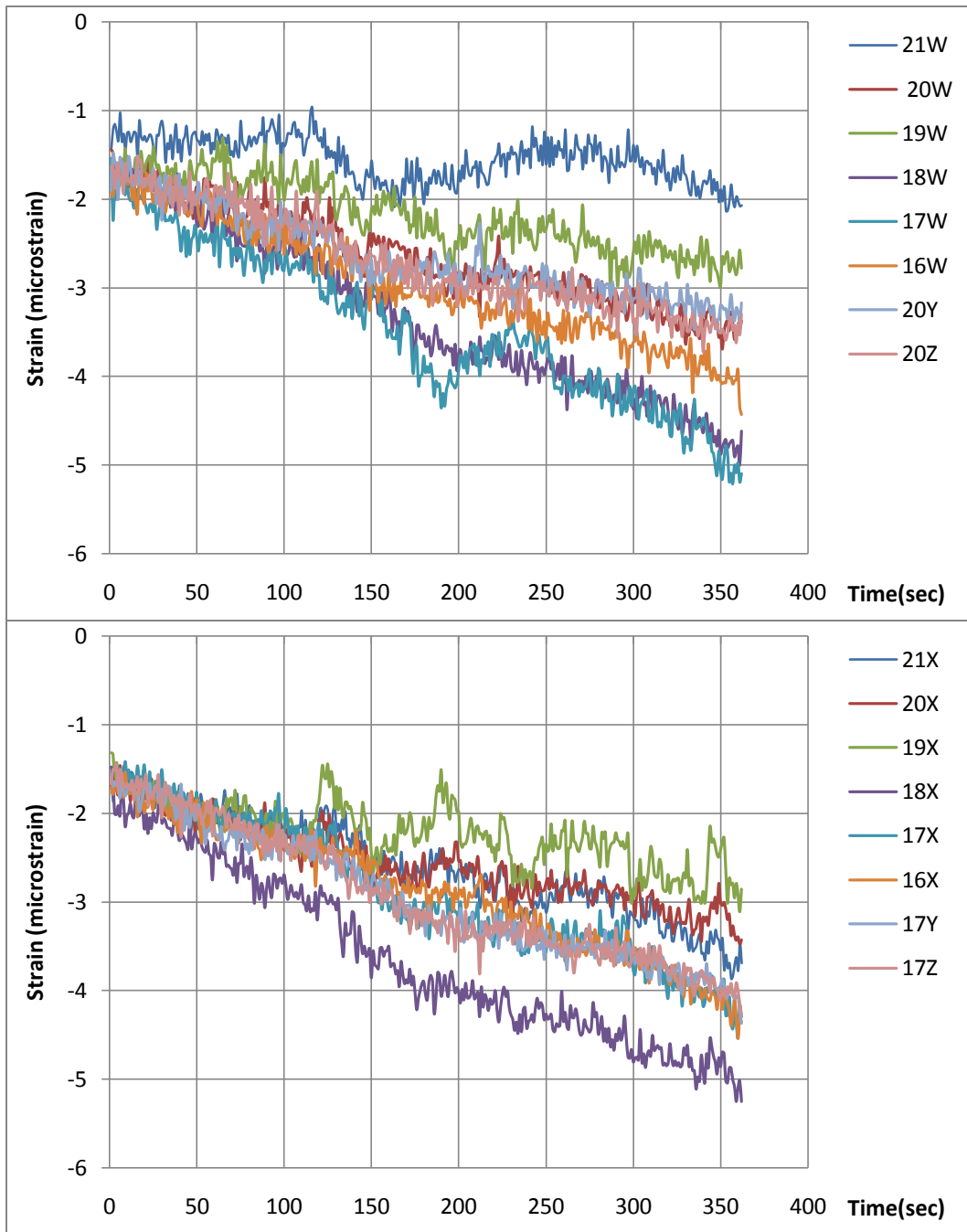


Figure C- 6: Strains in members of the FRP tower at 5:46-5:52PM on February 15, 2009

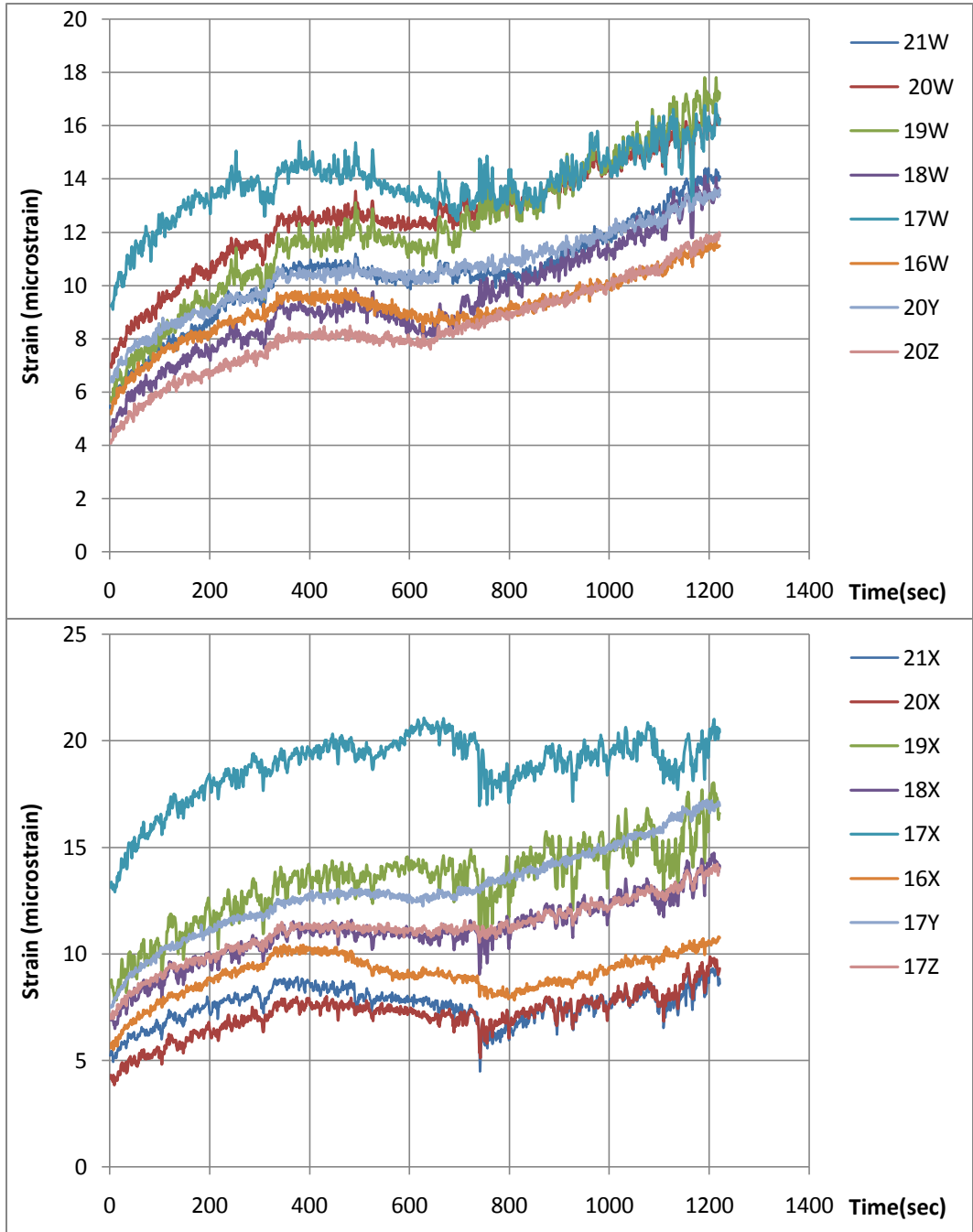


Figure C- 7: Strains in members of the FRP tower at 6:46-7:06PM on February 17, 2009

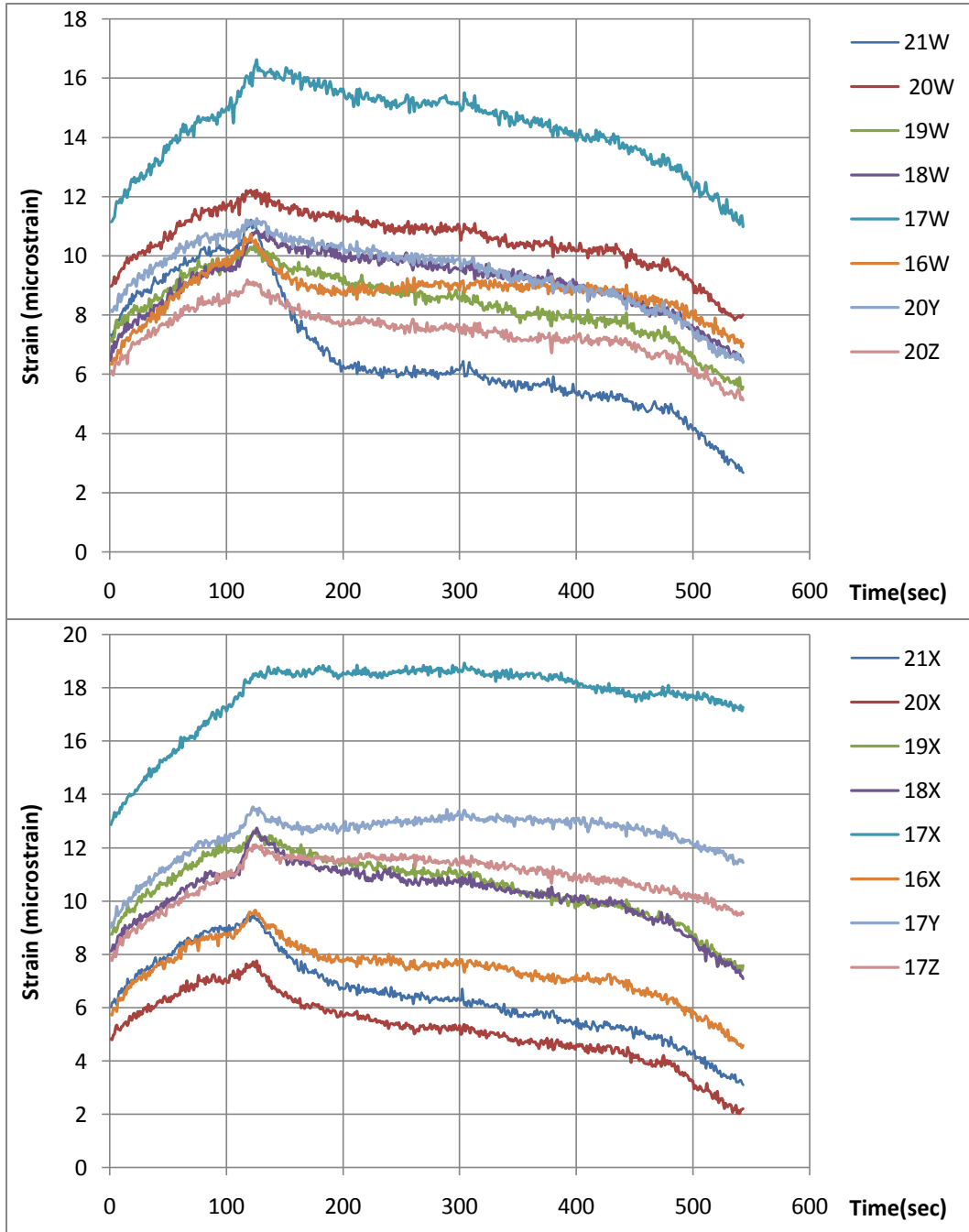


Figure C- 8: Strains in members of the FRP tower at 6:15-6:24PM on February 18, 2009

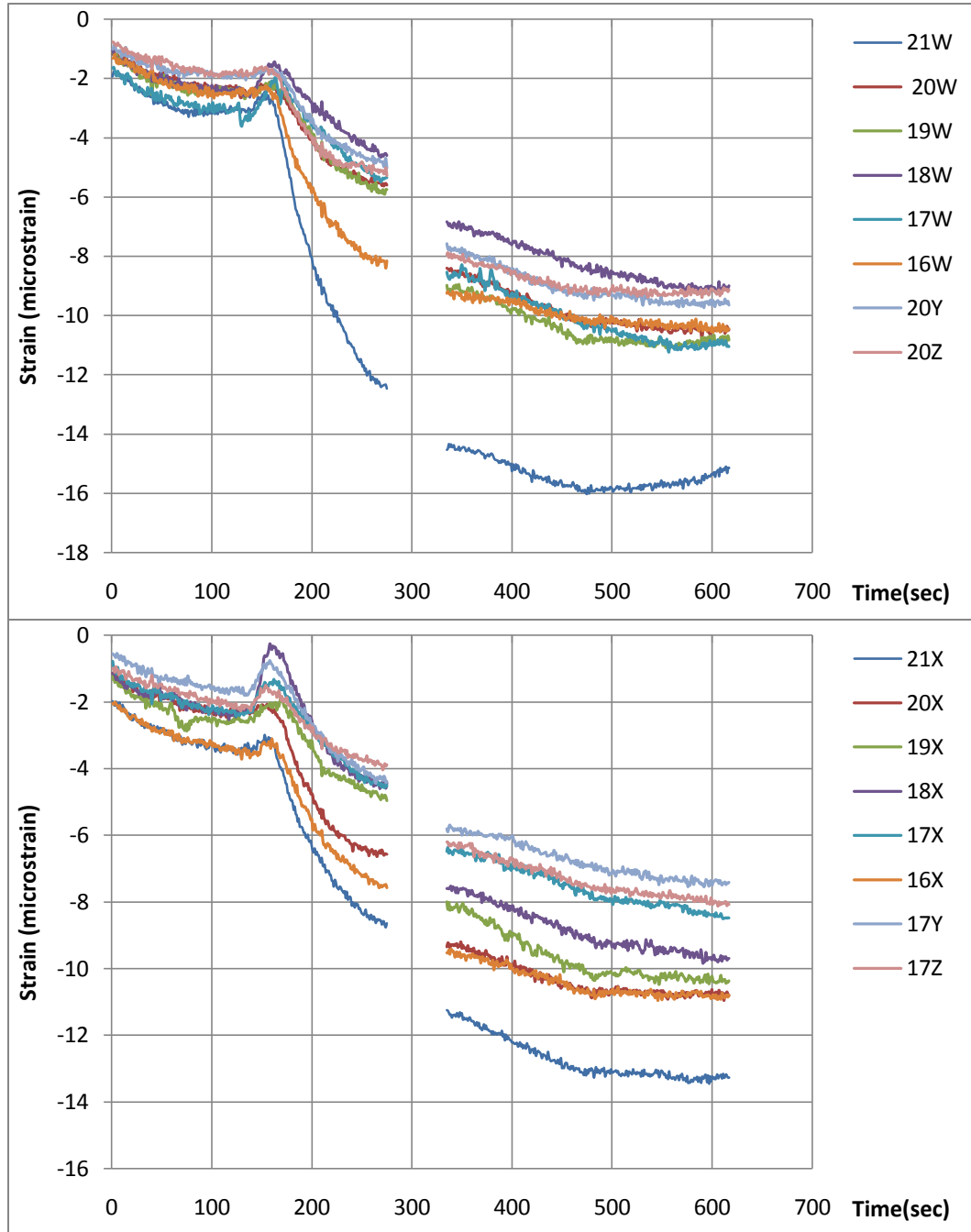


Figure C- 9: Strains in members of the FRP tower at 6:26-6:36PM on February 21, 2009 (1 min. interruption at 6:31)

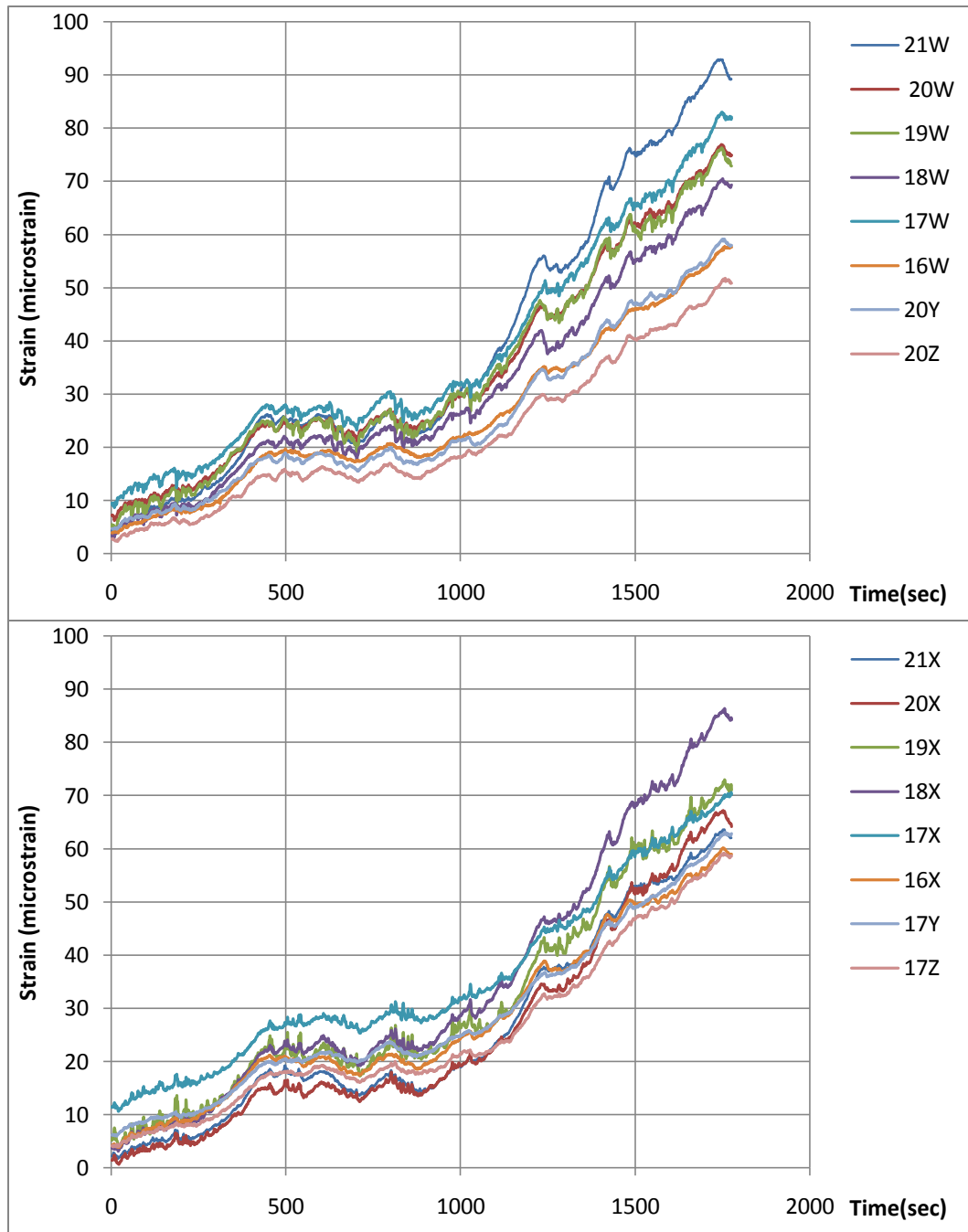


Figure C- 10: Strains in members of the FRP tower at 3:02-3:32PM on February 23, 2009

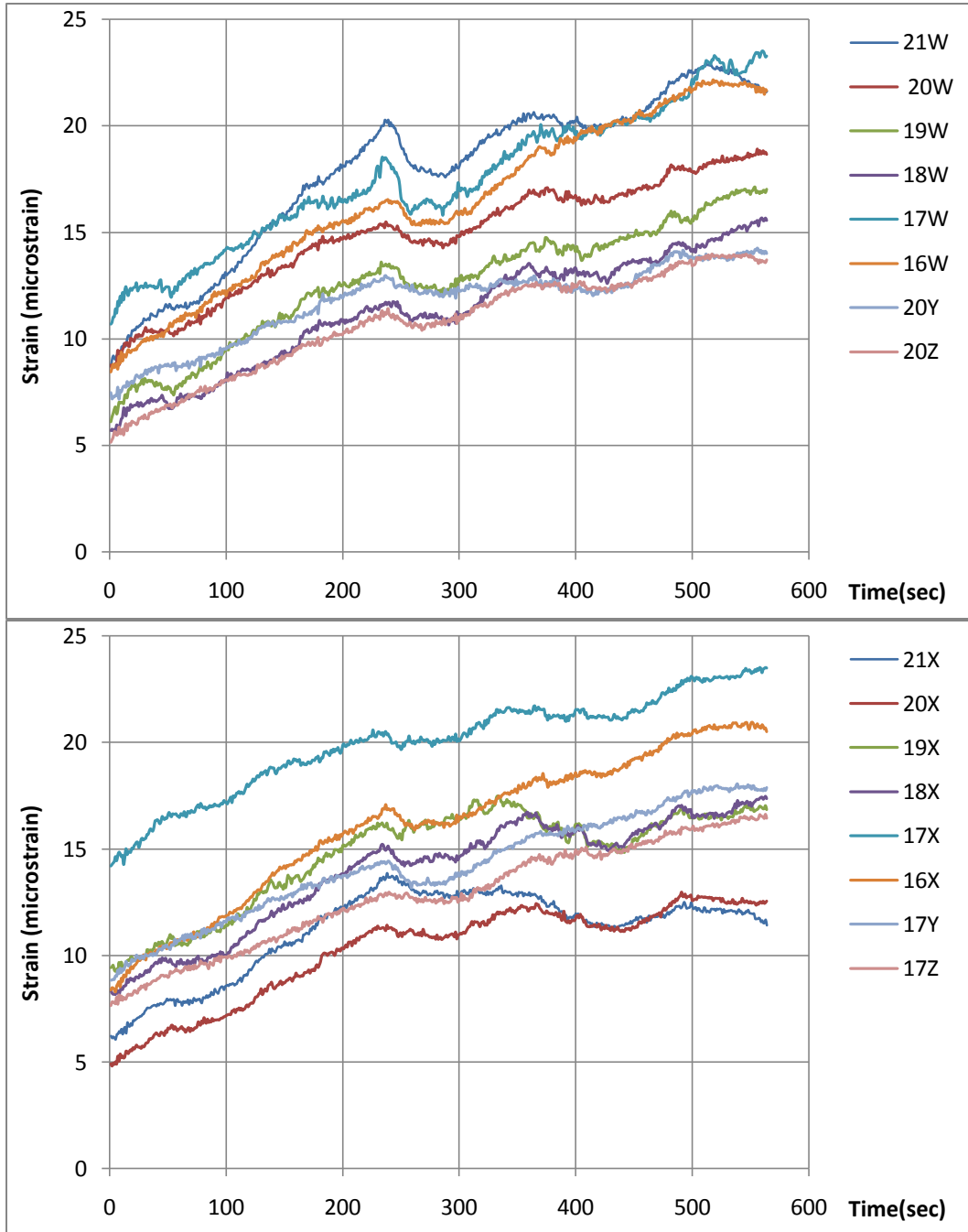


Figure C- 11: Strains in members of the FRP tower at 2:20-2:29PM on February 24, 2009

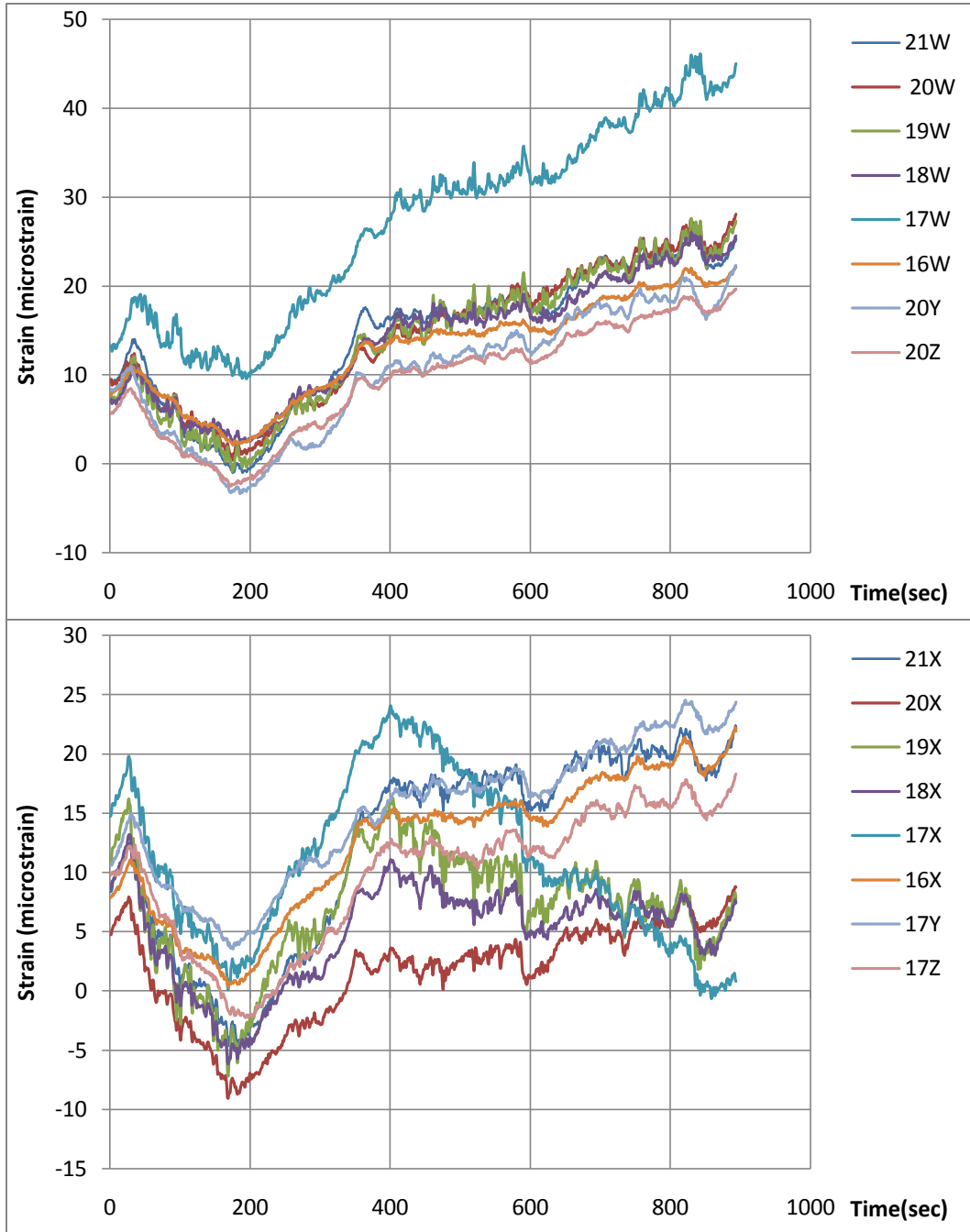


Figure C- 12: Strains in members of the FRP tower at 10:47-11:01AM on February 25, 2009

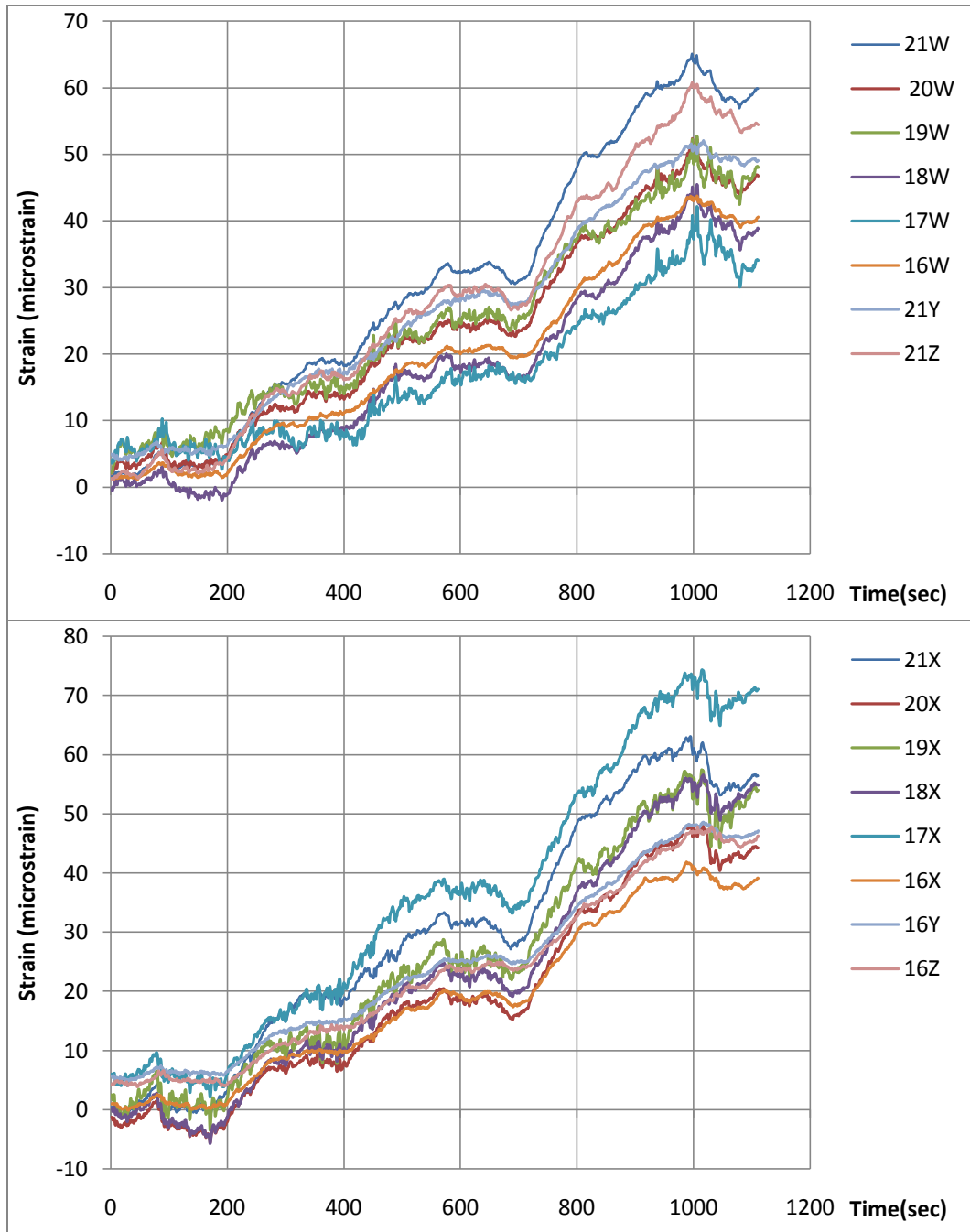


Figure C- 13: Strains in members of the FRP tower at 11:54-12:12AM on February 24, 2009

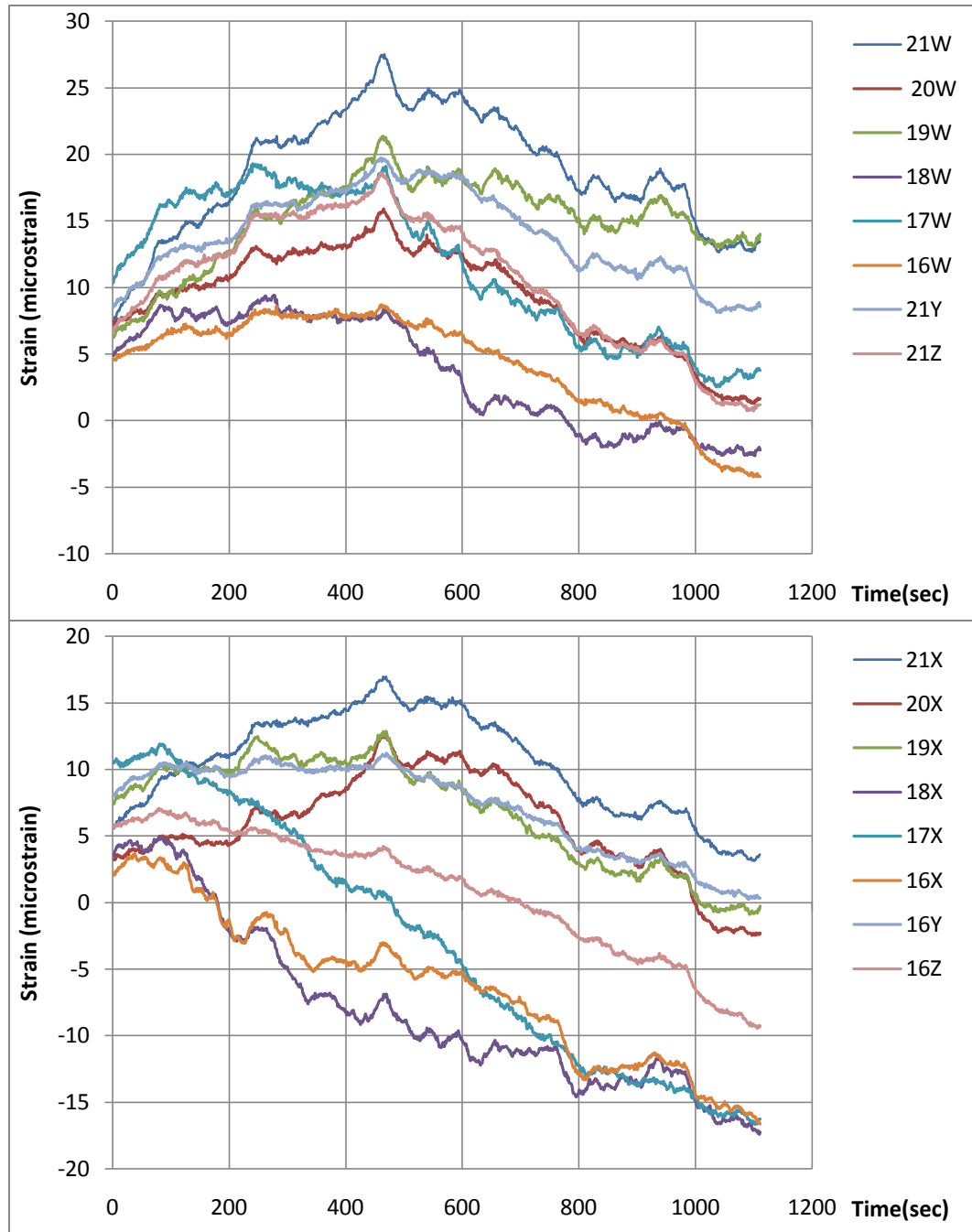


Figure C- 14: Strains in members of the iced FRP tower at 2:54-3:13PM on February 27, 2009

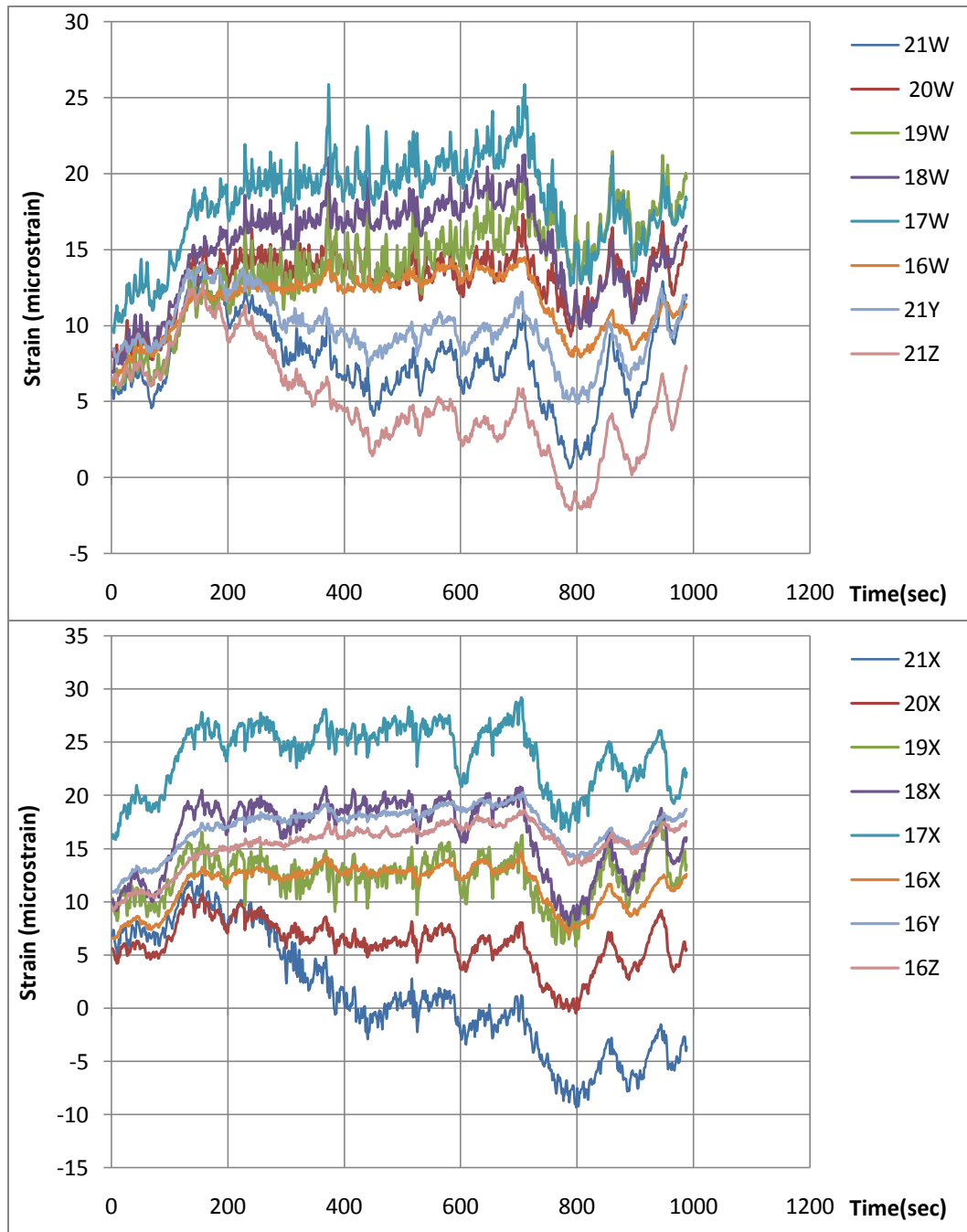


Figure C- 15: Strains in members of the iced FRP tower at 1:56-2:12PM on February 28, 2009

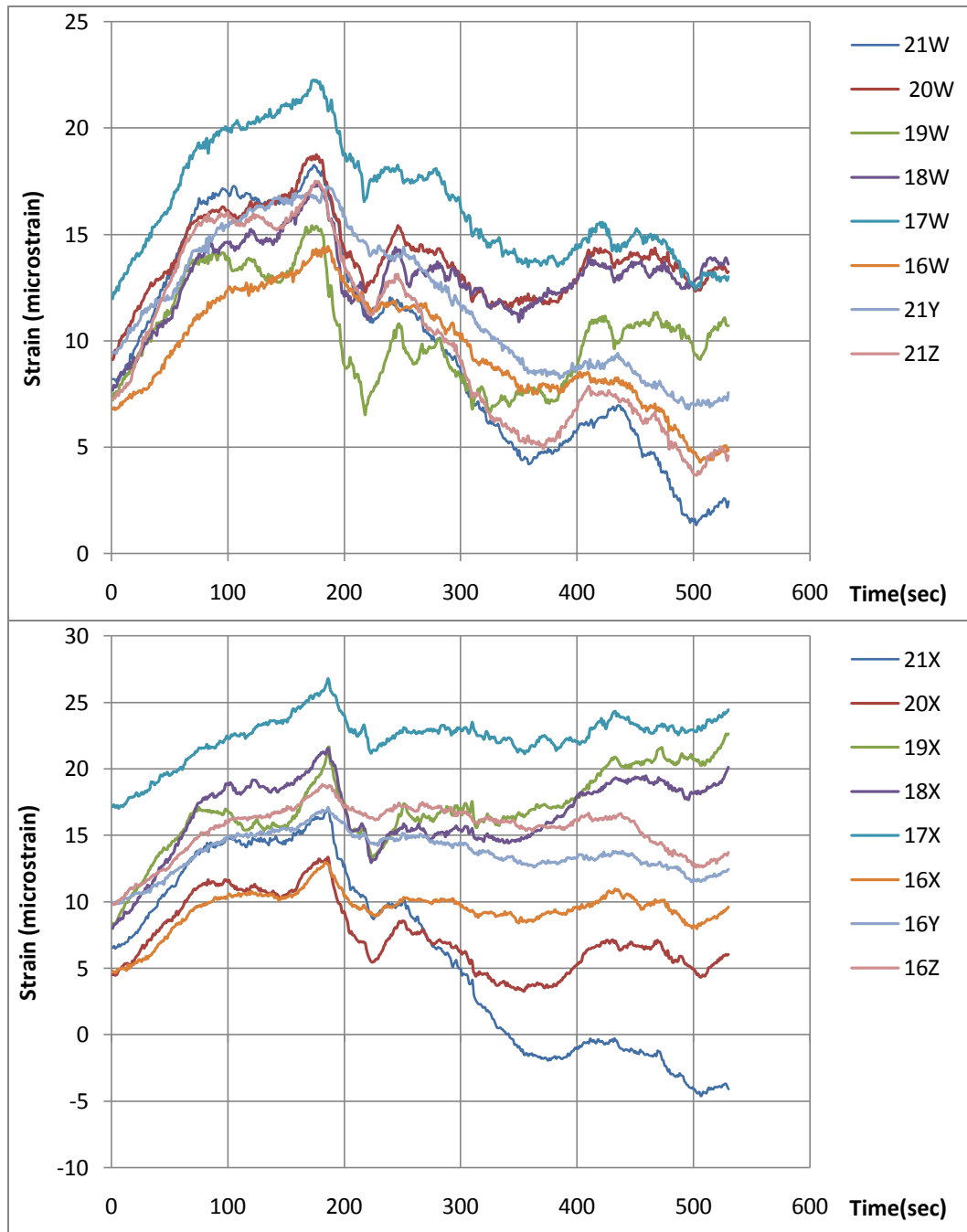


Figure C- 16: Strains in members of the iced FRP tower at 1:34-1:43PM on March 1, 2009

APPENDIX D: Vibration frequency spectra of the FRP tower.

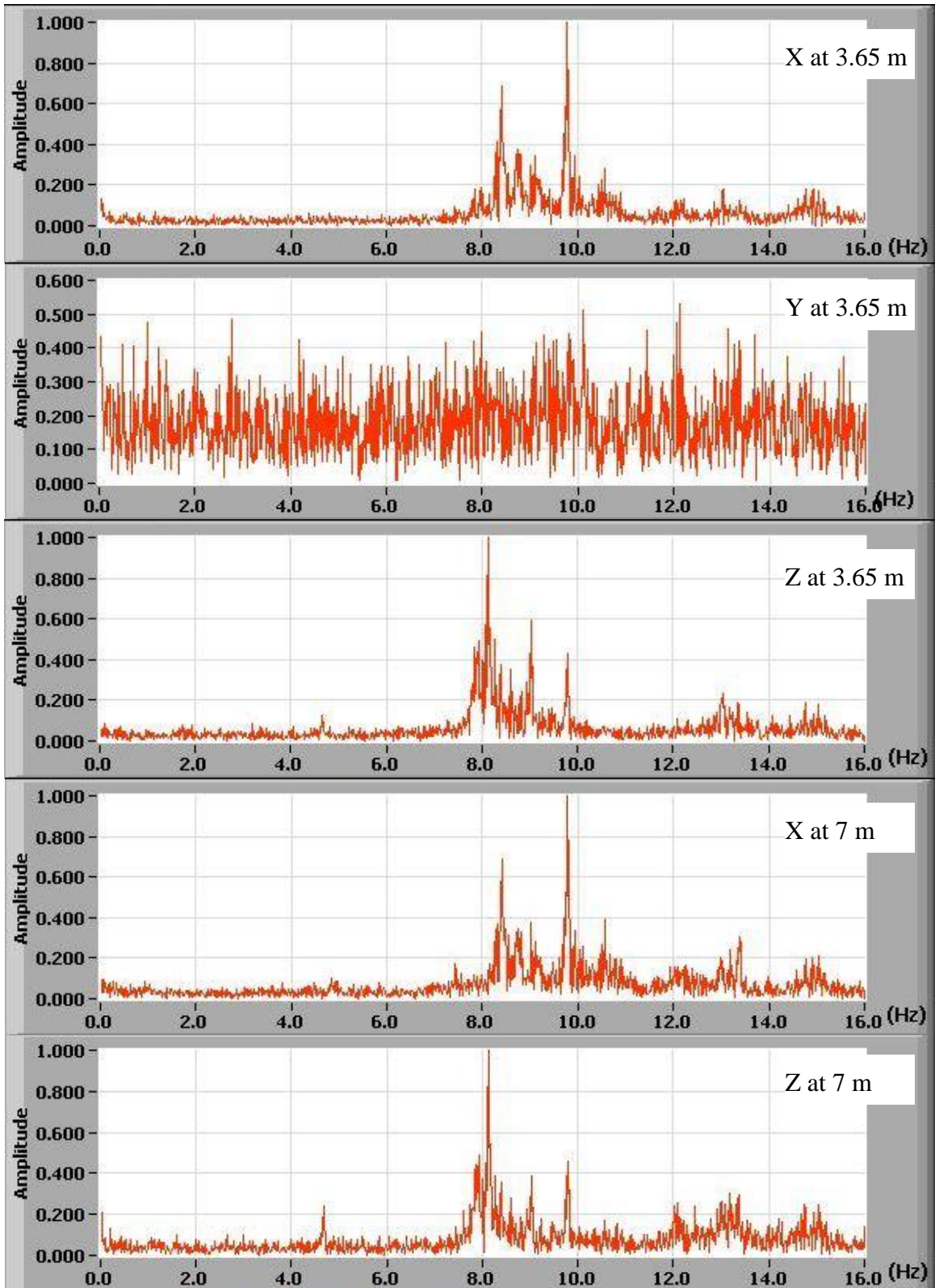


Figure D- 1: Vibration frequency spectrum of the FRP tower at 11:36-11:52AM on February 12, 2009

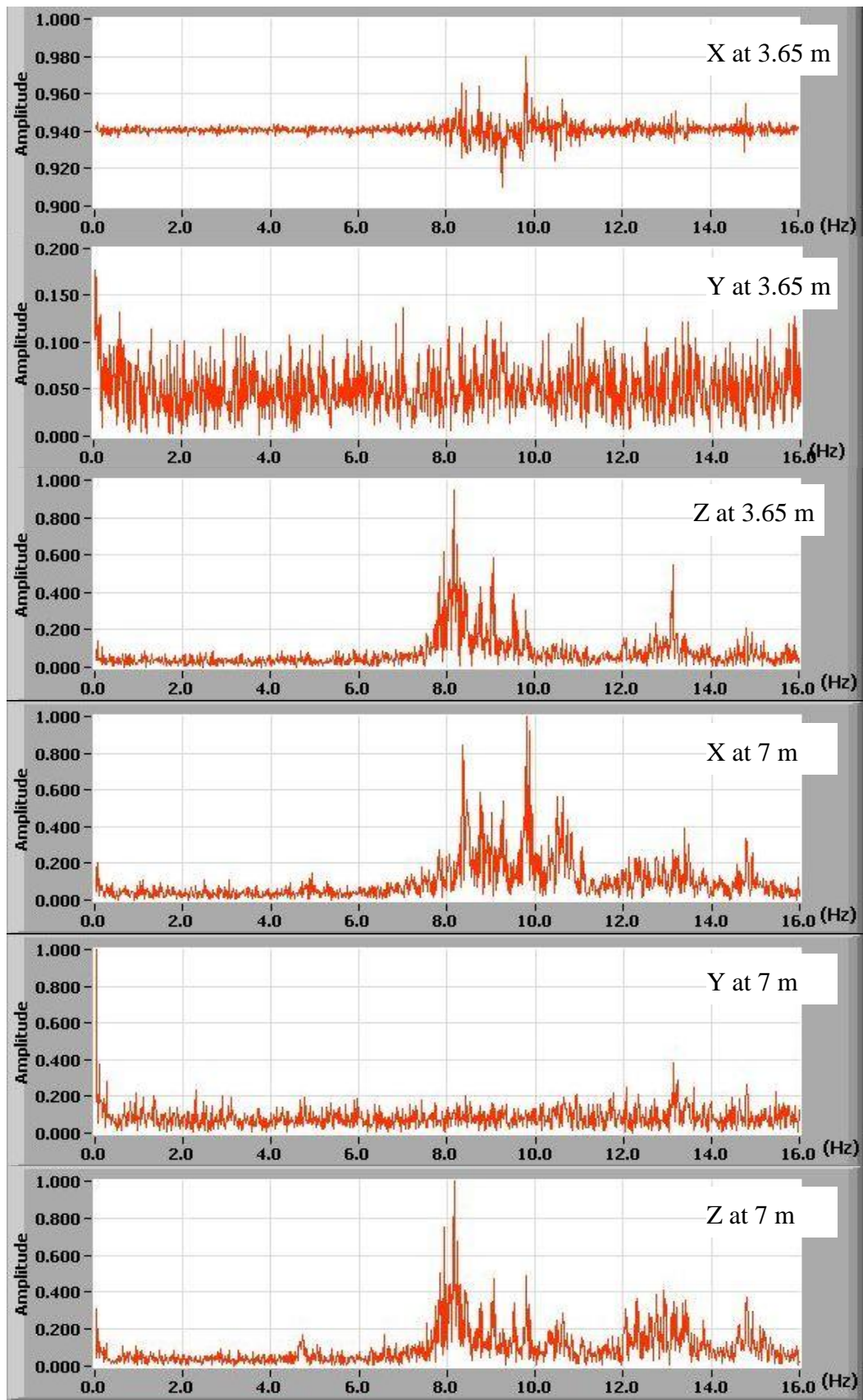


Figure D- 2: Vibration frequency spectrum of the FRP tower at 4:16-4:46PM on February 12, 2009

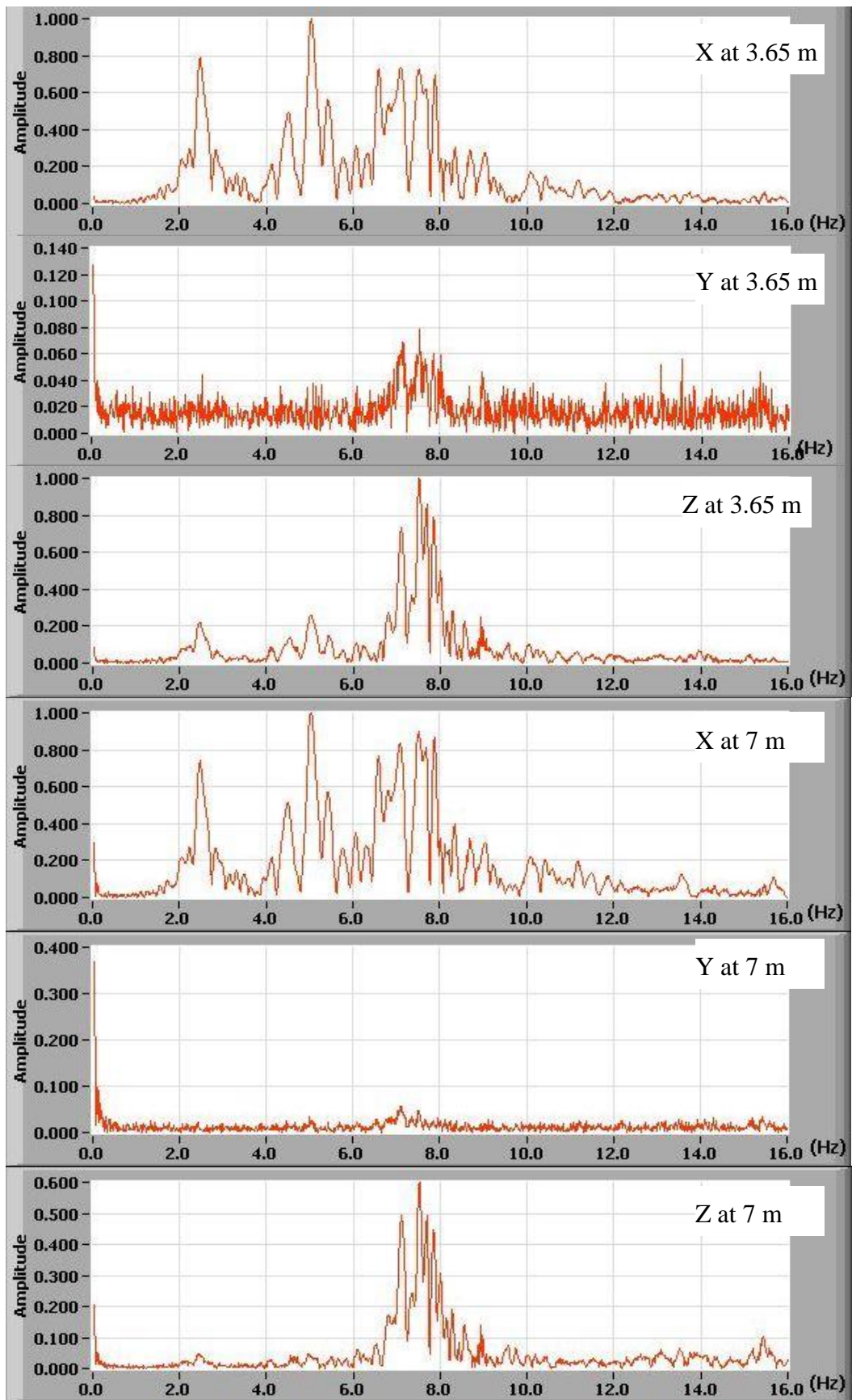


Figure D- 3: Vibration frequency spectrum of the FRP tower at 3:11-3:26PM on February 13, 2009

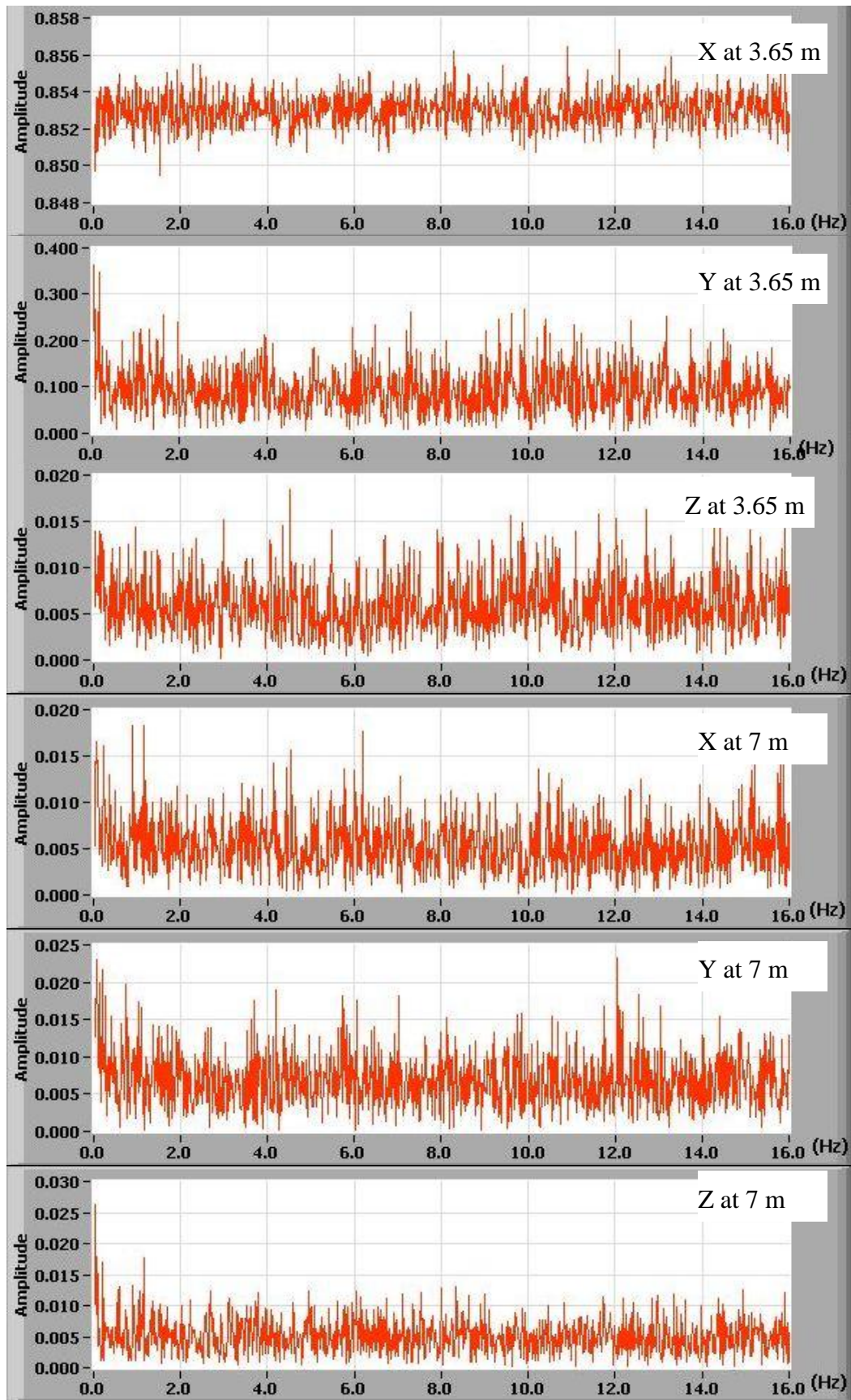


Figure D- 4: Vibration frequency spectrum of the FRP tower at 6:15-6:26PM on February 14, 2009

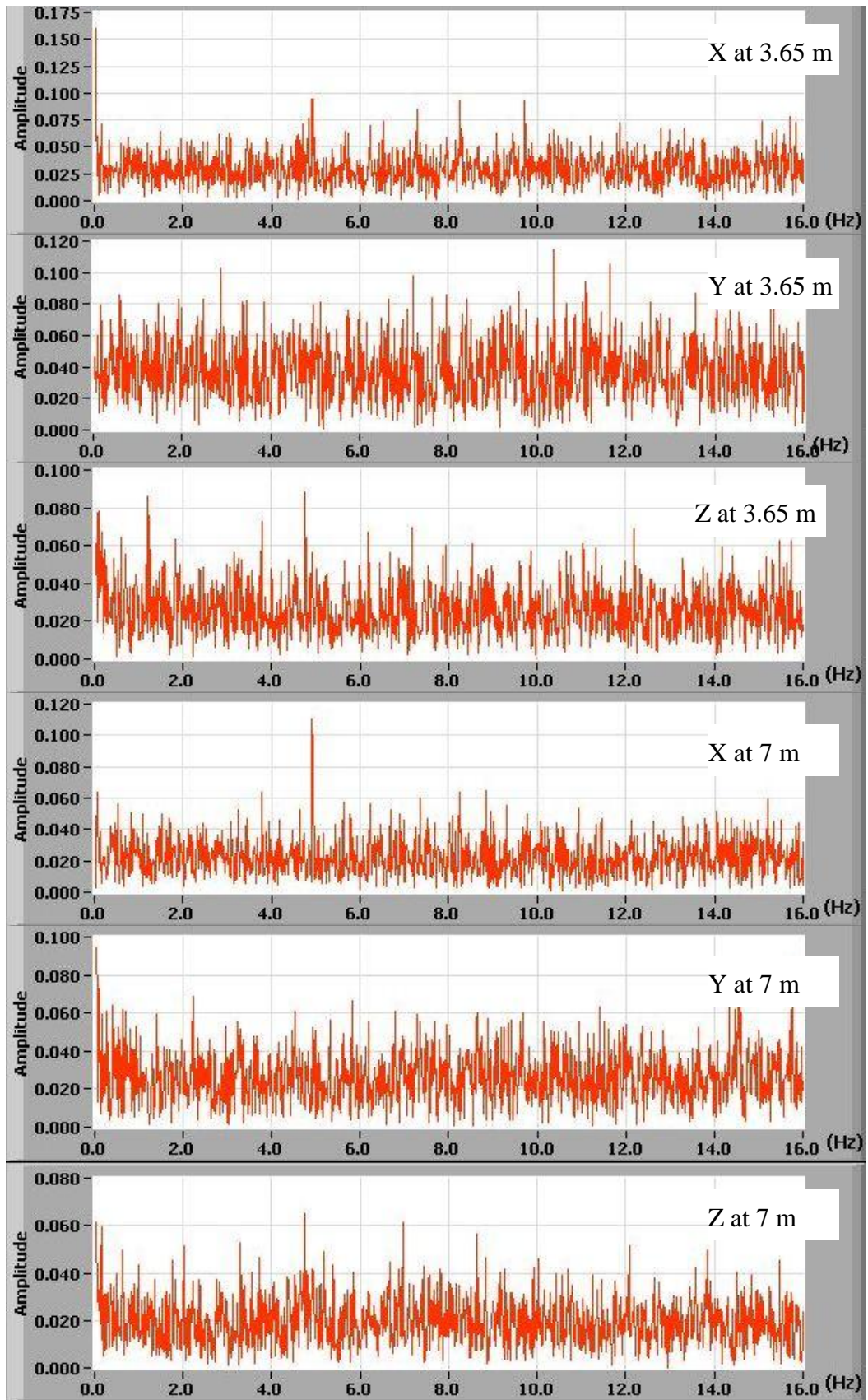


Figure D- 5: Vibration frequency spectrum of the FRP tower at 5:32-5:36PM on February 15, 2009

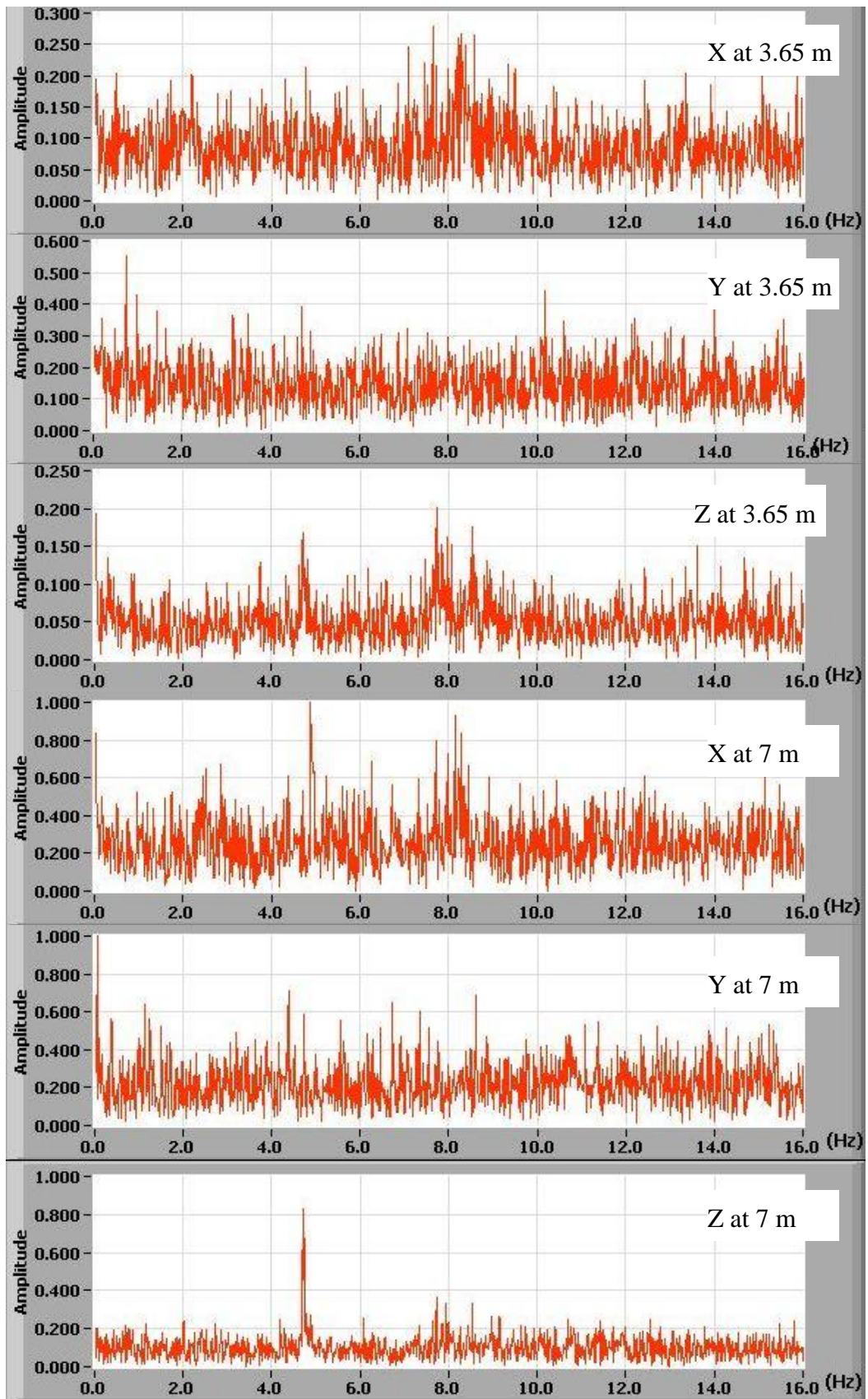


Figure D- 6: Vibration frequency spectrum of the FRP tower at 5:46-5:52PM on February 15, 2009

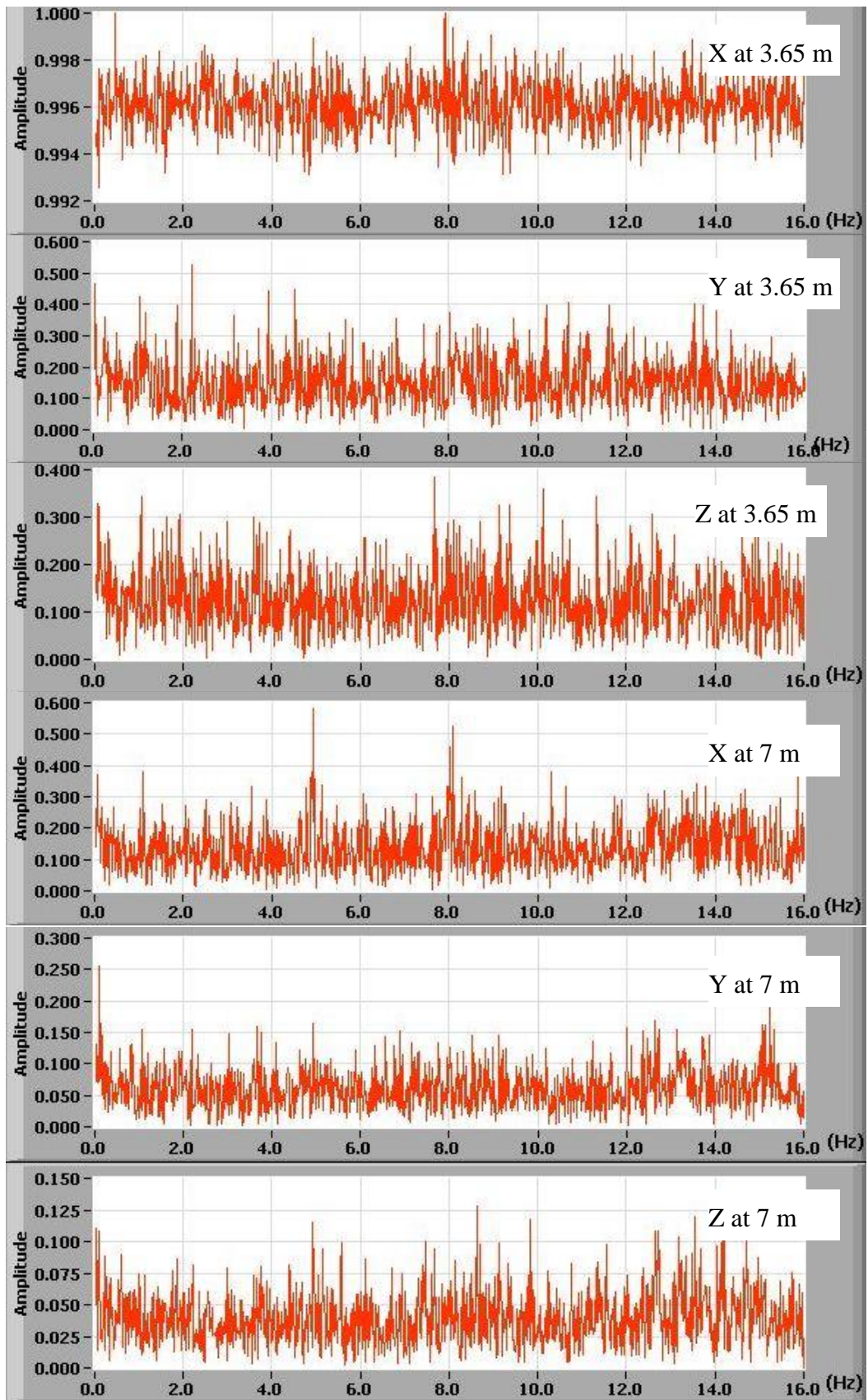


Figure D- 7: Vibration frequency spectrum of the FRP tower at 6:15-6:24PM on February 18, 2009

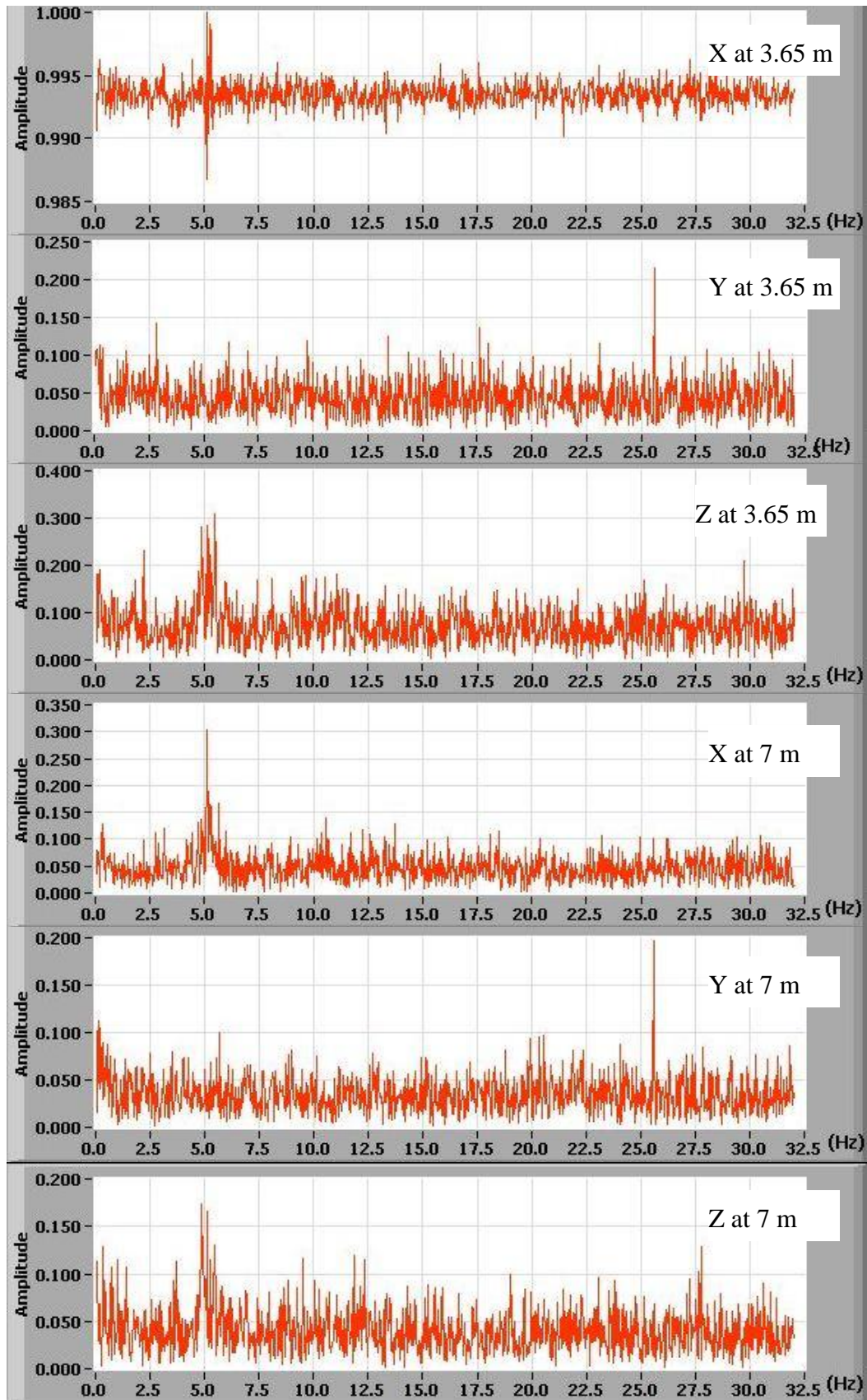


Figure D- 8: Vibration frequency spectrum of the FRP tower at 6:26-6:31PM on February 21, 2009

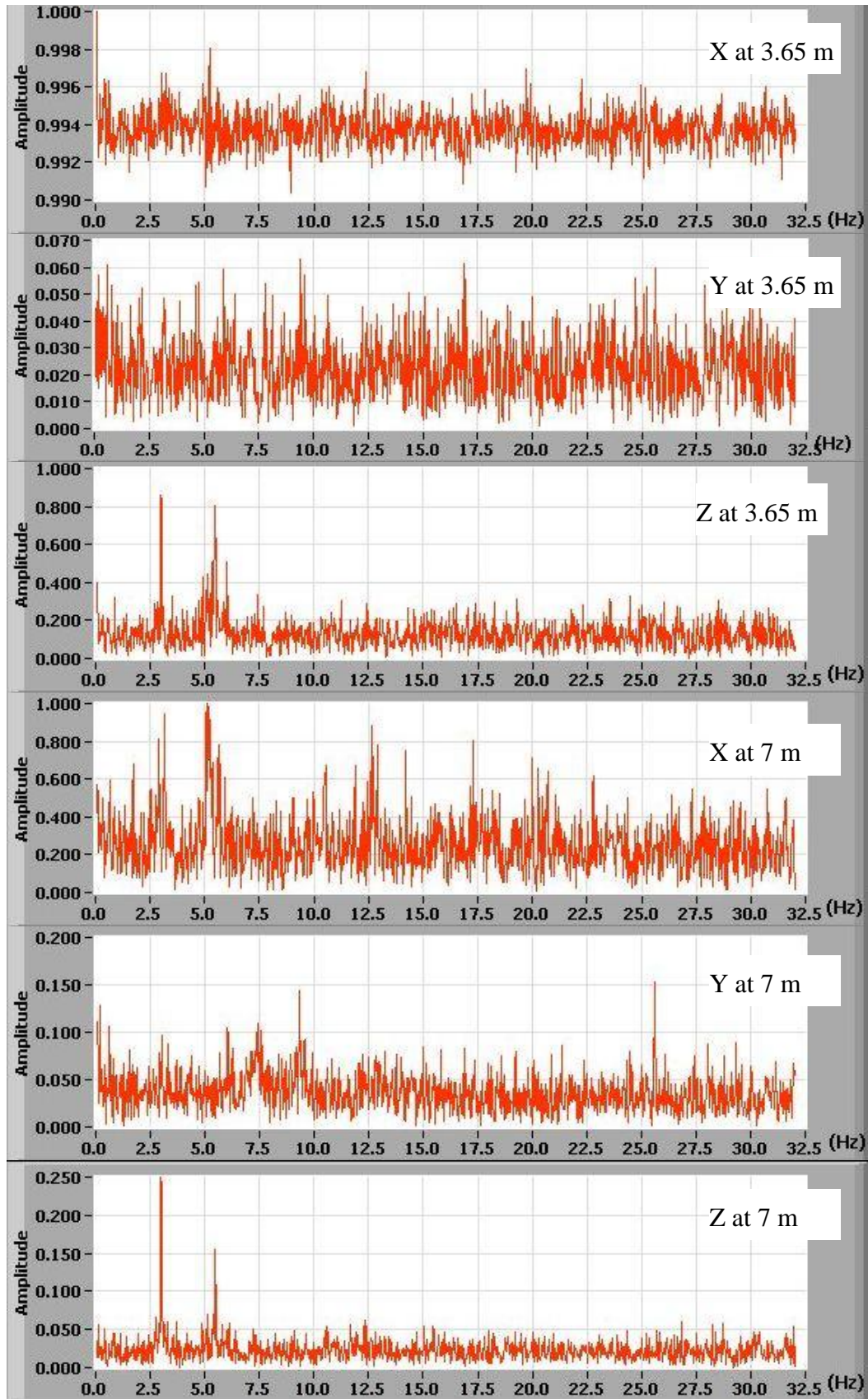


Figure D- 9: Vibration frequency spectrum of the FRP tower at 6:31-6:36PM on February 21, 2009

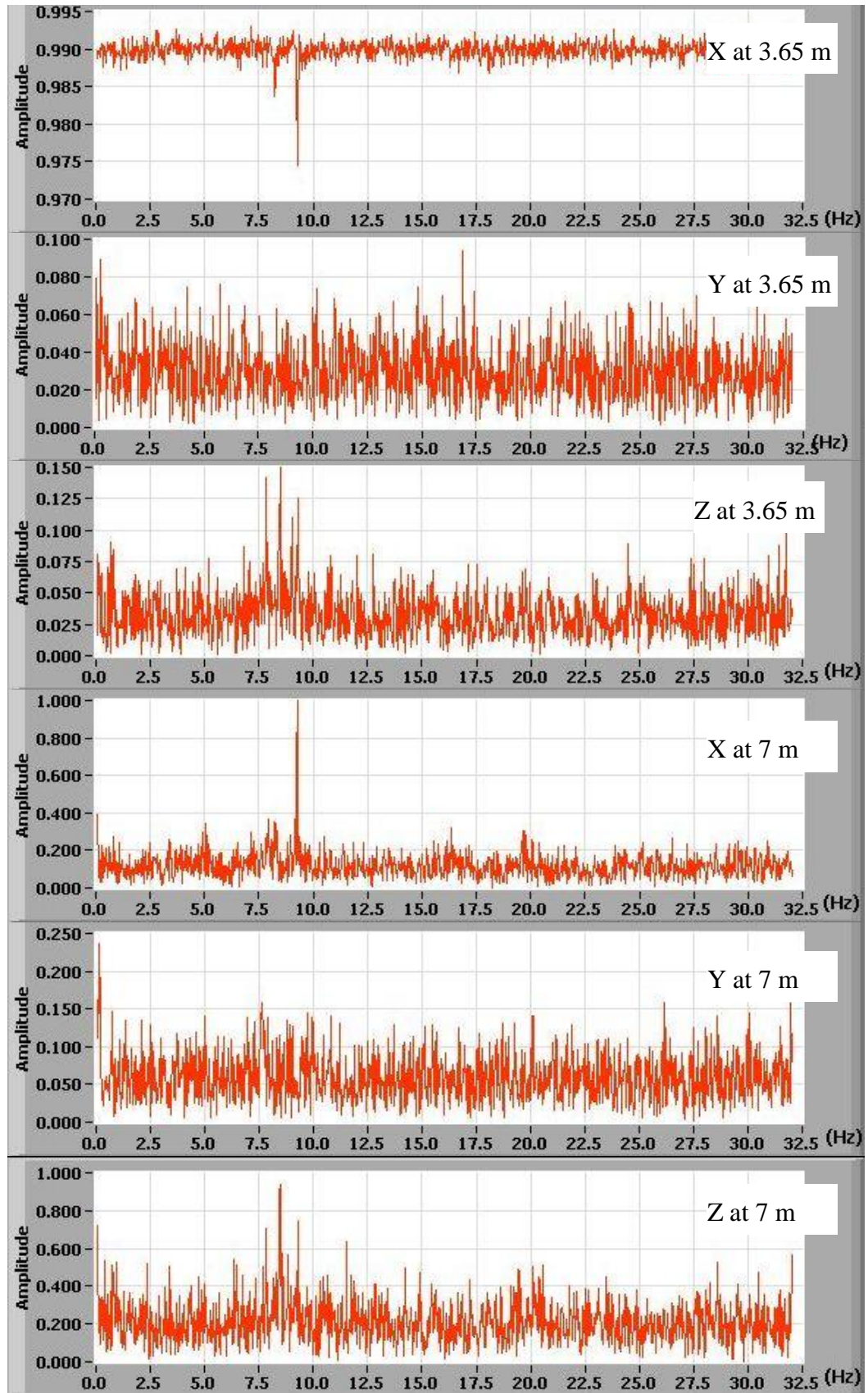


Figure D- 10: Vibration frequency spectrum of the FRP tower at 2:20-2:29PM on February 24, 2009

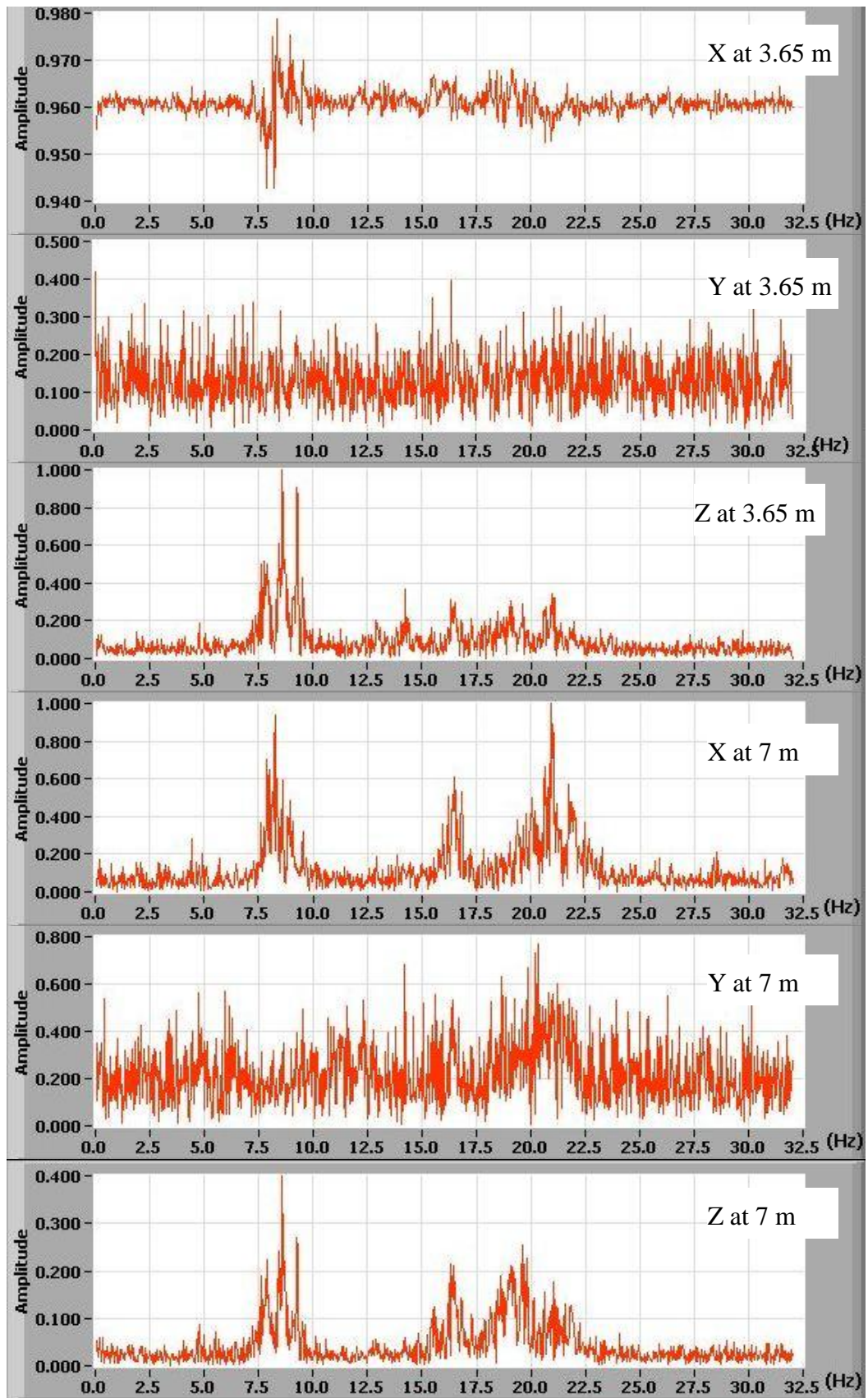


Figure D- 11: Vibration frequency spectrum of the FRP tower at 10:47-11:01PM on February 25, 2009

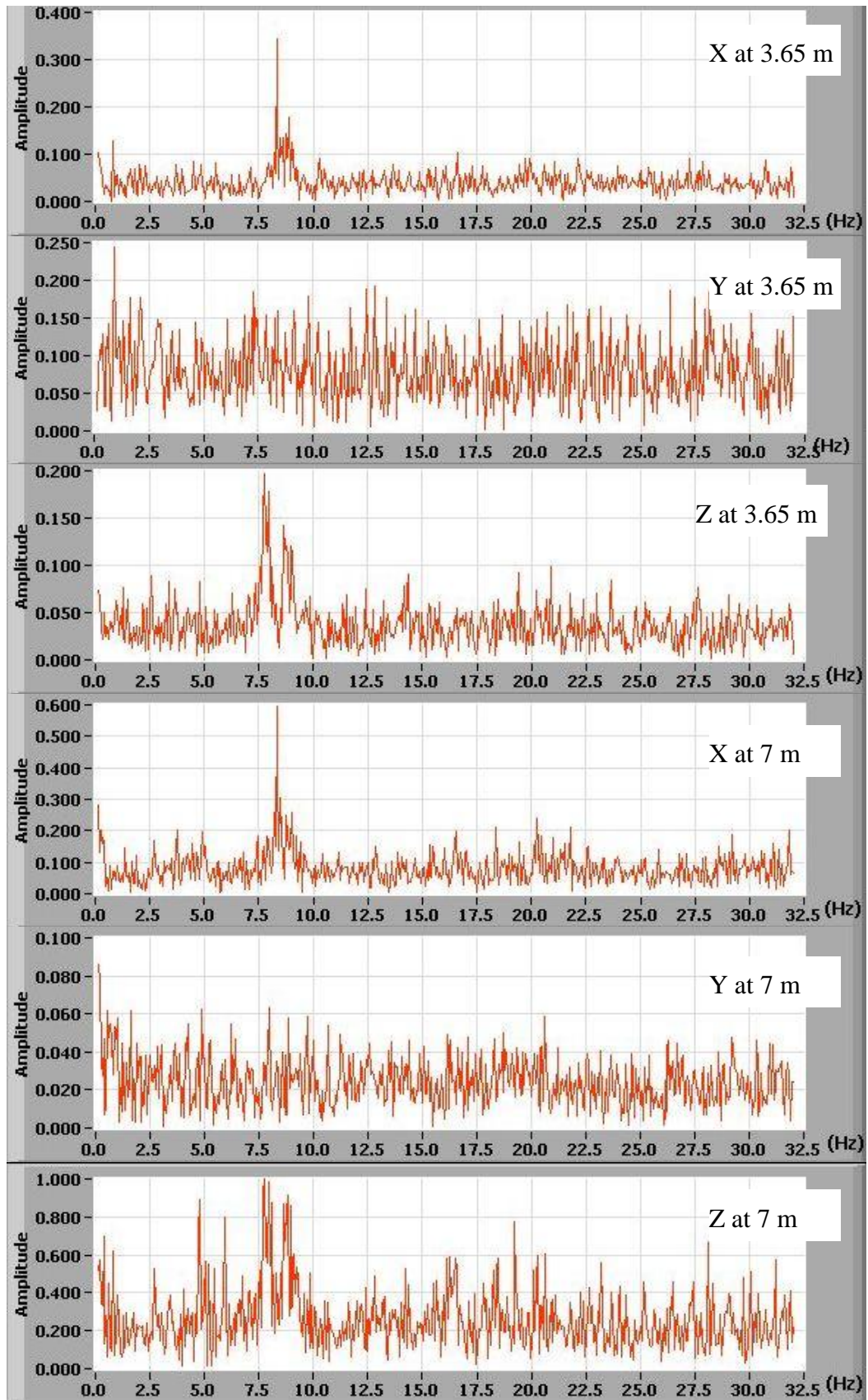


Figure D- 12: Vibration frequency spectrum of the iced FRP tower at 2:54-3:13PM on February 27, 2009

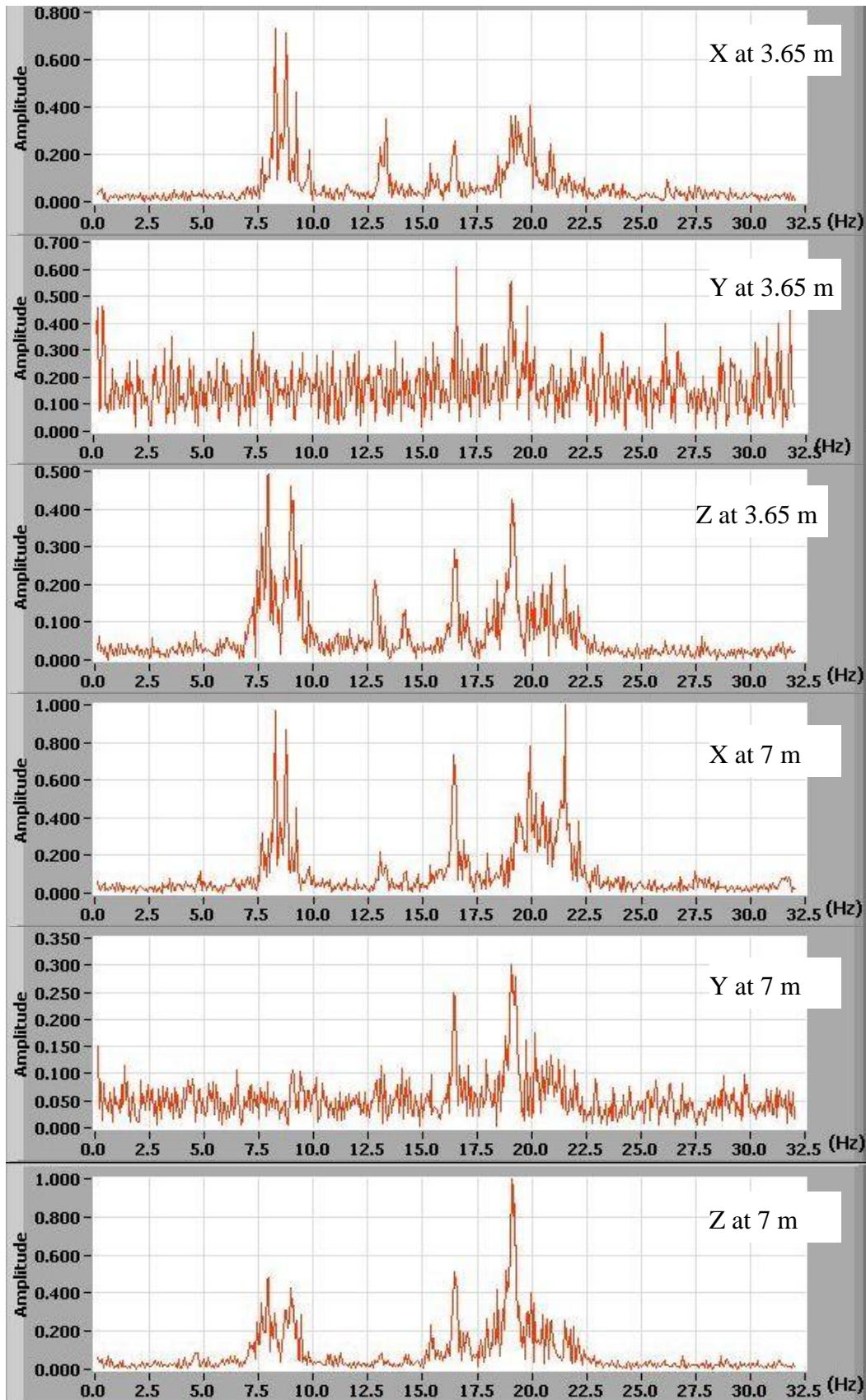


Figure D- 13: Vibration frequency spectrum of the iced FRP tower at 1:56-2:12PM on February 28, 2009

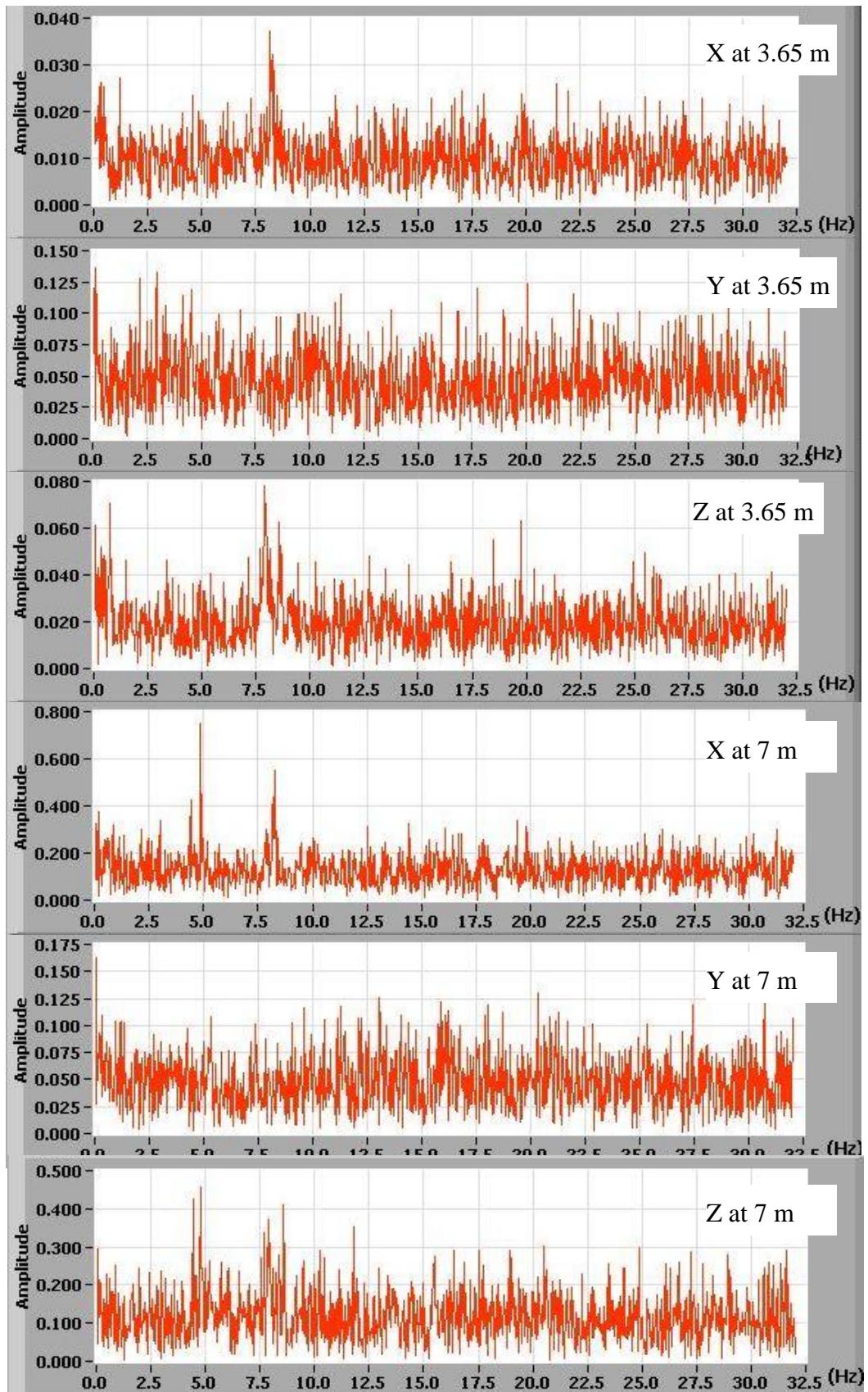


Figure D- 14: Vibration frequency spectrum of the iced FRP tower at 1:34-1:43PM on March 1, 2009